U.S.NRC
United States Nuclear Regulatory Commission
Protecting People and the Environment

Technical Letter Report
TLR-RES/DE/CIB-2020-09-Rev.1

RG 1.99 Revision 2 Update
FAVOR Scoping Study

Date:

May 6, 2021

Prepared in support of the RG 1.99 Rev. 2 revision project by:

Patrick Raynaud
Senior Materials Engineer
Component Integrity Branch

Division of Engineering
Office of Nuclear Regulatory Research
U.S. Nuclear Regulatory Commission
Washington, DC 20555–0001

DISCLAIMER

This report does not contain or imply legally binding requirements. Nor does this report establish or modify any regulatory guidance or positions of the U.S. Nuclear Regulatory Commission and is not binding on the Commission.

Errata

This TLR was modified after its initial publication to correct an error related to the PT100-50 transients modeled for PWRs and BWRs. Specifically, as initially modeled, the PT100-50 transients violated the PT limit for a 50°F/hour cooldown. The BWR and PWR definitions for this transient were updated to respect PT limits, and the analyses were re-run with the updated transient. The changes in the results resulted in CPI and CPF reductions for these transients, and did not affect the overall conclusions of the report.

There was also a paragraph added to the end of the executive summary, and associated editorial changes elsewhere in the executive summary, to provide a more fulsome description of the report's contents. Several editorial corrections were also made throughout the report.

Specific changes made are as follows:

- Executive summary was modified as previously described
- Section 2.1.2.3 and corresponding Figure 2-4 were replaced
- Figure 2-11 was updated
- Section 2.3.3 was updated (including the Figures and Tables) to reflect correct transient definition
- Section 3.1.2.3 and corresponding Figure 3-4 were replaced
- Figure 3-9 was updated
- Section 3.3.3 was updated (including the Figures and Tables) to reflect correct transient definition
- Figure 4-3 and the corresponding description of this figure in Section 4 was updated
- Throughout the report, the following typographical errors were fixed:
    - Kic was replaced by K_{Ic}
    - Kia was replaced by K_{Ia}

Contents

Executive Summary

This report documents the probabilistic fracture mechanics analyses performed between October 2019 and May 2020 in support of the RG 1.99 Rev.2 revision effort. The primary goal of the analyses was to evaluate the analytical impact of a proposed change in embrittlement correlation, from the one currently used in RG 1.99 Rev.2 to the one used in the ASTM E900-15 standard. The analyses were performed with the NRC's FAVOR v16.1 code.

The study specifically analyzed the change in conditional probability of crack growth initiation (CPI) and in conditional probability of vessel failure (CPF) as a function of the shift in embrittlement that might result from changing the embrittlement correlation in RG 1.99. The potential embrittlement shift deltas associated with switching from the RG 1.99, Rev. 2 to the E900-15 embrittlement correlation were predicted for the entire US fleet. The range of embrittlement shift deltas in this study were chosen to capture the variability of the entire fleet of PWRs and BWRs.

Several PWR and BWR transients deemed relevant for the purpose of this assessment were modeled assuming both a ¼ thickness flaw depth (as required by ASME code) and a shallow inner-surface flaw penetrating through the stainless steel cladding and barely into the reactor pressure vessel base metal (ferritic carbon steel).

With the modeling assumptions used in this study, the transients resulting in the highest CPF (i.e., CPF > $1x10^{-6}$) were PWR cooldowns along the pressure-temperature (P-T) limit for ¼ thickness flaws. For BWRs, the transients resulting in the highest CPF were leak tests, but CPF was < $1x10^{-6}$ unless the embrittlement shift data was > 100°F. Realistic cooldown transients resulted in the lowest CPF values, with most being zero, and the highest reaching around $1x10^{-9}$ for one actual PWR cooldown modeled.

In this study, CPF was used as a conservative risk surrogate and values below $1x10^{-6}$ are not considered to be significant. The associated through-wall cracking frequency (TWCF) is a more accurate risk metric and it accounts for the likelihood of both the evaluated transients and the existence of the cracks modeled. In this study, the expected TWCFs were evaluated, using previously estimated transient frequencies. The results show that the TWCFs are well below the $1x10^{-6}$ per year acceptance limit used in 10 CFR 50.61a.

1 Introduction

Beginning in 2019, the NRC evaluated whether to update Regulatory Guide 1.99, Revision 2 [1] (hereafter RG 1.99, Rev. 2), in particular with regards to the embrittlement correlations to be used in reactor pressure vessel safety analyses. Specifically, the NRC was proposing to replace the embrittlement correlation in RG 1.99, Rev. 2 with the embrittlement correlation from ASTM E900-15 [2] (hereafter E900-15). This report documents the analyses performed in support of the RG 1.99 Rev.2 revision effort between October 2019 and May 2020.

The primary purpose of this study is to evaluate the analytical impact of a change in embrittlement correlation from the one currently in RG 1.99, Rev. 2 to the one from E900-15. Specifically, this study focuses on the change in conditional probability of crack initiation (CPI) and conditional probability of vessel failure (CPF) at 72 Effective Full Power Years (EFPY), as a result of the change in embrittlement correlation. This report first presents the PWR analysis results, and then the BWR analysis results.

The study was performed at 72 EFPY because this bounds the US Fleet 80 year subsequent license renewal periods. The change in CPI and CPF as a result of the change in embrittlement correlation was studied for a postulated high embrittlement PWR and for a postulated high embrittlement BWR (high embrittlement plants are those with a high Adjusted Reference Temperature [ART]). Studies were performed for both a quarter-thickness ID surface flaw (¼ T flaw or 0.25 T flaw) and for the shallowest ID surface flaw whose crack tip penetrated through the cladding into the base metal (0.03 T for the PWR case and 0.04 T for the BWR case). These flaws were chosen based on NRC regulatory guidance and previous results concerning CPI and CPF sensitivity to flaw types [3].

The RT_{NDT} shifts associated with switching from the RG 1.99, Rev. 2 to the E900-15 embrittlement correlation were predicted using the embrittlement trend correlations. The values of the shift used in this study were chosen to capture the variability of the entire fleet of PWRs and BWRs. Calculations were performed for shifts of -40°F, 0°F (baseline), and then the 50^{th}, 75^{th}, 95^{th}, and 99^{th} percentiles of the predicted RT_{NDT} shift populations for the PWR and BWR fleets.

Finally, for each combination of reactor type, flaw depth, and RT_{NDT} shift, a variety of transients were studied, ranging from licensed maximum cooldown transients and leak tests to more realistic transients. The more realistic transients were studied to better understand the actual risk of vessel failure when considering actual practice in the US fleet. The FAVOR v16.1 code [4] [5] was used in all analyses.

2 PWR Scoping Study

2.1 Vessel and Transient Characteristics

2.1.1 Vessel Characteristics and Embrittlement Map

The PWR vessel modeled had the following characteristics:

- Inner radius 86 inches
- Cladding Thickness 0.25 inches
- Base metal thickness 8.5 inches
- Total wall thickness 8.75 inches

The material properties used in the FAVOR model are given in Table 2-1 and Table 2-2. The stress free temperature was assumed to be equal to 488°F. Pressure loading was applied since the calculations presented herein are for an ID surface flaw. Finally, weld residual stress (WRS) was included in calculations for axial and circumferential welds. These modeling parameters were chosen to match the analysis parameters historically used by NRC for regulatory analyses (e.g. 10 CFR 50.61a technical bases), and are the ones recommended in the FAVOR theory manual.

Table 2-1: PWR Base Metal Properties

Temperature	Thermal Conductivity	Specific Heat	Thermal Expansion Coefficient	Temperature	Young's Modulus
°F	BTU/(hr.ft.°F)	BTU/(lbm.°F)	1/°F	°F	ksi
70	24.8	0.1052		70	29200
100	25	0.1072	0.00000706	200	28500
150	25.1	0.1101	0.00000716	300	28000
200	25.2	0.1135	0.00000725	400	27400
250	25.2	0.1166	0.00000734	500	27000
300	25.1	0.1194	0.00000743	600	26400
350	25	0.1223	0.0000075	700	25300
400	25.1	0.1267	0.00000758	800	23900
450	24.6	0.1277	0.00000763	Temperature	Poisson's Ratio
500	24.3	0.1304	0.0000077	°F	
550	24	0.1326	0.00000777	0	0.3
600	23.7	0.135	0.00000783	1000	0.3
650	23.4	0.1375	0.0000079		
700	23	0.1404	0.00000794		
750	22.6	0.1435	0.000008		
800	22.2	0.1474	0.00000805		

Table 2-2: PWR Cladding Properties

Temperature	Thermal Conductivity	Specific Heat	Thermal Expansion Coefficient
°F	BTU/(hr.ft.°F)	BTU/(lbm.°F)	1/°F
70	8.1	0.1158	
100	8.4	0.1185	0.00000855
150	8.6	0.1196	0.00000867
200	8.8	0.1208	0.00000879
250	9.1	0.1232	0.0000089
300	9.4	0.1256	0.000009
350	9.6	0.1258	0.0000091
400	9.9	0.1281	0.00000919
450	10.1	0.1291	0.00000928
500	10.4	0.1305	0.00000937
550	10.6	0.1306	0.00000945
600	10.9	0.1327	0.00000953
650	11.1	0.1335	0.00000961
700	11.4	0.1348	0.00000969
750	11.6	0.1356	0.00000976
800	11.9	0.1367	0.00000982

Temperature	Young's Modulus
°F	ksi
68	22045.7
302	20160.2
482	18419.8

Temperature	Poisson's Ratio
°F	
0	0.3
1000	0.3

The PWR vessel rollout diagram and corresponding embrittlement information from the RVID database are provided in Figure 2-1 and Table 2-3 respectively.

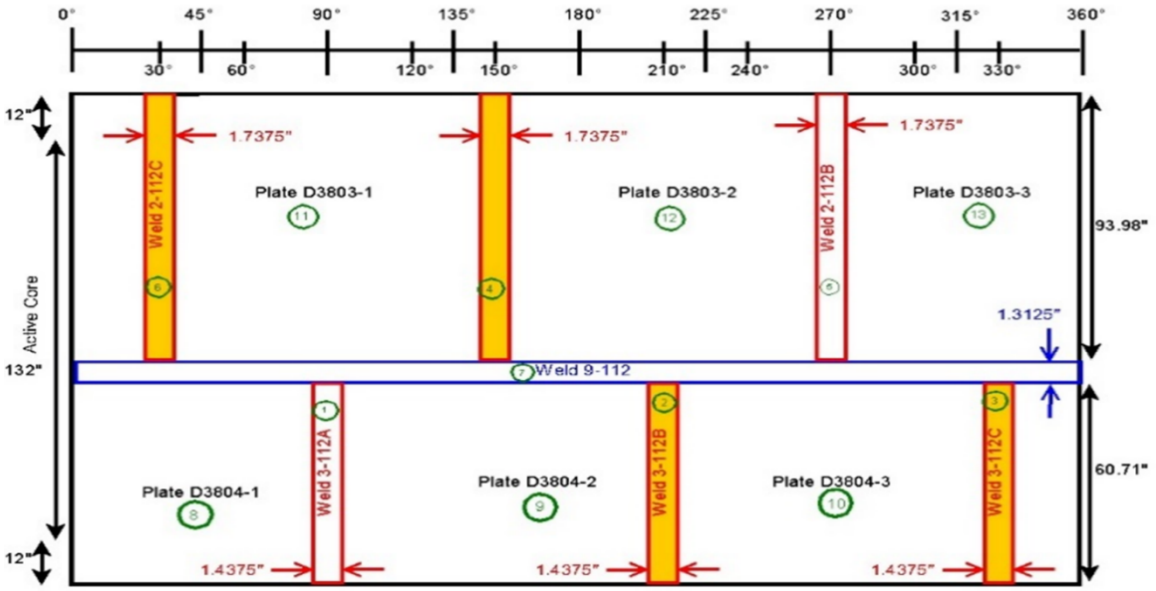

Figure 2-1: PWR Vessel Rollout Diagram

Table 2-3: PWR Vessel Embrittlement Map Information and Corresponding FAVOR Input

Major Region	Description	Heat ID	Plate or Weld ID	%Cu	%Ni	%P	ID RTndt (u) [Initial RTndt]	max neutron fluence @72 EFPY(1) 10^{19} n/cm^2	1/4T RT_{NDT} @ 72 EFPY(2) w/o Margin °F
1	Axial Weld	W5214	LOWER SHELL AXIAL WELDS 3-112A/C	0.213	1.010	0.019	-56.000	2.96	210.7
2	Axial Weld	W5214	LOWER SHELL AXIAL WELDS 3-112A/C	0.213	1.010	0.019	-56.000	3.81	225.9
3	Axial Weld	W5214	LOWER SHELL AXIAL WELDS 3-112A/C	0.213	1.010	0.019	-56.000	3.81	225.9
4	Axial Weld	W5214	INTERMEDIATE SHELL AXIAL WELDS 2-112 A/C	0.213	1.010	0.019	-56.000	3.86	226.6
5	Axial Weld	W5214	INTERMEDIATE SHELL AXIAL WELDS 2-112 A/C	0.213	1.010	0.019	-56.000	2.99	211.3
6	Axial Weld	W5214	INTERMEDIATE SHELL AXIAL WELDS 2-112 A/C	0.213	1.010	0.019	-56.000	3.86	226.6
7	CircWeld	27204	CIRC. WELD 9-112	0.203	1.018	0.013	-56.000	4.85	234.3
8	Plate	C-1308A	D-3804-1	0.190	0.480	0.016	0.000	4.85	164.8
9	Plate	C-1308B	D-3804-2	0.190	0.500	0.015	-30.000	4.85	137.7
10	Plate	B-5294	D-3804-3	0.120	0.550	0.010	-25.000	4.85	79.9
11	Plate	C-1279	D-3803-1	0.240	0.510	0.009	-5.000	4.90	198.9
12	Plate	A-0313	D-3803-2	0.240	0.520	0.010	-30.000	4.90	175.7
13	Plate	C-1279	D-3803-3	0.240	0.500	0.011	-5.000	4.90	197.0

The resulting FAVOR PWR embrittlement map input was as follows:

```
*=================================================================================================================*
*  1    2    3    4       5     6     7     8     9 10 11    12    13 14    15    16    17 18    19    20 *
*****************************************************************************************************************
   1    8    9    1 2.9625 0.213  1.01 0.019     1  1  0   -56    17 11 0.958 60.71   516  1 0.000 0.000
   2    9   10    2 3.8089 0.213  1.01 0.019     1  1  0   -56    17 11 0.958 60.71   516  1 0.000 0.000
   3   10    8    3 3.8089 0.213  1.01 0.019     1  1  0   -56    17 11 0.958 60.71   516  1 0.000 0.000
   4   11   12    4 3.8554 0.213  1.01 0.019     1  1  0   -56    17 11 1.158 93.98   799  1 0.000 0.000
   5   12   13    5 2.9892 0.213  1.01 0.019     1  1  0   -56    17 11 1.158 93.98   799  1 0.000 0.000
   6   13   11    6 3.8554 0.213  1.01 0.019     1  1  0   -56    17 11 1.158 93.98   799  1 0.000 0.000
   7    8   11    7 4.8502 0.203 1.018 0.013     1  2  0   -56    17 11   360  1.31  4833  2 0.000 0.000
   8    8    8    8 4.8456  0.19  0.48 0.016     1  0  0     0    17 21 119.0 60.71 0.000  0 0.000 0.000
   9    9    9    9 4.8456  0.19   0.5 0.015     1  0  0   -30    17 21 119.0 60.71 0.000  0 0.000 0.000
  10   10   10   10 4.8456  0.12  0.55  0.01     1  0  0   -25    17 21 119.0 60.71 0.000  0 0.000 0.000
  11   11   11   11 4.9015  0.24  0.51 0.009     1  0  0    -5    17 21 118.8 93.98 0.000  0 0.000 0.000
  12   12   12   12 4.9015  0.24  0.52  0.01     1  0  0   -30    17 21 118.8 93.98 0.000  0 0.000 0.000
  13   13   13   13 4.9015  0.24   0.5 0.011     1  0  0    -5    17 21 118.8 93.98 0.000  0 0.000 0.000
```

Of note, RG 1.99, Rev. 2 was used to calculate the RT_{NDT} at the 0.25 T location so as to calculate the P-T limit for a 100°F/hour cooldown (last column in Table 2-3). The maximum RT_{NDT} at the 0.25 T location at 72 EFPY was determined to be 234.3°F, which is the value that was used for the P-T limit calculation.

2.1.2 Transient Definitions

2.1.2.1 PT100-100: 100°F/Hour Cooldown at Maximum Allowed Pressure for 100°F/hour Cooldown

In order to determine the allowable pressure for the P-T limit cooldown at a rate of 100°F/hour, ASME Section XI, Appendix G, Paragraph G-2215 [6] was used. The risk-informed alternative was NOT used. Assuming the limiting case of an axial flaw and a wall thickness between 4 and 12 inches, the allowable pressure is given by:

$$P = \frac{K_{Ic} - K_{It}}{2M_m}\left(t/R_i\right)$$

with

$$K_{Ic} = 33.2 + 20.734\ exp[0.02(T - RT_{NDT})]$$

and

$$M_m = 0.926\sqrt{t}$$

In order to determine the applied stress intensity factor due to thermal stresses (K_{It}), FAVOR was used to simulate a 100°F/hour cooldown from 550°F to 70°F with no applied pressure, and using a stress free temperature of 550°F (such that the initial thermal stresses are zero). The resulting K calculated by FAVOR for a 0.25 T flaw and an aspect ratio of 6 was used to determine the allowable pressure using the equation above. The value of crack tip RT_{NDT} used was 234.3°F, as described in 2.1.1.

The resulting P-T limit transient for a 100°F/hour cooldown from 550°F to 70°F is shown in Figure 2-2. This transient is referred to as the 'PT100-100' transient in this document, and its frequency of occurrence is 6×10^{-6} events per year (based on the BTP 5-3 closure memo assessment [7]).

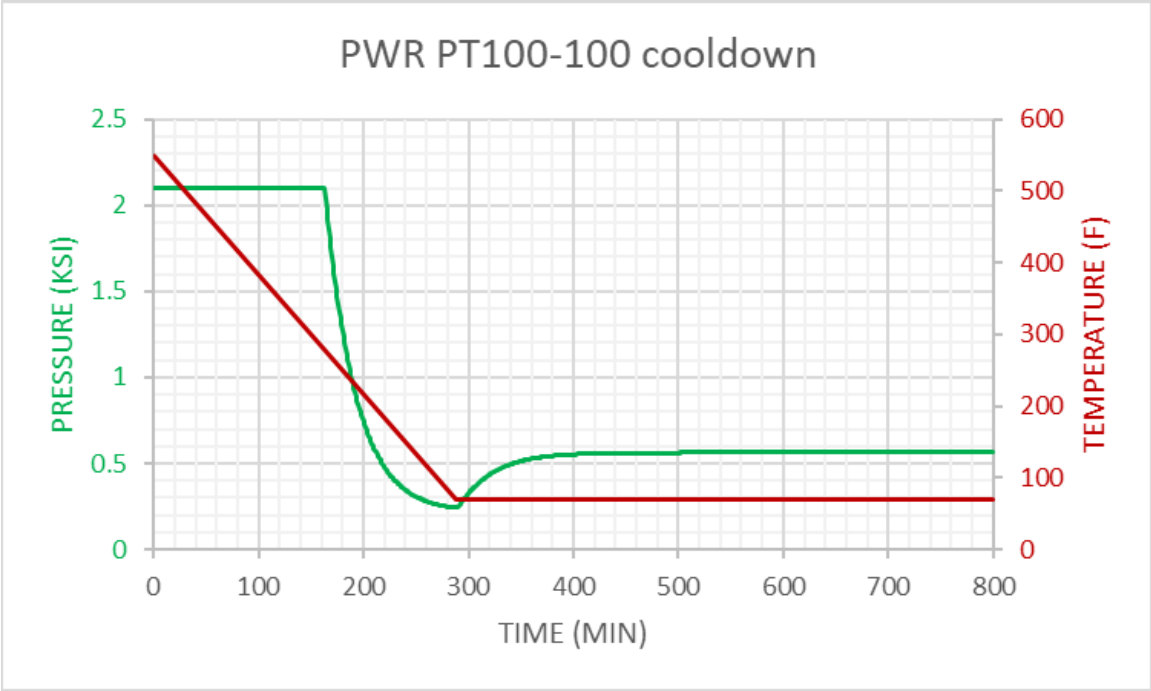

Figure 2-2: PWR PT100-100 Cooldown Transient Characteristics

2.1.2.2 PT50-50: 50°F/Hour Cooldown at Maximum Allowed Pressure for 50°F/hour Cooldown

In order to determine the allowable pressure for the P-T limit cooldown at a rate of 50°F/hour, ASME Section XI, Appendix G, Paragraph G-2215 [6] was used. The risk-informed alternative was NOT used. Assuming the limiting case of an axial flaw and a wall thickness between 4 and 12 inches, the allowable pressure is given by:

$$P = \frac{K_{Ic} - K_{It}}{2M_m}\left({}^{t}/_{R_i}\right)$$

with

$$K_{Ic} = 33.2 + 20.734\ exp[0.02(T - RT_{NDT})]$$

and

$$M_m = 0.926\sqrt{t}$$

In order to determine the applied stress intensity factor due to thermal stresses (K_{It}), FAVOR was used to simulate a 50°F/hour cooldown from 550°F to 70°F with no applied pressure, and using a stress free temperature of 550°F (such that the initial thermal stresses are zero). The resulting K calculated by FAVOR for a 0.25 T flaw and an aspect ratio of 6 was used to determine the allowable pressure using the equation above. The value of crack tip RT_{NDT} used was 234.3°F, as described in 2.1.1.

The resulting P-T limit transient for a 50°F/hour cooldown from 550°F to 70°F is shown in Figure 2-3. This transient is referred to as the 'PT50-50' transient in this document, and its frequency of occurrence is estimated at 6×10^{-6} events per year (based on the BTP 5-3 closure memo assessment [7]).

Figure 2-3: PWR PT50-50 Cooldown Transient Characteristics

2.1.2.3 PT100-50: 50°F/Hour Cooldown at Maximum Allowed Pressure for 100°F/hour Cooldown

The P-T limit pressure history based on a 100°F/hour cooldown (see section 2.1.2.1) was used along with a 50°F/hour cooldown temperature history. The pressure history was essentially the same as for the PT100-100 cooldown, except between ~450 minutes and ~650 minutes, where the pressure was reduced to match the PT limits for a 50°F/hour cooldown. The resulting transient for a 50°F/hour cooldown from 550°F to 70°F is shown in Figure 2-4. This transient is referred to as the 'PT100-50' transient in this document, and its frequency of occurrence is estimated at 6×10^{-6} events per year (based on the BTP 5-3 closure memo assessment [7]).

Figure 2-4: PWR PT100-50 Cooldown Transient Characteristics

2.1.2.4 C50P: 50th Percentile (Median) of Actual Cooldown Transients

A combined 42 actual normal operation plant cooldown histories were obtained from 17 different PWRs. These cooldown histories were analyzed to determine the pressure and temperature histories corresponding to various percentiles of the pressure and temperature history distributions based on the population considered.

It is important to note that no information was available regarding how representative these transients are of actual PWR fleet operations. These transients were simply those that were made available to NRC by Westinghouse in 2013 through an informal exchange of data, and they may or may not be statistically representative of normal PWR cooldowns. Nonetheless, they all appeared to represent successfully terminated cooldowns, and were treated as such.

Figure 2-5 and Figure 2-7 respectively show the actual 42 temperature and pressure histories obtained for a total of 17 different PWRs. Figure 2-6 and Figure 2-8 respectively show the temperature and pressure histories corresponding to various percentiles of the distribution of the temperature and pressure histories. Figure 2-9 and Figure 2-10 show the P-T curves for the actual plant cooldowns as well as the P-T histories corresponding to various percentiles of the population studied. The values of pressure and temperature corresponding to the various percentiles were calculated at each time step based on the distribution of the data for the 42 transients analyzed. The 50th percentile (median) histories are highlighted in bold red lines. Importantly, the time is given here in hours instead of minutes.

When comparing the actual cooldowns with the three P-T limit cooldowns studied (PT100-100, PT100-50, and PT50-50), the actual cooldown transients generally occur over a much longer period of time. Looking at the median histories (50th percentile), the cooldown rate is roughly ~50°F/hour from 550°F to 350°F, then ~20°F/hour from 350°F to 200°F, then ~2.5°F/hour from 200°F to 100°F. The corresponding pressure reduction rate is roughly 400psig/hour to 500psig/hour for the first 4 hours, such that in 4 to 5 hours, the pressure is reduced to about 350psig, then the pressure is maintained at ~350psig until the temperature reaches ~100°F, then rapidly dropped to zero (0psig).

The analysis results for the 50th percentile of actual cooldown transients are presented in Section2.3.4. This transient is referred to as the '50th percentile cooldown' or 'C50P' transient in this document, and its frequency of occurrence is estimated at 1.0 events per year (based on the BTP 5-3 closure memo assessment [7]).

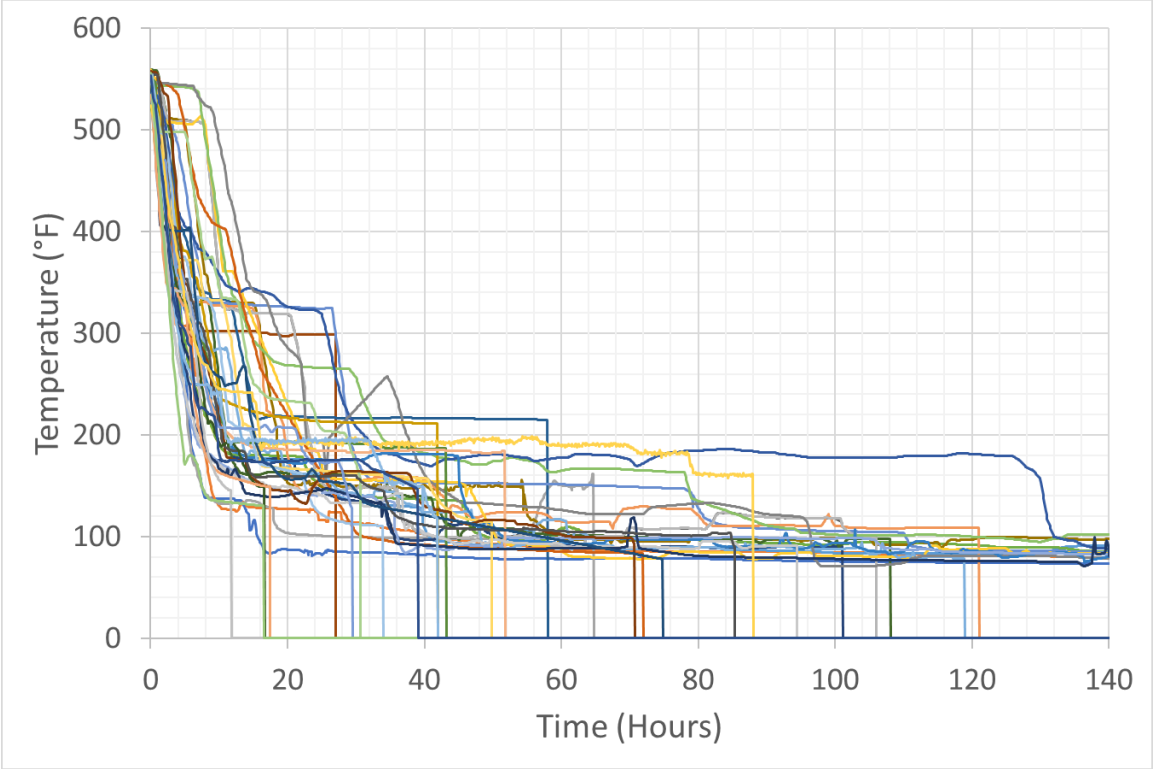

Figure 2-5: Temperature histories for 42 PWR cooldown transients

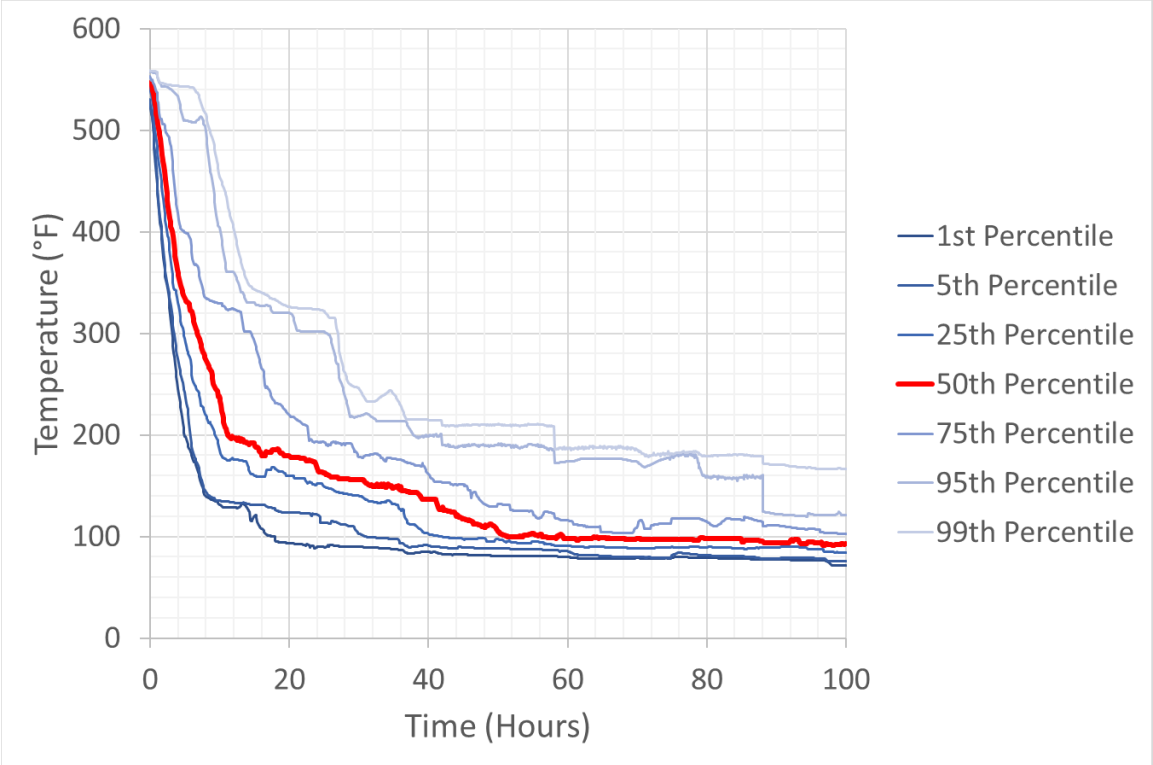

Figure 2-6: Temperature histories corresponding to various percentiles of the population of PWR cooldowns considered

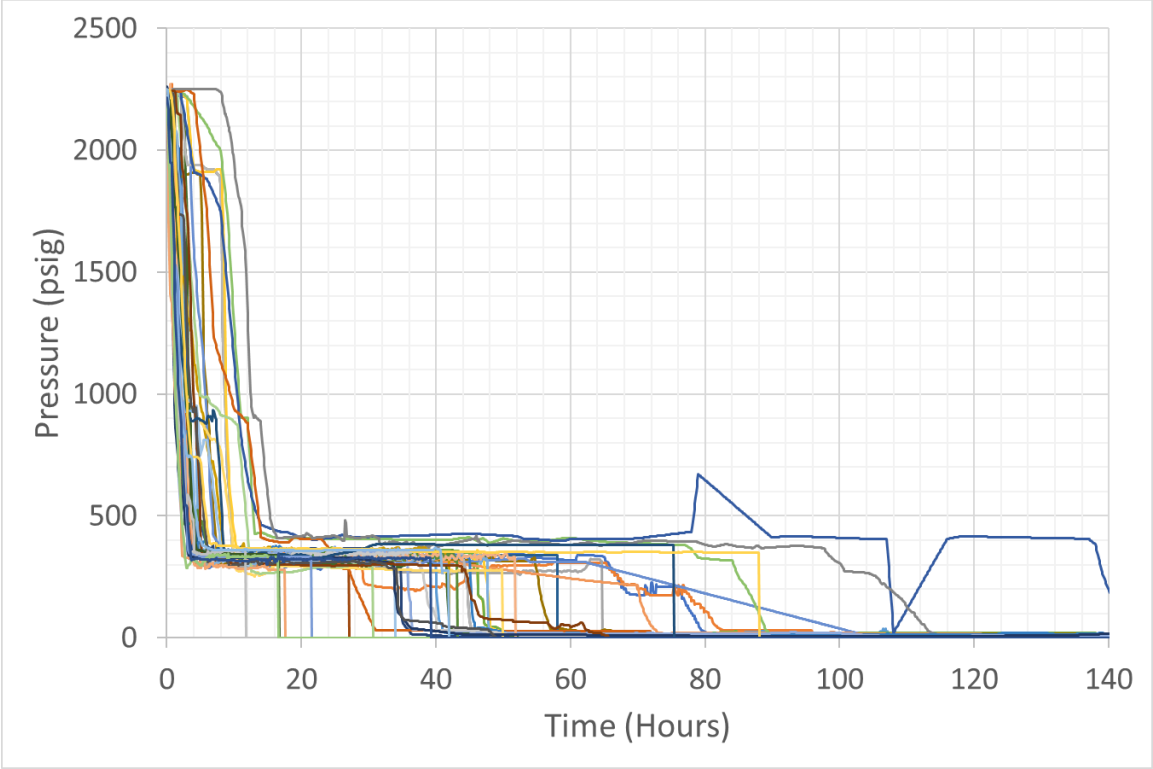

Figure 2-7: Pressure histories for 42 PWR cooldown transients

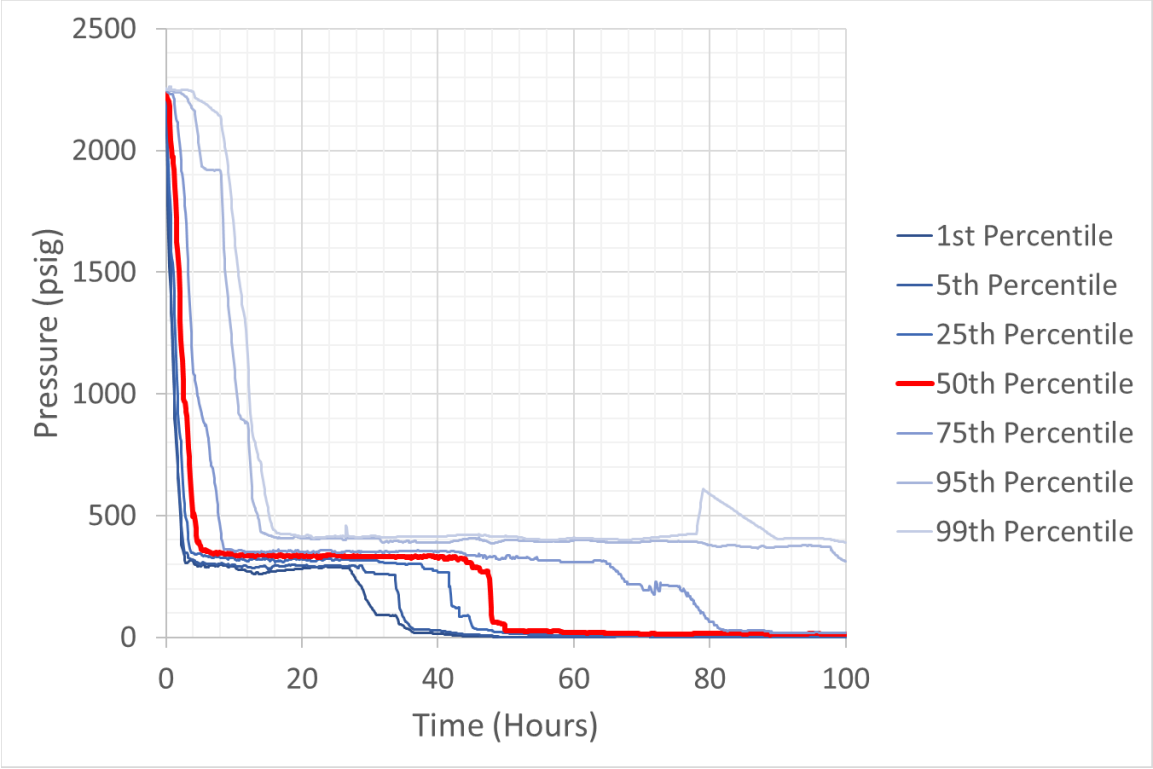

Figure 2-8: Pressure histories corresponding to various percentiles of the population of PWR cooldowns considered

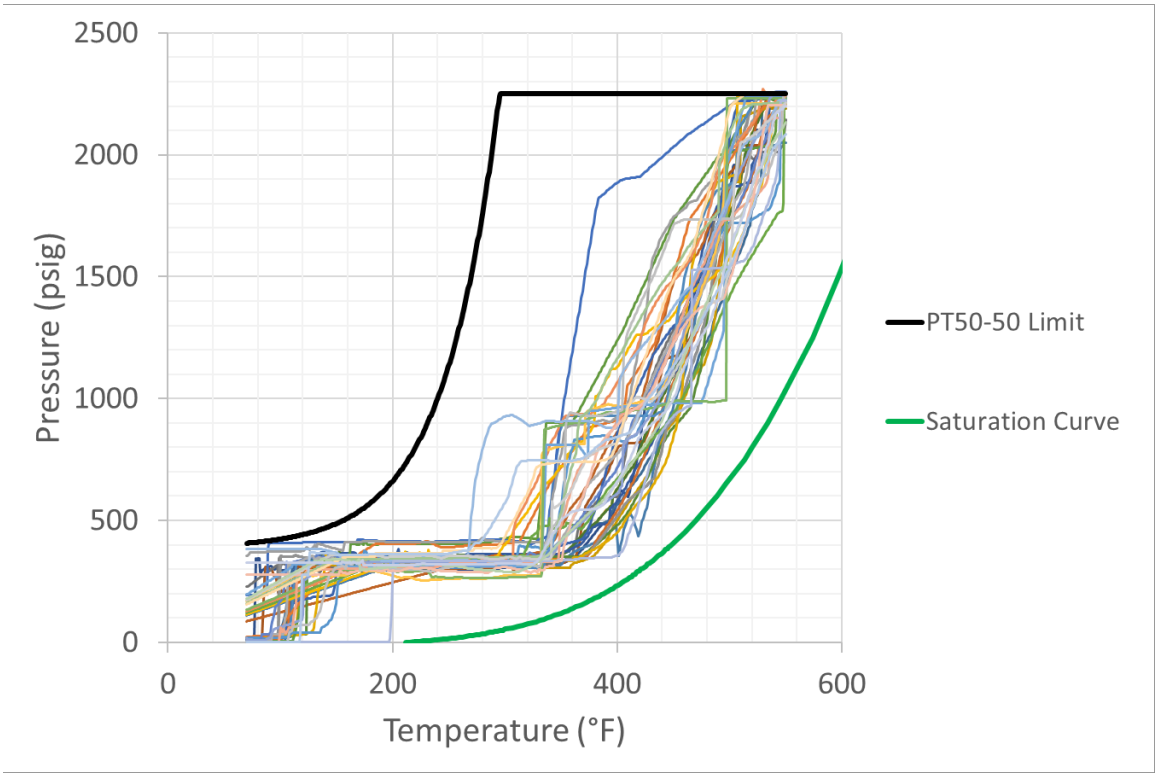

Figure 2-9: P-T histories for 42 PWR cooldown transients

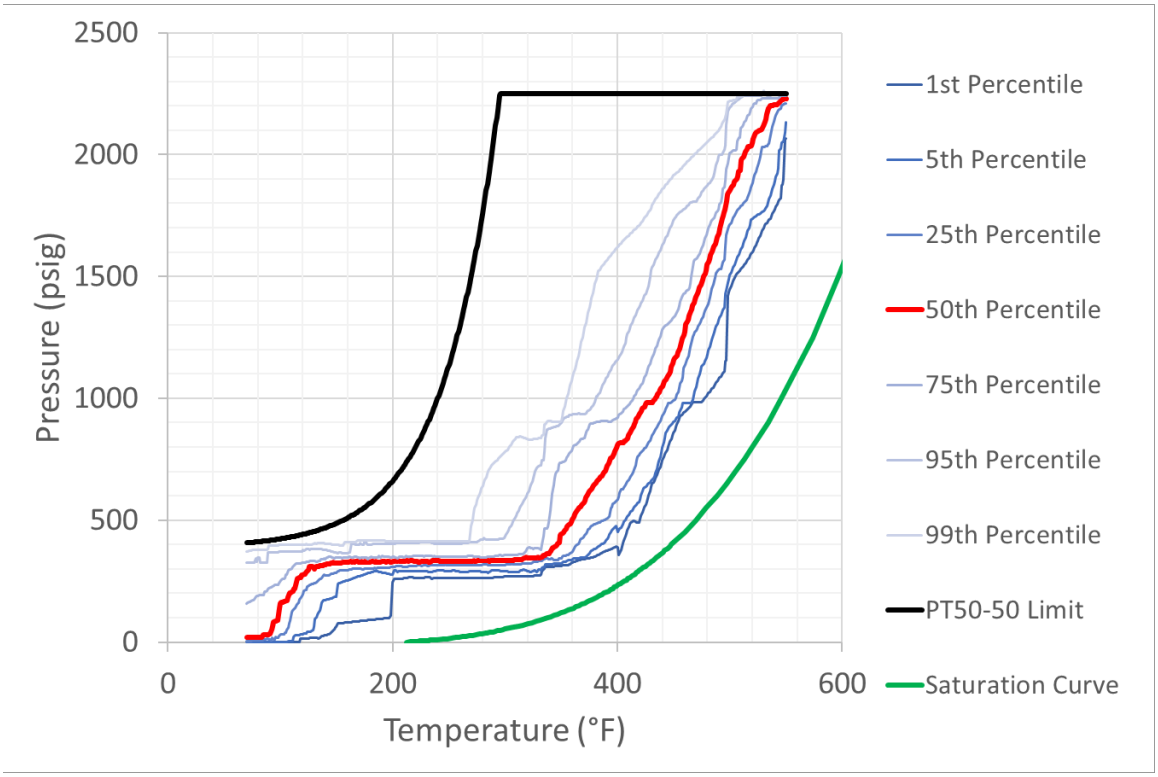

Figure 2-10: P-T histories corresponding to various percentiles of the population of PWR cooldowns considered

2.1.2.5 PWR Transient PT Curves

Figure 2-11 shows the PT curves for the 4 cooldown transients modeled for the PWR RT_{NDT} shift sensitivity studies. Overall, the PT100-100 and PT50-50 transients are similar on a PT curve, and one would thus expect relatively similar trends for stress intensity factor histories, as can be seen by comparing Figure 2-14 with Figure 2-20 and Figure 2-17 with Figure 2-23. Furthermore, based on the relative positions of the PT curves, one would expect that for a ¼ T flaw (which is the postulated flaw for the creation of PT curves), the CPI and CPF values for the transients shown would be ranked as follows from highest to lowest: PT50-50, PT100-100, PT100-50, and finally C50P. This is indeed generally the trend for ¼ T flaws, as described in Section 2.3. However, for shallow flaws, the trends are different, and the PT curves are not a good indication of the relative values of CPI and CPF for the cooldown transients.

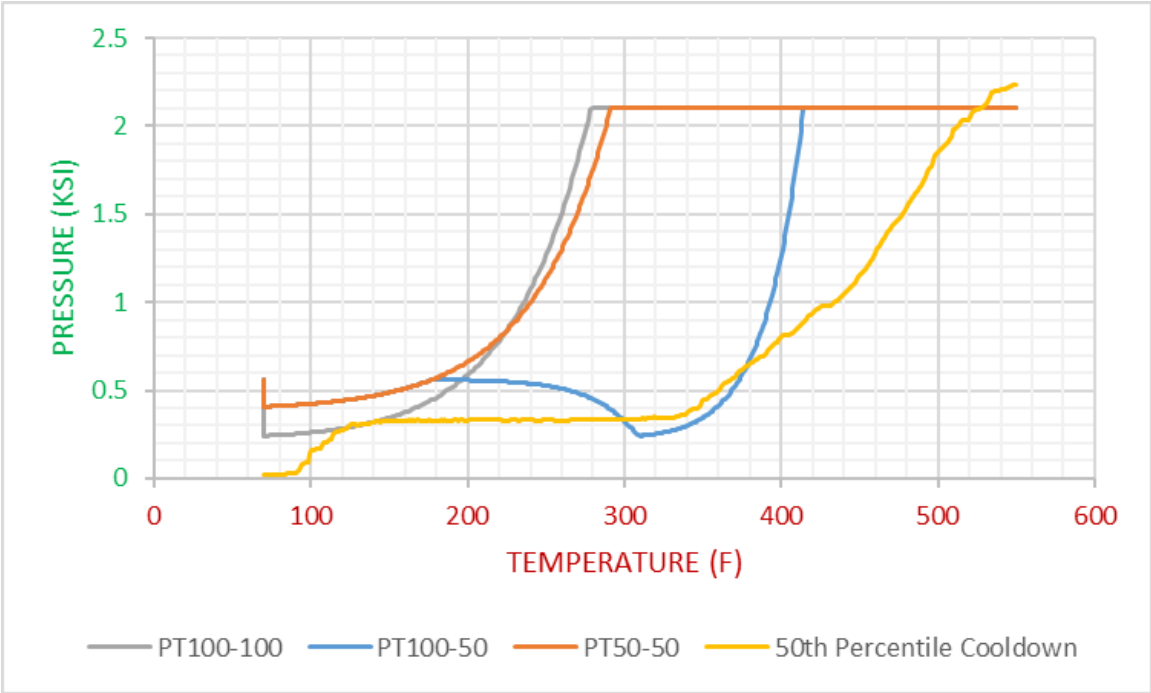

Figure 2-11: PT curves for the 4 PWR cooldown transients modeled for the RT_{NDT} shift sensitivity studies

2.1.3 Other FAVOR Simulation Input Information

In addition to the vessel and transient information, the following FAVOR simulation inputs were used:

Simulation Parameters	
Irradiation shift correlation choice	Regulatory Guide 1.99 Rev. 2
Normal operating coolant temperature	550°F
Plant operating time	72 EFPY
Ductile tearing model in IGA submodel	off
Ductile tearing initiation checks and reporting	off
Additional reports on CPI/CPF for major beltline regions	off
Flow stress for net-section plastic collapse failure model	80 ksi
Maximum value for K_{Ic} or K_{Ia}	200 ksi$\sqrt{in}$
Crack arrest model	High-constraint K_{Ia} (CCA specimens)
Resampling when advancing into new weld layer	on
Normalized crack depth corresponding to vessel failure	0.9

Fluence Sampling	
Multiplier for standard deviation of mean local fluence	0.118
Multiplier for standard deviation of local fluence	0.056

Weld Chemistry Sampling	
Standard deviation for Copper sampling in welds	0.167 wt%
Standard deviation for Nickel sampling in welds	0.162 wt%
Standard deviation for Phosphorus sampling in welds	0.0013 wt%

Plate Chemistry Sampling	
Standard deviation for Copper sampling in plates	0.0073 wt%
Standard deviation for Nickel sampling in plates	0.0244 wt%
Standard deviation for Phosphorus sampling in plates	0.0013 wt%

To produce FAVOR runs corresponding to a single ID surface flaw of depth 0.25 T and aspect ratio 6, the VFLAW input format was used to specify the flaw population as follows:

- The surface flaw density was set to result in a single flaw of depth 0.25 T and aspect ratio 6, with zeros everywhere else
- The embedded weld flaw density was set to zero for all flaw depths and aspect ratios
- The embedded plate flaw density was set to zero for all flaw depths and aspect ratios

To produce FAVOR runs corresponding to a single ID surface flaw of depth 0.03 T and aspect ratio 6, the VFLAW input format was used to specify the flaw population as follows:

- The surface flaw density was set to result in a single flaw of depth 0.03 T and aspect ratio 6, with zeros everywhere else
- The embedded weld flaw density was set to zero for all flaw depths and aspect ratios
- The embedded plate flaw density was set to zero for all flaw depths and aspect ratios

2.2 RT_{NDT} Shift Distribution

In order to simulate the effects of changing the embrittlement correlation from RG 1.99, Rev. 2 to E900-15 without changing the FAVOR code, the initial RT_{NDT} value was changed via input to the FAVOR embrittlement map. The RT_{NDT} shift amount was defined as follows:

$$RT_{NDT}^{SHIFT} = \Delta RT_{NDT}^{RG-1.99r2 \rightarrow E900}(72\ EFPY) = \Delta RT_{NDT}^{E900}(72\ EFPY) - \Delta RT_{NDT}^{RG-1.99r2}(72\ EFPY)$$

Furthermore, the adjusted reference temperature (ART) as a result of using the E900-15 embrittlement correlation is defined by:

$$ART(72\ EFPY) = RT_{NDT}^{0} + \Delta RT_{NDT}^{E900}(72\ EFPY)$$

leading to:

$$ART(72\ EFPY) = RT_{NDT}^{0} + RT_{NDT}^{SHIFT} + \Delta RT_{NDT}^{RG-1.99r2}(72\ EFPY)$$

By shifting the initial RT_{NDT} by $\mathrm{RT}_{\mathrm{NDT}}^{\mathrm{SHIFT}}$, FAVOR can thus simulate the effects of changing the embrittlement correlation from RG 1.99, Rev. 2 to E900-15 while still using the RG 1.99, Rev. 2 embrittlement correlation, and thus without needing to change the FAVOR code.

A compilation of $\mathrm{RT}_{\mathrm{NDT}}^{\mathrm{SHIFT}}$ values for the entire PWR fleet, based on all the available embrittlement capsule data, was performed as part of the RG 1.99, Rev. 2 update effort. Figure 2-12 shows the distribution of RT_{NDT}^{SHIFT} values across the US PWR fleet considering this large set of embrittlement information, and Table 2-4 shows the values of RT_{NDT}^{SHIFT} corresponding to key percentiles (and vice versa).

Figure 2-12 and Table 2-4 show that when considering all available capsule data for PWRs at 72 EFPY, changing the embrittlement correlation from RG 1.99, Rev. 2 to E900-15 would increase the adjusted reference temperature in most cases, since a 0°F shift (i.e. no shift) corresponds to the 23rd percentile for RT_{NDT}^{SHIFT}. Furthermore, the RT_{NDT}^{SHIFT} distribution is quite large, such that the median is 40°F and the upper 99th percentile is 193°F, which represents a very large shift.

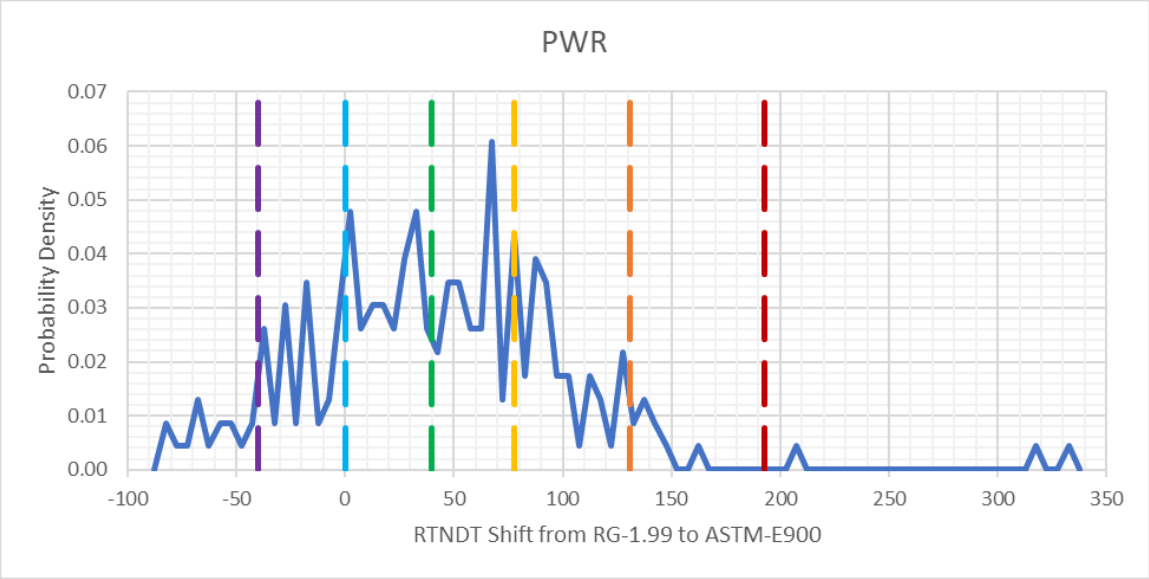

Figure 2-12: Probability Distribution of the PWR RT_{NDT} Shift as a Result of the Change from RG 1.99, Rev. 2 to E900-15 Embrittlement Correlations (all capsule data)

Table 2-4: PWR RT_{NDT} Shift as a Result of the Change from RG 1.99, Rev. 2 to E900-15 Embrittlement Correlations at Percentiles of Interest for this Study (all capsule data)

Percentiles	RT_{NDT} Shift from RG 1.99, Rev. 2 to E900-15
0.01	-74
0.05	-49
0.07	**-40**
0.1	-30
0.23	**0**
0.25	2
0.5	**40**
0.75	**78**
0.9	112
0.95	**131**
0.99	**193**

It is important to point out that considering all available capsule does not provide the most accurate picture of the actual material embrittlement in the US fleet, because some capsules pulled early in the reactor life and for which data has been extrapolated can result in large errors in the actual embrittlement of reactor materials. A more accurate method may consist of filtering the capsule data to only keep the fluence capsule data for the longest actual irradiation time for each reactor in the fleet, as shown in Figure 2-13 and Table 2-5. This reduces extrapolation error and results in a far more accurate picture of the material embrittlement for the vessels in the US fleet.

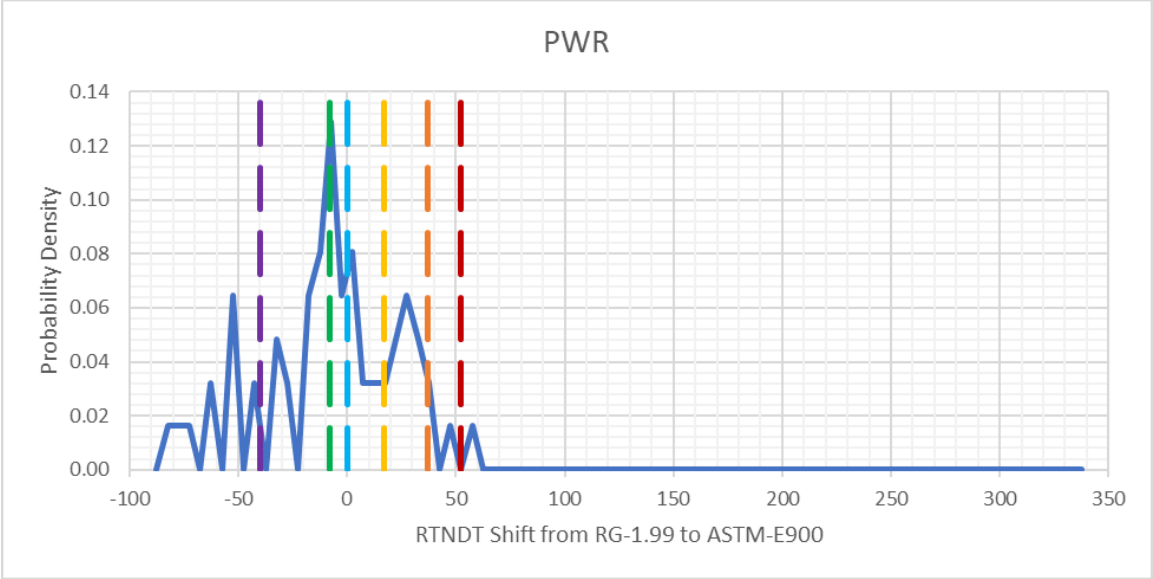

Figure 2-13: Probability Distribution of the PWR RT_{NDT} Shift as a Result of the Change from RG 1.99, Rev. 2 to E900-15 Embrittlement Correlations (filtered capsule data)

Table 2-5: PWR RT_{NDT} Shift as a Result of the Change from RG 1.99, Rev. 2 to E900-15 Embrittlement Correlations at Percentiles of Interest for this Study (filtered capsule data)

Percentiles	RT_{NDT} Shift from RG 1.99, Rev. 2 to E900-15
0.01	-86
0.05	-64
0.16	**-40**
0.1	-53
0.25	-24
0.5	**-8**
0.6	**0**
0.75	**17**
0.9	31
0.95	**37**
0.99	**52**

Figure 2-5 and Table 2-12 show that when considering only the highest fluence capsule for each reactor, the RT_{NDT}^{SHIFT} distribution is much narrower and the 99th percentile is only a little over 50°F.

2.3 Results

Probabilistic FAVOR runs were performed for the highlighted RT_{NDT}^{SHIFT} values from Table 2-4. The values chosen were -40°F, 0°F, followed by the 50th, 75th, 95th, and 99th percentile values, so as to cover the wide range of possible RT_{NDT}^{SHIFT} values (see Section 2.2). This section presents results for a PWR vessel containing a single flaw of aspect ratio equal to 6 and depths of 0.25 T and 0.03 T, for the transients described in section 2.1.2.

2.3.1 PT100-100 Cooldown

2.3.1.1 ¼-T Flaw Results

The stress intensity factor history for a 0.25 T ID surface flaw subjected to the PT100-100 cooldown transient described in 2.1.2.1 is shown in Figure 2-14 for flaws with aspect ratios of 2, 6, 10 and infinity. The arrest toughness K_{Ia}, below which no crack growth initiation can occur, as well as the median fracture toughness K_{Ic}, are also shown. It is important to note that all probabilistic analyses were performed with a flaw of aspect ratio equal to 6. Figure 2-14 clearly shows that K increases initially while the pressure is held constant and the temperature decreases linearly at a rate of 100°F/hour, reaching a maximum between 140 and 160 minutes. Then, at 164 minutes, the sudden pressure drop is accompanied by a sudden drop in K values. The rate of decrease in K is initially high but diminishes as time goes by. Finally, at 288 minutes, when the temperature reaches 70°F and remains constant, the rate of decrease in K values accelerates and creates an inflection point in the K versus time curves. After this inflection point, the rate of decrease in K values slowly diminishes until the end of the calculation.

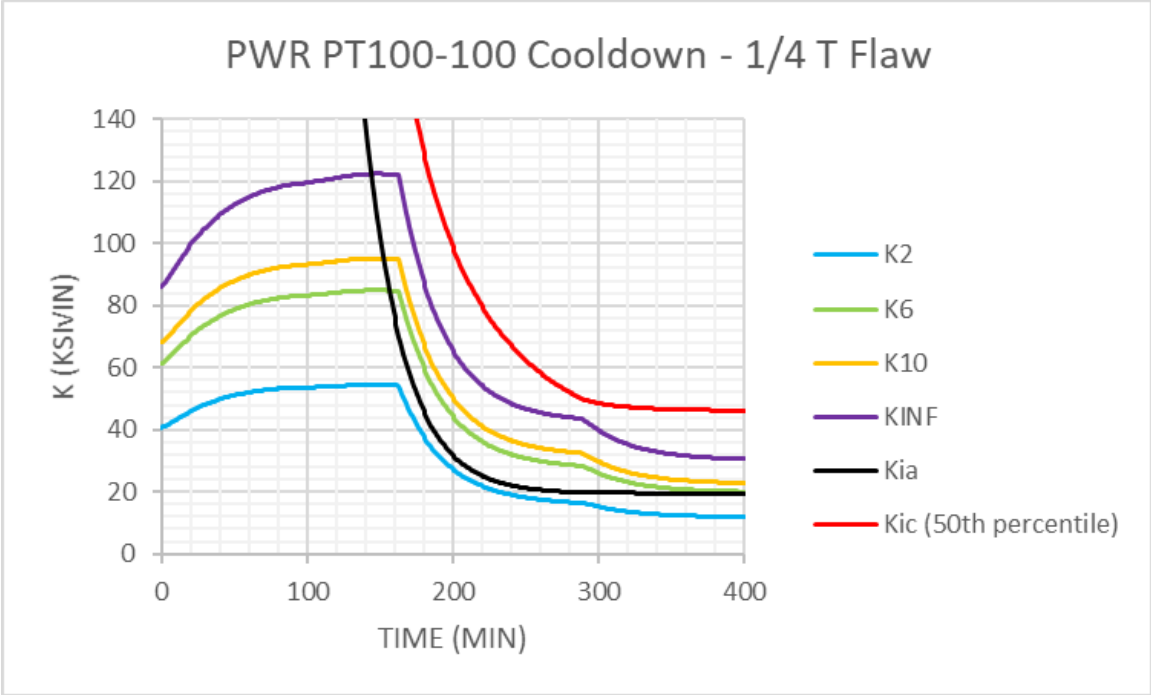

Figure 2-14: Stress Intensity Factor for the PWR PT100-100 Cooldown for a 0.25 T Flaw for Flaw Aspect Ratios of 2, 6, 10 and Infinity (note: in the legend, Kia is K_{Ia} and Kic is K_{Ic})

A probabilistic calculation assuming a 0.25 T flaw of aspect ratio equal to 6 and the PT100-100 cooldown resulted in a CPI of 9.4E-07 and a CPF of 6.2E-08 using the RG 1.99, Rev. 2 embrittlement correlation. This case corresponds to 0°F RT_{NDT} shift (i.e. 'no shift') for this transient. Figure 2-15 shows the calculated CPI and CPF as a function of the number of RPV trials in FAVOR for this reference case, and one can see that the FAVOR calculations are statistically converged after about 80,000 trials. Similar plots were generated for all the runs performed in this study, so as to assess statistical convergence of the results.

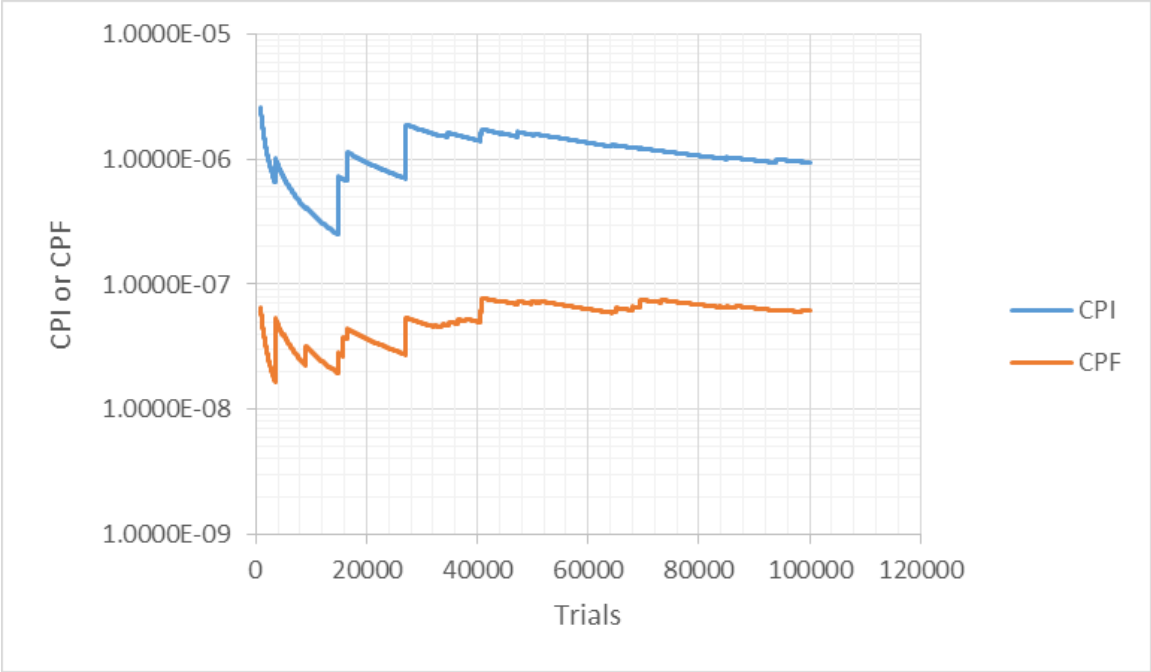

Figure 2-15: CPI and CPF versus Number of Trials for a 0.25 T Flaw in a PWR with 0°F RT_{NDT} Shift for the PT100-100 cooldown

The same PT100-100 cooldown determined using the RG 1.99, Rev. 2 embrittlement correlation (shown in Figure 2-2) was modeled for different values of RT_{NDT}^{SHIFT}, so as to understand the impact of shifting the RT_{NDT} for this transient. Of course, in actual safety analyses, the P-T limit would be adjusted as a function of the maximum ART in the vessel being analyzed, so a higher ART would reduce the allowed pressure, which In turn would result in lower CPI and CPF than presented here for cases where RT_{NDT}^{SHIFT} is greater than 0°F.

Table 2-6 and Figure 2-16 show the results of the probabilistic analyses for the 0.25 T flaw for the PT100-100 cooldown, as a function of RT_{NDT}^{SHIFT}. As expected, the CPI and CPF increase as RT_{NDT}^{SHIFT} increases. It should be noted that the analysis for $RT_{NDT}^{SHIFT} = -40°F$ did not statistically converge because of the very low calculated probabilities, but the CPI and CPF trend over the number of trials was beginning to stabilize, so the results are believed to be in the correct order of magnitude.

Table 2-6: Calculated CPI and CPF for a 0.25 T Flaw of Aspect Ratio 6 in a PWR Subjected to the PT100-100 Cooldown

RTNDT Shift (°F)	CPI	CPI Converged?	CPF	CPF Converged?	TWCF
-40	6.0759E-09	NO	9.4160E-12	NO	5.6496E-17
0	9.4399E-07	YES	6.2145E-08	YES	3.7287E-13
40	3.4276E-05	YES	1.9320E-05	YES	1.1592E-10
78	6.7942E-04	YES	5.8762E-04	YES	3.5257E-09
131	1.1926E-02	YES	1.1499E-02	YES	6.8994E-08
193	9.1868E-02	YES	9.0872E-02	YES	5.4523E-07

Figure 2-16: CPI and CPF for a 0.25 T Flaw of Aspect Ratio 6 in a PWR Subjected to the PT100-100 Cooldown, as a Function of RT_{NDT} Shift from RG 1.99, Rev. 2 to E900-15 Embrittlement Correlations (open symbols linked by dashed lines represent results that are not statistically converged)

2.3.1.2 Shallow Flaw Results

The stress intensity factor history for a 0.03 T ID surface flaw subjected to the PT100-100 cooldown transient described in 2.1.2.1 is shown in Figure 2-17 for flaws with aspect ratios of 2, 6, 10 and infinity. The arrest toughness K_{Ia}, below which no crack growth initiation can occur, as well as the median fracture toughness K_{Ic}, are also shown. Figure 2-17 clearly shows that K increases initially while the pressure is held constant and the temperature decreases linearly at a rate of 100°F/hour. The maximum K values are reached at 163 minutes, just before the sudden pressure drop that results in a sudden drop in K values. During the subsequent pressure and temperature decrease, the K values reach a minimum sometime between 230 and 240 minutes, and then increase again between 240 minutes and 288 minutes, when a second peak is observed. This second peak is characteristic of shallow surface flaws that barely penetrate the base metal because these cracks are highly affected by the stresses due to the mismatch in thermal expansion coefficient between the cladding and the base metal. After 288 minutes, the temperature is held constant at 70°F, and thus the thermal stresses and associated component of K decrease rapidly, hence there is a decrease in overall K values despite the increase in pressure.

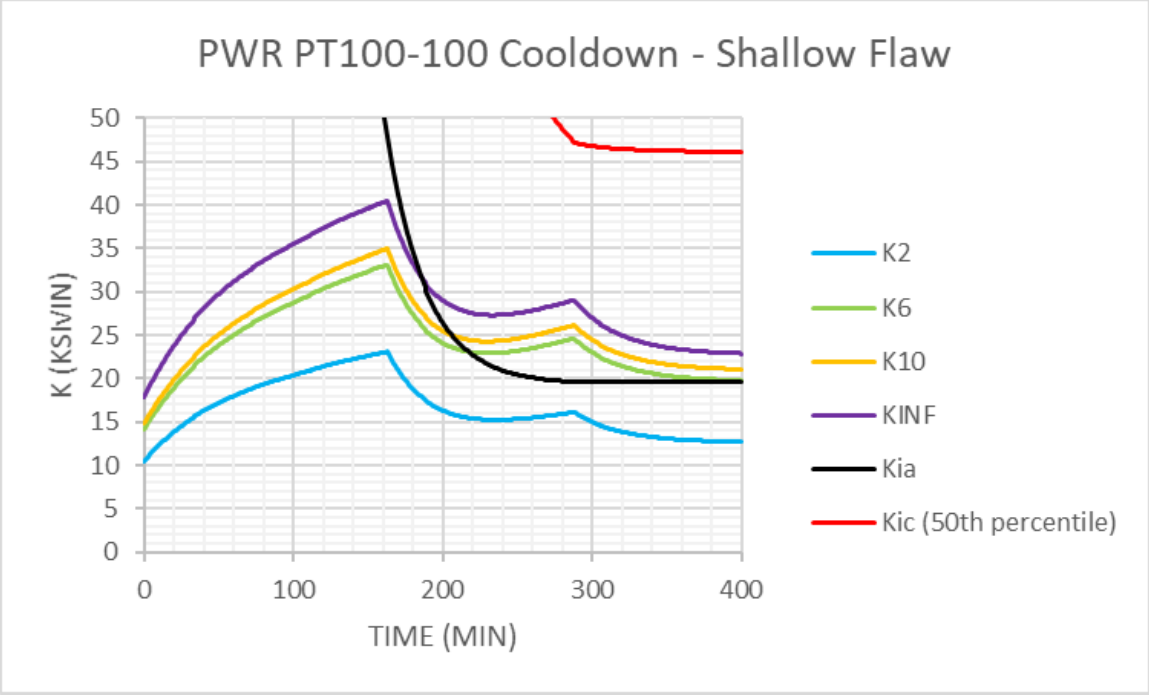

Figure 2-17: Stress Intensity Factor for the PWR PT100-100 Cooldown for a 0.03 T Flaw for Flaw Aspect Ratios of 2, 6, 10 and Infinity (note: in the legend, Kia is K_{Ia} and Kic is K_{Ic})

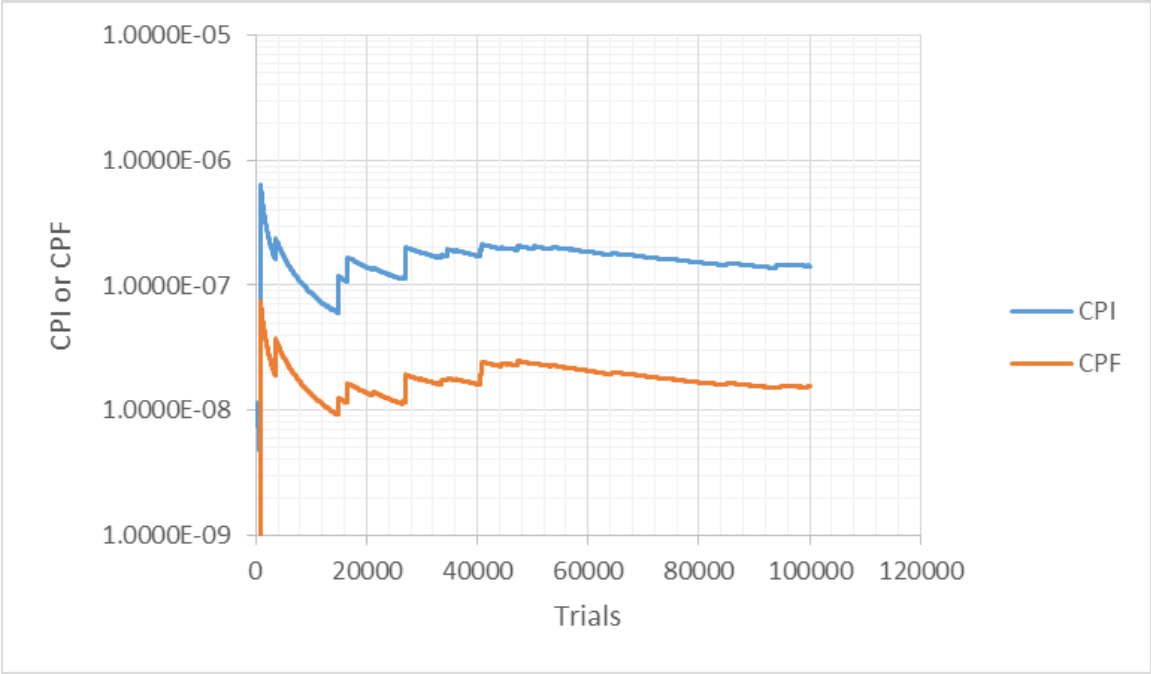

Figure 2-18: CPI and CPF versus Number of Trials for a 0.03 T Flaw in a PWR with 0°F RT_{NDT} Shift for the PT100-100 cooldown

A probabilistic calculation assuming a 0.03 T flaw of aspect ratio equal to 6 and the PT100-100 cooldown resulted in a CPI of 1.4E-07 and a CPF of 1.6E-08 using the RG 1.99, Rev. 2 embrittlement correlation. This case corresponds to 0°F RT_{NDT} shift (i.e. 'no shift') for this transient. Figure 2-18 shows the calculated CPI and CPF as a function of the number of RPV trials in FAVOR, and one can see that the FAVOR calculations are statistically converged after about 80,000 trials. Similar plots were generated for all the runs performed in this study, so as to assess statistical convergence of the results.

The same PT100-100 cooldown determined using the RG 1.99, Rev. 2 embrittlement correlation for a 0.25 T flaw (shown in Figure 2-2) was modeled for different values of RT_{NDT}^{SHIFT}, so as to understand the impact of shifting the RT_{NDT} for this transient. That is, a new P-T limit was not calculated for a 0.03 T shallow flaw, but was instead calculated using current practice based on ASME Section XI, Appendix G, which requires analysis based on a 0.25 T flaw. Furthermore, as for the 0.25 T case, in actual safety analyses, the P-T limit would be adjusted as a function of the maximum ART in the vessel being analyzed, which would result in a different CPI and CPF than presented here. If the P-T limit was recalculated for each RT_{NDT}^{SHIFT} value, the shallow flaw effect makes it difficult to predict a priori whether the CPI and CPF values would move up or down.

Table 2-7 and Figure 2-19 show the results of the probabilistic analyses for the 0.03 T flaw for the PT100-100 cooldown, as a function of RT_{NDT}^{SHIFT}. As expected, the CPI and CPF increase as RT_{NDT}^{SHIFT} increases. It should be noted that the analysis for $RT_{NDT}^{SHIFT} = -40°F$ did not statistically converge because of the very low calculated probabilities, but the CPI and CPF trend over the number of trials was beginning to stabilize, so the results are believed to be in the correct order of magnitude.

Table 2-7: Calculated CPI and CPF for a 0.03 T Flaw of Aspect Ratio 6 in a PWR Subjected to the PT100-100 Cooldown

RTNDT Shift (°F)	CPI	CPI Converged?	CPF	CPF Converged?	TWCF
-40	5.2829E-09	NO	1.1418E-10	NO	6.8508E-16
0	1.4259E-07	YES	1.5513E-08	YES	9.3078E-14
40	1.4816E-06	YES	4.6824E-07	YES	2.8094E-12
78	9.3457E-06	YES	5.5843E-06	YES	3.3506E-11
131	7.9849E-05	YES	6.9312E-05	YES	4.1587E-10
193	4.7912E-04	YES	4.6376E-04	YES	2.7826E-09

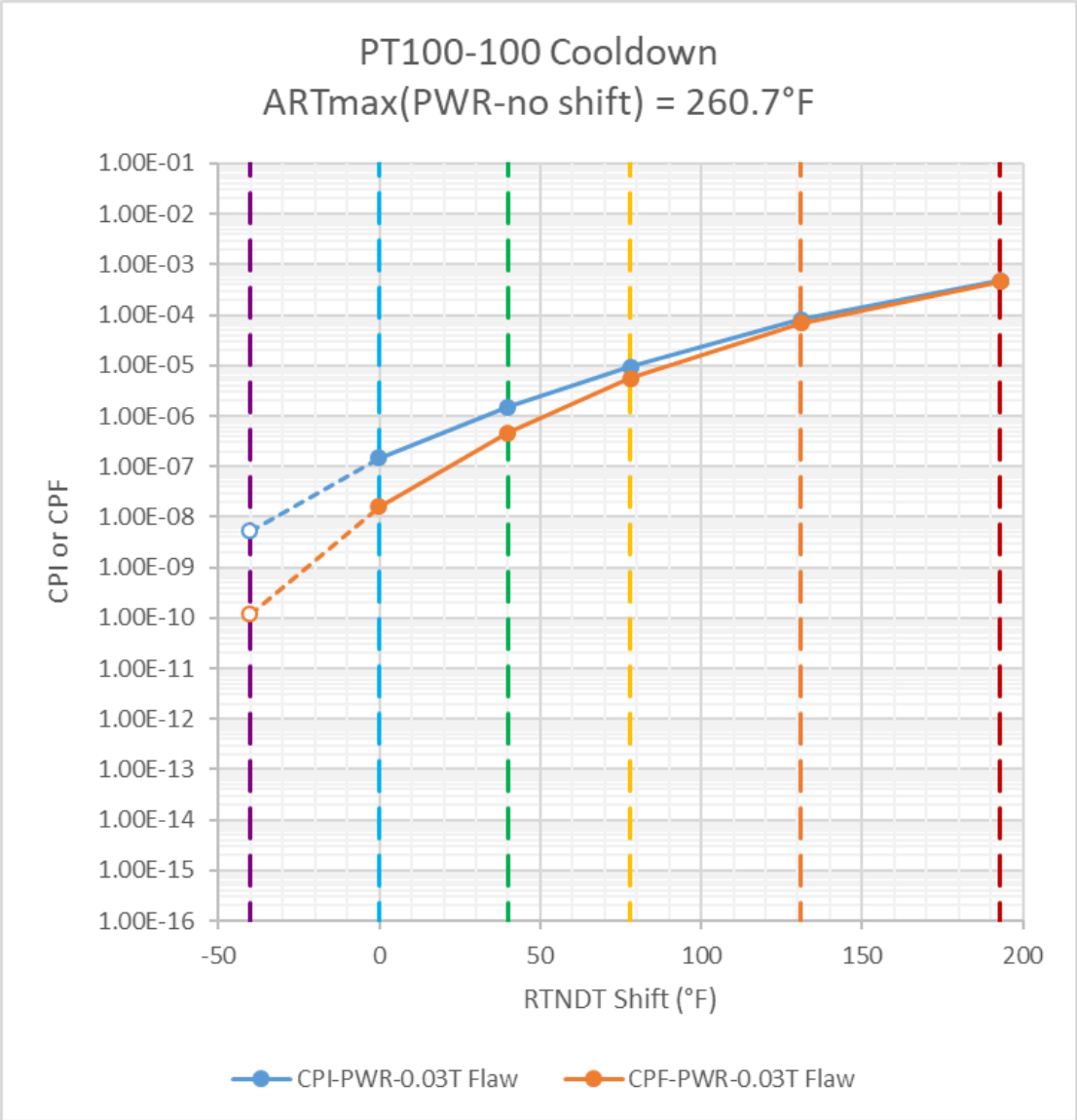

Figure 2-19: CPI and CPF for a 0.03 T Flaw of Aspect Ratio 6 in a PWR Subjected to the PT100-100 Cooldown, as a Function of RT_{NDT} Shift from RG 1.99, Rev. 2 to E900-15 Embrittlement Correlations (open symbols linked by dashed lines represent results that are not statistically converged)

2.3.2 PT50-50 Cooldown

2.3.2.1 ¼-T Flaw Results

The stress intensity factor history for a 0.25 T ID surface flaw subjected to the PT50-50 cooldown transient described in 2.1.2.2 is shown in Figure 2-20 for flaws with aspect ratios of 2, 6, 10 and infinity. The arrest toughness K_{Ia}, below which no crack growth initiation can occur, as well as the median fracture toughness K_{Ic}, are also shown. It is important to note that all probabilistic analyses were performed with a flaw of aspect ratio equal to 6. Figure 2-20 clearly shows that K increases initially while the pressure is held constant and the temperature decreases linearly at a rate of 50°F/hour, reaching a maximum between 300 and 320 minutes. Then, at 310 minutes, the sudden pressure drop is accompanied by a sudden drop in K values. The rate of decrease in K is initially high but diminishes as time goes by. Finally, at 576 minutes, when the temperature reaches 70°F and remains constant, the rate of decrease in K values accelerates and creates an inflection point in the K versus time curves. After this inflection point, the rate of decrease in K values slowly diminishes until the end of the calculation.

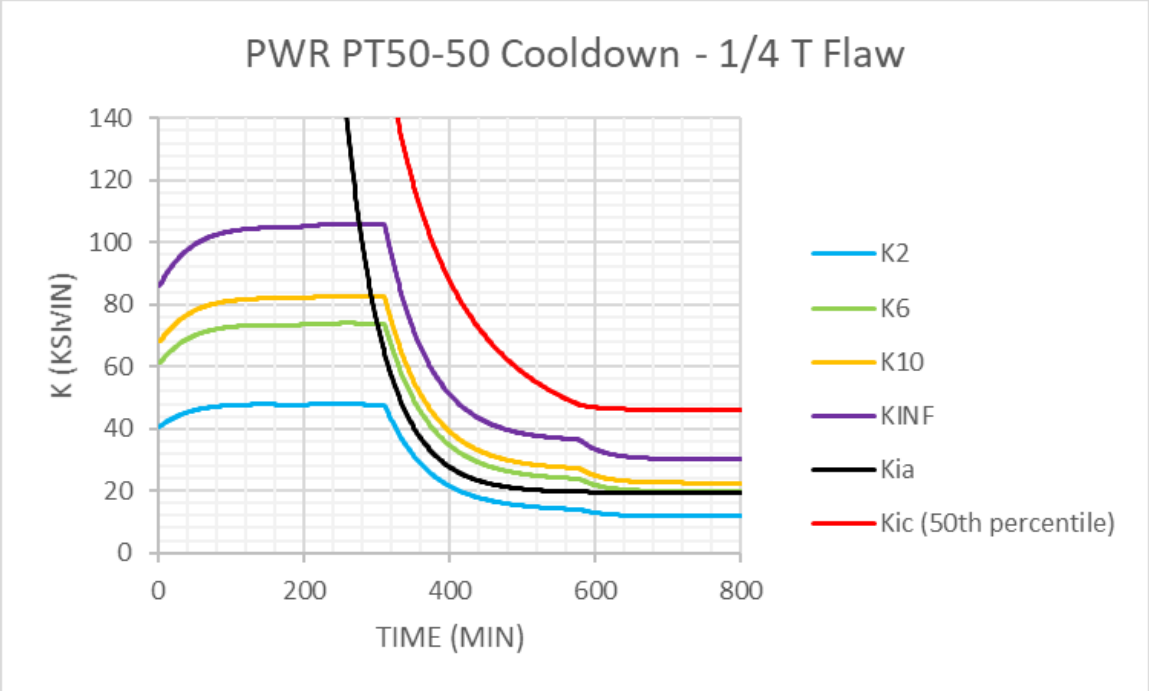

Figure 2-20: Stress Intensity Factor for the PWR PT50-50 Cooldown for a 0.25 T Flaw for Flaw Aspect Ratios of 2, 6, 10 and Infinity (note: in the legend, Kia is K_{Ia} and Kic is K_{Ic})

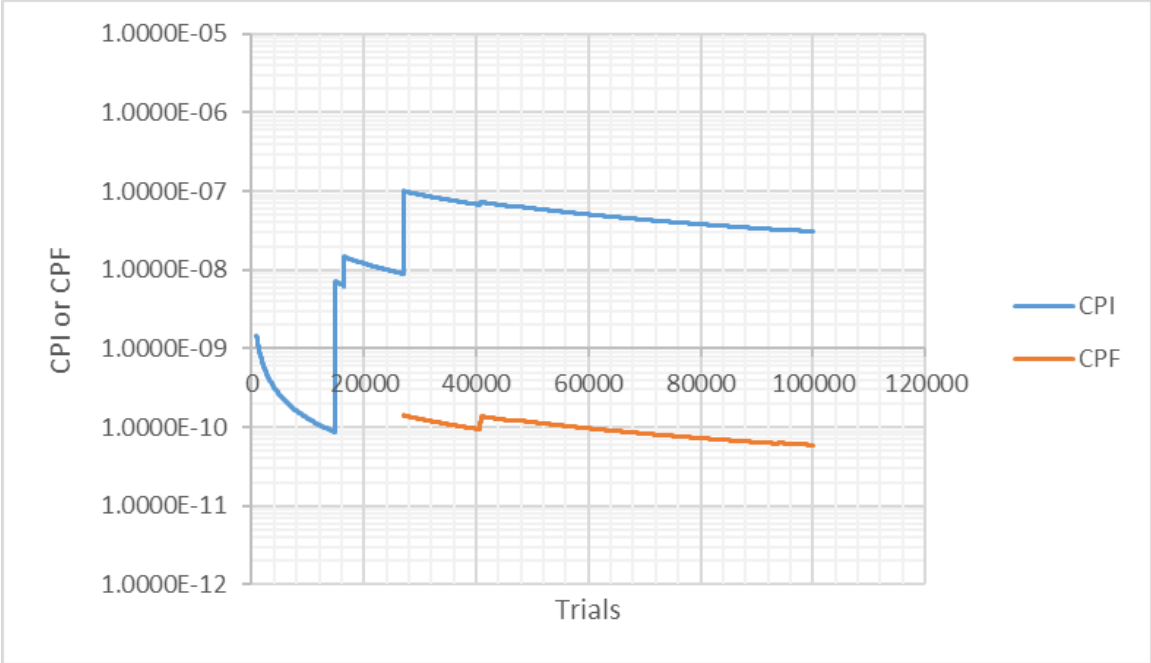

Figure 2-21: CPI and CPF versus Number of Trials for a 0.25 T Flaw in a PWR with 0°F RT_{NDT} Shift for the PT50-50 cooldown

A probabilistic calculation assuming a 0.25 T flaw of aspect ratio equal to 6 and the PT50-50 cooldown resulted in a CPI of 3.1E-08 and a CPF of 5.9E-11 using the RG 1.99, Rev. 2 embrittlement correlation. This case corresponds to 0°F RT_{NDT} shift (i.e. 'no shift') for this transient. Figure 2-21 shows the calculated CPI and CPF as a function of the number of RPV trials in FAVOR, and one can see that the FAVOR calculations are not quite statistically converged after 100,000 trials. However, the order of magnitude of CPI and CPF is believed to be sufficiently accurate for the purposes of this study. Similar plots were generated for all the runs performed in this study, so as to assess statistical convergence of the results.

The same PT50-50 cooldown (shown in Figure 2-3) was modeled for different values of RT_{NDT}^{SHIFT}, so as to understand the impact of shifting the RT_{NDT} for this transient. Of course, in actual safety analyses, the P-T limit would be adjusted as a function of the maximum ART in the vessel being analyzed, so a higher ART would reduce the allowed pressure, which In turn would result in lower CPI and CPF than presented here for cases where RT_{NDT}^{SHIFT} is greater than 0°F.

Table 2-8 and Figure 2-22 show the results of the probabilistic analyses for the 0.25 T flaw for the PT50-50 cooldown, as a function of RT_{NDT}^{SHIFT}. As expected, the CPI and CPF increase as RT_{NDT}^{SHIFT} increases. It should be noted that the analysis for $RT_{NDT}^{SHIFT} < 0°F$ resulted in CPI and CPF predictions equal to zero. Furthermore, for $RT_{NDT}^{SHIFT} = 0°F$, the CPF and the CPI did not statistically converge because of the very low calculated probability, but the CPI and CPF trend over the number of trials was beginning to stabilize, so the results are believed to be in the correct order of magnitude.

Table 2-8: Calculated CPI and CPF for a 0.25 T Flaw of Aspect Ratio 6 in a PWR Subjected to the PT50-50 Cooldown

RTNDT Shift (°F)	CPI	CPI Converged?	CPF	CPF Converged?	TWCF
-40	0.0000E+00	YES	0.0000E+00	YES	0.0000E+00
0	3.0806E-08	NO	5.9409E-11	NO	3.5645E-16
40	1.7008E-06	YES	2.3462E-07	YES	1.4077E-12
78	3.9427E-05	NO	2.3607E-05	YES	1.4164E-10
131	1.2837E-03	YES	1.1396E-03	YES	6.8376E-09
193	1.6079E-02	YES	1.5494E-02	YES	9.2964E-08

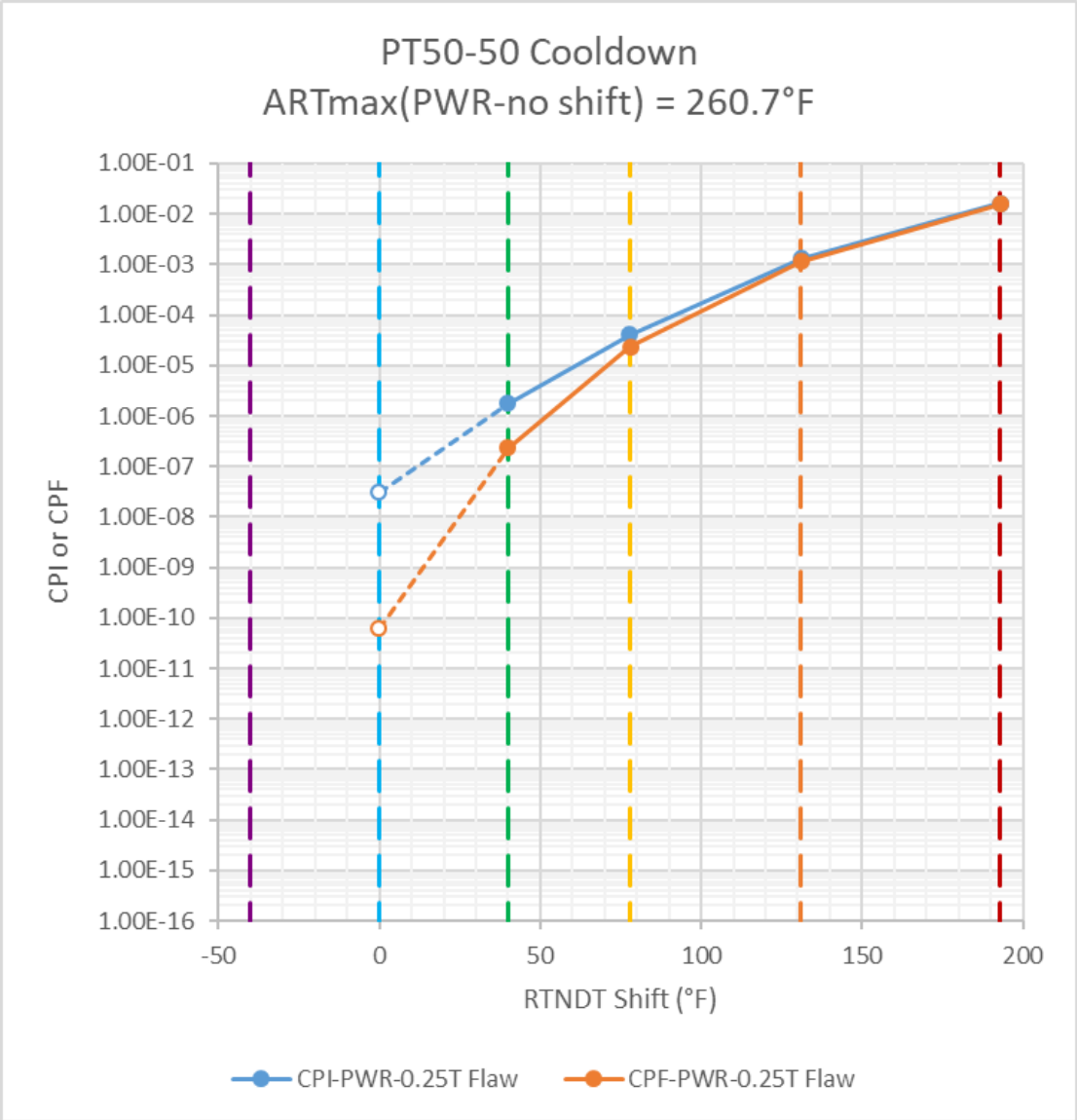

Figure 2-22: CPI and CPF for a 0.25 T Flaw of Aspect Ratio 6 in a PWR Subjected to the PT50-50 Cooldown, as a Function of RT_{NDT} Shift from RG 1.99, Rev. 2 to E900-15 Embrittlement Correlations (open symbols linked by dashed lines represent results that are not statistically converged)

2.3.2.2 Shallow Flaw Results

The stress intensity factor history for a 0.03 T ID surface flaw subjected to the PT50-50 transient described in 2.1.2.2 is shown in Figure 2-23 for flaws with aspect ratios of 2, 6, 10 and infinity. The arrest toughness K_{Ia}, below which no crack growth initiation can occur, as well as the median fracture toughness K_{Ic}, are also shown. Figure 2-23 clearly shows that K increases initially while the pressure is held constant and the temperature decreases linearly at a rate of 50°F/hour. The maximum K values are reached at 310 minutes, just before the sudden pressure drop that results in a sudden drop in K values. During the subsequent temperature and temperature decrease (with pressure going down to about 400psi), the K values reach a minimum sometime between 430 and 450 minutes, and then increase again between 450 minutes and 576 minutes, when a second peak is observed at 576 minutes. This second peak is characteristic of shallow surface flaws that barely penetrate the base metal because these cracks are highly affected by the stresses due to the mismatch in thermal expansion coefficient between the cladding and the base metal. After 576 minutes, the temperature is held constant at 70°F, and thus the thermal stresses and associated component of K decrease rapidly, hence there is a decrease in overall K values despite the pressure coming back up to stabilize around 575psi.

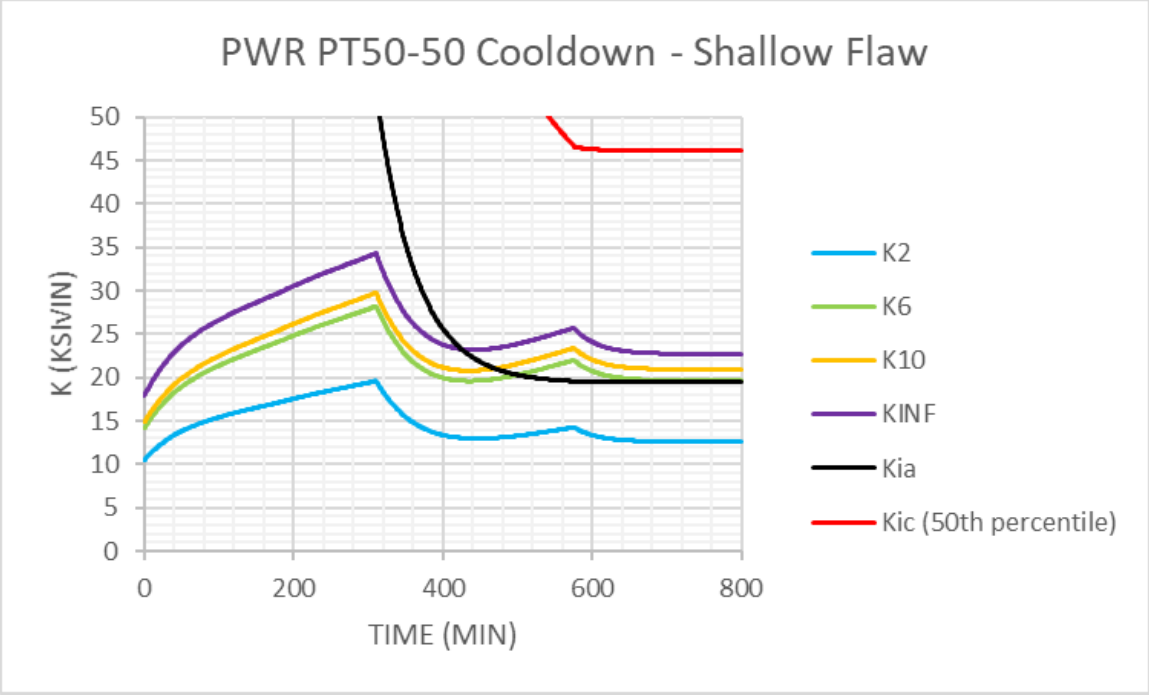

Figure 2-23: Stress Intensity Factor for the PWR PT50-50 Cooldown for a 0.03 T Flaw for Flaw Aspect Ratios of 2, 6, 10 and Infinity (note: in the legend, Kia is K_{Ia} and Kic is K_{Ic})

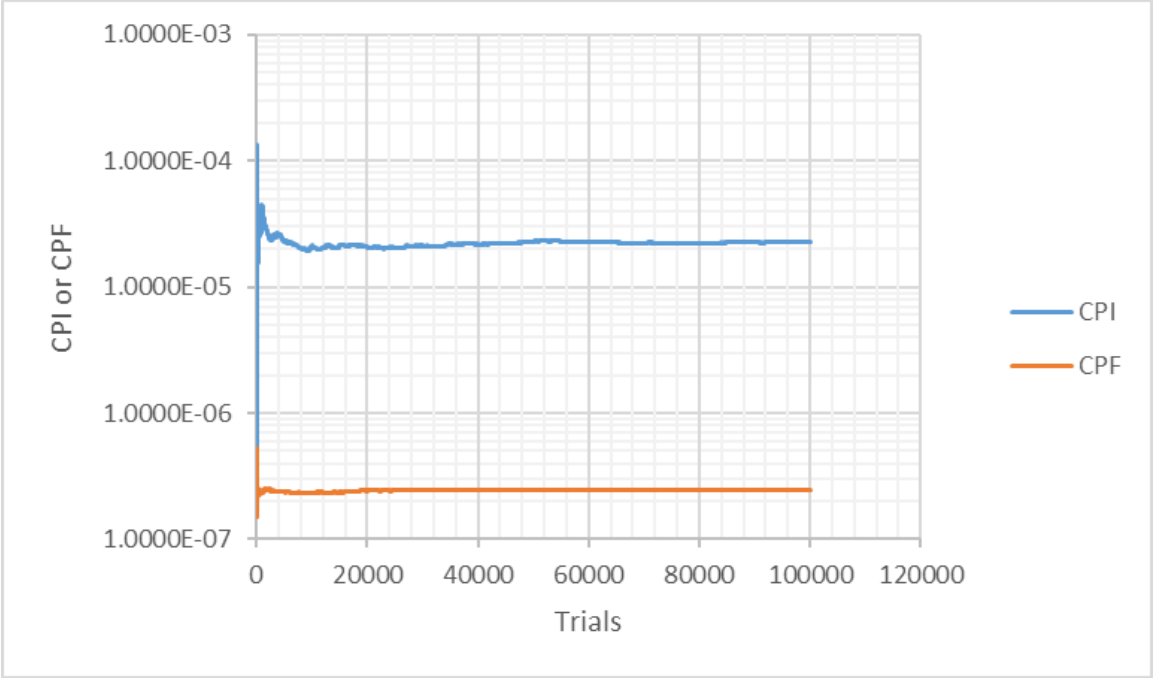

Figure 2-24: CPI and CPF versus Number of Trials for a 0.03 T Flaw in a PWR with 0°F RT_{NDT} Shift for the PT50-50 cooldown

A probabilistic calculation assuming a 0.03 T flaw of aspect ratio equal to 6 and the PT50-50 cooldown resulted in a CPI of 2.3E-05 and a CPF of 2.4E-07 using the RG 1.99, Rev. 2 embrittlement correlation. This case corresponds to 0°F RT_{NDT} shift (i.e. 'no shift') for this transient. Figure 2-24 shows the calculated CPI and CPF as a function of the number of RPV trials in FAVOR, and one can see that the FAVOR calculations are statistically converged after about 20,000 trials. Similar plots were generated for all the runs performed in this study, so as to assess statistical convergence of the results.

The same PT50-50 cooldown (shown in Figure 2-3) was modeled for different values of RT_{NDT}^{SHIFT}, so as to understand the impact of shifting the RT_{NDT} for this transient. That is, a new P-T limit was not calculated for a 0.03 T shallow flaw, but was instead calculated using current practice based on ASME Section XI, Appendix G, which requires analysis based on a 0.25 T flaw. Furthermore, as for the 0.25 T case, in actual safety analyses, the P-T limit would be adjusted as a function of the maximum ART in the vessel being analyzed, which would result in a different CPI and CPF than presented here. If the P-T limit was recalculated for each RT_{NDT}^{SHIFT} value, the shallow flaw effect makes it difficult to predict a priori whether the CPI and CPF values would move up or down.

Table 2-9 and Figure 2-25 show the results of the probabilistic analyses for the 0.03 T flaw for the PT50-50 cooldown, as a function of RT_{NDT}^{SHIFT}. As expected, the CPI and CPF increase as RT_{NDT}^{SHIFT} increases. Because of the relatively high CPI and CPF values calculated and the relatively large (100,000) number of runs, all calculated conditional probabilities achieved statistical convergence.

Table 2-9: Calculated CPI and CPF for a 0.03 T Flaw of Aspect Ratio 6 in a PWR Subjected to the PT50-50 Cooldown

RTNDT Shift (°F)	CPI	CPI Converged?	CPF	CPF Converged?	TWCF
-40	1.0140E-05	YES	3.4793E-08	YES	2.0876E-13
0	2.2891E-05	YES	2.4388E-07	YES	1.4633E-12
40	4.3563E-05	YES	9.0718E-07	YES	5.4431E-12
78	7.1213E-05	YES	2.3264E-06	YES	1.3958E-11
131	1.2150E-04	YES	7.5567E-06	YES	4.5340E-11
193	1.9106E-04	YES	2.8034E-05	YES	1.6820E-10

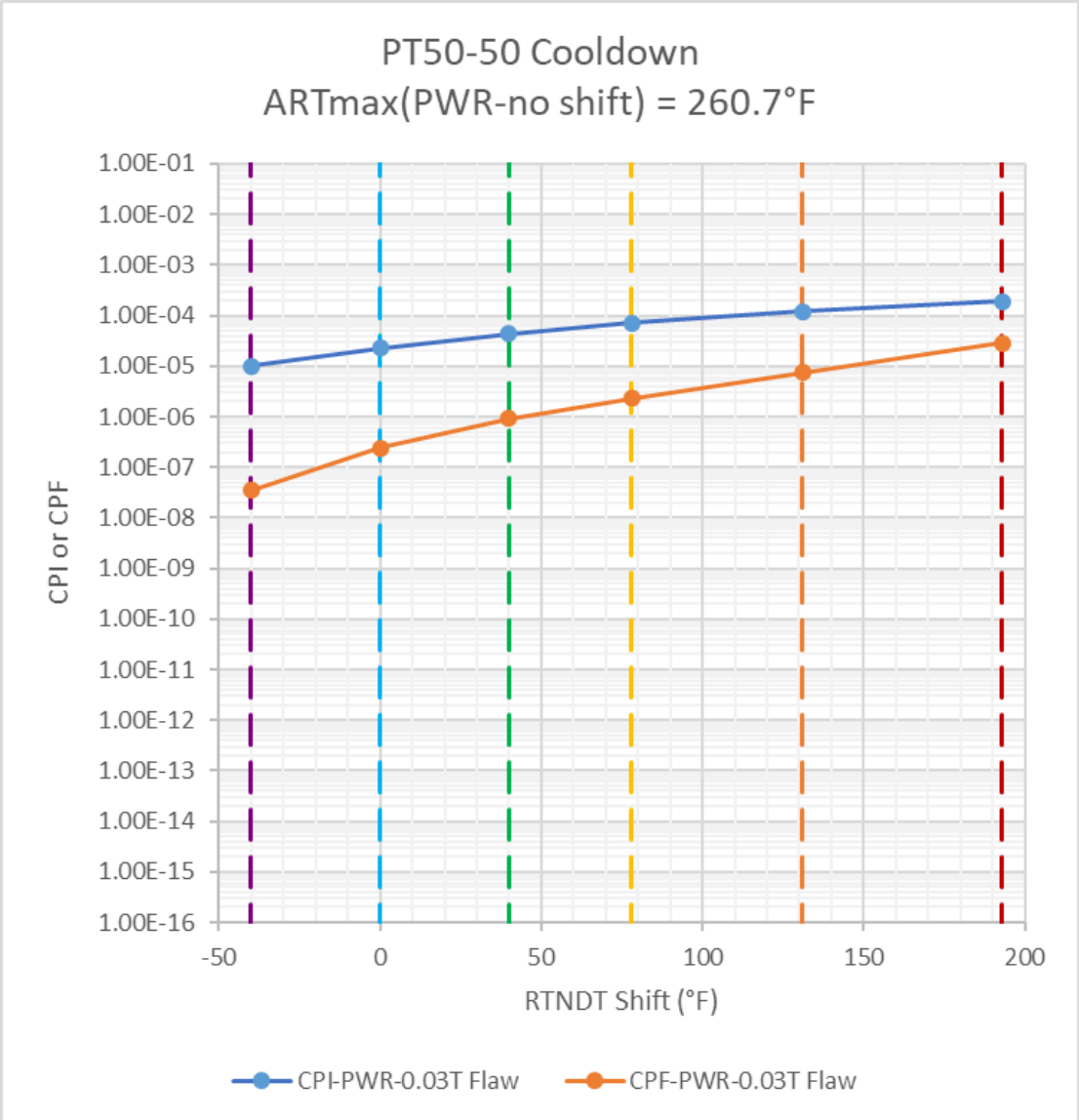

Figure 2-25: CPI and CPF for a 0.03 T Flaw of Aspect Ratio 6 in a PWR Subjected to the PT50-50 Cooldown, as a Function of RT_{NDT} Shift from RG 1.99, Rev. 2 to E900-15 Embrittlement Correlations (open symbols linked by dashed lines represent results that are not statistically converged)

2.3.3 PT100-50 Cooldown

2.3.3.1 ¼-T Flaw Results

The stress intensity factor history for a 0.25 T ID surface flaw subjected to the PT100-50 cooldown transient described in 2.1.2.3 is shown in Figure 2-26 for flaws with aspect ratios of 2, 6, 10 and infinity. The arrest toughness K_{Ia}, below which no crack growth initiation can occur, as well as the median fracture toughness K_{Ic}, are also shown. It is important to note that all probabilistic analyses were performed with a flaw of aspect ratio equal to 6. Figure 2-26 clearly shows that K increases initially while the pressure is held constant and the temperature decreases linearly at a rate of 50°F/hour, reaching a maximum between 140 and 160 minutes. Then, at 164 minutes, the sudden pressure drop is accompanied by a sudden drop in K values. The rate of decrease in K is initially high but diminishes as time goes by. At 288 minutes, when the pressure increases again, a corresponding increase in K is observed. At about 440 minutes, the pressure is reduced to match the PT limit curve for a 50°F/hour cooldown, resulting in a decrease in K. Finally, at 576 minutes, when the temperature reaches 70°F and remains constant, K decreases at a higher rate because the portion of K due to thermal stresses decreases. After this point, the rate of decrease in K values slowly diminishes until the end of the calculation.

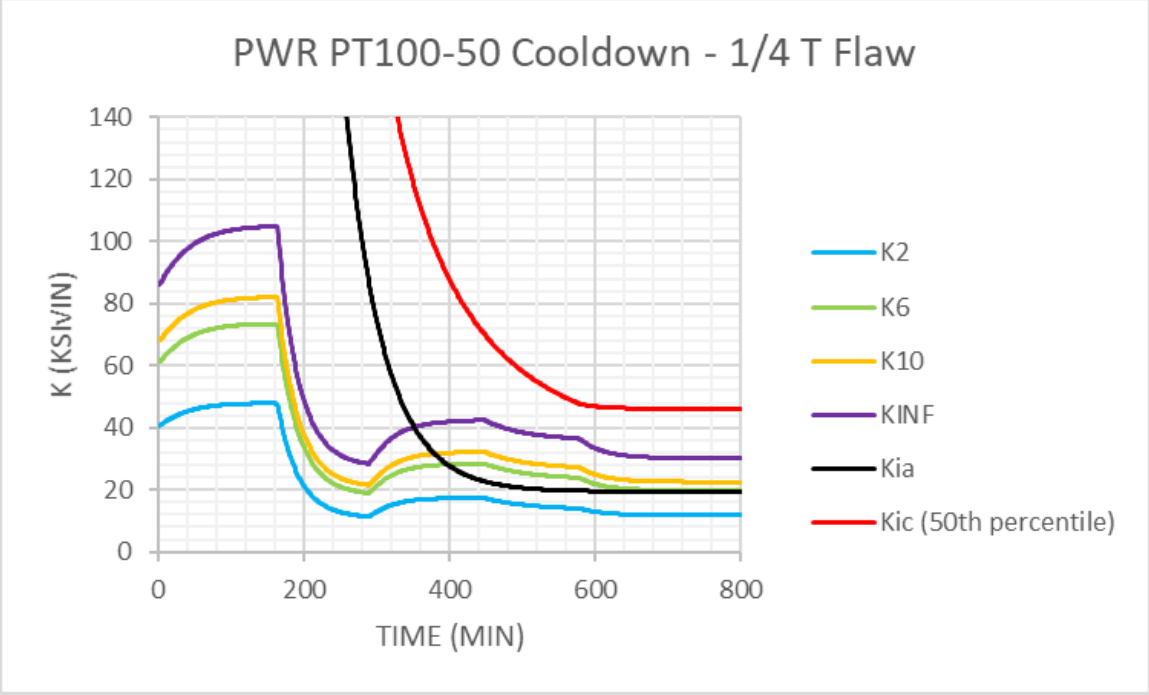

Figure 2-26: Stress Intensity Factor for the PWR PT100-50 Cooldown for a 0.25 T Flaw for Flaw Aspect Ratios of 2, 6, 10 and Infinity (note: in the legend, Kia is K_{Ia} and Kic is K_{Ic})

A probabilistic calculation assuming a 0.25 T flaw of aspect ratio equal to 6 and the PT100-50 cooldown resulted in a CPI and a CPF of zero using the RG 1.99, Rev. 2 embrittlement correlation. This case corresponds to 0°F RT_{NDT} shift (i.e. 'no shift') for this transient.

The same PT100-50 cooldown (shown in Figure 2-4) was modeled for different values of RT_{NDT}^{SHIFT}, so as to understand the impact of shifting the RT_{NDT} for this transient. Of course, in actual safety analyses, the

P-T limit would be adjusted as a function of the maximum ART in the vessel being analyzed, so a higher ART would reduce the allowed pressure, which In turn would result in lower CPI and CPF than presented here for cases where RT_{NDT}^{SHIFT} is greater than 0°F.

Table 2-10 and Figure 2-27 show the results of the probabilistic analyses for the 0.25 T flaw for the PT100-50 cooldown, as a function of RT_{NDT}^{SHIFT}. As expected, the CPI and CPF increase as RT_{NDT}^{SHIFT} increases. It should be noted that the analyses for $RT_{NDT}^{SHIFT} < 78°F$ resulted in CPI and CPF predictions equal to zero. Furthermore, for $RT_{NDT}^{SHIFT} = 78°F$, the CPF was zero and the CPI did not statistically converge because of the very low calculated probability, but the CPI trend over the number of trials was beginning to stabilize, so the results are believed to be in the correct order of magnitude.

Table 2-10: Calculated CPI and CPF for a 0.25 T Flaw of Aspect Ratio 6 in a PWR Subjected to the PT100-50 Cooldown

RTNDT Shift (°F)	CPI	CPI Converged?	CPF	CPF Converged?	TWCF
-40	0.0000E+00	YES	0.0000E+00	YES	0.0000E+00
0	0.0000E+00	YES	0.0000E+00	YES	0.0000E+00
40	0.0000E+00	YES	0.0000E+00	YES	0.0000E+00
78	4.8419E-09	NO	0.0000E+00	YES	0.0000E+00
131	1.6005E-06	YES	1.9420E-07	YES	1.1652E-12
193	2.1283E-04	YES	1.6256E-04	YES	9.7536E-10

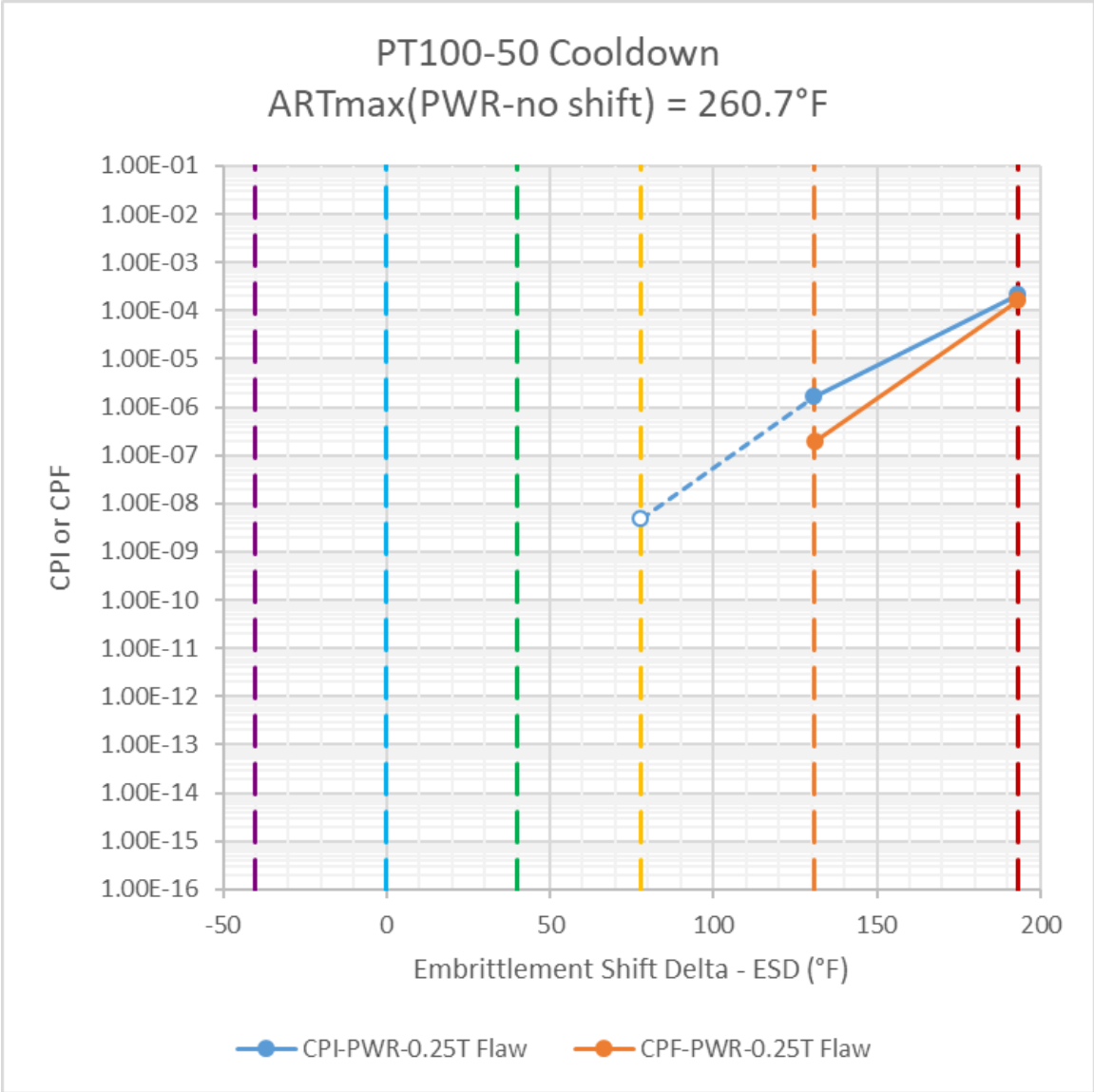

Figure 2-27: CPI and CPF for a 0.25 T Flaw of Aspect Ratio 6 in a PWR Subjected to the PT100-50 Cooldown, as a Function of RT_{NDT} Shift from RG 1.99, Rev. 2 to E900-15 Embrittlement Correlations (open symbols linked by dashed lines represent results that are not statistically converged)

2.3.3.2 Shallow Flaw Results

The stress intensity factor history for a 0.03 T ID surface flaw subjected to the PT100-50 cooldown transient described in 2.1.2.3 is shown in Figure 2-28 for flaws with aspect ratios of 2, 6, 10 and infinity. The arrest toughness K_{Ia}, below which no crack growth initiation can occur, as well as the median fracture toughness K_{Ic}, are also shown. Figure 2-28 clearly shows that K increases initially while the pressure is held constant and the temperature decreases linearly at a rate of 50°F/hour. The maximum K values are reached at 163 minutes, just before the sudden pressure drop that results in a sudden drop in K values. During the subsequent temperature decrease (with pressure initially going down to about 250psi and then coming back up to stabilize around 575psi, with a dip between ~445 minutes and 576 minutes to match the PT limit), the K values reach a minimum sometime between 230 and 288 minutes,

and then increase again between 288 minutes and 576 minutes, when a second peak is observed at 576 minutes. This second peak is characteristic of shallow surface flaws that barely penetrate the base metal because these cracks are highly affected by the stresses due to the mismatch in thermal expansion coefficient between the cladding and the base metal. An inflexion point around 445 minutes is the result of the pressure being reduced to remain below the PT limit for this transient. After 576 minutes, the temperature is held constant at 70°F, and thus the thermal stresses and associated component of K decrease rapidly, hence there is a decrease in overall K values despite the constant pressure.

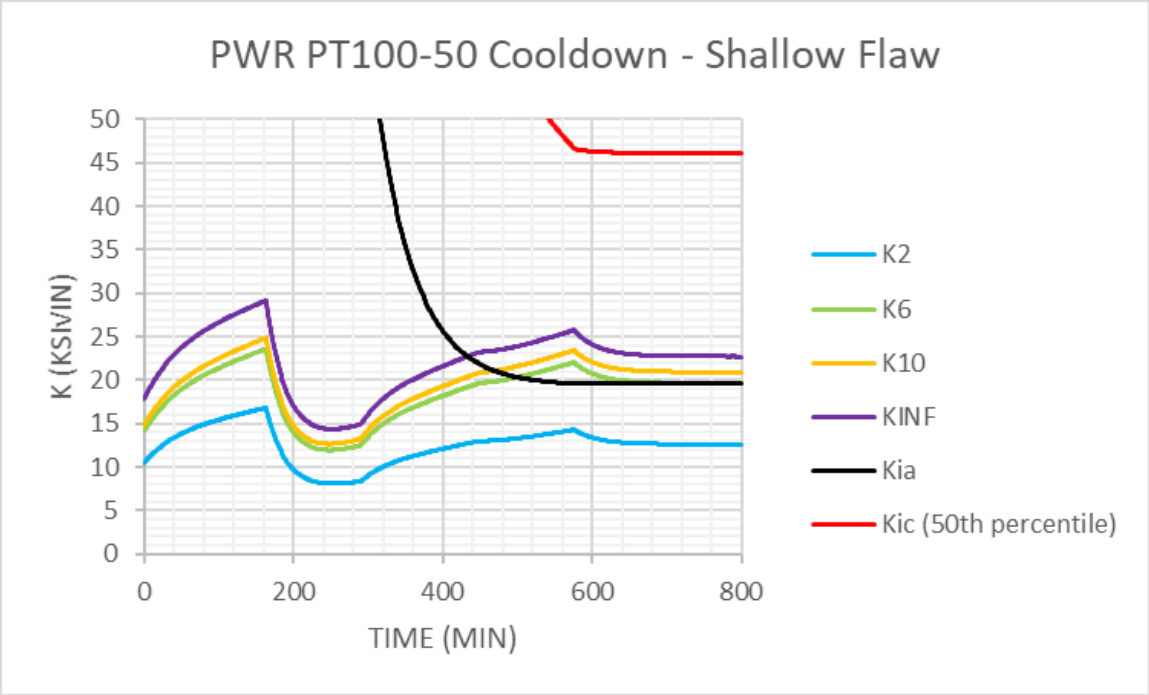

Figure 2-28: Stress Intensity Factor for the PWR PT100-50 Cooldown for a 0.03 T Flaw for Flaw Aspect Ratios of 2, 6, 10 and Infinity (note: in the legend, Kia is K_{Ia} and Kic is K_{Ic})

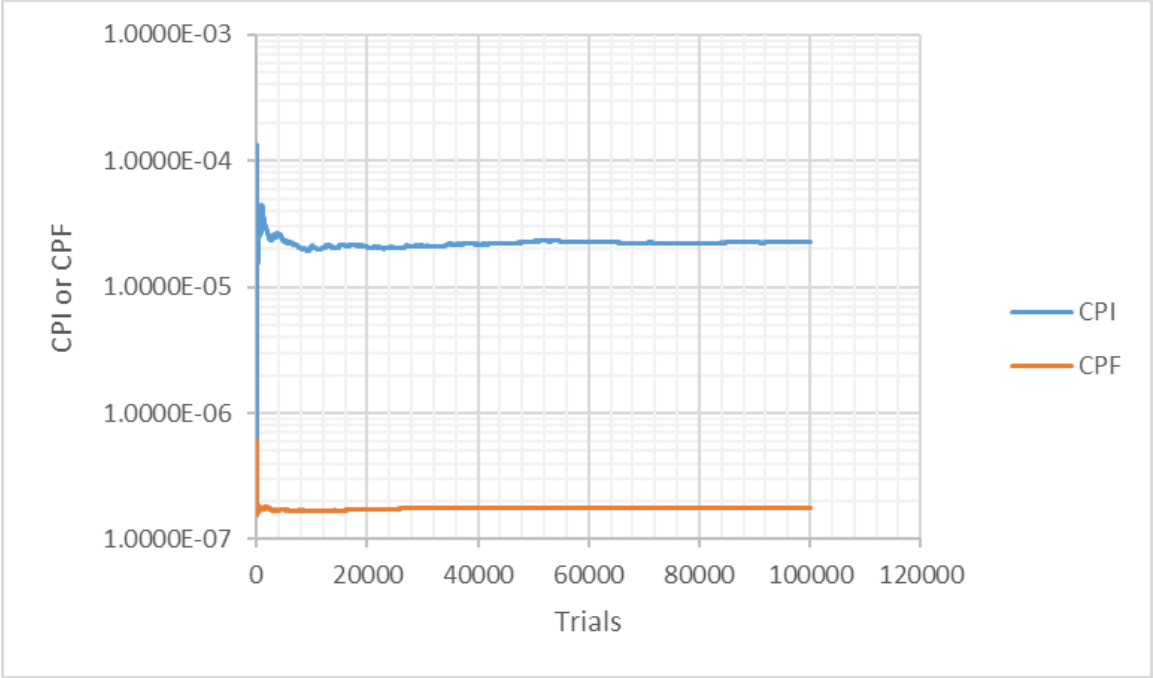

Figure 2-29: CPI and CPF versus Number of Trials for a 0.03 T Flaw in a PWR with 0°F RT_{NDT} Shift for the PT100-50 cooldown

A probabilistic calculation assuming a 0.03 T flaw of aspect ratio equal to 6 and the PT100-50 cooldown resulted in a CPI of 2.3E-05 and a CPF of 1.8E-07 using the RG 1.99, Rev. 2 embrittlement correlation. This case corresponds to 0°F RT_{NDT} shift (i.e. 'no shift') for this transient. Figure 2-29 shows the calculated CPI and CPF as a function of the number of RPV trials in FAVOR, and one can see that the FAVOR calculations are statistically converged after about 20,000 trials. Similar plots were generated for all the runs performed in this study, so as to assess statistical convergence of the results.

The same PT100-50 cooldown (shown in Figure 2-4) was modeled for different values of RT_{NDT}^{SHIFT}, so as to understand the impact of shifting the RT_{NDT} for this transient. That is, a new P-T limit was not calculated for a 0.03 T shallow flaw, but was instead calculated using current practice based on ASME Section XI, Appendix G, which requires analysis based on a 0.25 T flaw. Furthermore, as for the 0.25 T case, in actual safety analyses, the P-T limit would be adjusted as a function of the maximum ART in the vessel being analyzed, which would result in a different CPI and CPF than presented here. If the P-T limit was recalculated for each RT_{NDT}^{SHIFT} value, the shallow flaw effect makes it difficult to predict a priori whether the CPI and CPF values would move up or down.

Table 2-11 and Figure 2-30 show the results of the probabilistic analyses for the 0.03 T flaw for the PT100-50 cooldown, as a function of RT_{NDT}^{SHIFT}. As expected, the CPI and CPF increase as RT_{NDT}^{SHIFT} increases. Because of the relatively high CPI and CPF values calculated and the relatively large (100,000) number of runs, all calculated conditional probabilities achieved statistical convergence.

Table 2-11: Calculated CPI and CPF for a 0.03 T Flaw of Aspect Ratio 6 in a PWR Subjected to the PT100-50 Cooldown

RTNDT Shift (°F)	CPI	CPI Converged?	CPF	CPF Converged?	TWCF
-40	1.0140E-05	YES	2.5599E-08	YES	1.5359E-13
0	2.2891E-05	YES	1.7802E-07	YES	1.0681E-12
40	4.3563E-05	YES	6.6744E-07	YES	4.0046E-12
78	7.1213E-05	YES	1.6717E-06	YES	1.0030E-11
131	1.2150E-04	YES	4.5909E-06	YES	2.7545E-11
193	1.9106E-04	YES	1.3886E-05	YES	8.3316E-11

Figure 2-30: CPI and CPF for a 0.03 T Flaw of Aspect Ratio 6 in a PWR Subjected to the PT100-50 Cooldown, as a Function of RT_{NDT} Shift from RG 1.99, Rev. 2 to E900-15 Embrittlement Correlations (open symbols linked by dashed lines represent results that are not statistically converged)

2.3.4 C50P Cooldown

2.3.4.1 ¼-T Flaw Results

The stress intensity factor history for a 0.25 T ID surface flaw subjected to the '50th percentile' cooldown transient described in 2.1.2.4 is shown in Figure 2-31 for flaws with aspect ratios of 2, 6, 10 and infinity. The arrest toughness K_{Ia}, below which no crack growth initiation can occur, as well as the median fracture toughness K_{Ic}, are also shown. It is important to note that all probabilistic analyses were performed with a flaw of aspect ratio equal to 6. Figure 2-31 shows that for this transient, K continuously decreases as temperature and pressure decrease over time. The initial decrease is very sharp, dominated by the sharp pressure drop until about 300 minutes. After the initial pressure drop in the system, the value of K is driven by thermal stresses and basically correlate to the cooldown rate. In fact, one can observe a first plateau from ~300 minutes to ~600 minutes, a second plateau from ~600 minutes to ~2800 minutes, and finally a step down at ~2800 minutes with final values of K essentially flat after 2900 minutes.

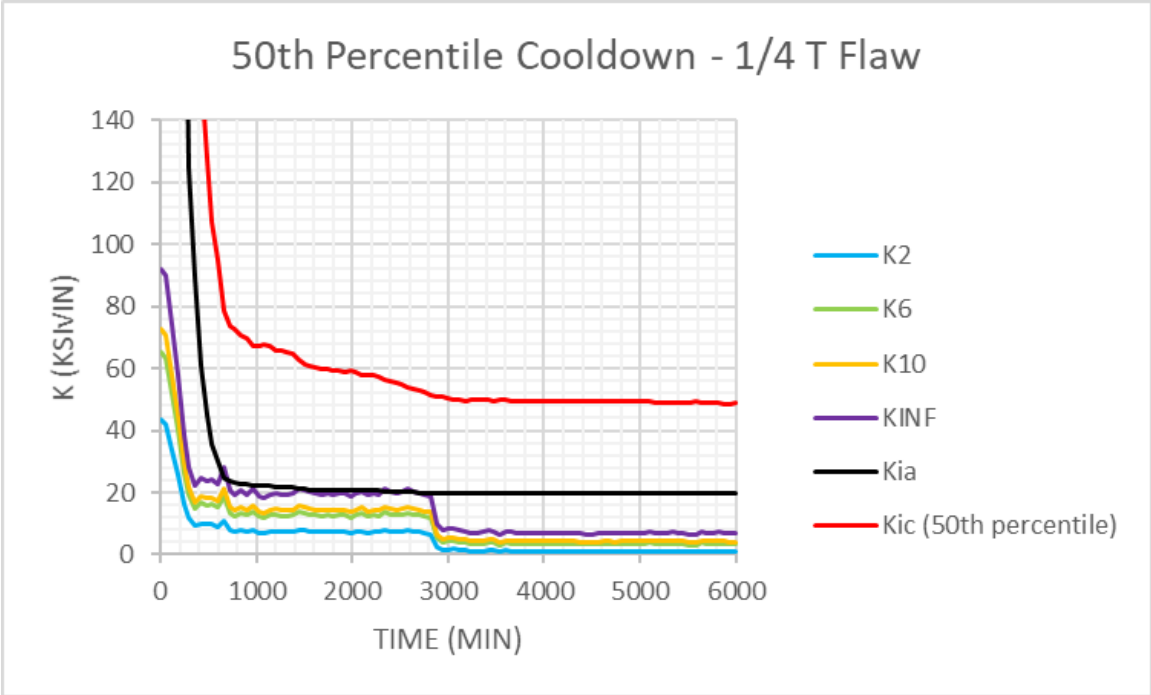

Figure 2-31: Stress Intensity Factor for PWR 50th Percentile Cooldown for 0.25 T Flaw for Flaw Aspect Ratios of 2, 6, 10 and Infinity (note: in the legend, Kia is K_{Ia} and Kic is K_{Ic})

A probabilistic calculation assuming a 0.25 T flaw of aspect ratio equal to 6 and the 50th percentile cooldown resulted in a CPI and a CPF of zero using the RG 1.99, Rev. 2 embrittlement correlation. This case corresponds to 0°F RT_{NDT} shift (i.e. 'no shift') for this transient. The same 50th percentile cooldown (shown in Figure 2-6 and Figure 2-8) was modeled for different values of RT_{NDT}^{SHIFT}, so as to understand the impact of shifting the RT_{NDT} for this transient.

Table 2-12 and Figure 2-32 show the results of the probabilistic analyses for the 0.25 T flaw for the 50th percentile cooldown, as a function of RT_{NDT}^{SHIFT}. All values of CPI and CPF calculated were zero using

100,000 vessel simulations, except the CPI value for a RT_{NDT}^{SHIFT} value of 193°F (resulting in a very high ART of around 427°F).

Table 2-12: Calculated CPI and CPF for a 0.25 T Flaw of Aspect Ratio 6 in a PWR Subjected to the 50th Percentile Cooldown

RTNDT Shift (°F)	CPI	CPI Converged?	CPF	CPF Converged?	TWCF
-40	0.0000E+00	YES	0.0000E+00	YES	0.0000E+00
0	0.0000E+00	YES	0.0000E+00	YES	0.0000E+00
40	0.0000E+00	YES	0.0000E+00	YES	0.0000E+00
78	0.0000E+00	YES	0.0000E+00	YES	0.0000E+00
131	0.0000E+00	YES	0.0000E+00	YES	0.0000E+00
193	2.5504E-08	NO	0.0000E+00	YES	0.0000E+00

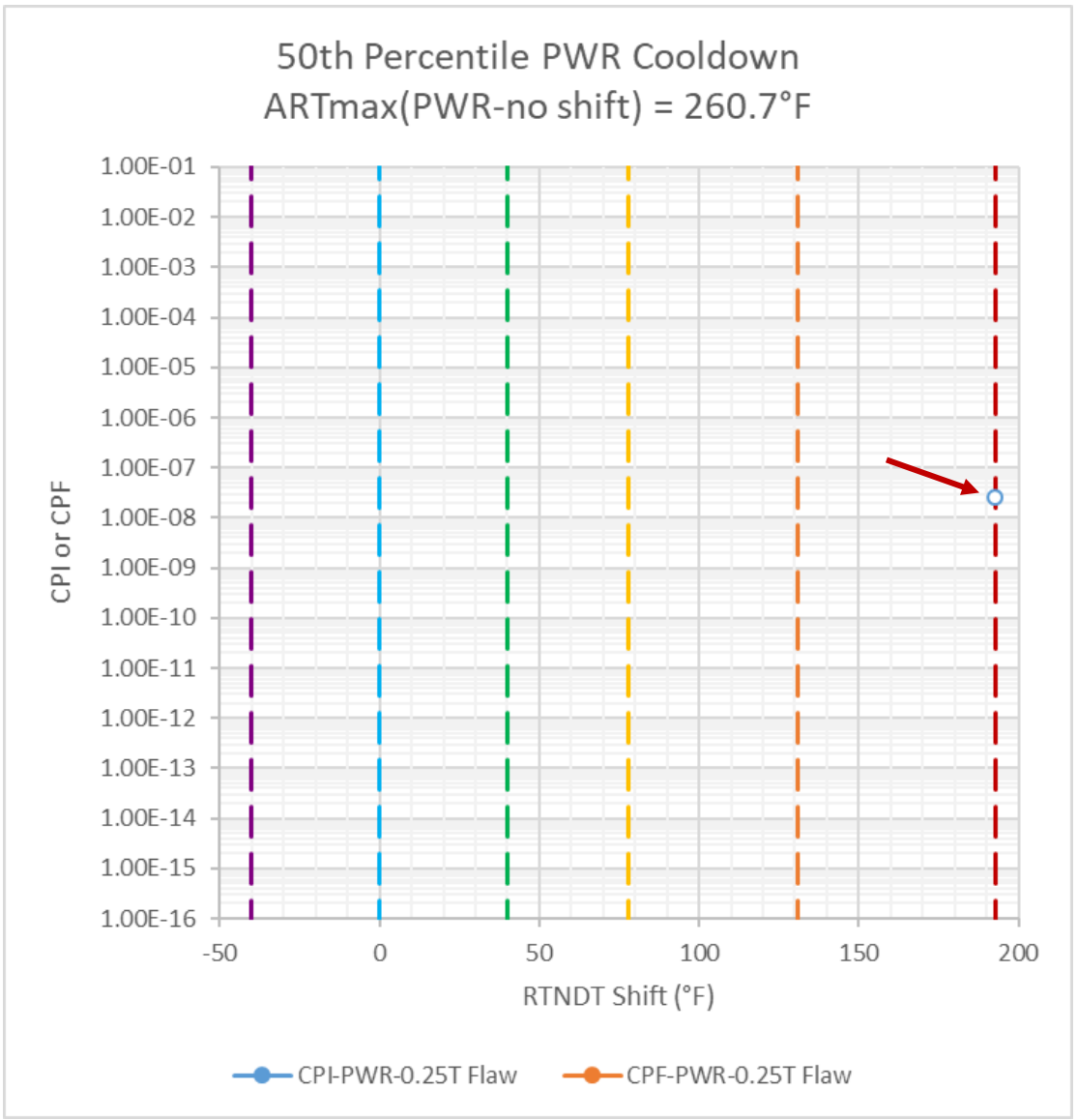

Figure 2-32: CPI and CPF for a 0.25 T Flaw of Aspect Ratio 6 in a PWR Subjected to the 50th Percentile Cooldown, as a Function of RT_{NDT} Shift from RG 1.99, Rev. 2 to E900-15 Embrittlement Correlations (open symbols linked by dashed lines represent results that are not statistically converged). Note that all CPF values were zero, and thus are not shown, and the only non-zero value of CPI is shown as an open symbol.

2.3.4.2 Shallow Flaw Results

The stress intensity factor history for a 0.03 T ID surface flaw subjected to the 50th percentile cooldown transient described in 2.1.2.4 is shown in Figure 2-33 for flaws with aspect ratios of 2, 6, 10 and infinity. The arrest toughness K_{Ia}, below which no crack growth initiation can occur, as well as the median fracture toughness K_{Ic}, are also shown. Figure 2-33 shows that in the early part of the cooldown, K increases as a result of the temperature drop, but the simultaneous pressure reduction results in a large decrease in K between the peak around 60 minutes and the minimum reached at about 360 minutes. Beyond 360 minutes, the pressure remains essentially constant until the final pressure drop at ~2800

minutes, and the K increase between 360 minutes and 2800 minutes is driven by the decrease in temperature. After 2800 minutes, K remains almost constant as both the pressure and temperature remain roughly constant.

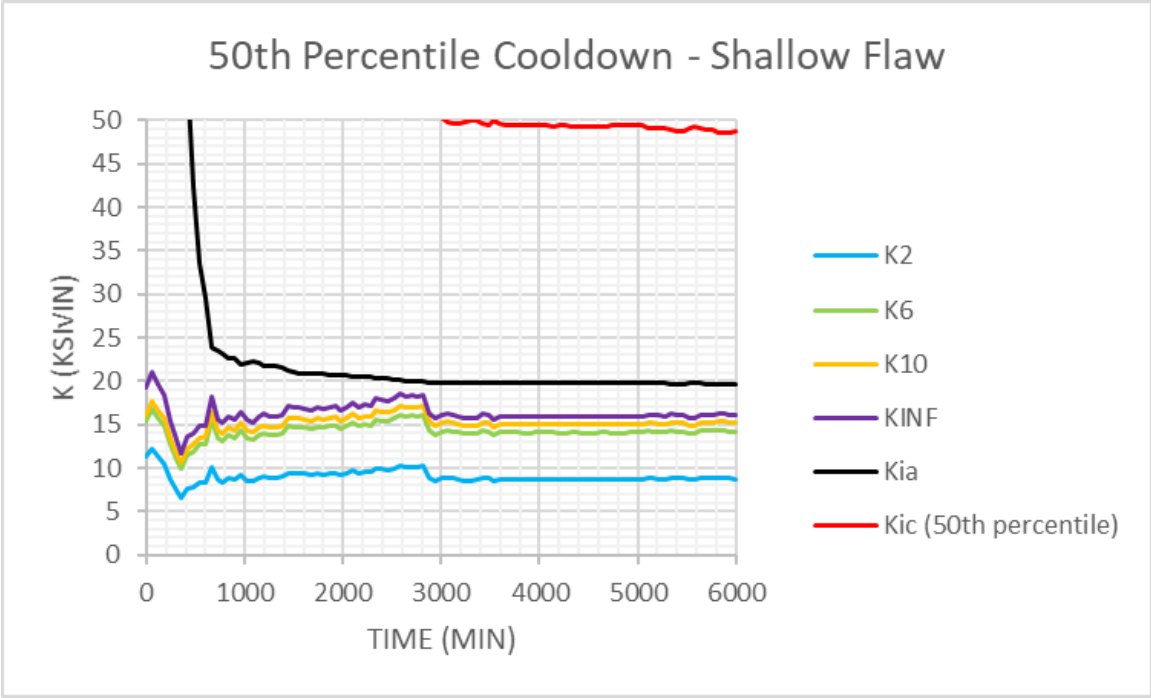

Figure 2-33: Stress Intensity Factor for PWR 50°F/hour P-T Limit Cooldown for 0.03 T Flaw for Flaw Aspect Ratios of 2, 6, 10 and Infinity (note: in the legend, Kia is K_{Ia} and Kic is K_{Ic})

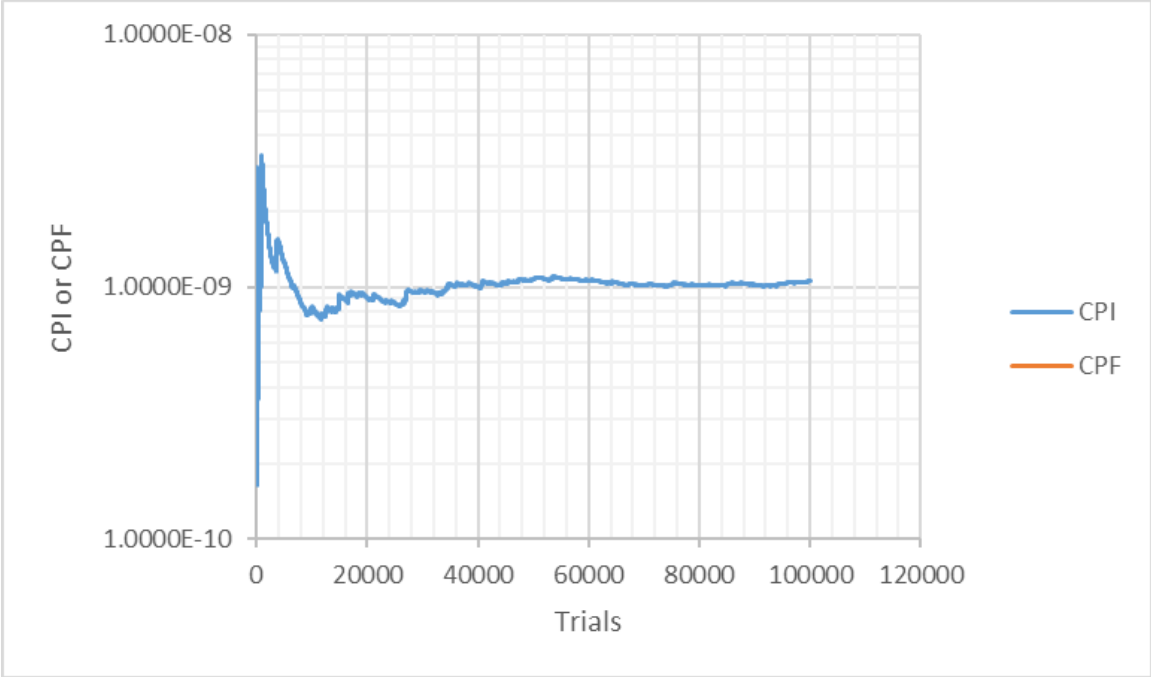

Figure 2-34: CPI and CPF versus Number of Trials for the 0.03 T Flaw in a PWR with 0°F RT_{NDT} Shift for the 50th Percentile Cooldown

A probabilistic calculation assuming a 0.03 T flaw of aspect ratio equal to 6 and the 50th percentile cooldown resulted in a CPI of 1.0E-09 and a CPF of zero using the RG 1.99, Rev. 2 embrittlement correlation. This case corresponds to 0°F RT_{NDT} shift (i.e. 'no shift') for this transient. Figure 2-34 shows the calculated CPI as a function of the number of RPV trials in FAVOR, and one can see that the FAVOR calculations are statistically converged after about 40,000 trials. Similar plots were generated for all the runs performed in this study, so as to assess statistical convergence of the results.

The same 50th percentile cooldown (shown in Figure 2-6 and Figure 2-8) was modeled for different values of RT_{NDT}^{SHIFT}, so as to understand the impact of shifting the RT_{NDT} for this transient. Table 2-13 and Figure 2-35 show the results of the probabilistic analyses for the 0.03 T flaw for the 50th percentile cooldown, as a function of RT_{NDT}^{SHIFT}. As expected, the CPI increases as RT_{NDT}^{SHIFT} increases, but CPF remained zero in all cases. All calculated conditional probabilities achieved statistical convergence.

Table 2-13: Calculated CPI and CPF for a 0.03 T Flaw of Aspect Ratio 6 in a PWR Subjected to a 50°F/hour Cooldown at the P-T Limit

RTNDT Shift (°F)	CPI	CPI Converged?	CPF	CPF Converged?	TWCF
-40	1.6441E-10	YES	0.0000E+00	YES	0.0000E+00
0	1.0556E-09	YES	0.0000E+00	YES	0.0000E+00
40	4.0286E-09	YES	0.0000E+00	YES	0.0000E+00
78	1.0078E-08	YES	0.0000E+00	YES	0.0000E+00
131	2.4315E-08	YES	0.0000E+00	YES	0.0000E+00
193	4.7276E-08	YES	0.0000E+00	YES	0.0000E+00

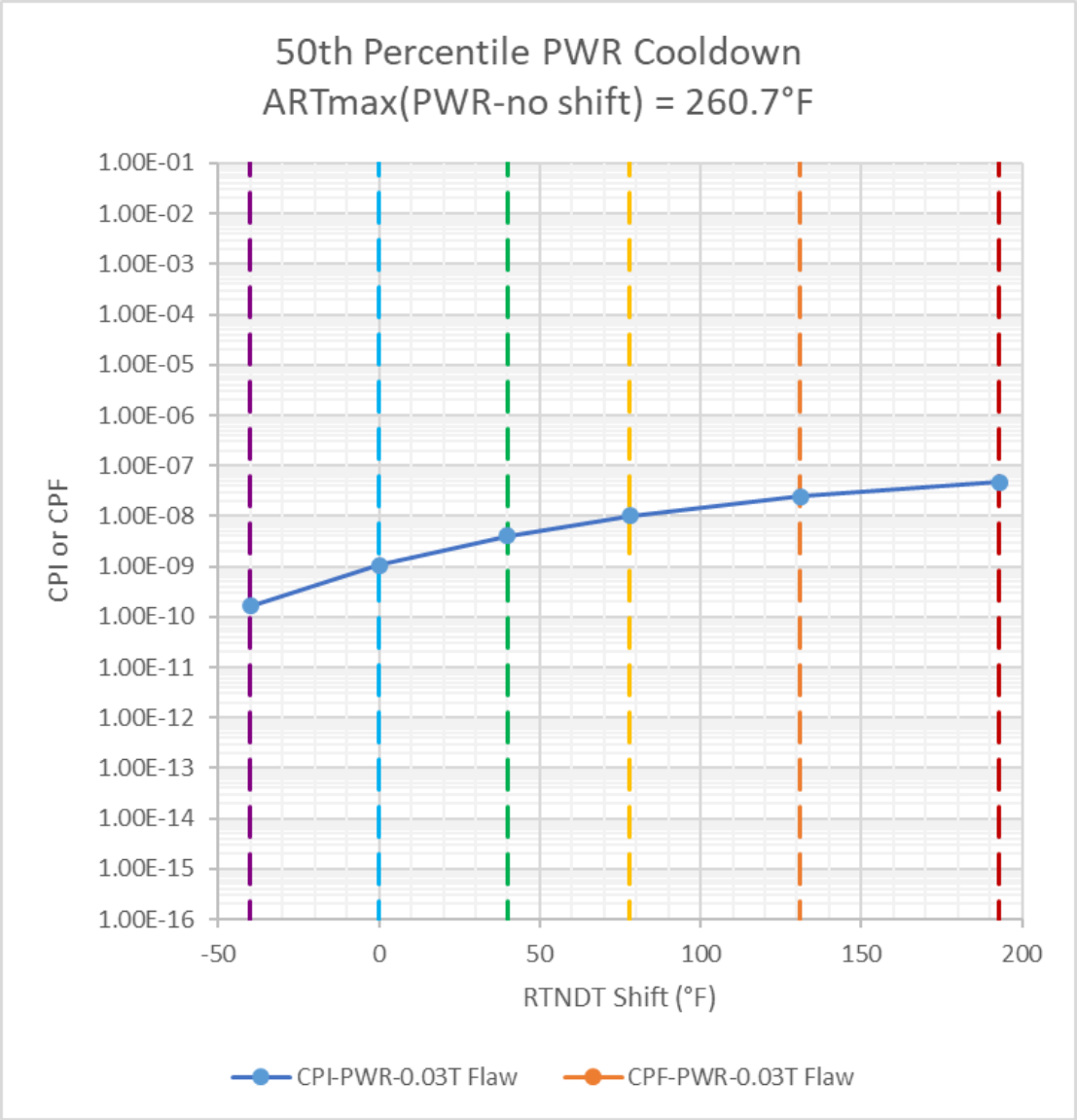

Figure 2-35: CPI and CPF for a 0.03 T Flaw of Aspect Ratio 6 in a PWR Subjected to a 50°F/hour Cooldown at the P-T Limit, as a Function of RT_{NDT} Shift from RG 1.99, Rev. 2 to E900-15 Embrittlement Correlations (open symbols linked by dashed lines represent results that are not statistically converged)

2.3.5 Sensitivity Study on Actual PWR Cooldowns for Shallow Flaw

In order to better understand the possible CPI and CPF variability (i.e. the range of risk) associated with normal cooldowns, the 42 actual cooldown transients were simulated for a single value of RT_{NDT} shift equal to 100°F. Since the risk of crack growth initiation (CPI) associated with shallow flaws is greater than that associated with ¼ T flaws for the 50th percentile of actual transients, the simulations of the 42 actual cooldowns were performed only for the case of a 0.03 T shallow flaw. It is important to note that calculated CPF values for this transient were equal to zero in all the cases analyzed (for both the ¼ T and 0.03 T flaw).

Figure 2-36 show the distribution of CPI and CPF values for the 42 actual cooldowns simulated. The CPI values range from 4.9E-12 to 2.0E-05, with a mean of 1.5E-06, a median of 1.3E-07, and a 99th percentile of 1.6E-05. 6 of the 42 actual cooldowns resulted in a CPI of zero. The CPF values range from 4.2E-15 to 1.1E-10, with a mean of 2.6E-12, a median of zero, and a 99th percentile of 6.4E-11. 38 of the 42 actual cooldown transients resulted in a CPF of zero. In summary, none of the 42 actual cooldown transients presented any significant vessel failure risk, and all were at least roughly 4 orders of magnitude below 1.0E-06 events per year.

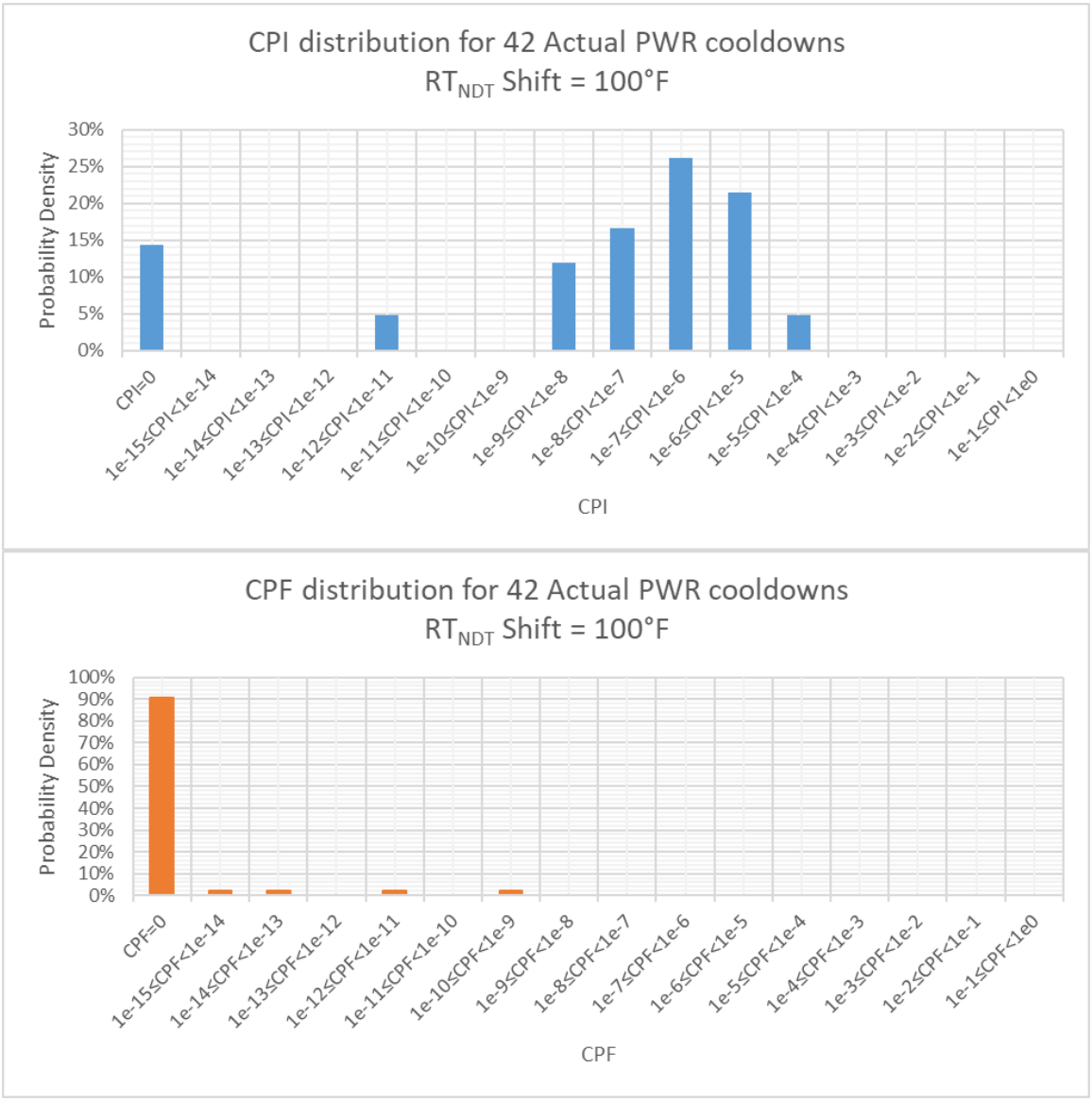

Figure 2-36: CPI (top) and CPF (bottom) Distribution for the 42 Actual PWR Cooldown Transients Modeled, for RT_{NDT} Shift of 100°F

Figure 2-37 shows the calculated CPI and CPF values for the 42 actual PWR cooldowns in comparison with the CPI and CPF calculated for the 50th percentile cooldown as a function of RT_{NDT} shift. One can see that the value of CPI for the 50th percentile cooldown for a RT_{NDT} shift value of 100°F is about $2x10^{-8}$, which corresponds roughly to the 35th percentile of the calculated CPI values for the 42 actual

cooldowns. As described above, none of the CPF values calculated were of any concern from a vessel integrity and safety point of view. In fact, for the actual cooldowns simulated, the transient frequency can be set equal to 1. As a result, for these transients, CPF = TWCF (through-wall cracking frequency). The highest TWCF value predicted for the 42 actual cooldowns is thus 1.1E-10, which is almost 4 orders of magnitude below 1.0E-06 events per year.

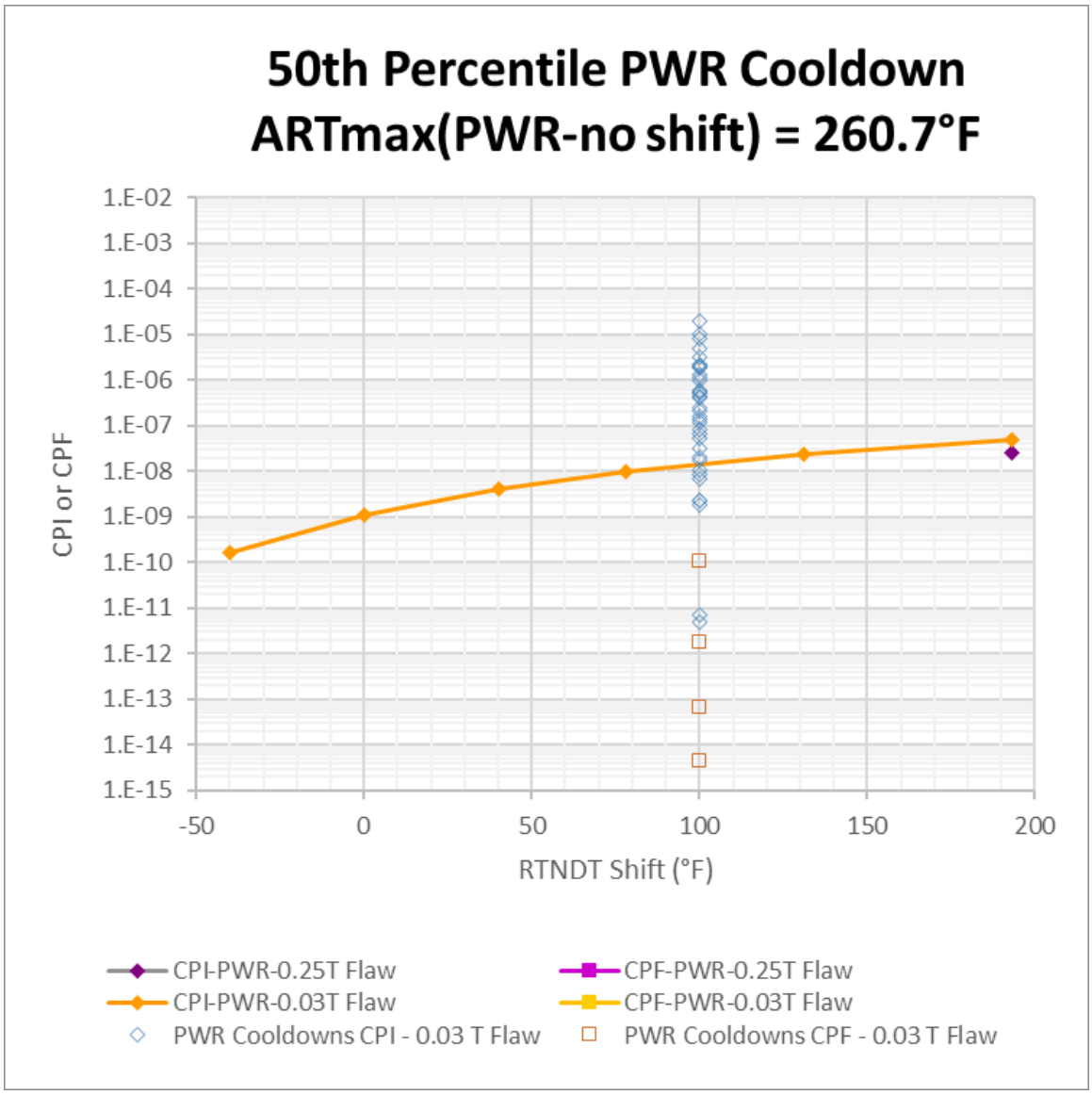

Figure 2-37: Comparison of the 0.03 T Flaw CPI and CPF at a RT_{NDT} Shift of 100°F for the 42 Actual PWR Cooldowns with the CPI as a Function of RT_{NDT} Shift for the 50th Percentile Cooldown (CPF Values Were all Zero for the 50th Percentile Cooldown)

3 BWR Scoping Study

3.1 Vessel and Transient Characteristics

3.1.1 Vessel Characteristics and Embrittlement Map

The BWR vessel modeled had the following characteristics:

- Inner radius 110.37 inches
- Cladding Thickness 0.21 inches
- Base metal thickness 5.62 inches
- Total wall thickness 5.83 inches

The material properties used in the FAVOR model are the same as for the PWR cases, and are given in Table 2-1 and Table 2-2. The stress free temperature was again assumed to be equal to 488°F. Pressure loading was applied since the calculations presented herein are for an ID surface flaw. Finally, WRS was included in calculations for axial and circumferential welds. These modeling parameters were chosen to match the analysis parameters historically used by NRC for regulatory analyses (e.g. 10 CFR 50.61a technical bases), and are the ones recommended in the FAVOR theory manual.

The BWR vessel rollout diagram and corresponding basic embrittlement information from the RVID database are provided in Figure 3-1 and Table 3-1 respectively.

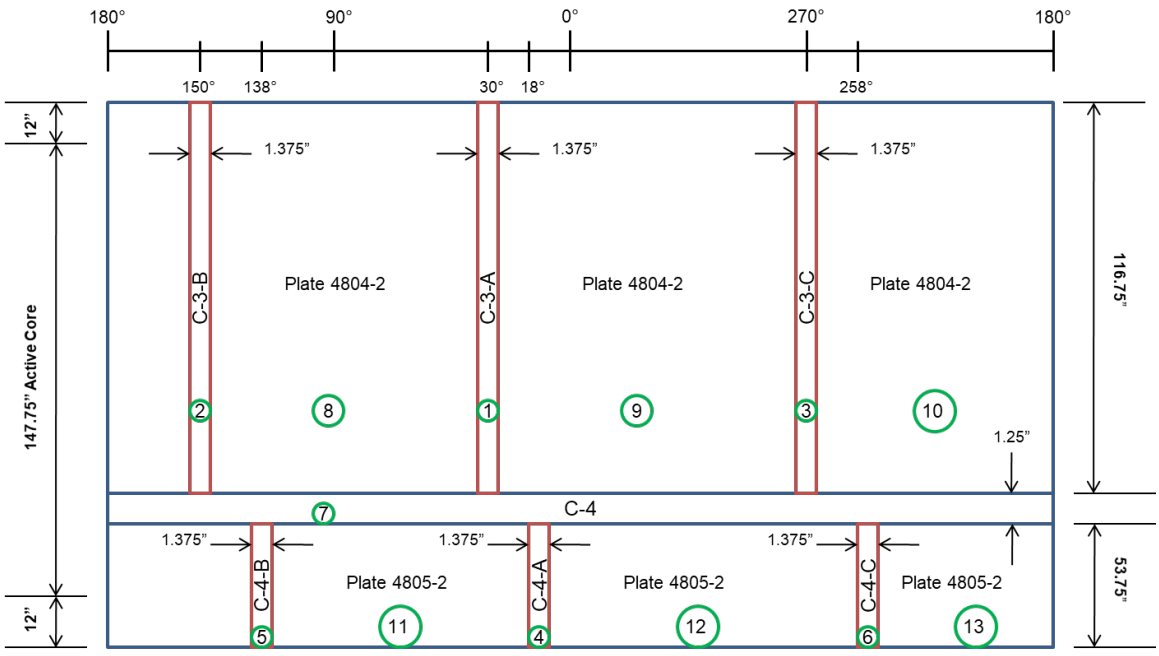

Figure 3-1: BWR Vessel Rollout Diagram

Table 3-1: BWR Vessel Embrittlement Map Information and Corresponding FAVOR Input

Major Region	Description	Heat ID	Plate or Weld ID	%Cu	%Ni	%P	ID RTndt (u) [Initial RTndt]	max neutron fluence @72 EFPY 10^{19} n/cm^2	1/4T RT_{NDT} @ 72 EFPY w/o Margin °F
1	Axial Weld	1P2809	LOWER INTERMEDIATE AXIAL WELDS 1-308	0.270	0.735	0.013	-50.000	0.47	92.7
2	Axial Weld	1P2809	LOWER INTERMEDIATE AXIAL WELDS 1-308	0.270	0.735	0.013	-50.000	0.47	92.7
3	Axial Weld	1P2809	LOWER INTERMEDIATE AXIAL WELDS 1-308	0.270	0.735	0.013	-50.000	0.47	92.7
4	Axial Weld	13253	LOWER SHELL AXIAL WELDS 1-307A/C	0.221	0.732	0.023	-50.000	0.32	63.1
5	Axial Weld	13253	LOWER SHELL AXIAL WELDS 1-307A/C	0.221	0.732	0.023	-50.000	0.32	63.1
6	Axial Weld	13253	LOWER SHELL AXIAL WELDS 1-307A/C	0.221	0.732	0.023	-50.000	0.32	63.1
7	CircWeld	33A277	CIRC WELD 1-313B	0.258	0.165	0.017	-50.000	0.32	25.6
8	Plate	C4337-1	LOWER INT. SHELL G-4803-7	0.170	0.620	0.011	-20.000	0.47	68.5
9	Plate	C3985-2	LOWER INT. SHELL G-4804-1	0.130	0.580	0.015	-20.000	0.47	42.8
10	Plate	C4114-2	LOWER INT. SHELL G-4804-2	0.130	0.700	0.010	-20.000	0.47	44.9
11	Plate	C4112-1	LOWER SHELL G-4805-1	0.130	0.640	0.011	8.000	0.32	63.1
12	Plate	C4112-2	LOWER SHELL G-4805-2	0.130	0.640	0.011	10.000	0.32	65.1
13	Plate	C4149-1	LOWER SHELL G-4805-3	0.140	0.570	0.009	-10.000	0.32	49.0

The resulting FAVOR BWR embrittlement map input was as follows:

```
*=============================================================================================================*
*  1    2    3    4      5     6     7     8     9 10 11    12    13 14    15    16    17 18    19    20 *
*************************************************************************************************************
   1    8    9    1 0.4666  0.27 0.735 0.013     1  2  0   -50    10 11 0.714 116.7   656  1 0.000 0.000
   2   10    8    2 0.4666  0.27 0.735 0.013     1  2  0   -50    10 11 0.714 116.7   656  1 0.000 0.000
   3    9   10    3 0.4666  0.27 0.735 0.013     1  2  0   -50    10 11 0.714 116.7   656  1 0.000 0.000
   4   11   12    4   0.32 0.221 0.732 0.023     1  2  0   -50    10 11 0.714 53.75   302  1 0.000 0.000
   5   13   11    5   0.32 0.221 0.732 0.023     1  2  0   -50    10 11 0.714 53.75   302  1 0.000 0.000
   6   12   13    6   0.32 0.221 0.732 0.023     1  2  0   -50    10 11 0.714 53.75   302  1 0.000 0.000
   7    8   11    7   0.32 0.258 0.165 0.017     1  2  0   -50    10 11   360  1.25  4005  2 0.000 0.000
   8    8    8    8 0.4666  0.17  0.62 0.011     1  0  0   -20    10 21 119.2 116.7 0.000  0 0.000 0.000
   9    9    9    9 0.4666  0.13  0.58 0.015     1  0  0   -20    10 21 119.2 116.7 0.000  0 0.000 0.000
  10   10   10   10 0.4666  0.13   0.7  0.01     1  0  0   -20    10 21 119.2 116.7 0.000  0 0.000 0.000
  11   11   11   11   0.32  0.13  0.64 0.011     1  0  0     8    10 21 119.2 53.75 0.000  0 0.000 0.000
  12   12   12   12   0.32  0.13  0.64 0.011     1  0  0    10    10 21 119.2 53.75 0.000  0 0.000 0.000
  13   13   13   13   0.32  0.14  0.57 0.009     1  0  0   -10    10 21 119.2 53.75 0.000  0 0.000 0.000
```

Of note, RG 1.99, Rev. 2 was used to calculate the RT_{NDT} at the 0.25 T location so as to calculate the P-T limit for a 100°F/hour cooldown (last column in Table 3-1). The maximum RT_{NDT} at the 0.25 T location at 72 EFPY was determined to be 92.7°F, which is the value that was used for the P-T limit calculation.

3.1.2 Transient Definitions

3.1.2.1 PT100-100: 100°F/Hour Cooldown at Maximum Allowed Pressure for 100°F/hour Cooldown

As was done for the PWR analysis, in order to determine the allowable pressure for the P-T limit cooldown at a rate of 100°F/hour, ASME Section XI, Appendix G, Paragraph G-2215 [6] was used. The risk-informed alternative was NOT used. Assuming the limiting case of an axial flaw and a wall thickness between 4 and 12 inches, the allowable pressure is given by:

$$P = \frac{K_{Ic} - K_{It}}{2M_m}\left({}^{t}/_{R_i}\right)$$

with

$$K_{Ic} = 33.2 + 20.734\ exp[0.02(T - RT_{NDT})]$$

and

$$M_m = 0.926\sqrt{t}$$

In order to determine the applied stress intensity factor due to thermal stresses (K_{It}), FAVOR was used to simulate a 100°F/hour cooldown from 550°F to 70°F with no applied pressure, and using a stress free temperature of 550°F (such that the initial thermal stresses are zero). The resulting K calculated by FAVOR for a 0.25 T flaw and an aspect ratio of 6 was used to determine the allowable pressure using the equation above. The value of crack tip RT_{NDT} used was92.7°F, as described in 3.1.1.

The resulting P-T limit transient for a 100°F/hour cooldown from 550°F to 70°F is shown in Figure 3-2. This transient is referred to as the 'PT100-100' transient in this document, and its frequency of occurrence is $1x10^{-7}$ events per year (based on the BTP 5-3 closure memo assessment [7]).

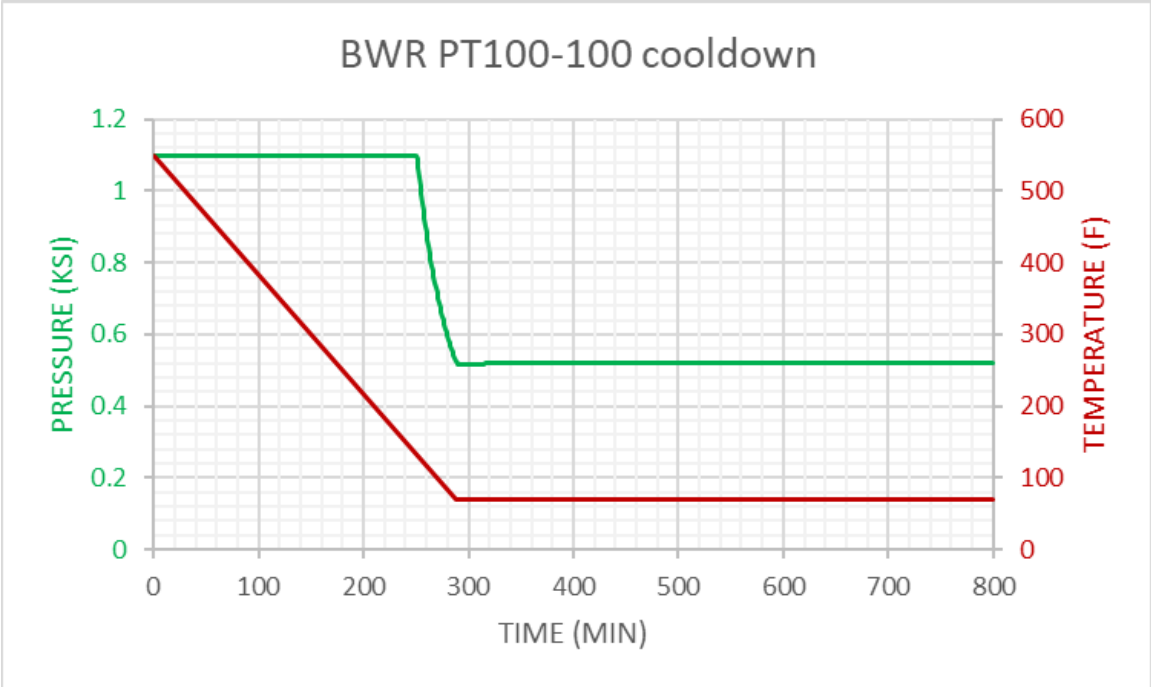

Figure 3-2: BWR PT100-100 Cooldown Transient Characteristics

3.1.2.2 PT50-50: 50°F/Hour Cooldown at Maximum Allowed Pressure for 50°F/hour Cooldown

As was done for the PWR analysis, in order to determine the allowable pressure for the P-T limit cooldown at a rate of 50°F/hour, ASME Section XI, Appendix G, Paragraph G-2215 [6] was used. The risk-informed alternative was NOT used. Assuming the limiting case of an axial flaw and a wall thickness between 4 and 12 inches, the allowable pressure is given by:

$$P = \frac{K_{Ic} - K_{It}}{2M_m}\left({}^{t}/_{R_i}\right)$$

with

$$K_{Ic} = 33.2 + 20.734\ exp[0.02(T - RT_{NDT})]$$

and

$$M_m = 0.926\sqrt{t}$$

In order to determine the applied stress intensity factor due to thermal stresses (K_{It}), FAVOR was used to simulate a 50°F/hour cooldown from 550°F to 70°F with no applied pressure, and using a stress free temperature of 550°F (such that the initial thermal stresses are zero). The resulting K calculated by FAVOR for a 0.25 T flaw and an aspect ratio of 6 was used to determine the allowable pressure using the equation above. The value of crack tip RT_{NDT} used was 92.7°F, as described in 3.1.1.

The resulting P-T limit transient for a 50°F/hour cooldown from 550°F to 70°F is shown in Figure 3-2. This transient is referred to as the 'PT50-50' transient in this document, and its frequency of occurrence is $1x10^{-7}$ events per year (based on the BTP 5-3 closure memo assessment [7]).

Figure 3-3: BWR PT50-50 Cooldown Transient Characteristics

3.1.2.3 PT100-50: 50°F/Hour Cooldown at Maximum Allowed Pressure for 100°F/hour Cooldown

The P-T limit pressure history based on a 100°F/hour cooldown (see section3.1.2.1) was used along with a 50°F/hour cooldown temperature history. The pressure history was essentially the same as for the PT100-100 cooldown, except between ~570 minutes and ~640 minutes, where the pressure was reduced to match the PT limits for a 50°F/hour cooldown. The resulting transient for a 50°F/hour cooldown from 550°F to 70°F is shown in Figure 3-4. This transient is referred to as the 'PT100-50' transient in this document, and its frequency of occurrence is $1x10^{-7}$ events per year (based on the BTP 5-3 closure memo assessment [7]).

Figure 3-4: BWR PT100-50 Cooldown Transient Characteristics

3.1.2.4 S50: 50°F/Hour Saturation Pressure Cooldown

Figure 3-5 Shows the pressure and temperature histories for a 50°F/hour cooldown at saturation pressure and temperature. This transient is hereafter referred to as the '50°F/hour saturation cooldown' or 'S50' transient in this document, and its frequency of occurrence is 1.0 events per year (based on the BTP 5-3 closure memo assessment [7]).

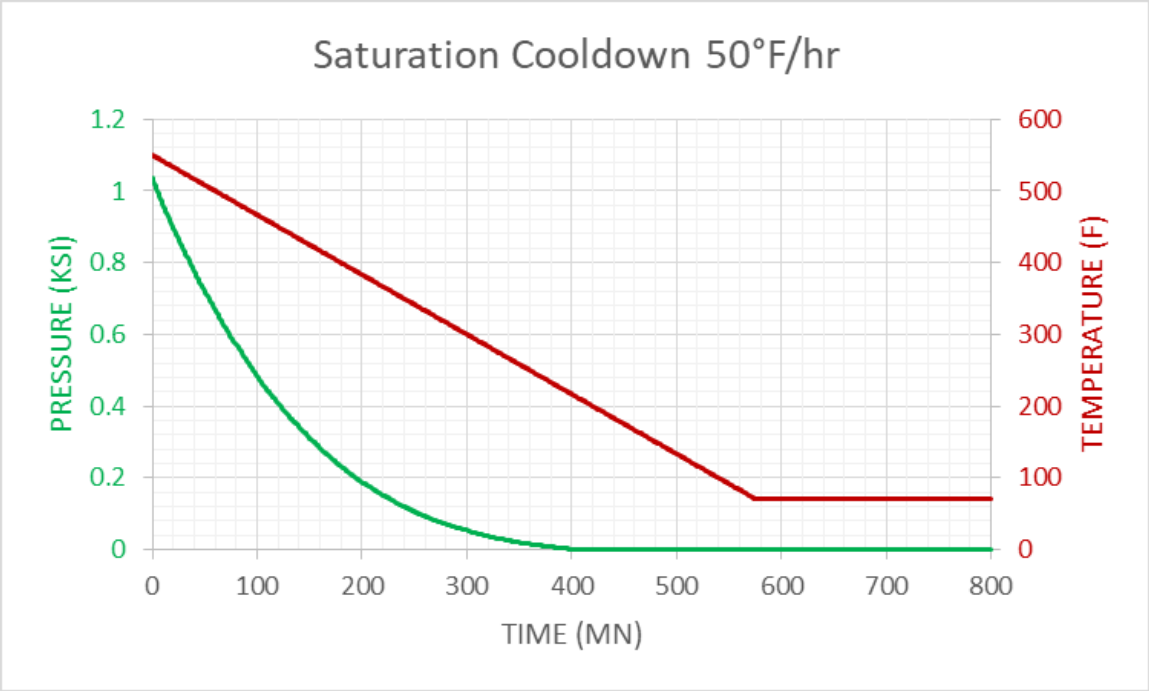

Figure 3-5: BWR Saturation Cooldown at 50°F/hour Transient Characteristics

3.1.2.5 LT40-40: Leak Test with 40°F/Hour Heatup and 40°F/Hour Cooldown

Figure 3-6 shows the pressure and temperature histories used for a BWR leak test transient with a 40°F/hour heatup rate and a 40°F/hour cooldown rate. The allowable pressure and temperature were derived from the ASME Section XI Appendix G, Paragraph G-2215 rules [6], as was done for the P-T limit cooldowns. For this transient, the leak test pressure and temperature were 1.1 ksi and 167°F, respectively.

This transient is referred to as the 'LT40-40' transient in this document, and its frequency of occurrence is estimated at $1x10^{-3}$ events per year (based on the BTP 5-3 closure memo assessment [7]).

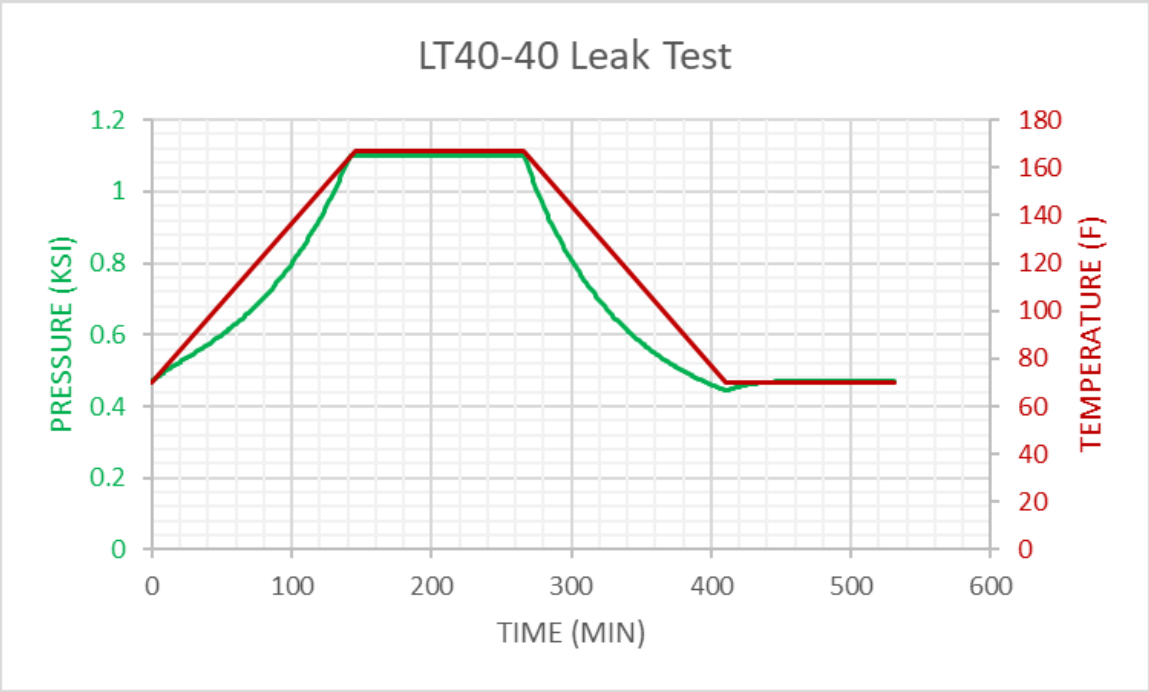

Figure 3-6: BWR LT40-40 Leak Test Transient Characteristics

3.1.2.6 LT40-100: 40°F/Hour Heatup and 100°F/Hour Cooldown Leak Test

Figure 3-7 shows the pressure and temperature histories used for a BWR leak test transient with a 40°F/hour heatup rate and a 100°F/hour cooldown rate. The allowable pressure and temperature were derived from the ASME Section XI Appendix G, Paragraph G-2215 rules [6], as was done for the P-T limit cooldowns. For this transient, the test pressure and temperature were 1.1 ksi and 167°F, respectively.

This transient is referred to as the 'LT40-100' transient in this document, and its frequency of occurrence is estimated at 1×10^{-3} events per year (based on the BTP 5-3 closure memo assessment [7]).

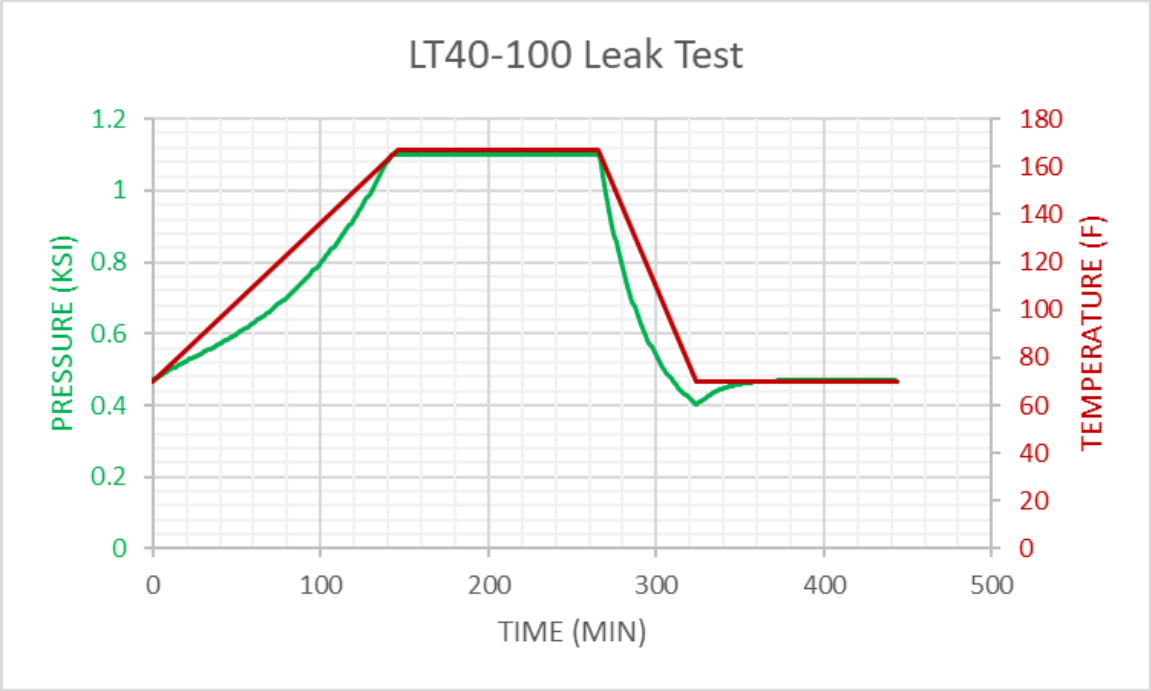

Figure 3-7: BWR LT40-100 Leak Test Transient Characteristics

3.1.2.7 LTA: Actual Leak Test

Figure 3-8 shows the pressure and temperature histories used for the actual leak test transient obtained from EPRI. For this transient, the leak test pressure and temperature were 1.0 ksi and 208.5°F, respectively.

This transient is referred to as the 'LTA' transient in this document, and its frequency of occurrence is estimated at 1.0 events per year.

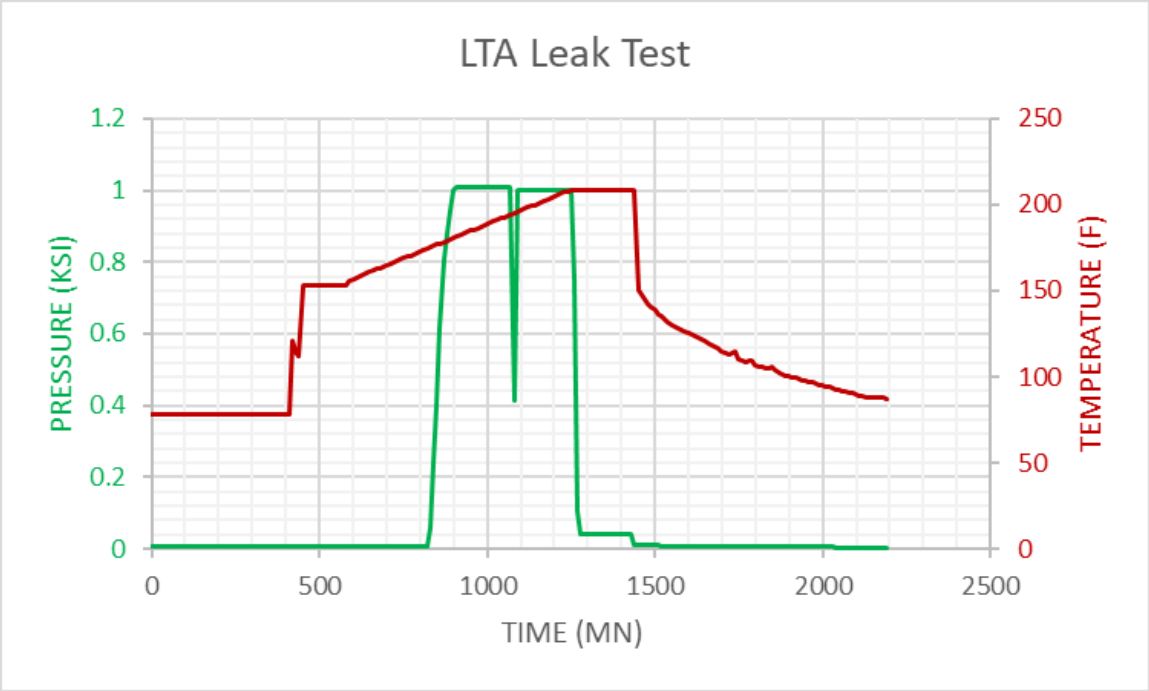

Figure 3-8: BWR LTA Leak Test Transient Characteristics

3.1.2.8 BWR Transient PT Curves

Figure 3-9 shows the PT curves for the 4 cooldown transients and 3 leak test transients modeled for the BWR RT_{NDT} shift sensitivity studies. Overall, the PT100-100 and PT50-50 transients are similar on a PT curve, and one would thus expect relatively similar trends for stress intensity factor histories, as can be seen by comparing Figure 3-12 with Figure 3-18 and Figure 3-15 with Figure 3-21. Furthermore, based on the relative positions of the PT curves, one would expect that for a ¼ T flaw (which is the postulated flaw for the creation of PT curves), the CPI and CPF values for the cooldown transients shown would be ranked as follows from highest to lowest: PT100-100, PT50-50, PT100-50, and finally S50. This is indeed generally the trend for ¼ T flaws, as described in Section 3.3. However, for shallow flaws, the trends are different, and the PT curves are not a good indication of the relative values of CPI and CPF for the cooldown transients.

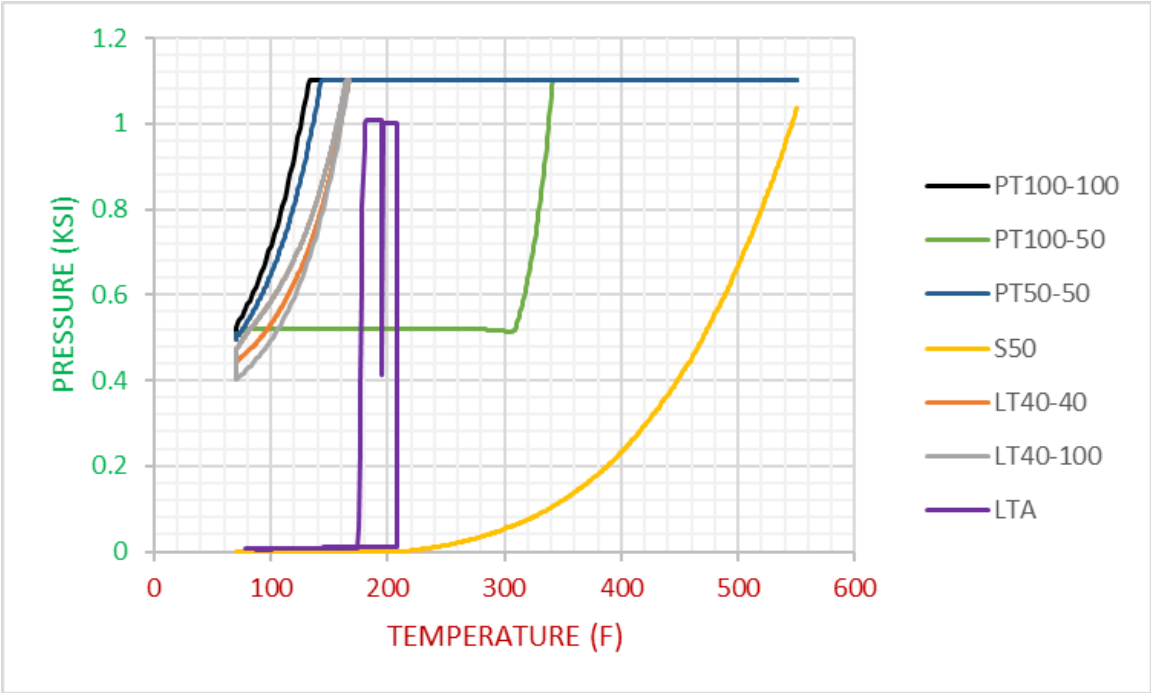

Figure 3-9: PT curves for the BWR cooldown and leak test transients modeled for the RTNDT shift sensitivity studies

3.1.3 Other FAVOR Simulation Input Information

Aside from the vessel and transient information, the following FAVOR simulation inputs were used:

Simulation Parameters	
Irradiation shift correlation choice	Regulatory Guide 1.99 Rev. 2
Normal operating coolant temperature	550°F
Plant operating time	72 EFPY
Ductile tearing model in IGA submodel	off
Ductile tearing initiation checks and reporting	off
Additional reports on CPI/CPF for major beltline regions	off
Flow stress for net-section plastic collapse failure model	80 ksi
Maximum value for K_{Ic} or K_{Ia}	200 ksi√in
Crack arrest model	High-constraint K_{Ia} (CCA specimens)
Resampling when advancing into new weld layer	on
Normalized crack depth corresponding to vessel failure	0.9
Fluence Sampling	
Multiplier for standard deviation of mean local fluence	0.118
Multiplier for standard deviation of local fluence	0.056
Weld Chemistry Sampling	
Standard deviation for Copper sampling in welds	0.167 wt%
Standard deviation for Nickel sampling in welds	0.162 wt%
Standard deviation for Phosphorus sampling in welds	0.0013 wt%
Plate Chemistry Sampling	
Standard deviation for Copper sampling in plates	0.0073 wt%
Standard deviation for Nickel sampling in plates	0.0244 wt%
Standard deviation for Phosphorus sampling in plates	0.0013 wt%

3.2 RT_{NDT} Shift Distribution

As was done for PWR analyses, the initial RT_{NDT} value was changed via input to the FAVOR embrittlement map to simulate the effects of changing the embrittlement correlation from RG 1.99, Rev. 2 to E900-15 without changing the FAVOR code. A compilation of $\mathrm{RT}_{\mathrm{NDT}}^{\mathrm{SHIFT}}$ values for the entire BWR fleet, based on embrittlement capsule data, was performed as part of the RG 1.99, Rev. 2 update effort. Figure 3-10 shows the distribution of RT_{NDT}^{SHIFT} values across the US BWR fleet, and Table 3-2 shows the values of RT_{NDT}^{SHIFT} corresponding to key percentiles (and vice versa).

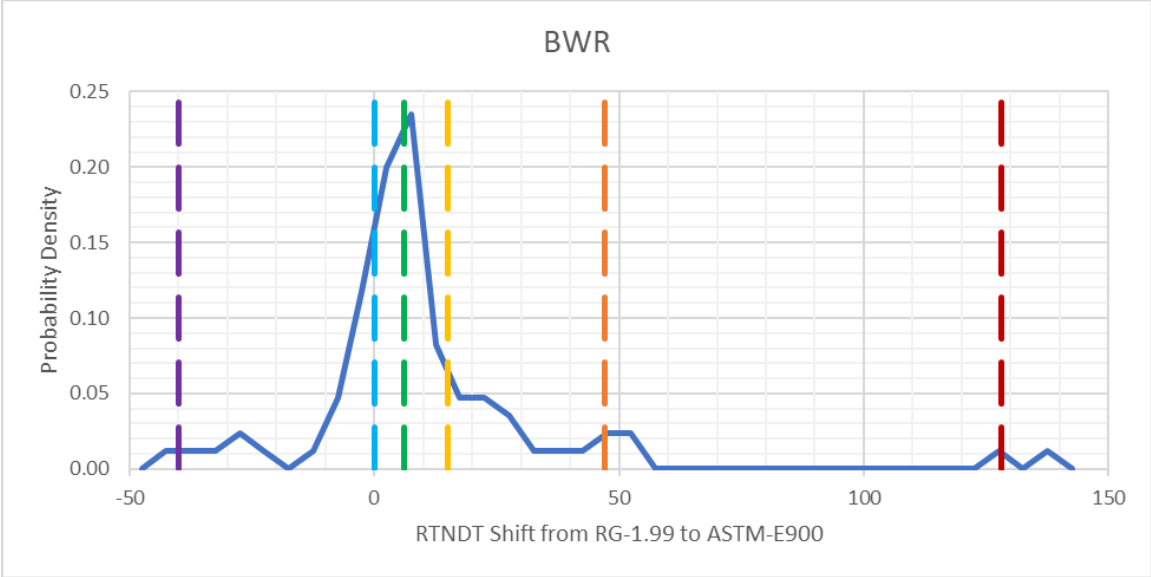

Figure 3-10: Probability Distribution of the BWR RT_{NDT} Shift as a Result of the Change from RG 1.99, Rev. 2 to E900-15 Embrittlement Correlations (all capsule data)

Table 3-2: BWR RTNDT Shift as a Result of the Change from RG 1.99, Rev. 2 to E900-15 Embrittlement Correlations at Percentiles of Interest for this Study (all capsule data)

Percentiles	RT_{NDT} Shift from RG 1.99, Rev. 2 to E900-15
0.005	**-40**
0.01	-39
0.05	-27
0.1	-8
0.25	**0**
0.5	**6**
0.75	**15**
0.9	31
0.95	**47**
0.99	**128**

Figure 3-10 and Table 3-2 show that for BWRs at 72 EFPY, changing the embrittlement correlation from RG 1.99, Rev. 2 to E900-15 would increase the adjusted reference temperature in most cases, since a 0°F

shift (i.e. no shift) corresponds to the 25th percentile for RT_{NDT}^{SHIFT}. However, the RT_{NDT}^{SHIFT} distribution for BWRs is narrower than that reported for PWRs in 2.2, such that the median is only 6°F and the upper 99th percentile is 128°F.

It is important to point out that considering all available capsule does not provide the most accurate picture of the actual material embrittlement in the US fleet, because some capsules pulled early in the reactor life and for which data has been extrapolated can result in large errors in the actual embrittlement of reactor materials. A more accurate method may consist of filtering the capsule data to only keep the fluence capsule data for the longest actual irradiation time for each reactor in the fleet. This reduces extrapolation error and results in a far more accurate picture of the material embrittlement for the vessels in the US fleet.

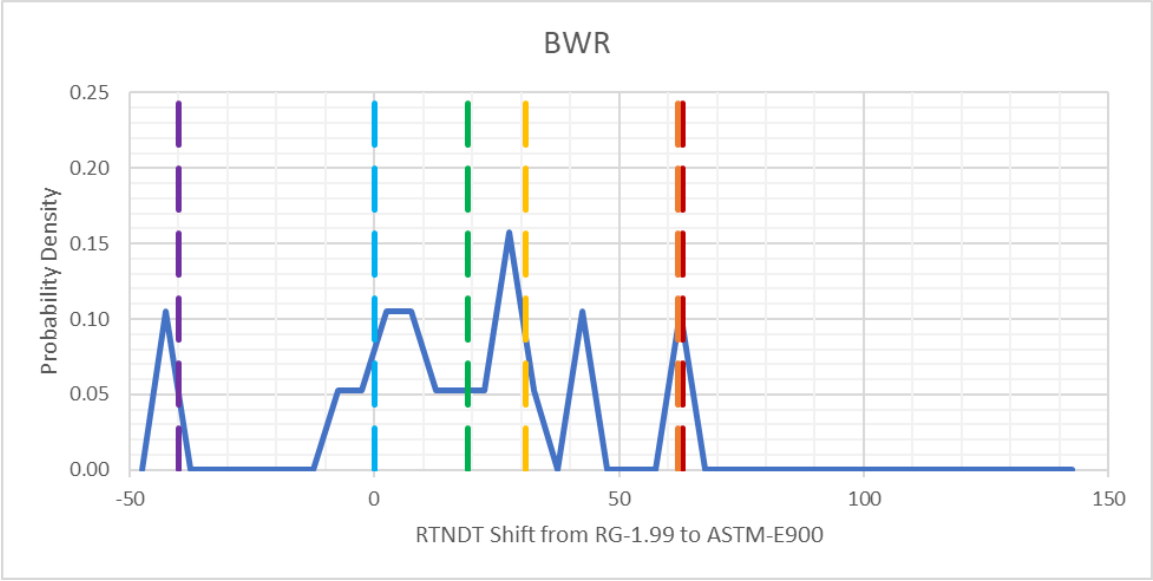

Figure 3-11: Probability Distribution of the BWR RT_{NDT} Shift as a Result of the Change from RG 1.99, Rev. 2 to E900-15 Embrittlement Correlations (filtered capsule data)

Table 3-3: BWR RT_{NDT} Shift as a Result of the Change from RG 1.99, Rev. 2 to E900-15 Embrittlement Correlations at Percentiles of Interest for this Study (filtered capsule data)

Percentiles	RT_{NDT} Shift from RG 1.99, Rev. 2 to E900-15
0.01	-50
0.05	-44
0.06	**-40**
0.1	-14
0.17	**0**
0.25	3
0.5	**19**
0.75	**31**
0.9	48
0.95	**62**
0.99	**63**

Figure 3-11 and Table 3-3 show that when considering only the highest fluence capsule for each reactor, the RT_{NDT}^{SHIFT} distribution is narrower and shift downward, such that the 99th percentile is around 63°F.

3.3 Results

Probabilistic FAVOR runs were performed for the highlighted RT_{NDT}^{SHIFT} values from Table 3-2. The values chosen were -40°F, 0°F, followed by the 50th, 75th, 95th, and 99th percentile values, so as to cover the wide range of possible RT_{NDT}^{SHIFT} values (see Section 3.2). This section presents results for a BWR vessel containing a single flaw of aspect ratio equal to 6 and depths of 0.25 T and 0.04 T, for the transients described in Section 3.1.2.

3.3.1 PT100-100 Cooldown

3.3.1.1 ¼-T Flaw Results

The stress intensity factor history for a 0.25 T ID surface flaw subjected to the PT100-100 cooldown transient described in 3.1.2.1 is shown in Figure 3-12 for flaws with aspect ratios of 2, 6, 10 and infinity. The arrest toughness K_{Ia}, below which no crack growth initiation can occur, as well as the median fracture toughness K_{Ic}, are also shown. It is important to note that all probabilistic analyses were performed with a flaw of aspect ratio equal to 6. Figure 3-12 clearly shows that K increases initially while the pressure is held constant and the temperature decreases linearly at a rate of 100°F/hour, reaching a maximum around 250 minutes. One exception is for the flaw aspect ratio of 2, where the maximum is reached around 80 minutes and then K is held almost constant until the pressure drops at 250 minutes. Then, at 250 minutes, the sudden pressure drop is accompanied by a sudden drop in K values. Finally, at 288 minutes, when the temperature reaches 70°F and remains constant, the rate of decrease in K values diminishes and K versus time curves plateau at their minimum value.

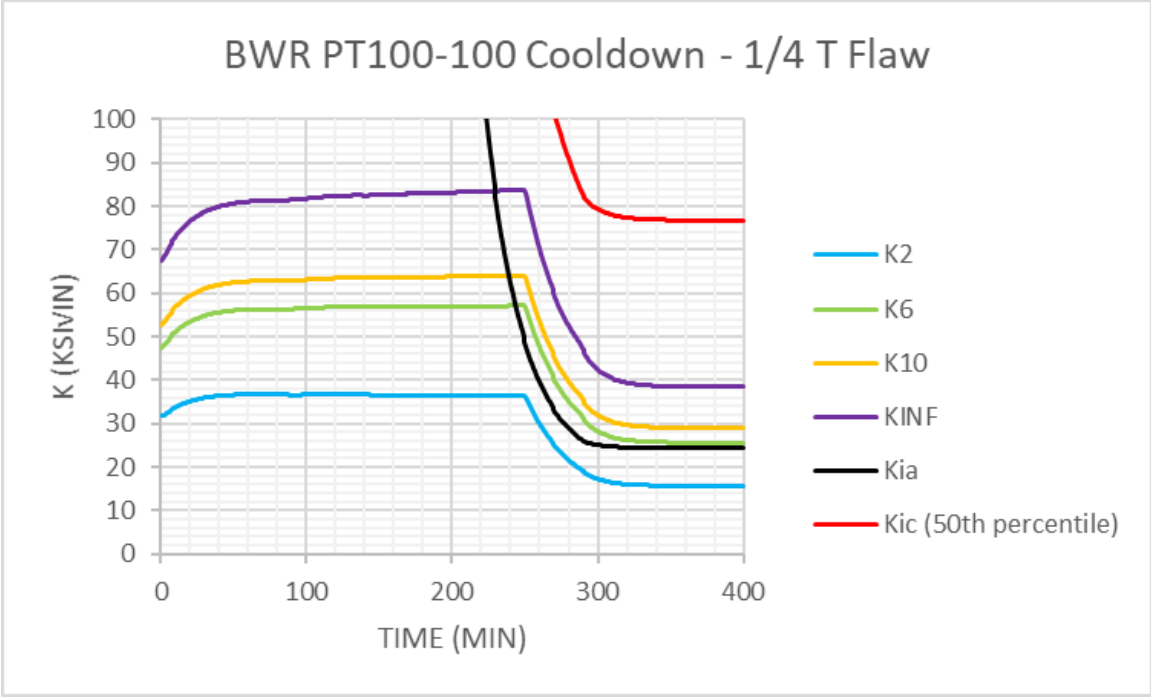

Figure 3-12: Stress Intensity Factor for the BWR PT100-100 Cooldown for a 0.25 T Flaw for Flaw Aspect Ratios of 2, 6, 10 and Infinity (note: in the legend, Kia is K_{Ia} and Kic is K_{Ic})

A probabilistic calculation assuming a 0.25 T flaw of aspect ratio equal to 6 and the PT100-100 cooldown resulted in a CPI of 1.6E-08 and a CPF of 2.3E-10 using the RG 1.99, Rev. 2 embrittlement correlation. This case corresponds to 0°F RT_{NDT} shift (i.e. 'no shift') for this transient. Figure 3-13 shows the calculated CPI and CPF as a function of the number of RPV trials in FAVOR. Although it looks like the CPF value may have sufficiently converged, the CPI value has not converged, but the order of magnitude of CPI is believed to be sufficiently accurate for the purposes of this study.

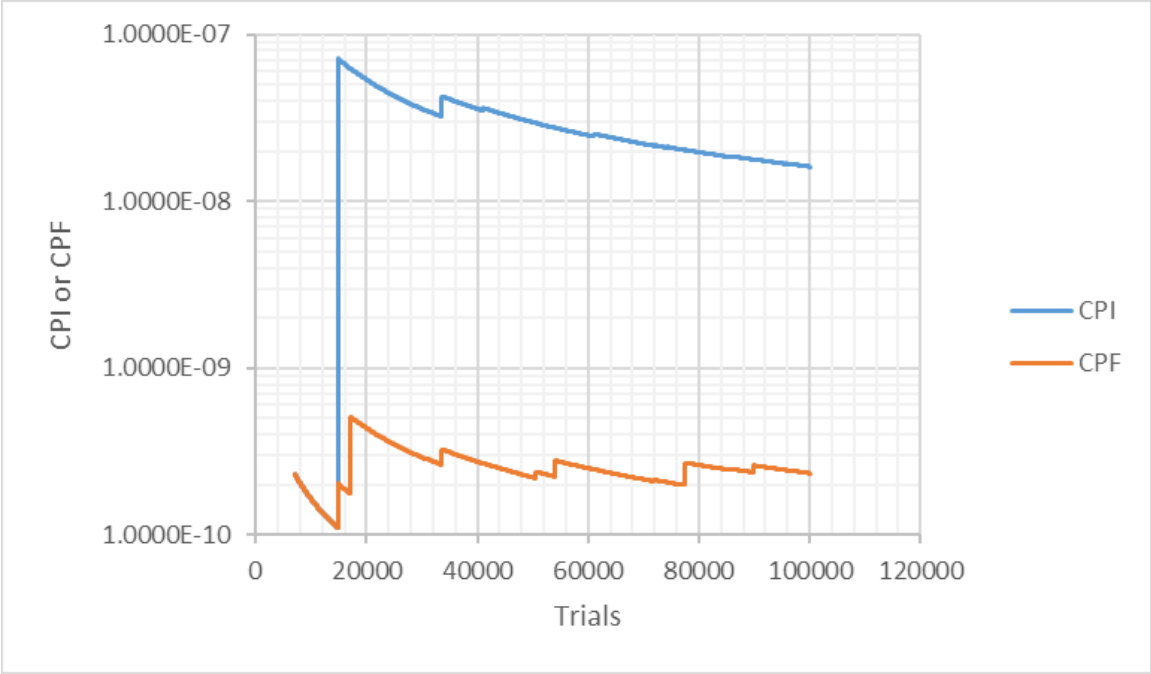

Figure 3-13: CPI and CPF versus Number of Trials for a 0.25 T Flaw in a BWR with 0°F RT_{NDT} Shift for the PT100-100 cooldown

To produce FAVOR runs corresponding to a single ID surface flaw of depth 0.25 T and aspect ratio 6, the VFLAW input format was used to specify the flaw population as follows:

- The surface flaw density was set to result in a single flaw of depth 0.25 T and aspect ratio 6, with zeros everywhere else
- The embedded weld flaw density was set to zero for all flaw depths and aspect ratios
- The embedded plate flaw density was set to zero for all flaw depths and aspect ratios

The PT100-100 cooldown determined using the RG 1.99, Rev. 2 embrittlement correlation (shown in Figure 3-2) was modeled for different values of RT_{NDT}^{SHIFT}, so as to understand the impact of shifting the RT_{NDT} for this transient. Of course, in actual safety analyses, the P-T limit would be adjusted as a function of the maximum ART in the vessel being analyzed, so a higher ART would reduce the allowed pressure, which In turn would result in significantly lower CPI and CPF than presented here for cases where RT_{NDT}^{SHIFT} is greater than 0°F.

Table 3-4: Calculated CPI and CPF for a 0.25 T Flaw of Aspect Ratio 6 in a BWR Subjected to the PT100-100 Cooldown

RTNDT Shift (°F)	CPI	CPI Converged?	CPF	CPF Converged?	TWCF
-40	3.9308E-13	NO	0.0000E+00	YES	0.0000E+00
0	1.6133E-08	NO	2.3416E-10	NO	2.3416E-17
6	3.0774E-08	YES	1.3237E-09	YES	1.3237E-16
15	8.1789E-08	YES	1.1164E-08	YES	1.1164E-15
47	3.3045E-06	YES	2.2012E-06	YES	2.2012E-13
128	1.0648E-03	YES	1.0060E-03	YES	1.0060E-10

Figure 3-14: CPI and CPF for a 0.25 T Flaw of Aspect Ratio 6 in a BWR Subjected to the PT100-100 Cooldown, as a Function of RT_{NDT} Shift from RG 1.99, Rev. 2 to E900-15 Embrittlement Correlations (open symbols linked by dashed lines represent results that are not statistically converged)

Table 3-4 and Figure 3-14 show the results of the probabilistic analyses for the 0.25 T flaw for the PT100-100 cooldown, as a function of RT_{NDT}^{SHIFT}. As expected, the CPI and CPF increase as RT_{NDT}^{SHIFT} increases. It should be noted that the analyses for $RT_{NDT}^{SHIFT} \leq 0°F$ did not statistically converge because of the very low calculated probabilities, but the CPI and CPF trend over the number of trials was beginning to stabilize, so the results are believed to be in the correct order of magnitude. Overall, it can be said that CPI and CPF for BWRs with a ¼ T flaw are about 1 or 2 orders of magnitude lower than for PWRs for the PT100-100 cooldown.

3.3.1.2 Shallow Flaw Results

The stress intensity factor history for a 0.04 T ID surface flaw subjected to the PT100-100 cooldown transient described in 3.1.2.1 is shown in Figure 3-15 for flaws with aspect ratios of 2, 6, 10 and infinity. The arrest toughness K_{Ia}, below which no crack growth initiation can occur, as well as the median fracture toughness K_{Ic}, are also shown. Figure 3-15 clearly shows that K increases initially while the pressure is held constant and the temperature decreases linearly at a rate of 100°F/hour. The maximum K values are reached at 250 minutes, just before the sudden pressure drop that results in a sudden drop in K values. During the subsequent pressure and temperature decrease, the K values reach a minimum sometime between 330 and 350 minutes, and then remain at this minimum value. It should be noted that a small inflection point can be observed in the decreasing K trend at 288 minutes, where the temperature reaches 70°F and subsequently remains there.

A probabilistic calculation assuming a 0.04 T flaw of aspect ratio equal to 6 and the PT100-100 cooldown resulted in a CPI of 1.5E-11 and a CPF of 4.0E-15 using the RG 1.99, Rev. 2 embrittlement correlation. This case corresponds to 0°F RT_{NDT} shift (i.e. 'no shift') for this transient. Figure 3-16 shows the calculated CPI and CPF as a function of the number of RPV trials in FAVOR, and one can see that the FAVOR calculations are not statistically converged after 100,000 trials. However, the values calculated are believed to have reached the correct order of magnitude.

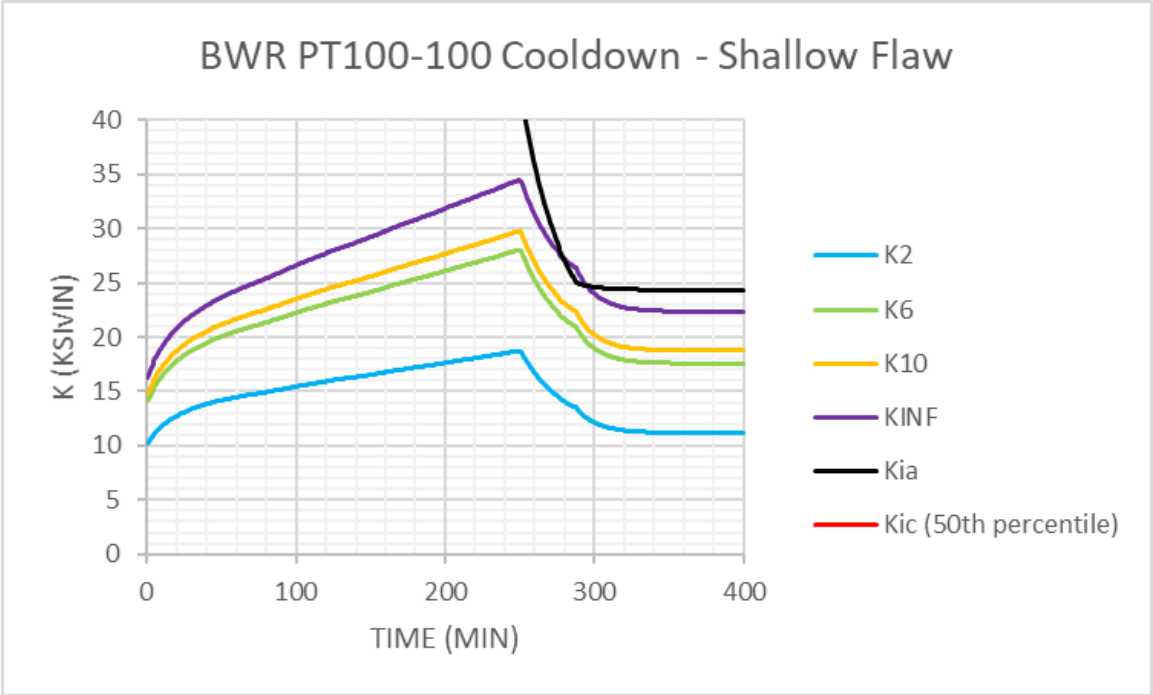

Figure 3-15 Stress Intensity Factor for the BWR PT100-100 Cooldown for 0.04 T Flaw for Flaw Aspect Ratios of 2, 6, 10 and Infinity (note: in the legend, Kia is K_{Ia} and Kic is K_{Ic})

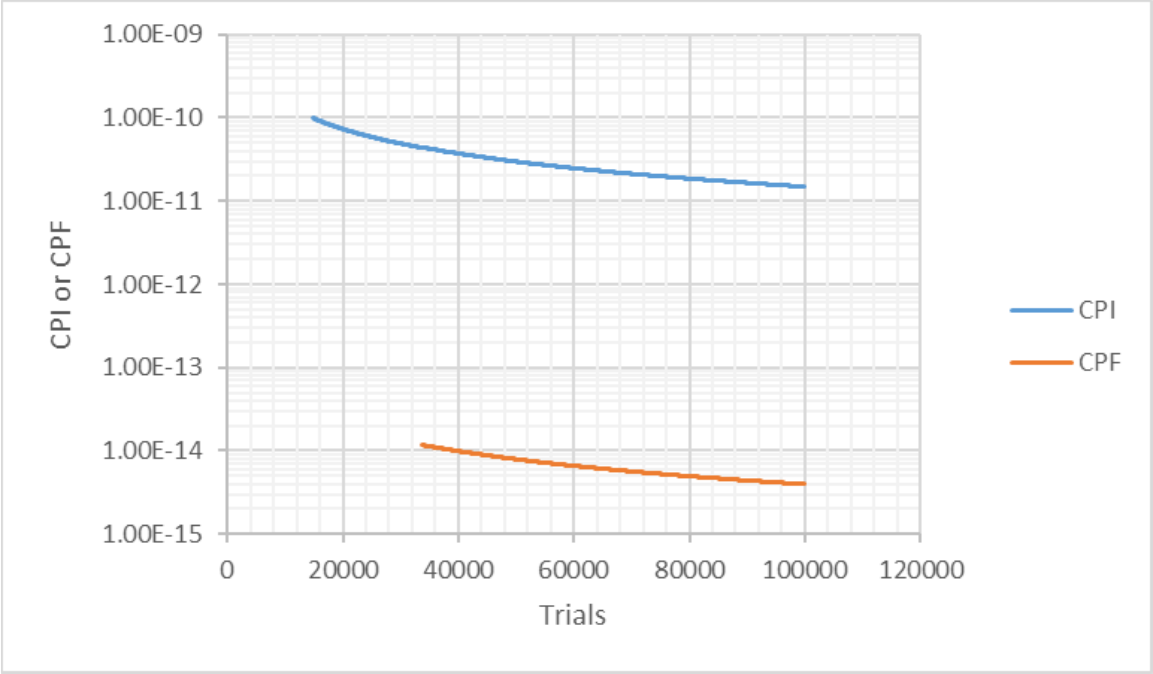

Figure 3-16: CPI and CPF versus Number of Trials for a 0.04 T Flaw in a BWR with 0°F RT_{NDT} Shift for the PT100-100 cooldown t

To produce FAVOR runs corresponding to a single ID surface flaw of depth 0.04 T and aspect ratio 6, the VFLAW input format was used to specify the flaw population as follows:

- The surface flaw density was set to result in a single flaw of depth 0.04 T and aspect ratio 6, with zeros everywhere else
- The embedded weld flaw density was set to zero for all flaw depths and aspect ratios
- The embedded plate flaw density was set to zero for all flaw depths and aspect ratios

The same PT100-100 cooldown determined using the RG 1.99, Rev. 2 embrittlement correlation for a 0.25 T flaw (shown in Figure 3-2) was modeled for different values of RT_{NDT}^{SHIFT}, so as to understand the impact of shifting the RT_{NDT} for this transient. That is, a new P-T limit was not calculated for a 0.04 T shallow flaw, but was instead calculated using current practice based on ASME Section XI, Appendix G, which requires analysis based on a 0.25 T flaw. Furthermore, as for the 0.25 T case, in actual safety analyses, the P-T limit would be adjusted as a function of the maximum ART in the vessel being analyzed, which would result in a different CPI and CPF than presented here. If the P-T limit was recalculated for each RT_{NDT}^{SHIFT} value, the shallow flaw effect makes it difficult to predict a priori whether the CPI and CPF values would move up or down.

Table 3-5 and Figure 3-17 show the results of the probabilistic analyses for the 0.04 T flaw for the PT100-100 cooldown, as a function of RT_{NDT}^{SHIFT}. As expected, the CPI and CPF increase as RT_{NDT}^{SHIFT} increases. It should be noted that the analyses for $RT_{NDT}^{SHIFT} < 47°F$ did not statistically converge because of the very low calculated probabilities, but the CPI and CPF trend over the number of trials was beginning to stabilize, so the results are believed to be in the correct order of magnitude. Overall, it can be said that CPI and CPF for BWRs with a 0.04 T flaw are at least 2 orders of magnitude lower than for PWRs for the PT100-100 cooldown.

Table 3-5: Calculated CPI and CPF for a 0.04 T Flaw of Aspect Ratio 6 in a BWR Subjected to the PT100-100 Cooldown

RTNDT Shift (°F)	CPI	CPI Converged?	CPF	CPF Converged?	TWCF
-40	0.0000E+00	Maybe	0.0000E+00	Maybe	0.0000E+00
0	1.4841E-11	NO	3.9582E-15	NO	3.9582E-22
6	4.5757E-11	NO	2.2927E-13	NO	2.2927E-20
15	1.6055E-10	NO	2.3249E-12	NO	2.3249E-19
47	4.0525E-09	YES	2.3711E-10	YES	2.3711E-17
128	7.2475E-07	YES	1.8924E-07	YES	1.8924E-14

Figure 3-17: CPI and CPF for a 0.04 T Flaw of Aspect Ratio 6 in a BWR Subjected to the PT100-100 Cooldown, as a Function of RT_{NDT} Shift from RG 1.99, Rev. 2 to E900-15 Embrittlement Correlations (open symbols linked by dashed lines represent results that are not statistically converged)

3.3.2 PT50-50 Cooldown

3.3.2.1 ¼-T Flaw Results

The stress intensity factor history for a 0.25 T ID surface flaw subjected to the PT50-50 cooldown transient described in 3.1.2.2 is shown in Figure 3-18 for flaws with aspect ratios of 2, 6, 10 and infinity. The arrest toughness K_{Ia}, below which no crack growth initiation can occur, as well as the median fracture toughness K_{Ic}, are also shown. It is important to note that all probabilistic analyses were performed with a flaw of aspect ratio equal to 6. Figure 3-18 clearly shows that K increases initially while the pressure is held constant and the temperature decreases linearly at a rate of 50°F/hour, reaching a maximum around 488 minutes. Then, at 488 minutes, the sudden pressure drop is accompanied by a sudden drop in K values. Finally, at 576 minutes, when the temperature reaches 70°F and remains constant, the rate of decrease in K values diminishes and K versus time curves plateau at their minimum value.

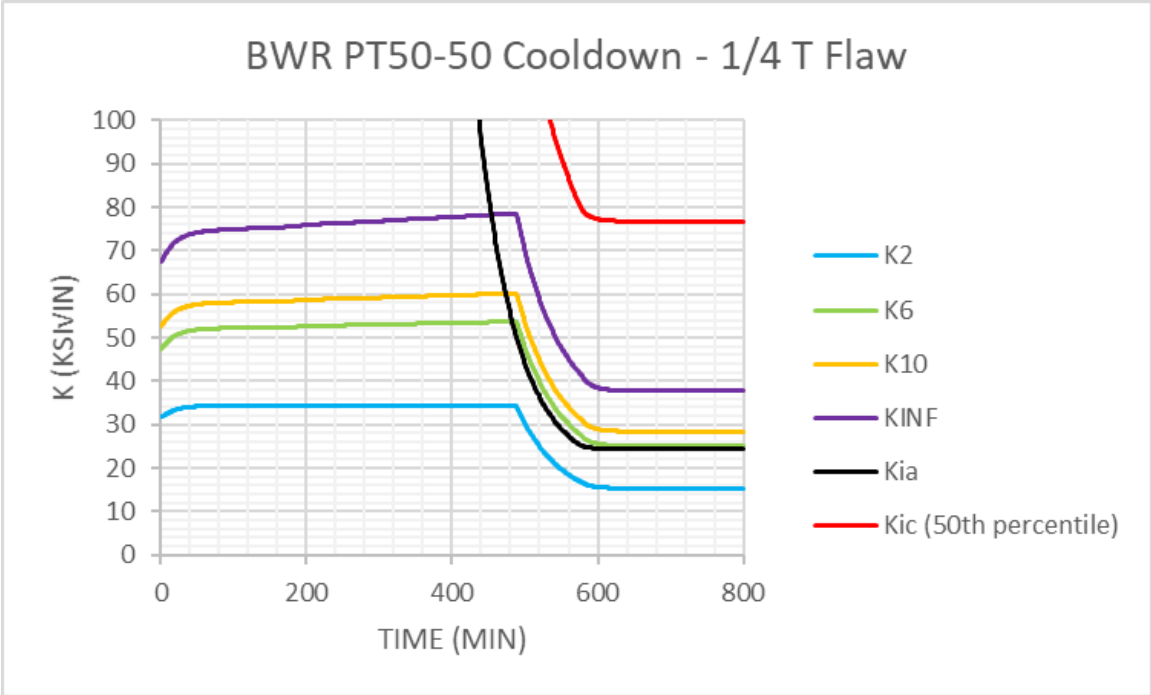

Figure 3-18: Stress Intensity Factor for the BWR PT50-50 Cooldown for a 0.25 T Flaw for Flaw Aspect Ratios of 2, 6, 10 and Infinity (note: in the legend, Kia is K_{Ia} and Kic is K_{Ic})

A probabilistic calculation assuming a 0.25 T flaw of aspect ratio equal to 6 and the PT50-50 cooldown resulted in a CPI of 2.3E-09 and a CPF of 2.0E-14 using the RG 1.99, Rev. 2 embrittlement correlation. This case corresponds to 0°F RT_{NDT} shift (i.e. 'no shift') for this transient. Figure 3-19 shows the calculated CPI and CPF as a function of the number of RPV trials in FAVOR. The CPI and CPF values have not converged, but the order of magnitude is believed to be sufficiently accurate for the purposes of this study.

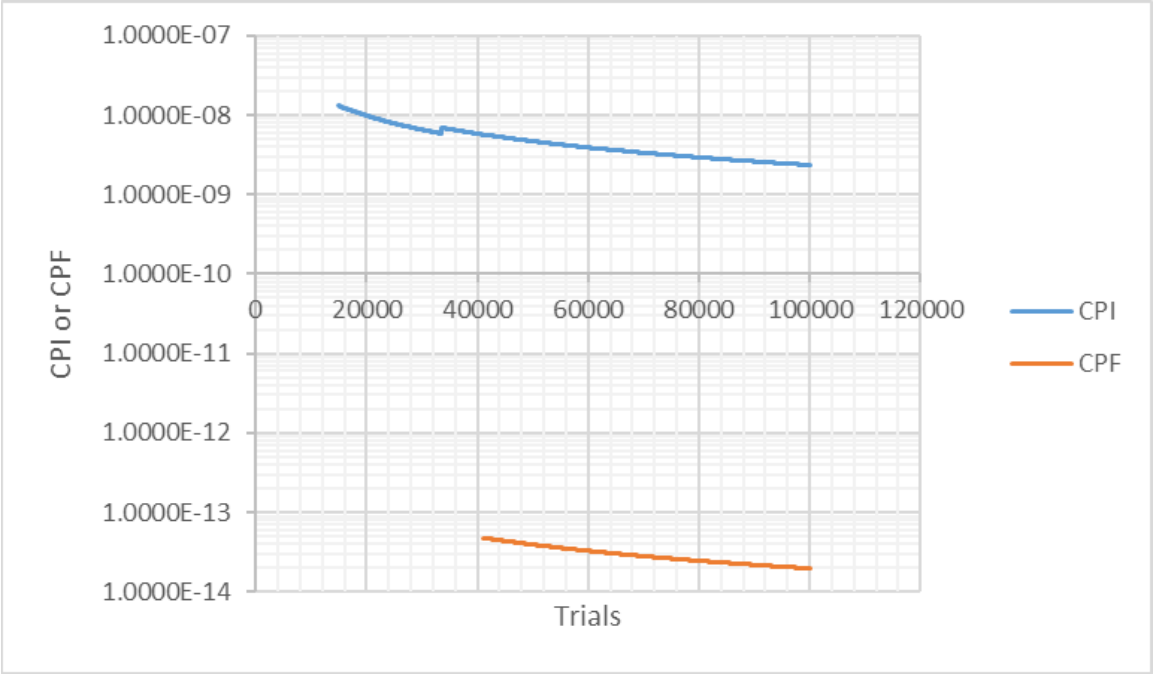

Figure 3-19: CPI and CPF versus Number of Trials for a 0.25 T Flaw in a BWR with 0°F RT_{NDT} Shift for the PT50-50 cooldown

To produce FAVOR runs corresponding to a single ID surface flaw of depth 0.25 T and aspect ratio 6, the VFLAW input format was used to specify the flaw population as follows:

- The surface flaw density was set to result in a single flaw of depth 0.25 T and aspect ratio 6, with zeros everywhere else
- The embedded weld flaw density was set to zero for all flaw depths and aspect ratios
- The embedded plate flaw density was set to zero for all flaw depths and aspect ratios

The same PT50-50 cooldown following the P-T limit determined using the RG 1.99, Rev. 2 embrittlement correlation (shown in Figure 3-3) was modeled for different values of RT_{NDT}^{SHIFT}, so as to understand the impact of shifting the RT_{NDT} for this transient. Of course, in actual safety analyses, the P-T limit would be adjusted as a function of the maximum ART in the vessel being analyzed, so a higher ART would reduce the allowed pressure, which In turn would result in significantly lower CPI and CPF than presented here for cases where RT_{NDT}^{SHIFT} is greater than 0°F.

Table 3-6: Calculated CPI and CPF for a 0.25 T Flaw of Aspect Ratio 6 in a BWR Subjected to the PT50-50 Cooldown

RTNDT Shift (°F)	CPI	CPI Converged?	CPF	CPF Converged?	TWCF
-40	0.0000E+00	YES	0.0000E+00	YES	0.0000E+00
0	2.3475E-09	NO	1.9693E-14	NO	1.9693E-21
6	4.7785E-09	NO	1.2400E-12	NO	1.2400E-19
15	1.2570E-08	NO	1.0564E-10	YES	1.0564E-17
47	3.6727E-07	YES	1.2292E-07	YES	1.2292E-14
128	2.3713E-04	YES	2.1340E-04	YES	2.1340E-11

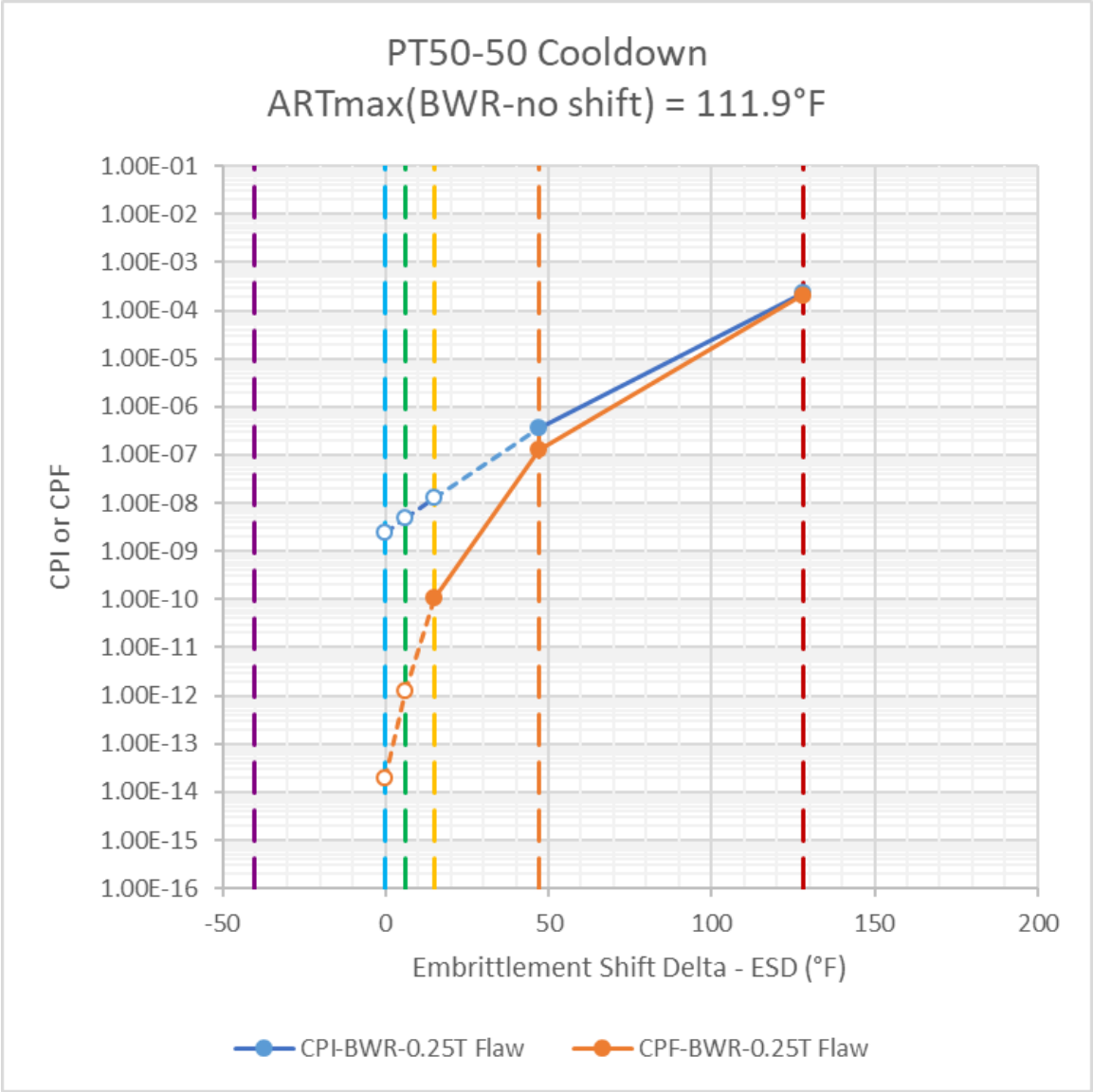

Figure 3-20: CPI and CPF for a 0.25 T Flaw of Aspect Ratio 6 in a BWR Subjected to the PT50-50 Cooldown at the P-T Limit, as a Function of RT_{NDT} Shift from RG 1.99, Rev. 2 to E900-15 Embrittlement Correlations (open symbols linked by dashed lines represent results that are not statistically converged)

Table 3-6 and Figure 3-20 show the results of the probabilistic analyses for the 0.25 T flaw for the PT50-50 cooldown, as a function of RT_{NDT}^{SHIFT}. As expected, the CPI and CPF increase as RT_{NDT}^{SHIFT} increases. It should be noted that the analyses with $RT_{NDT}^{SHIFT} \leq 15°F$ and with $RT_{NDT}^{SHIFT} \leq 6°F$ did not statistically converge, respectively for CPI and CPF, because of the very low calculated probabilities. However, the CPI and CPF trend over the number of trials was beginning to stabilize, so the results are believed to be in the correct order of magnitude. Overall, it can be said that CPI and CPF for BWRs with a ¼ T flaw are at least 1 order of magnitude lower than for PWRs for the PT50-50 cooldown.

3.3.2.2 Shallow Flaw Results

The stress intensity factor history for a 0.04 T ID surface flaw subjected to the PT50-50 cooldown transient described in 3.1.2.2 is shown in Figure 3-21 for flaws with aspect ratios of 2, 6, 10 and infinity. The arrest toughness K_{Ia}, below which no crack growth initiation can occur, as well as the median fracture toughness K_{Ic}, are also shown. Figure 3-21 clearly shows that K increases initially while the pressure is held constant and the temperature decreases linearly at a rate of 50°F/hour. The maximum K values are reached at 488 minutes, just before the sudden pressure drop that results in a sudden drop in K values. During the subsequent pressure and temperature decrease, the K values reach a minimum sometime between 640 and 660 minutes, and then remain at this minimum value. It should be noted that a small inflection point can be observed in the decreasing K trend at 576 minutes, where the temperature reaches 70°F and subsequently remains there.

A probabilistic calculation assuming a 0.04 T flaw of aspect ratio equal to 6 and the 100°F/hour P-T limit cooldown resulted in a CPI and CPF of zero using the RG 1.99, Rev. 2 embrittlement correlation. This case corresponds to 0°F RT_{NDT} shift (i.e. 'no shift') for this transient.

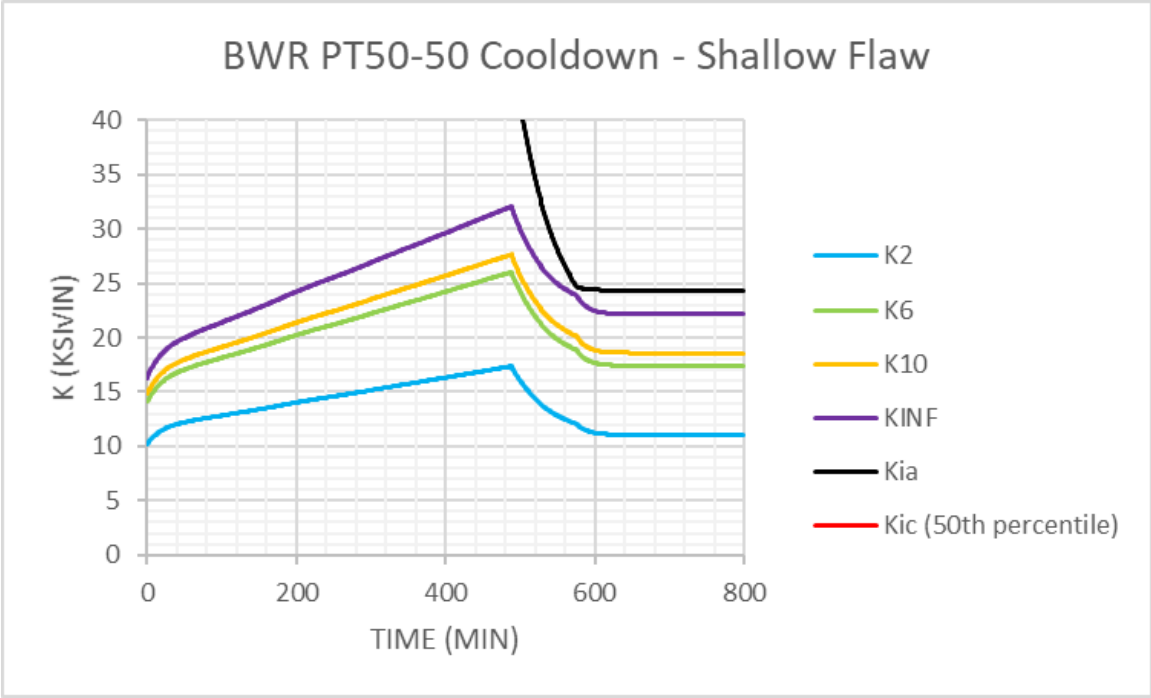

Figure 3-21 Stress Intensity Factor for the BWR PT50-50 Cooldown for a 0.04 T Flaw for Flaw Aspect Ratios of 2, 6, 10 and Infinity (note: in the legend, Kia is K_{Ia} and Kic is K_{Ic})

To produce FAVOR runs corresponding to a single ID surface flaw of depth 0.04 T and aspect ratio 6, the VFLAW input format was used to specify the flaw population as follows:

- The surface flaw density was set to result in a single flaw of depth 0.04 T and aspect ratio 6, with zeros everywhere else
- The embedded weld flaw density was set to zero for all flaw depths and aspect ratios
- The embedded plate flaw density was set to zero for all flaw depths and aspect ratios

The same PT50-50 cooldown following the P-T limit determined using the RG 1.99, Rev. 2 embrittlement correlation for a 0.25 T flaw (shown in Figure 3-3) was modeled for different values of RT_{NDT}^{SHIFT}, so as to understand the impact of shifting the RT_{NDT} for this transient. That is, a new P-T limit was not calculated for a 0.04 T shallow flaw, but was instead calculated using current practice based on ASME Section XI, Appendix G, which requires analysis based on a 0.25 T flaw. Furthermore, as for the 0.25 T case, in actual safety analyses, the P-T limit would be adjusted as a function of the maximum ART in the vessel being analyzed, which would result in a different CPI and CPF than presented here. If the P-T limit was recalculated for each RT_{NDT}^{SHIFT} value, the shallow flaw effect makes it difficult to predict a priori whether the CPI and CPF values would move up or down.

Table 3-7 and Figure 3-22 show the results of the probabilistic analyses for the 0.04 T flaw for the PT50-50 cooldown, as a function of RT_{NDT}^{SHIFT}. As expected, the CPI and CPF increase as RT_{NDT}^{SHIFT} increases. It should be noted that the analyses with $RT_{NDT}^{SHIFT} < 47°F$ did not statistically converge because of the very low calculated probabilities. However, the CPI and CPF trend over the number of trials was beginning to stabilize, so the results are believed to be in the correct order of magnitude. Overall, it can be said that CPI and CPF for BWRs with a 0.04 T flaw are several orders of magnitude lower than for PWRs for the PT50-50 cooldown.

Table 3-7: Calculated CPI and CPF for a 0.04 T Flaw of Aspect Ratio 6 in a BWR Subjected to the PT50-50 Cooldown

RTNDT Shift (°F)	CPI	CPI Converged?	CPF	CPF Converged?	TWCF
-40	0.0000E+00	YES	0.0000E+00	YES	0.0000E+00
0	0.0000E+00	YES	0.0000E+00	YES	0.0000E+00
6	0.0000E+00	YES	0.0000E+00	YES	0.0000E+00
15	9.8045E-14	NO	0.0000E+00	YES	0.0000E+00
47	8.6349E-11	NO	1.6261E-12	NO	1.6261E-19
128	5.5078E-08	YES	8.2949E-09	YES	8.2949E-16

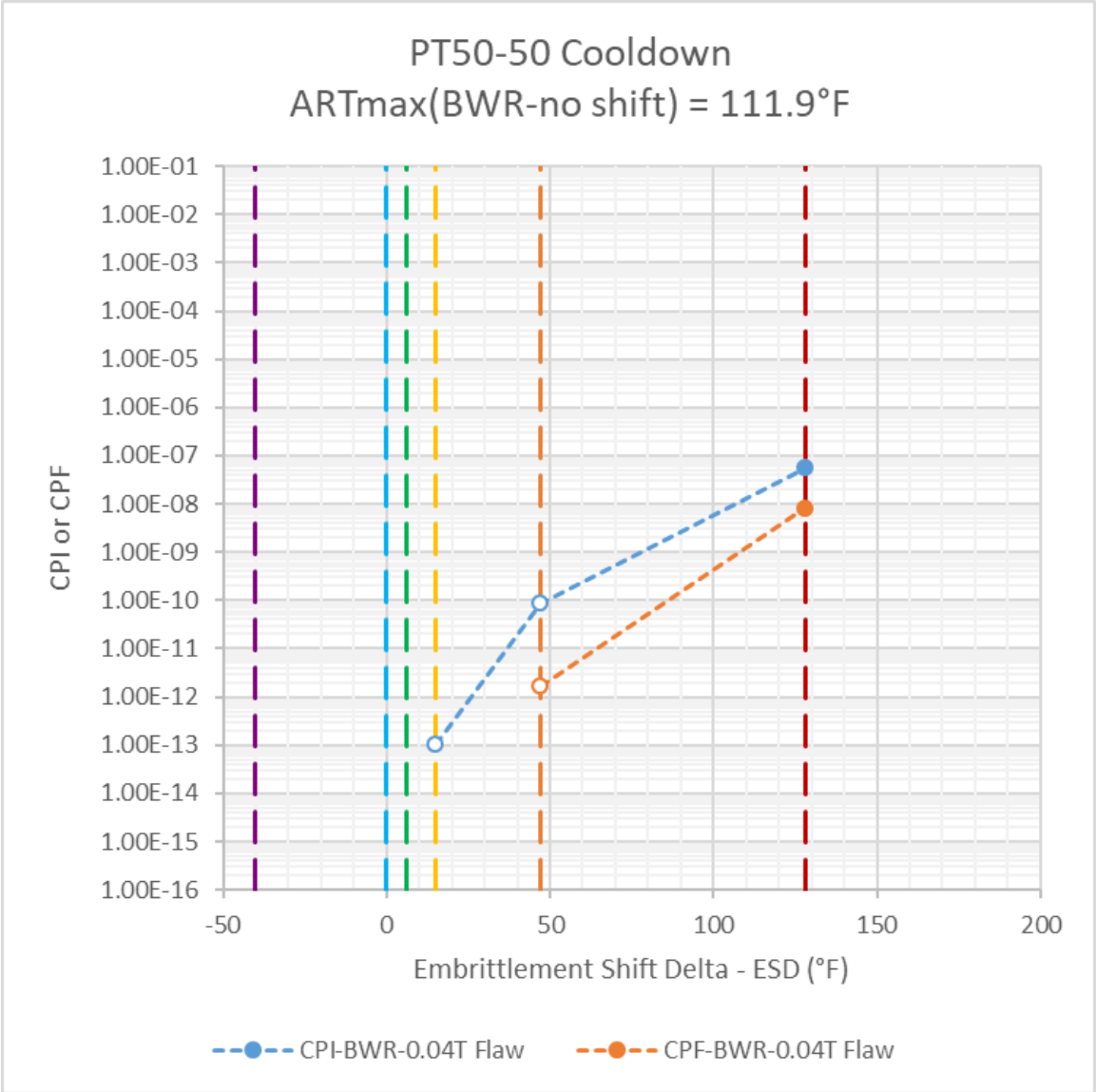

Figure 3-22: CPI and CPF for a 0.04 T Flaw of Aspect Ratio 6 in a BWR Subjected to the PT50-50 Cooldown, as a Function of RT_{NDT} Shift from RG 1.99, Rev. 2 to E900-15 Embrittlement Correlations (open symbols linked by dashed lines represent results that are not statistically converged)

3.3.3 PT100-50 Cooldown

3.3.3.1 ¼-T Flaw Results

The stress intensity factor history for a 0.25 T ID surface flaw subjected to the PT100-50 cooldown transient described in 3.1.2.3 is shown in Figure 3-23 for flaws with aspect ratios of 2, 6, 10 and infinity. The arrest toughness K_{Ia}, below which no crack growth initiation can occur, as well as the median fracture toughness K_{Ic}, are also shown. It is important to note that all probabilistic analyses were performed with a flaw of aspect ratio equal to 6. Figure 3-23 clearly shows that K increases initially while the pressure is held constant and the temperature decreases linearly at a rate of 50°F/hour, reaching a maximum between around 250 minutes. Then, at 250 minutes, the sudden pressure drop is accompanied by a sudden drop in K values. The rate of decrease in K is high but at 288 minutes, when the pressure stabilizes, K begins to increase again as a result of the continued temperature decrease. Finally, at 576 minutes, when the temperature reaches 70°F and remains constant, K begins to decrease again as the portion of K due to thermal stresses decreases. After this point, the rate of decrease in K values slowly diminishes until the end of the calculation.

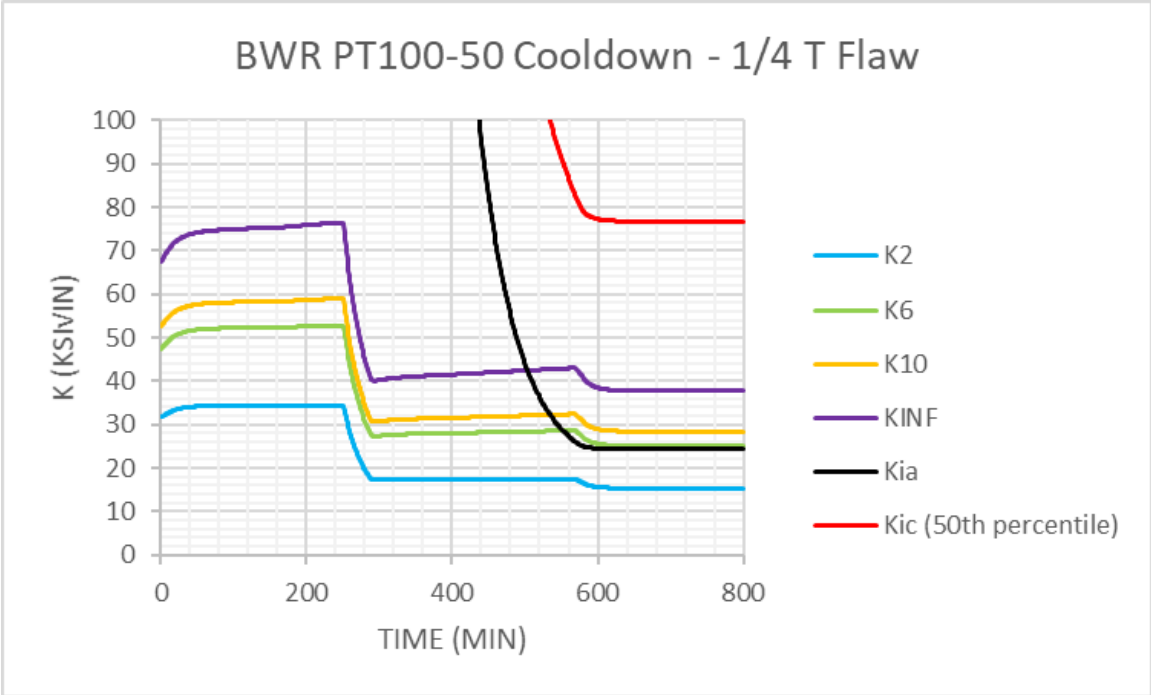

Figure 3-23: Stress Intensity Factor for the BWR PT100-50 Cooldown for a 0.25 T Flaw for Flaw Aspect Ratios of 2, 6, 10 and Infinity (note: in the legend, Kia is K_{Ia} and Kic is K_{Ic})

A probabilistic calculation assuming a 0.25 T flaw of aspect ratio equal to 6 and the PT100-50 cooldown resulted in a CPI and a CPF of zero using the RG 1.99, Rev. 2 embrittlement correlation. This case corresponds to 0°F RT_{NDT} shift (i.e. 'no shift') for this transient.

The same PT100-50 cooldown (shown in Figure 3-4) was modeled for different values of RT_{NDT}^{SHIFT}, so as to understand the impact of shifting the RT_{NDT} for this transient. Of course, in actual safety analyses, the P-T limit would be adjusted as a function of the maximum ART in the vessel being analyzed, so a higher

ART would reduce the allowed pressure, which In turn would result in lower CPI and CPF than presented here for cases where RT_{NDT}^{SHIFT} is greater than 0°F.

Table 3-8 shows the results of the probabilistic analyses for the 0.25 T flaw for the PT100-50 cooldown, as a function of RT_{NDT}^{SHIFT}. Interestingly, regardless of the RT_{NDT}^{SHIFT} value, the CPI and CPF predictions were equal to zero.

Table 3-8: Calculated CPI and CPF for a 0.25 T Flaw of Aspect Ratio 6 in a BWR Subjected to the PT100-50 Cooldown

RTNDT Shift (°F)	CPI	CPI Converged?	CPF	CPF Converged?	TWCF
-40	0.0000E+00	YES	0.0000E+00	YES	0.0000E+00
0	0.0000E+00	YES	0.0000E+00	YES	0.0000E+00
6	0.0000E+00	YES	0.0000E+00	YES	0.0000E+00
15	0.0000E+00	YES	0.0000E+00	YES	0.0000E+00
47	0.0000E+00	YES	0.0000E+00	YES	0.0000E+00
128	0.0000E+00	YES	0.0000E+00	YES	0.0000E+00

3.3.3.2 Shallow Flaw Results

The stress intensity factor history for a 0.04 T ID surface flaw subjected to the PT100-50 cooldown transient described in 3.1.2.3 is shown in Figure 3-24 for flaws with aspect ratios of 2, 6, 10 and infinity. The arrest toughness K_{Ia}, below which no crack growth initiation can occur, as well as the median fracture toughness K_{Ic}, are also shown. Figure 3-24 clearly shows that K increases initially while the pressure is held constant and the temperature decreases linearly at a rate of 50°F/hour. The maximum K values are reached at 250 minutes, just before the sudden pressure drop that results in a sudden drop in K values. The rate of decrease in K is high but at 288 minutes, when the pressure stabilizes, K begins to increase again as a result of the continued temperature decrease. Finally, at 576 minutes, when the temperature reaches 70°F and remains constant, K begins to decrease again as the portion of K due to thermal stresses decreases, resulting in a second peak in K values. After this point, the rate of decrease in K values slowly diminishes until the end of the calculation. The second peak is characteristic of shallow surface flaws that barely penetrate the base metal because these cracks are highly affected by the stresses due to the mismatch in thermal expansion coefficient between the cladding and the base metal.

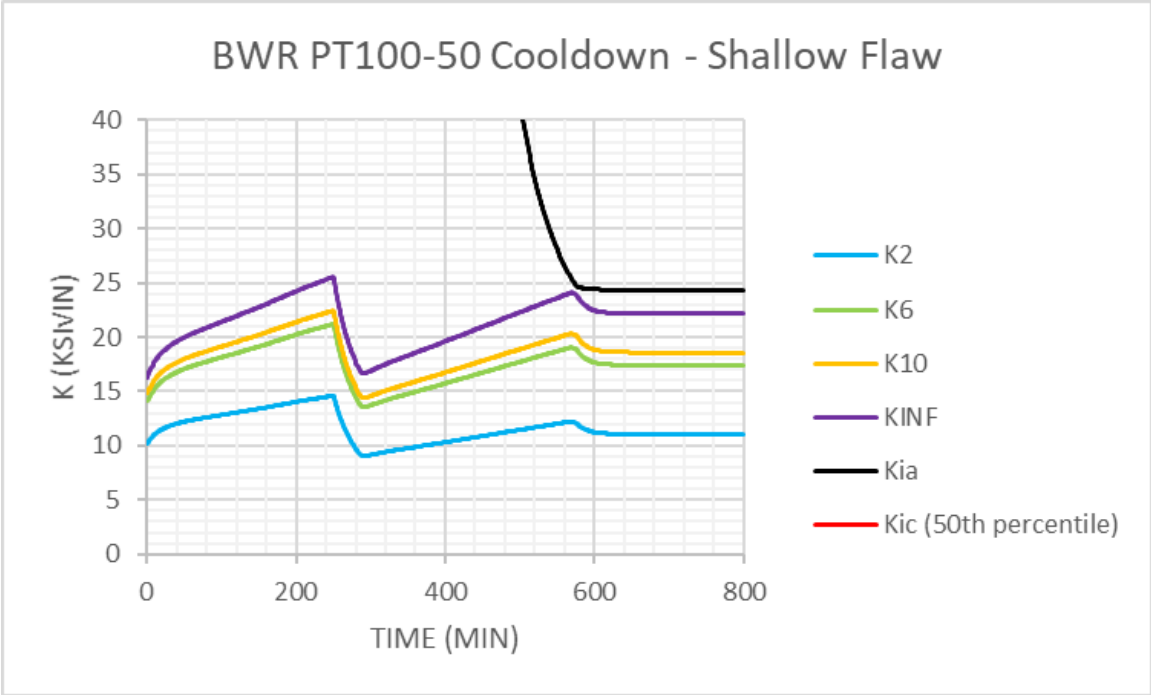

Figure 3-24: Stress Intensity Factor for the BWR PT100-50 Cooldown for a 0.04 T Flaw for Flaw Aspect Ratios of 2, 6, 10 and Infinity (note: in the legend, Kia is K_{Ia} and Kic is K_{Ic})

A probabilistic calculation assuming a 0.04 T flaw of aspect ratio equal to 6 and the PT100-50 cooldown resulted in a CPI and a CPF of zero using the RG 1.99, Rev. 2 embrittlement correlation. This case corresponds to 0°F RT_{NDT} shift (i.e. 'no shift') for this transient.

The same PT100-50 cooldown (shown in Figure 3-4) was modeled for different values of RT_{NDT}^{SHIFT}, so as to understand the impact of shifting the RT_{NDT} for this transient. That is, a new P-T limit was not calculated for a 0.04 T shallow flaw, but was instead calculated using current practice based on ASME Section XI, Appendix G, which requires analysis based on a 0.25 T flaw. Furthermore, as for the 0.25 T case, in actual safety analyses, the P-T limit would be adjusted as a function of the maximum ART in the vessel being analyzed, which would result in a different CPI and CPF than presented here. If the P-T limit was recalculated for each RT_{NDT}^{SHIFT} value, the shallow flaw effect makes it difficult to predict a priori whether the CPI and CPF values would move up or down.

Table 3-9 and Figure 3-25 show the results of the probabilistic analyses for the 0.04 T flaw for the PT100-50 cooldown, as a function of RT_{NDT}^{SHIFT}. As expected, the CPI increases as RT_{NDT}^{SHIFT} increases. CPF was always zero except for the highest value of RT_{NDT}^{SHIFT}. It should be noted that the analyses for $RT_{NDT}^{SHIFT} < 15°F$ did not statistically converge for CPI because of the very low calculated probabilities, but the CPI trend over the number of trials was beginning to stabilize, so the results are believed to be in the correct order of magnitude. Overall, it can be said that CPI and CPF for BWRs with a 0.04 T flaw are many orders of magnitude lower than for PWRs for the PT100-50 cooldown.

Table 3-9: Calculated CPI and CPF for a 0.04 T Flaw of Aspect Ratio 6 in a BWR Subjected to the PT100-50 Cooldown

RTNDT Shift (°F)	CPI	CPI Converged?	CPF	CPF Converged?	TWCF
-40	0.0000E+00	YES	0.0000E+00	YES	0.0000E+00
0	0.0000E+00	NO	0.0000E+00	YES	0.0000E+00
6	2.2204E-21	NO	0.0000E+00	YES	0.0000E+00
15	4.0261E-15	NO	0.0000E+00	YES	0.0000E+00
47	1.1199E-12	YES	0.0000E+00	YES	0.0000E+00
128	5.4778E-10	YES	9.5736E-13	YES	9.5736E-20

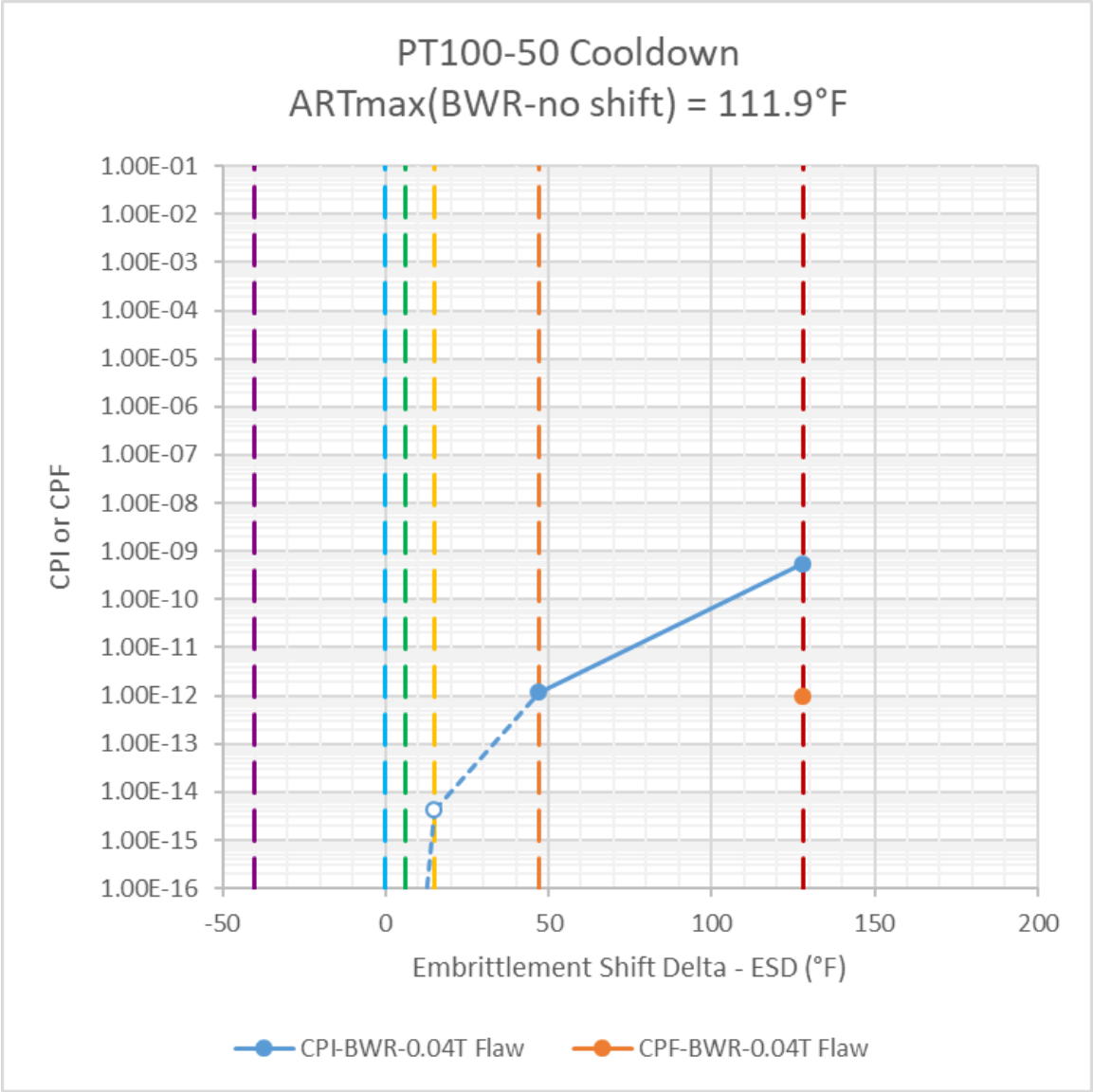

Figure 3-25: CPI and CPF for a 0.04 T Flaw of Aspect Ratio 6 in a BWR Subjected to the PT100-50 Cooldown, as a Function of RT_{NDT} Shift from RG 1.99, Rev. 2 to E900-15 Embrittlement Correlations (open symbols linked by dashed lines represent results that are not statistically converged)

3.3.4 S50 Cooldown

3.3.4.1 ¼-T Flaw Results

The stress intensity factor history for a 0.25 T ID surface flaw subjected to the 50°F/hour saturation cooldown transient described in 3.1.2.4 is shown in Figure 3-26 for flaws with aspect ratios of 2, 6, 10 and infinity. The arrest toughness K_{Ia}, below which no crack growth initiation can occur, as well as the median fracture toughness K_{Ic}, are also shown. It is important to note that all probabilistic analyses were performed with a flaw of aspect ratio equal to 6. Figure 3-26 shows that K decreases as both the pressure and the temperature decrease along the saturation curve. A local minimum is reached between 400 and 500 minutes, with a very small subsequent increase in K values between the time of the minimum and 576 minutes, at which point the temperature reaches 70°F and remains constant. After 576 minutes, K begins to decrease again as the portion of K due to thermal stresses decreases. After this point, the rate of decrease in K values slowly diminishes until the end of the calculation.

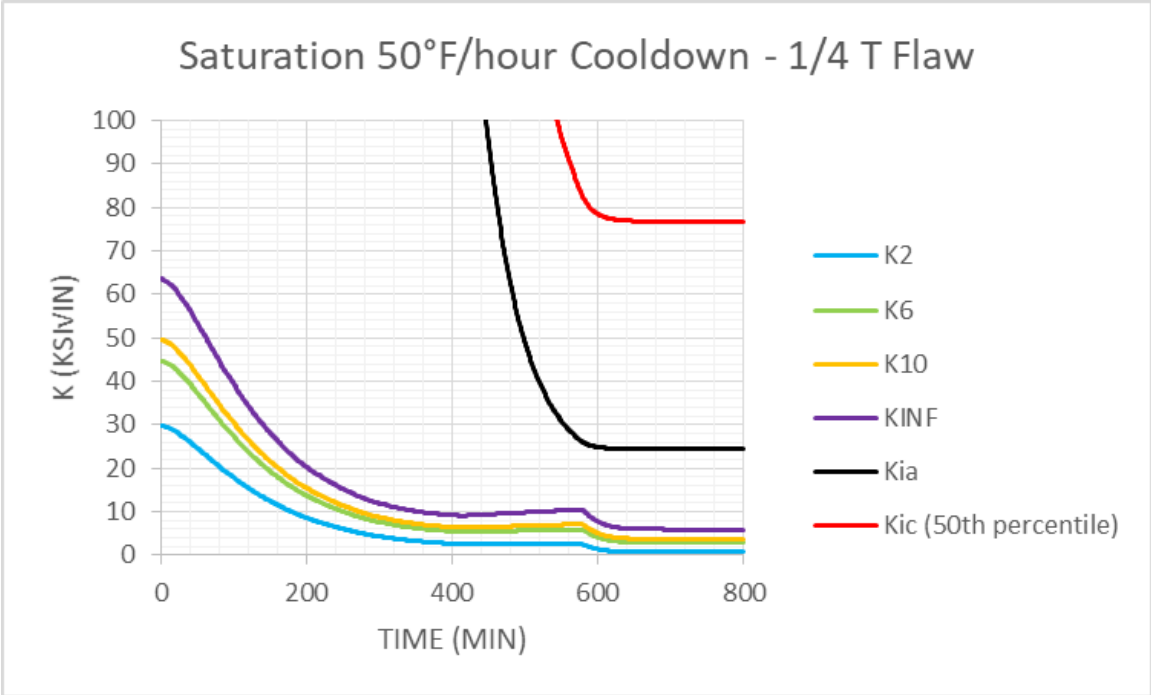

Figure 3-26: Stress Intensity Factor for BWR Saturation Cooldown for 0.25 T Flaw for Flaw Aspect Ratios of 2, 6, 10 and Infinity (note: in the legend, Kia is K_{Ia} and Kic is K_{Ic})

A probabilistic calculation assuming a 0.25 T flaw of aspect ratio equal to 6 and the 50°F/hour saturation cooldown resulted in a CPI and a CPF of zero using the RG 1.99, Rev. 2 embrittlement correlation. This case corresponds to 0°F RT_{NDT} shift (i.e. 'no shift') for this transient.

The same 50°F/hour saturation cooldown (shown in Figure 3-5) was modeled for different values of RT_{NDT}^{SHIFT}, so as to understand the impact of shifting the RT_{NDT} for this transient. Table 3-10 shows the results of the probabilistic analyses for the 0.25 T flaw for the 50°F/hour saturation cooldown, as a function of RT_{NDT}^{SHIFT}. All values of calculated CPI and CPF were equal to zero.

Table 3-10: Calculated CPI and CPF for a 0.25 T Flaw of Aspect Ratio 6 in a BWR Subjected to Saturation Cooldown

RTNDT Shift (°F)	CPI	CPI Converged?	CPF	CPF Converged?	TWCF
-40	0.0000E+00	YES	0.0000E+00	YES	0.0000E+00
0	0.0000E+00	YES	0.0000E+00	YES	0.0000E+00
6	0.0000E+00	YES	0.0000E+00	YES	0.0000E+00
15	0.0000E+00	YES	0.0000E+00	YES	0.0000E+00
47	0.0000E+00	YES	0.0000E+00	YES	0.0000E+00
128	0.0000E+00	YES	0.0000E+00	YES	0.0000E+00

3.3.4.2 Shallow Flaw Results

The stress intensity factor history for a 0.04 T ID surface flaw subjected to the P-T limit cooldown transient described in 3.1.2.4 is shown in Figure 3-27 for flaws with aspect ratios of 2, 6, 10 and infinity. The arrest toughness K_{Ia}, below which no crack growth initiation can occur, as well as the median fracture toughness K_{Ic}, are also shown. Figure 3-27 shows that K increases slightly from 0 to ~20 minutes, and then decreases as both the pressure and the temperature decrease along the saturation curve. A minimum is reached between 200 and 300 minutes, with a subsequent increase in K values between the time of the minimum and 576 minutes, at which point the temperature reaches 70°F and remains constant. A second peak in K values is observed at 576 minutes that can sometimes exceed the value of the first peak early in the transient. This second peak is characteristic of shallow surface flaws that barely penetrate the base metal because these cracks are highly affected by the stresses due to the mismatch in thermal expansion coefficient between the cladding and the base metal. After 576 minutes, the temperature is held constant at 70°F, and thus the thermal stresses and associated component of K decrease rapidly, hence there is a decrease in overall K values despite the constant pressure.

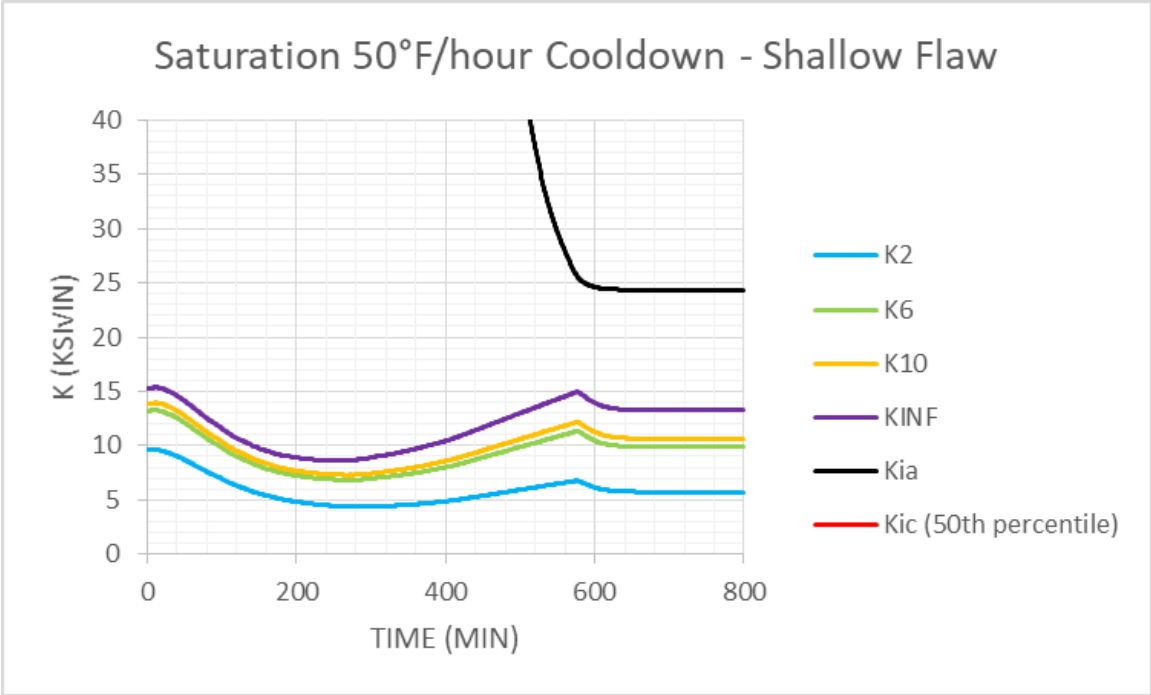

Figure 3-27: Stress Intensity Factor for BWR 50°F/hour Saturation Cooldown for 0.04 T Flaw for Flaw Aspect Ratios of 2, 6, 10 and Infinity (note: in the legend, Kia is K_{Ia} and Kic is K_{Ic})

A probabilistic calculation assuming a 0.04 T flaw of aspect ratio equal to 6 and the 50°F/hour saturation cooldown resulted in a CPI and a CPF of zero using the RG 1.99, Rev. 2 embrittlement correlation. This case corresponds to 0°F RT_{NDT} shift (i.e. 'no shift') for this transient.

The same 50°F/hour saturation cooldown (shown in Figure 3-5) was modeled for different values of RT_{NDT}^{SHIFT}, so as to understand the impact of shifting the RT_{NDT} for this transient. Table 3-11 shows the results of the probabilistic analyses for the 0.25 T flaw for the 50°F/hour saturation cooldown, as a function of RT_{NDT}^{SHIFT}. All values of calculated CPI and CPF were equal to zero.

Table 3-11: Calculated CPI and CPF for a 0.04 T Flaw of Aspect Ratio 6 in a BWR Subjected to a Saturation Cooldown

RTNDT Shift (°F)	CPI	CPI Converged?	CPF	CPF Converged?	TWCF
-40	0.0000E+00	YES	0.0000E+00	YES	0.0000E+00
0	0.0000E+00	YES	0.0000E+00	YES	0.0000E+00
6	0.0000E+00	YES	0.0000E+00	YES	0.0000E+00
15	0.0000E+00	YES	0.0000E+00	YES	0.0000E+00
47	0.0000E+00	YES	0.0000E+00	YES	0.0000E+00
128	0.0000E+00	YES	0.0000E+00	YES	0.0000E+00

3.3.5 LT40-40 Leak Test

3.3.5.1 ¼-T Flaw Results

The stress intensity factor history for a 0.25 T ID surface flaw subjected to the LT40-40 leak test transient described in 3.1.2.5 is shown in Figure 3-28 for flaws with aspect ratios of 2, 6, 10 and infinity. The arrest toughness K_{Ia}, below which no crack growth initiation can occur, as well as the median fracture toughness K_{Ic}, are also shown. It is important to note that all probabilistic analyses were performed with a flaw of aspect ratio equal to 6. Figure 3-28 shows that K increases as the temperature and pressure increase between 0 and 146 minutes. At 146 minutes, the pressure and temperature reach their maxima of 1.1 ksi and 167°F, respectively, and remain constant until 266 minutes (for 2 hours). During this time, K increases slower to eventually stabilize at its maximum value, which takes about 1 hour. The temperature and pressure then decrease from 266 minutes until 411 minutes, at which point they are held more or less constant until the end of the transient. This results in a steady decrease in K. The rate of decrease in K decreases over time, and becomes near zero by 450 minutes, at which point K reaches a minimum value roughly equal to its value at the start of the transient.

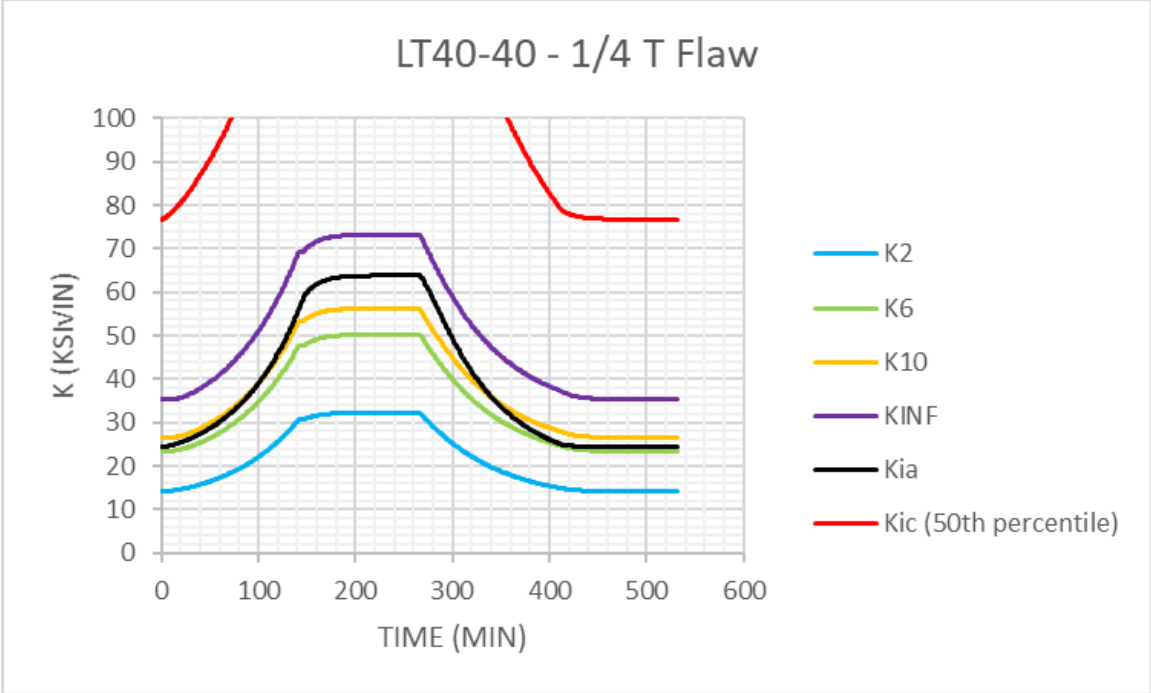

Figure 3-28: Stress Intensity Factor for the BWR LT40-40 Leak Test for a 0.25 T Flaw for Flaw Aspect Ratios of 2, 6, 10 and Infinity (note: in the legend, Kia is K_{Ia} and Kic is K_{Ic})

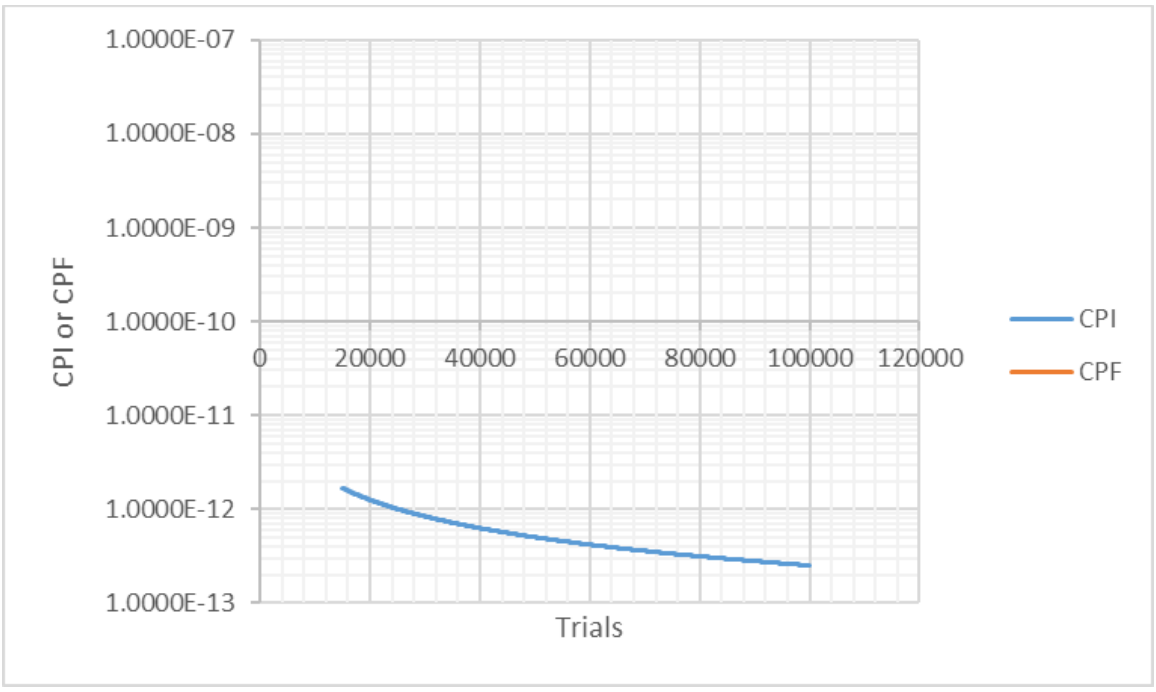

Figure 3-29: CPI and CPF versus Number of Trials for a 0.25 T Flaw in a BWR with 0°F RT_{NDT} Shift for the LT40-40 Leak Test

A probabilistic calculation assuming a 0.25 T flaw of aspect ratio equal to 6 and the PT40-40 leak test resulted in a CPI of 2.5E-13 and a CPF of zero using the RG 1.99, Rev. 2 embrittlement correlation. This case corresponds to 0°F RT_{NDT} shift (i.e. 'no shift') for this transient. Figure 3-29 shows the calculated CPI as a function of the number of RPV trials in FAVOR. Although the CPI value has not quite converged, the order of magnitude of CPI is believed to be sufficiently accurate for the purposes of this study.

The same LT40-40 leak test (shown in Figure 3-6) was modeled for different values of RT_{NDT}^{SHIFT}, so as to understand the impact of shifting the RT_{NDT} for this transient. Table 3-12 and Figure 3-30 show the results of the probabilistic analyses for the 0.25 T flaw for the LT40-40 leak test, as a function of RT_{NDT}^{SHIFT}. As expected, the CPI and CPF increase as RT_{NDT}^{SHIFT} increases. It should be noted that the analyses for $RT_{NDT}^{SHIFT} \leq 15°F$ resulted in a CPF prediction equal to zero. Furthermore, for $RT_{NDT}^{SHIFT} \leq 47°F$, the CPI did not statistically converge because of the low calculated probability, but the CPI trend over the number of trials was beginning to stabilize, so the results are believed to be in the correct order of magnitude.

Table 3-12: Calculated CPI and CPF for a 0.25 T Flaw of Aspect Ratio 6 in a BWR Subjected to the LT40-40 Leak Test

RTNDT Shift (°F)	CPI	CPI Converged?	CPF	CPF Converged?	TWCF
-40	0.0000E+00	YES	0.0000E+00	YES	0.0000E+00
0	2.5060E-13	NO	0.0000E+00	YES	0.0000E+00
6	1.1497E-11	NO	0.0000E+00	YES	0.0000E+00
15	1.4125E-10	NO	0.0000E+00	YES	0.0000E+00
47	8.7213E-09	NO	2.2284E-11	YES	2.2284E-14
128	1.1423E-05	YES	7.9051E-06	YES	7.9051E-09

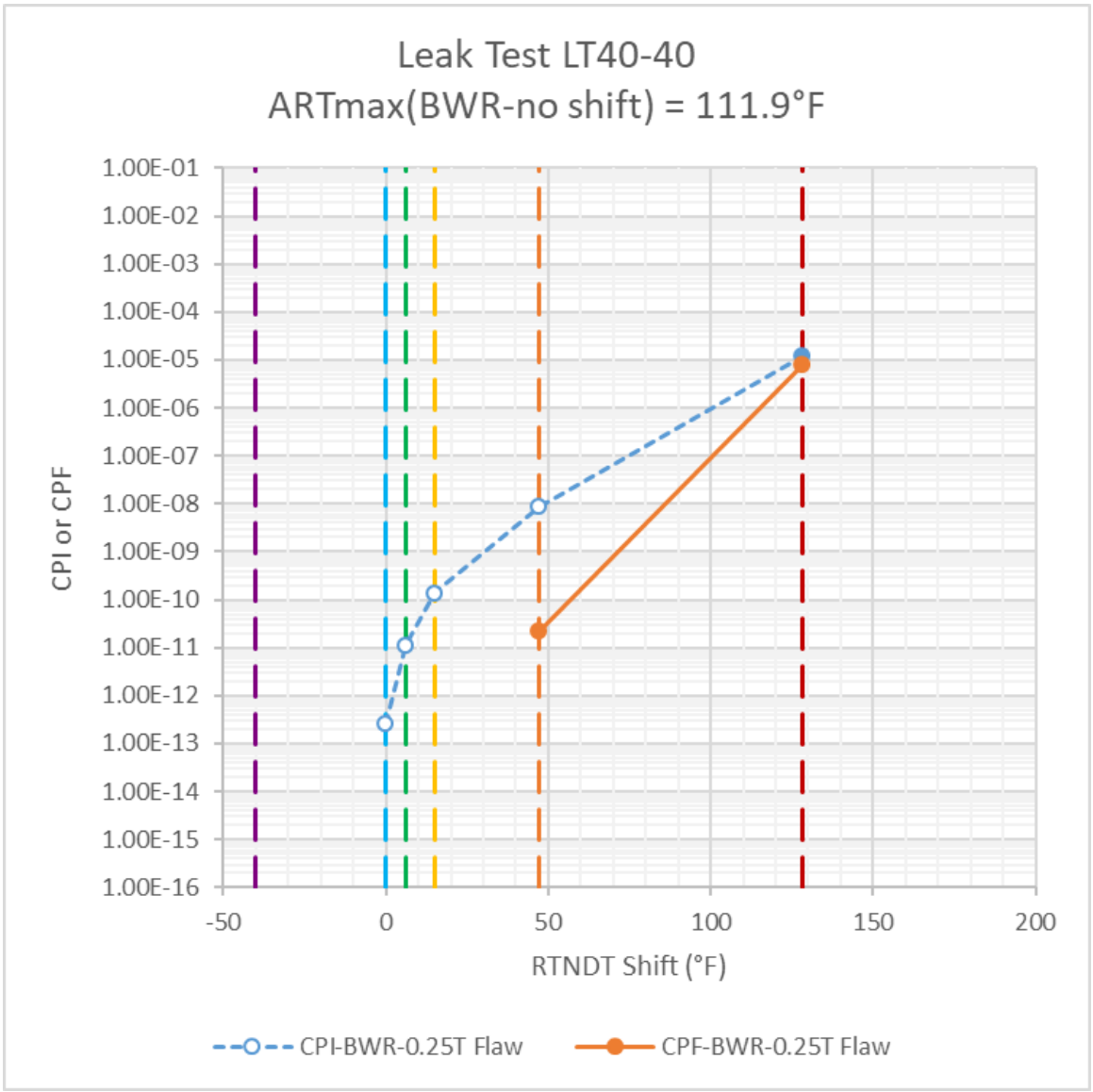

Figure 3-30: CPI and CPF for a 0.25 T Flaw of Aspect Ratio 6 in a BWR Subjected to the LT40-40 Leak Test, as a Function of RT_{NDT} Shift from RG 1.99, Rev. 2 to E900-15 Embrittlement Correlations (open symbols linked by dashed lines represent results that are not statistically converged)

3.3.5.2 Shallow Flaw Results

The stress intensity factor history for a 0.04 T ID surface flaw subjected to the LT40-40 leak test transient described in 3.1.2.5 is shown in Figure 3-31 for flaws with aspect ratios of 2, 6, 10 and infinity. The arrest toughness K_{Ia}, below which no crack growth initiation can occur, as well as the median fracture toughness K_{Ic}, are also shown. Figure 3-31 shows that K initially decreases slightly and then increases as the temperature and pressure increase between 0 and 146 minutes. The initial decrease in K can be explained by the fact that the shallow flaw is subjected to compressive thermal stresses as the temperature increases, resulting in a decrease in the thermal K component. This decrease is initially greater than the increase in pressure induced membrane K, resulting in a decrease in total K until the pressure induced membrane K component increases faster than the thermal K component decreases. At 146 minutes, the pressure and temperature reach their maxima of 1.1 ksi and 167°F, respectively, and remain constant until 266 minutes (for 2 hours). During this time, K increases slower to eventually stabilize at its maximum value, which takes about 1 hour. The temperature and pressure then decrease from 266 minutes until 411 minutes, at which point they are held more or less constant until the end of the transient. This results in a steady decrease in K. The decrease in K displays an inflection point at 411 minutes, due to the temperature being held constant after that time. At 450 minutes, K reaches a minimum value roughly equal to its value at the start of the transient.

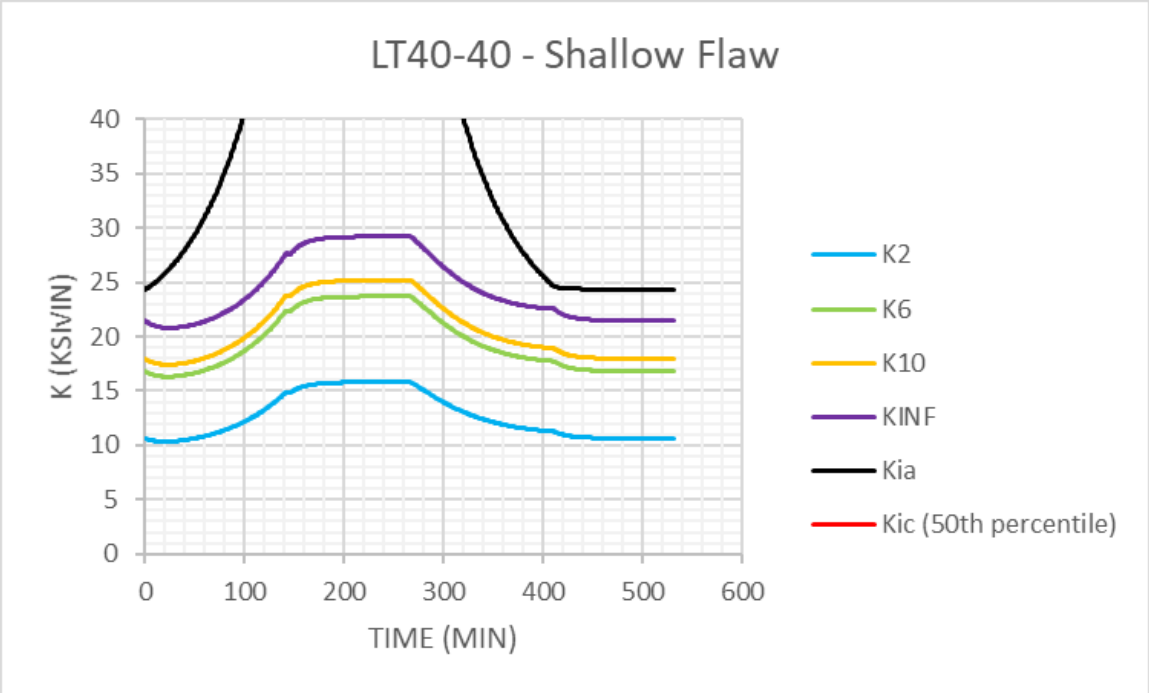

Figure 3-31: Stress Intensity Factor for the BWR LT40-100 Leak Test for a 0.04 T Flaw for Flaw Aspect Ratios of 2, 6, 10 and Infinity (note: in the legend, Kia is K_{Ia} and Kic is K_{Ic})

A probabilistic calculation assuming a 0.04 T flaw of aspect ratio equal to 6 and the LT40-40 leak test resulted in a CPI and a CPF of zero using the RG 1.99, Rev. 2 embrittlement correlation. This case corresponds to 0°F RT_{NDT} shift (i.e. 'no shift') for this transient.

The same LT40-40 leak test (shown in Figure 3-6) was modeled for different values of RT_{NDT}^{SHIFT}, so as to understand the impact of shifting the RT_{NDT} for this transient. Table 3-13 and Figure 3-32 show the results of the probabilistic analyses for the 0.04 T flaw for the LT40-40 leak test, as a function of RT_{NDT}^{SHIFT}. As expected, the CPI and CPF increase as RT_{NDT}^{SHIFT} increases. For $RT_{NDT}^{SHIFT} \leq 47°F$, the CPI and CPF were zero.

Table 3-13: Calculated CPI and CPF for a 0.04 T Flaw of Aspect Ratio 6 in a BWR Subjected to the LT40-40 Leak Test

RTNDT Shift (°F)	CPI	CPI Converged?	CPF	CPF Converged?	TWCF
-40	0.0000E+00	YES	0.0000E+00	YES	0.0000E+00
0	0.0000E+00	YES	0.0000E+00	YES	0.0000E+00
6	0.0000E+00	YES	0.0000E+00	YES	0.0000E+00
15	0.0000E+00	YES	0.0000E+00	YES	0.0000E+00
47	0.0000E+00	YES	0.0000E+00	YES	0.0000E+00
128	5.5368E-11	YES	3.8897E-12	YES	3.8897E-15

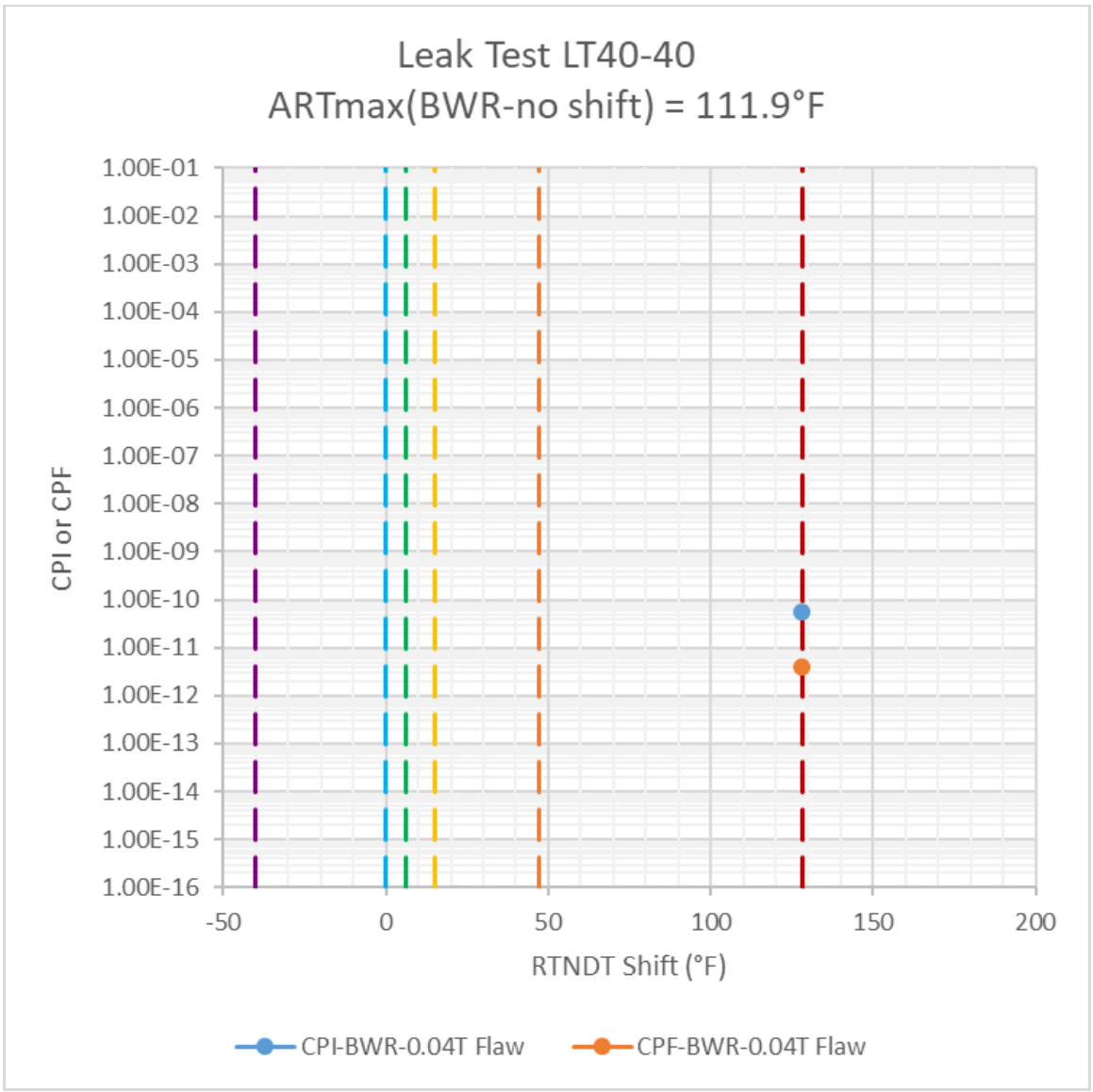

Figure 3-32: CPI and CPF for a 0.04 T Flaw of Aspect Ratio 6 in a BWR Subjected to the LT40-40 Leak Test, as a Function of RT_{NDT} Shift from RG 1.99, Rev. 2 to E900-15 Embrittlement Correlations (open symbols linked by dashed lines represent results that are not statistically converged)

3.3.6 LT40-100 Leak Test

3.3.6.1 ¼-T Flaw Results

The stress intensity factor history for a 0.25 T ID surface flaw subjected to the LT40-100 leak test transient described in 3.1.2.6 is shown in Figure 3-33 for flaws with aspect ratios of 2, 6, 10 and infinity. The arrest toughness K_{Ia}, below which no crack growth initiation can occur, as well as the median fracture toughness K_{Ic}, are also shown. It is important to note that all probabilistic analyses were performed with a flaw of aspect ratio equal to 6. Figure 3-33 shows that K increases as the temperature and pressure increase between 0 and 146 minutes. At 146 minutes, the pressure and temperature reach their maxima of 1.1 ksi and 167°F, respectively, and remain constant until 266 minutes (for 2 hours). During this time, K increases slower to eventually stabilize at its maximum value, which takes about 1 hour. The temperature and pressure then decrease from 266 minutes until 324 minutes, at which point they are held more or less constant until the end of the transient. This results in a steady decrease in K. The rate of decrease in K decreases over time, and becomes near zero by 380 minutes, at which point K reaches a minimum value roughly equal to its value at the start of the transient.

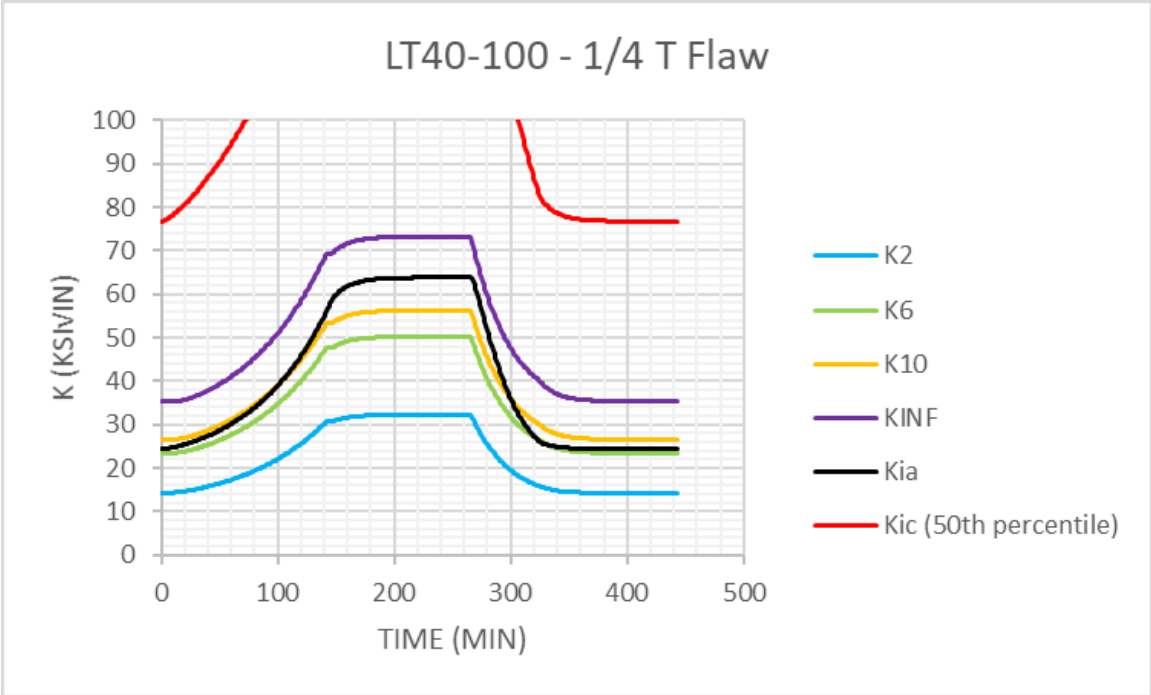

Figure 3-33: Stress Intensity Factor for the BWR LT40-100 Leak Test for a 0.25 T Flaw for Flaw Aspect Ratios of 2, 6, 10 and Infinity (note: in the legend, Kia is K_{Ia} and Kic is K_{Ic})

A probabilistic calculation assuming a 0.25 T flaw of aspect ratio equal to 6 and the LT40-100 leak test resulted in a CPI and a CPF of zero using the RG 1.99, Rev. 2 embrittlement correlation. This case corresponds to 0°F RT_{NDT} shift (i.e. 'no shift') for this transient.

The same LT40-100 leak test (shown in Figure 3-7) was modeled for different values of RT_{NDT}^{SHIFT}, so as to understand the impact of shifting the RT_{NDT} for this transient. Table 3-14 and Figure 3-34 show the results of the probabilistic analyses for the 0.25 T flaw for LT40-100 the leak test, as a function of RT_{NDT}^{SHIFT}. As expected, the CPI and CPF increase as RT_{NDT}^{SHIFT} increases. It should be noted that the

analyses for $RT_{NDT}^{SHIFT} \leq 15°F$ resulted in a CPF prediction equal to zero. Furthermore, for $RT_{NDT}^{SHIFT} \leq 15°F$, the CPI did not statistically converge because of the low calculated probability, but the CPI trend over the number of trials was beginning to stabilize, so the results are believed to be in the correct order of magnitude.

Table 3-14: Calculated CPI and CPF for a 0.25 T Flaw of Aspect Ratio 6 in a BWR Subjected to the LT40-100 Leak Test

RTNDT Shift (°F)	CPI	CPI Converged?	CPF	CPF Converged?	TWCF
-40	0.0000E+00	YES	0.0000E+00	YES	0.0000E+00
0	0.0000E+00	YES	0.0000E+00	YES	0.0000E+00
6	1.0905E-11	NO	0.0000E+00	YES	0.0000E+00
15	1.3700E-10	NO	0.0000E+00	YES	0.0000E+00
47	8.5617E-09	YES	1.9619E-11	YES	1.9619E-14
128	1.1188E-05	YES	7.7124E-06	YES	7.7124E-09

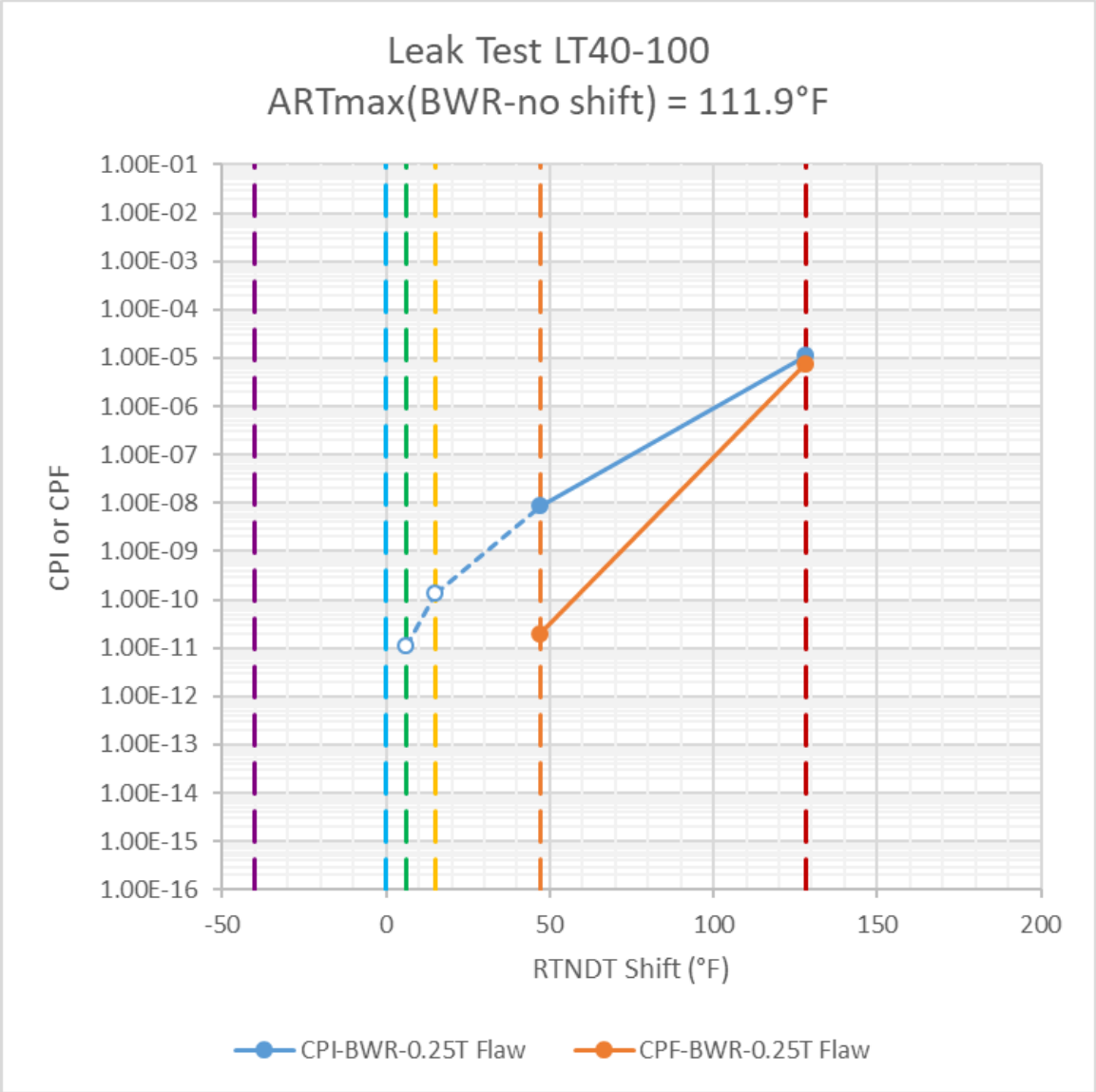

Figure 3-34: CPI and CPF for a 0.25 T Flaw of Aspect Ratio 6 in a BWR Subjected to the LT40-100 Leak Test, as a Function of RT_{NDT} Shift from RG 1.99, Rev. 2 to E900-15 Embrittlement Correlations (open symbols linked by dashed lines represent results that are not statistically converged)

3.3.6.2 Shallow Flaw Results

The stress intensity factor history for a 0.04 T ID surface flaw subjected to the LT40-100 leak test transient described in 3.1.2.6 is shown in Figure 3-35 for flaws with aspect ratios of 2, 6, 10 and infinity. The arrest toughness K_{Ia}, below which no crack growth initiation can occur, as well as the median fracture toughness K_{Ic}, are also shown. Figure 3-35 shows that K initially decreases slightly and then increases as the temperature and pressure increase between 0 and 146 minutes. The initial decrease in K can be explained by the fact that the shallow flaw is subjected to compressive thermal stresses as the temperature increases, resulting in a decrease in the thermal K component. This decrease is initially greater that the increase in pressure induced membrane K, resulting in a decrease in total K until the pressure induced membrane K component increases faster than the thermal K component decreases.

At 146 minutes, the pressure and temperature reach their maxima of 1.1 ksi and 167°F, respectively, and remain constant until 266 minutes (for 2 hours). During this time, K increases slower to eventually stabilize at its maximum value, which takes about 1 hour. The temperature and pressure then decrease from 266 minutes until 324 minutes, at which point they are held more or less constant until the end of the transient. This results in a steady decrease in K. The decrease in K displays an inflection point at 324 minutes, due to the temperature being held constant after that time. At 380 minutes, K reaches a minimum value roughly equal to its value at the start of the transient.

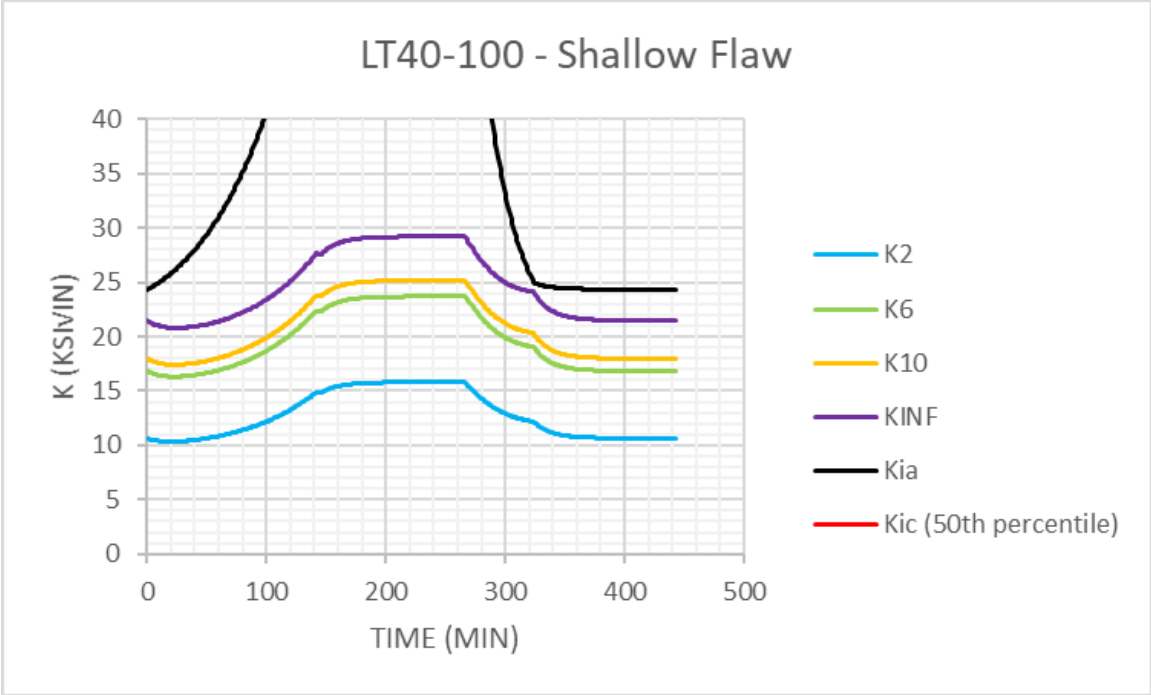

Figure 3-35: Stress Intensity Factor for the BWR LT40-100 Leak Test for a 0.04 T Flaw for Flaw Aspect Ratios of 2, 6, 10 and Infinity (note: in the legend, Kia is K_{Ia} and Kic is K_{Ic})

A probabilistic calculation assuming a 0.04 T flaw of aspect ratio equal to 6 and the LT40-100 leak test resulted in a CPI and a CPF of zero using the RG 1.99, Rev. 2 embrittlement correlation. This case corresponds to 0°F RT_{NDT} shift (i.e. 'no shift') for this transient.

The same LT40-100 leak test (shown in Figure 3-7) was modeled for different values of RT_{NDT}^{SHIFT}, so as to understand the impact of shifting the RT_{NDT} for this transient. Table 3-15 and Figure 3-36 show the results of the probabilistic analyses for the 0.04 T flaw for the LT40-100 leak test, as a function of RT_{NDT}^{SHIFT}. As expected, the CPI and CPF increase as RT_{NDT}^{SHIFT} increases. For $RT_{NDT}^{SHIFT} \leq 15°F$, the CPI was zero and for $RT_{NDT}^{SHIFT} \leq 47°F$, CPF was zero. Furthermore, for $RT_{NDT}^{SHIFT} = 47°F$, the CPI did not statistically converge because of the low calculated probability, but the CPI trend over the number of trials was beginning to stabilize, so the results are believed to be in the correct order of magnitude.

Table 3-15: Calculated CPI and CPF for a 0.04 T Flaw of Aspect Ratio 6 in a BWR Subjected to the LT40-100 Leak Test

RTNDT Shift (°F)	CPI	CPI Converged?	CPF	CPF Converged?	TWCF
-40	0.0000E+00	YES	0.0000E+00	YES	0.0000E+00
0	0.0000E+00	YES	0.0000E+00	YES	0.0000E+00
6	0.0000E+00	YES	0.0000E+00	YES	0.0000E+00
15	0.0000E+00	YES	0.0000E+00	YES	0.0000E+00
47	1.2425E-16	NO	0.0000E+00	YES	0.0000E+00
128	4.4753E-10	YES	1.4824E-11	YES	1.4824E-14

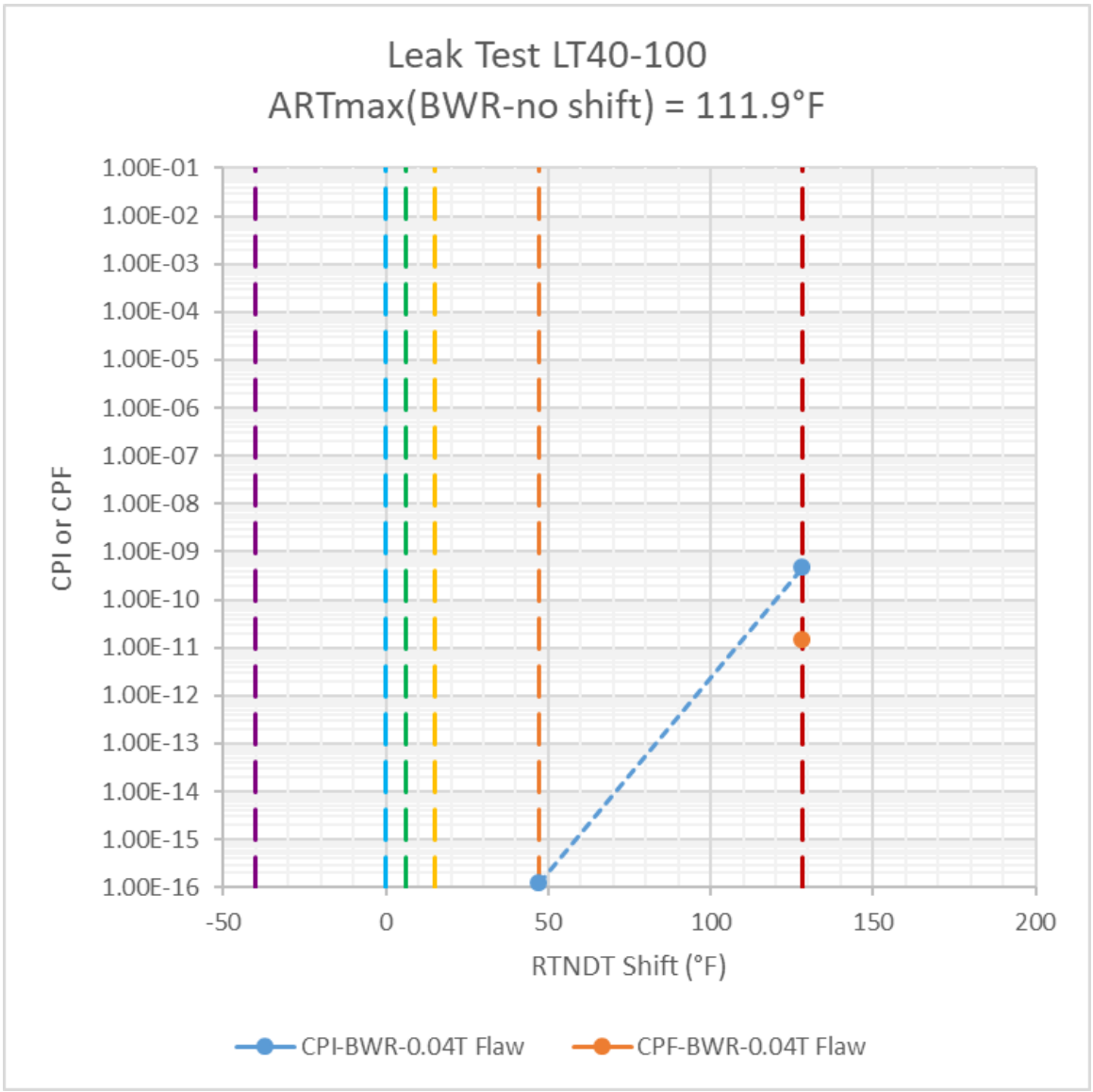

Figure 3-36: CPI and CPF for a 0.04 T Flaw of Aspect Ratio 6 in a BWR Subjected to the LT40-100 Leak Test, as a Function of RT_{NDT} Shift from RG 1.99, Rev. 2 to E900-15 Embrittlement Correlations (open symbols linked by dashed lines represent results that are not statistically converged)

3.3.7 LTA Leak Test

3.3.7.1 ¼-T Flaw Results

The stress intensity factor history for a 0.25 T ID surface flaw subjected to the LTA leak test transient described in 3.1.2.7 is shown in Figure 3-37 for flaws with aspect ratios of 2, 6, 10 and infinity. The arrest toughness K_{Ia}, below which no crack growth initiation can occur, as well as the median fracture toughness K_{Ic}, are also shown. It is important to note that all probabilistic analyses were performed with a flaw of aspect ratio equal to 6. Figure 3-37 shows that K is initially constant along while the temperature and pressure are held constant. When the temperature increases a little after 400 minutes, K become negative as the pressure is still zero and the temperature increase puts the inner surface flaw in compression. Around 825 minutes, the pressure increases rapidly up to the leak test pressure of 1.0 ksi, resulting in a corresponding increase in K to its maximum value. The pressure is momentarily reduced around 1100 minutes, and then raised back to 1.0 ksi. The K values decrease and then come back up accordingly. Around 1250 minutes, the pressure is dropped back to zero, and K decreases accordingly. Finally, as the temperature decreases (initially rapidly and then slower) beginning at 1450 minutes, a rapid rise in K is observed followed by a rapid decrease as the temperature is dropped more slowly. The K values then slowly stabilize near their values at the start of the transient.

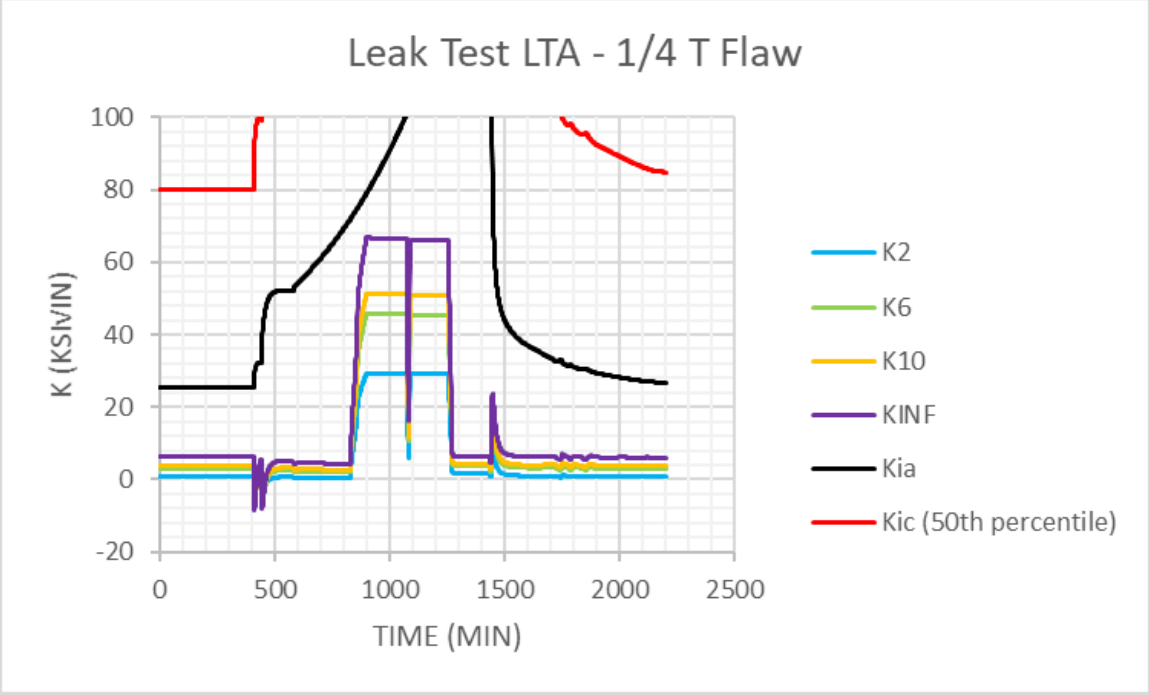

Figure 3-37: Stress Intensity Factor for the BWR LTA Leak Test for a 0.25 T Flaw for Flaw Aspect Ratios of 2, 6, 10 and Infinity (note: in the legend, Kia is K_{Ia} and Kic is K_{Ic})

A probabilistic calculation assuming a 0.25 T flaw of aspect ratio equal to 6 and the LTA leak test resulted in a CPI and a CPF of zero using the RG 1.99, Rev. 2 embrittlement correlation. This case corresponds to 0°F RT_{NDT} shift (i.e. 'no shift') for this transient.

The same LTA leak test (shown in Figure 3-8) was modeled for different values of RT_{NDT}^{SHIFT}, so as to understand the impact of shifting the RT_{NDT} for this transient. Table 3-16 and Figure 3-38 show the

results of the probabilistic analyses for the 0.25 T flaw for the LTA leak test, as a function of RT_{NDT}^{SHIFT}. As expected, the CPI and CPF increase as RT_{NDT}^{SHIFT} increases. It should be noted that the analyses for $RT_{NDT}^{SHIFT} \leq 47°F$ resulted in a CPF prediction equal to zero and analyses for $RT_{NDT}^{SHIFT} \leq 15°F$ resulted in a CPI prediction equal to zero. Furthermore, for $RT_{NDT}^{SHIFT} = 47°F$, the CPI did not statistically converge because of the low calculated probability, but the CPI trend over the number of trials was beginning to stabilize, so the results are believed to be in the correct order of magnitude.

Table 3-16: Calculated CPI and CPF for a 0.25 T Flaw of Aspect Ratio 6 in a BWR Subjected to the LTA Leak Test

RTNDT Shift (°F)	CPI	CPI Converged?	CPF	CPF Converged?	TWCF
-40	0.0000E+00	YES	0.0000E+00	YES	0.0000E+00
0	0.0000E+00	YES	0.0000E+00	YES	0.0000E+00
6	0.0000E+00	YES	0.0000E+00	YES	0.0000E+00
15	0.0000E+00	YES	0.0000E+00	YES	0.0000E+00
47	2.6317E-10	NO	0.0000E+00	YES	0.0000E+00
128	5.3999E-07	YES	9.5373E-08	YES	9.5373E-08

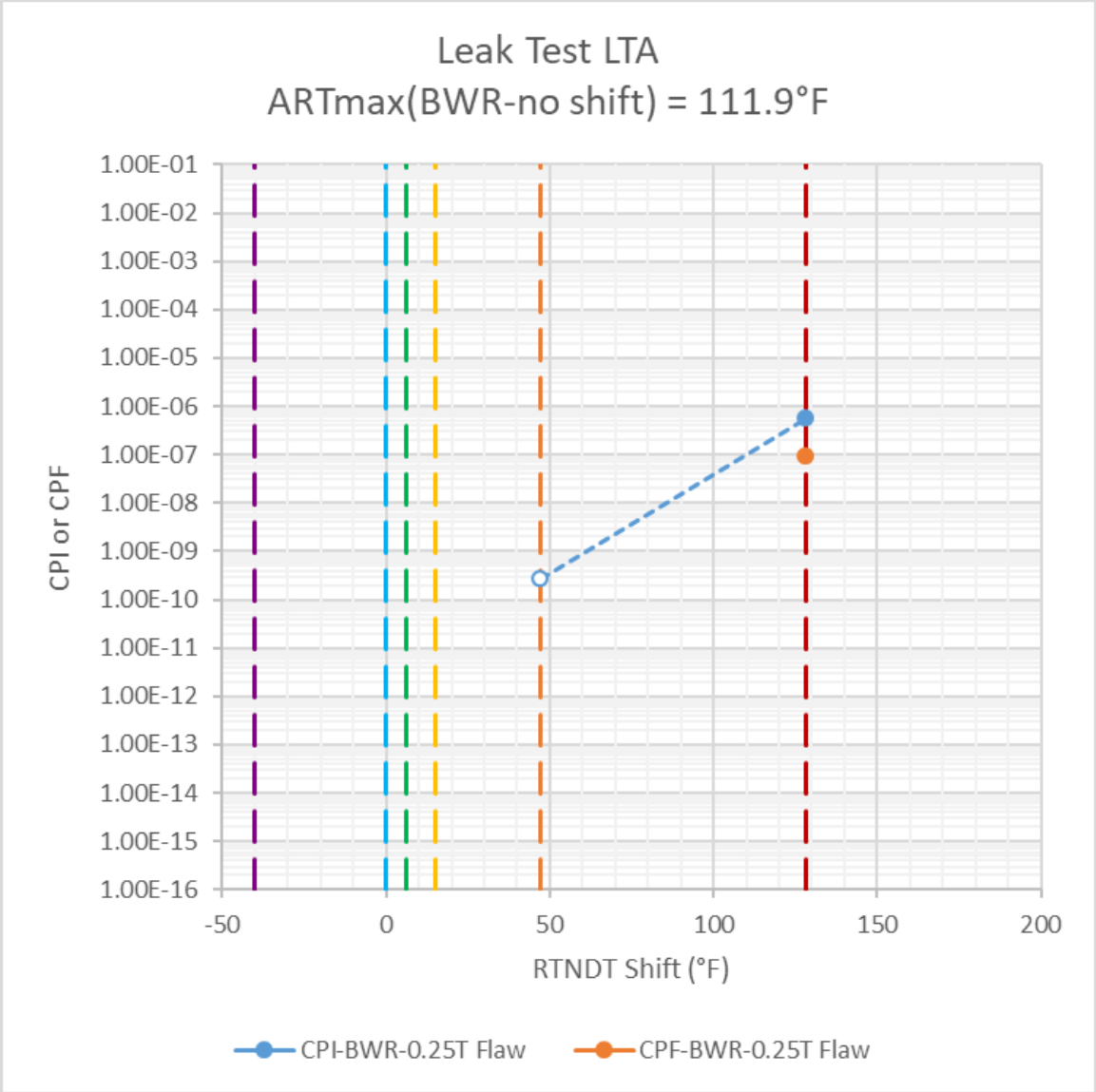

Figure 3-38: CPI and CPF for a 0.25 T Flaw of Aspect Ratio 6 in a BWR Subjected to the LTA Leak Test, as a Function of RT_{NDT} Shift from RG 1.99, Rev. 2 to E900-15 Embrittlement Correlations (open symbols linked by dashed lines represent results that are not statistically converged)

3.3.7.2 Shallow Flaw Results

The stress intensity factor history for a 0.04 T ID surface flaw subjected to the LTA leak test transient described in 3.1.2.7 is shown in Figure 3-39 for flaws with aspect ratios of 2, 6, 10 and infinity. The arrest toughness K_{Ia}, below which no crack growth initiation can occur, as well as the median fracture toughness K_{Ic}, are also shown. Figure 3-39 shows that K is initially constant along while the temperature and pressure are held constant. When the temperature increases a little after 400 minutes, K decreases sharply as the pressure is still zero and the temperature increase puts the inner surface flaw in compression, thus offsetting some of the tensile residual stresses affecting the shallow flaw. Around 825 minutes, the pressure increases rapidly up to the leak test pressure of 1.0 ksi, resulting in a corresponding increase in K to its maximum value. The pressure is momentarily reduced around 1100

minutes, and then raised back to 1.0 ksi. The K values decrease and then come back up accordingly. Around 1250 minutes, the pressure is dropped back to zero, and K decreases accordingly. Finally, as the temperature decreases (initially rapidly and then slower) beginning at 1450 minutes, a rapid rise in K is observed followed by a rapid decrease as the temperature is dropped more slowly. The K values then slowly stabilize near their values at the start of the transient.

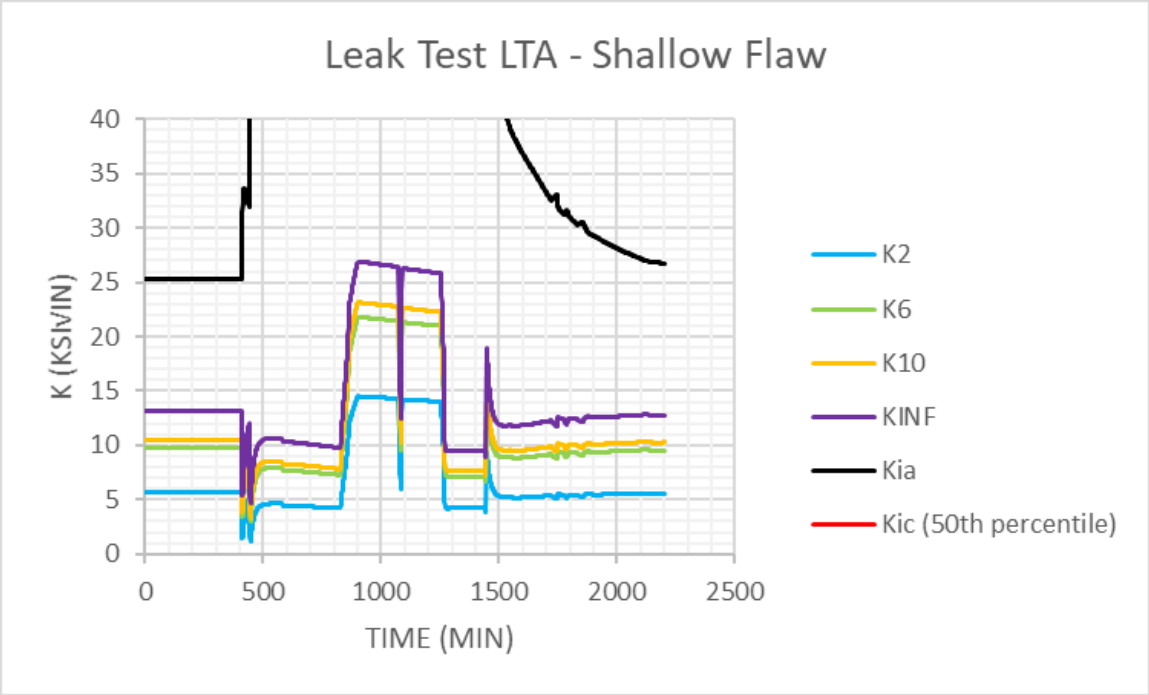

Figure 3-39: Stress Intensity Factor for the BWR LTA Leak Test for a 0.04 T Flaw for Flaw Aspect Ratios of 2, 6, 10 and Infinity (note: in the legend, Kia is K_{Ia} and Kic is K_{Ic})

A probabilistic calculation assuming a 0.04 T flaw of aspect ratio equal to 6 and the LTA leak test resulted in a CPI and a CPF of zero using the RG 1.99, Rev. 2 embrittlement correlation. This case corresponds to 0°F RT_{NDT} shift (i.e. 'no shift') for this transient.

The same LTA leak test (shown in Figure 3-8) was modeled for different values of RT_{NDT}^{SHIFT}, so as to understand the impact of shifting the RT_{NDT} for this transient. Table 3-17 shows the results of the probabilistic analyses for the 0.045 T flaw for the LTA leak test, as a function of RT_{NDT}^{SHIFT}. All values of calculated CPI and CPF were equal to zero.

Table 3-17: Calculated CPI and CPF for a 0.04 T Flaw of Aspect Ratio 6 in a BWR Subjected to the LTA Leak Test

RTNDT Shift (°F)	CPI	CPI Converged?	CPF	CPF Converged?	TWCF
-40	0.0000E+00	YES	0.0000E+00	YES	0.0000E+00
0	0.0000E+00	YES	0.0000E+00	YES	0.0000E+00
6	0.0000E+00	YES	0.0000E+00	YES	0.0000E+00
15	0.0000E+00	YES	0.0000E+00	YES	0.0000E+00
47	0.0000E+00	YES	0.0000E+00	YES	0.0000E+00
128	0.0000E+00	YES	0.0000E+00	YES	0.0000E+00

4 Summary

Figure 4-1 through Figure 4-7 show the calculated CPI and CPF calculated for all the analyses performed in this study. The PT100-100, PT100-50, and PT50-50 cooldowns were simulated for both PWR and BWR. The C50P cooldown was only simulated for PWR. Finally, the LT40-40, LT40-100, and LTA leak tests, as well as the S50 saturation cooldown were only simulated for BWR. Since all the predictions were zero for the BWR S50 saturation cooldown, no summary figure is shown for this transient. As expected, in all cases resulting in non-zero predictions, the calculated CPI and CPF increase as a function of the RT_{NDT} shift associated with going from RG 1.99, Rev. 2 to E900-15 for all combinations studied.

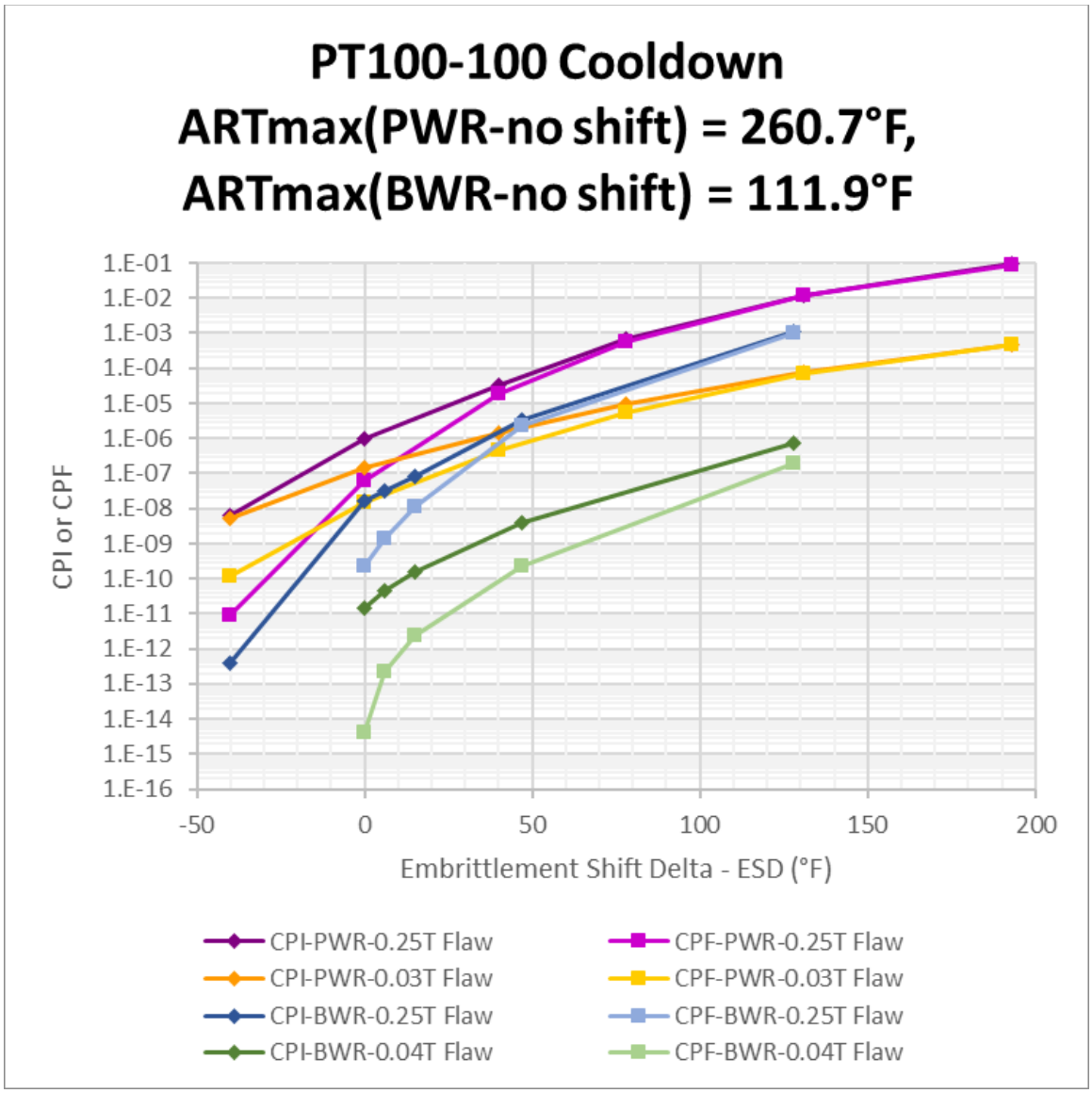

Figure 4-1: CPI and CPF for PWR and BWR, ¼ T and Shallow Flaws, as a Function of RT_{NDT} Shift for the PT100-100 Cooldown

Figure 4-1 shows that the CPI and CPF associated with the PT100-100 cooldown can be high and exceed $1x10^{-6}$ for relatively small RT_{NDT} shift amounts (~50°F). This is particularly true for the case of the 1/4T flaw in PWR and BWR, and for the PWR shallow flaw, which produce the higher CPI and CPF for this transient. However, since the PT100-100 cooldown is estimated to have a very low frequency of occurrence of $6x10^{-6}$ events per year for PWRs and $1x10^{-7}$ events per year for BWRs per BTP 5-3 [7], the overall TWCF (though-Wall Crack Frequency) remains well below the $1x10^{-6}$ per year limit despite the high CPI and CPF calculated in some cases. It is also interesting to note that for a given set of conditions, all CPI and CPF predictions for BWR are lower than those for PWR, which was expected for this transient.

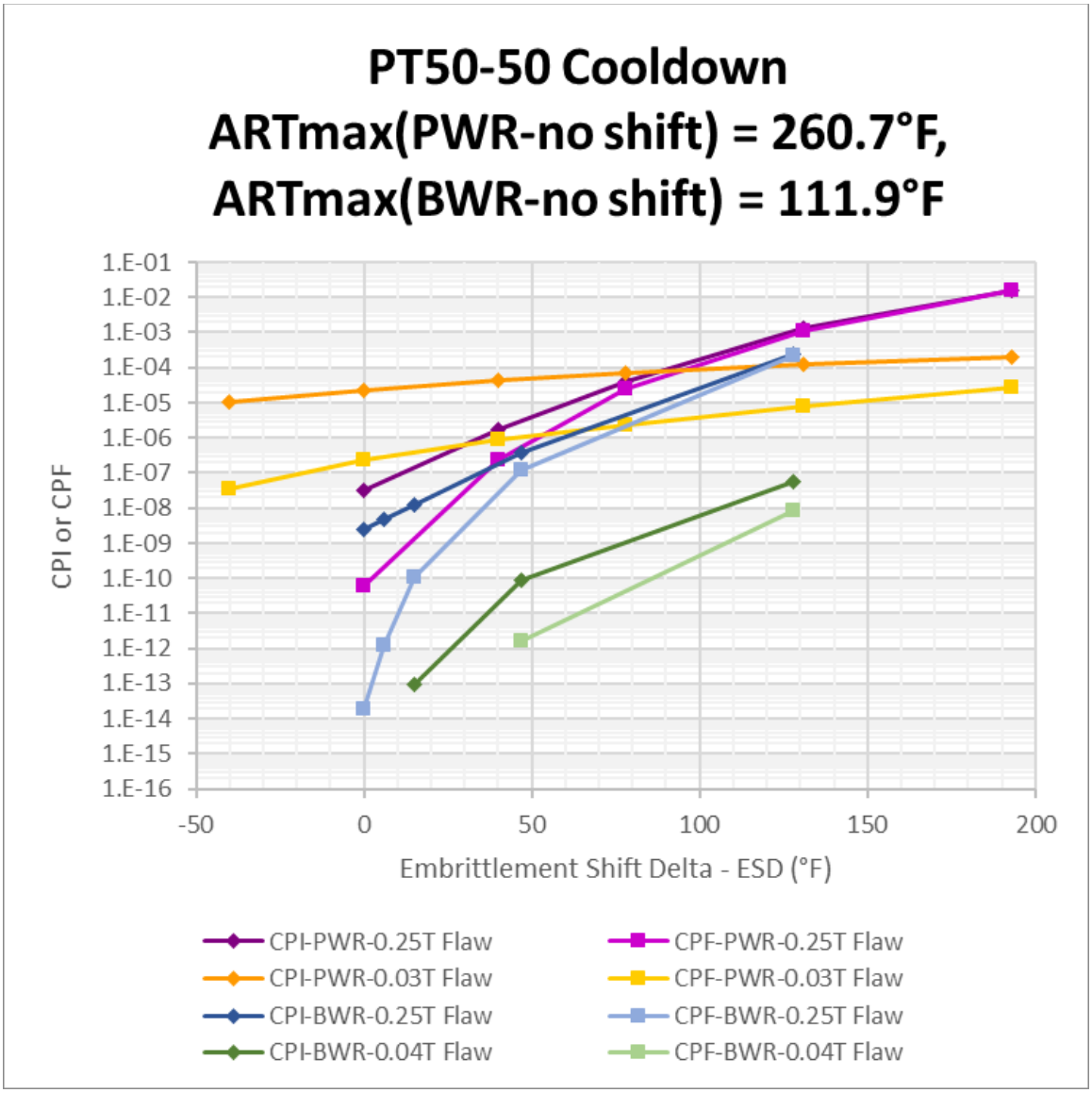

Figure 4-2: CPI and CPF for PWR and BWR, ¼ T and Shallow Flaws, as a Function of RT_{NDT} Shift for the PT50-50 Cooldown

Figure 4-2 shows that the CPI and CPF associated with the PT50-50 cooldown can be high and exceed $1x10^{-6}$ for relatively small RT_{NDT} shift amounts (from 50°F to 75°F). This is particularly true for the case of the 1/4T flaw in PWR and BWR, and for the PWR shallow flaw, which produce the higher CPI and CPF for this transient. However, since the PT50-50 cooldown is estimated to have a very low frequency of occurrence of $6x10^{-6}$ events per year for PWRs and $1x10^{-7}$ events per year for BWRs per BTP 5-3 [7], the overall TWCF (though-Wall Crack Frequency) remains well below the $1x10^{-6}$ per year limit despite the high CPI and CPF calculated in some cases. Once again, all CPI and CPF predictions for BWR are lower than those for PWR, which was expected for this transient.

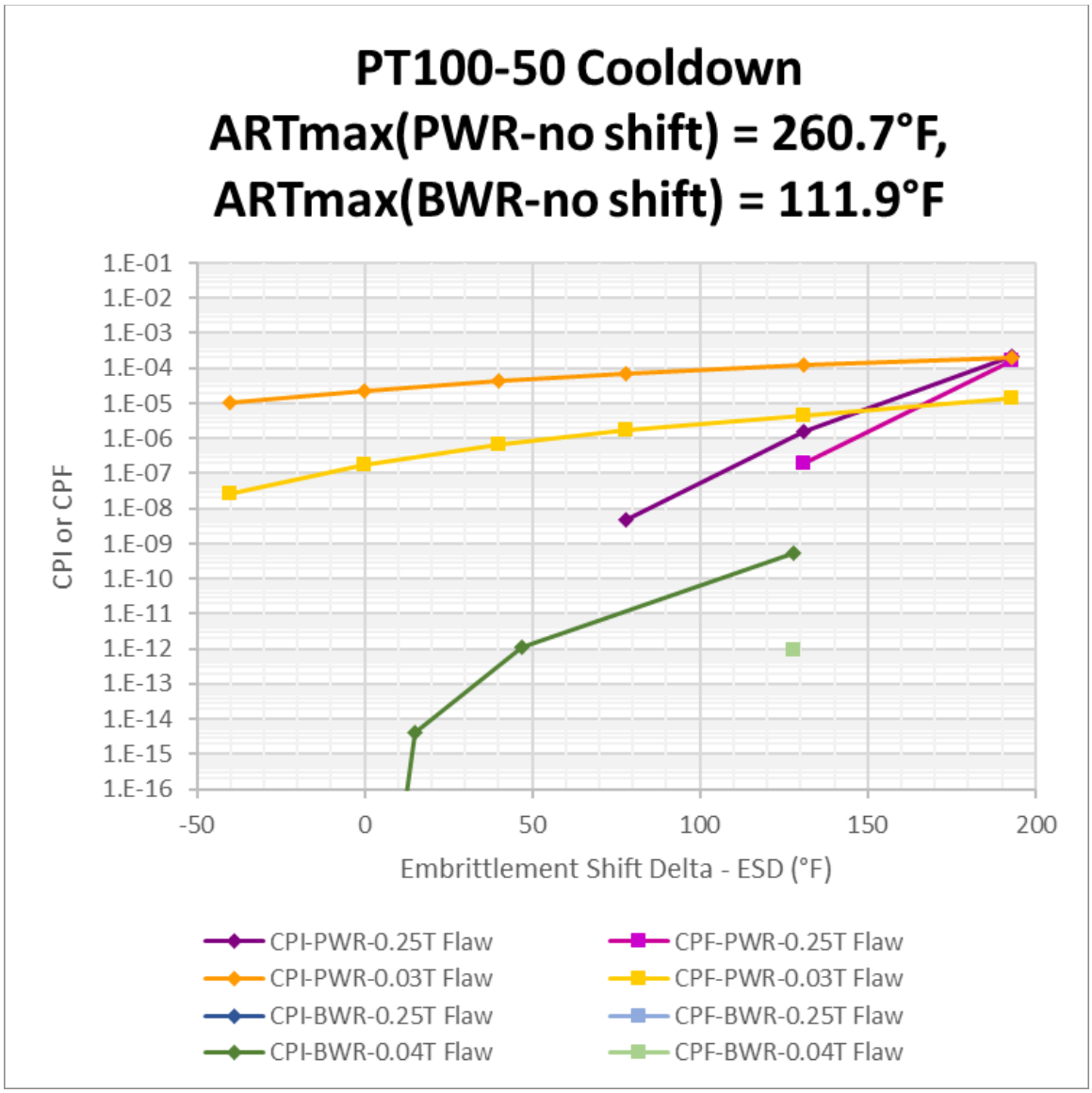

Figure 4-3: CPI and CPF for PWR and BWR, ¼ T and Shallow Flaws, as a Function of RT_{NDT} Shift for the PT100-50 Cooldown

Figure 4-3 shows that the CPI and CPF associated with the PT100-50 cooldown is generally lower than for the 100°F/hour and 50°F/hour P-T limit cooldowns (PT100-100 and PT50-50 respectively), except for the case of PWR shallow flaws. In fact, for PWR shallow flaws, even for 0°F RT_{NDT} shift, the calculated CPI and CPF are above $1x10^{-6}$. Furthermore, it is interesting to note that for both BWR and PWR, the CPI and CPF associated with shallow flaws exceed the CPI and CPF associated with ¼ T flaws by several orders of magnitude for this transient. However, since the PT100-50 cooldown is estimated to have a very low frequency of occurrence of $6x10^{-6}$ events per year for PWRs and $1x10^{-7}$ events per year for BWRs per BTP 5-3 [7], the overall TWCF (though-Wall Crack Frequency) remains well below the $1x10^{-6}$ per year limit despite the high CPI and CPF calculated in some cases. Once again, all CPI and CPF predictions for BWR are lower than those for PWR, which was expected for this transient.

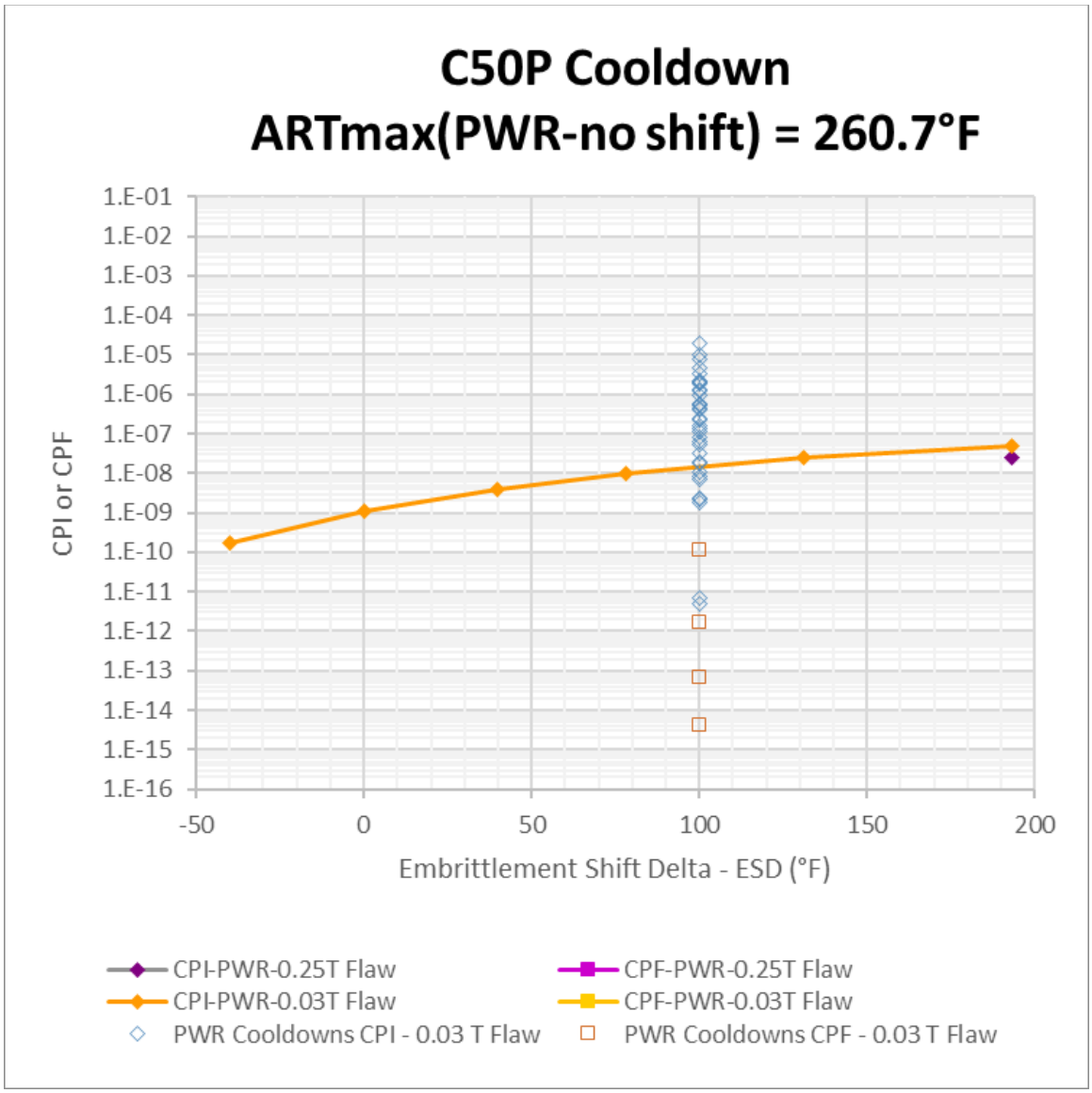

Figure 4-4: CPI and CPF for PWR, ¼ T and Shallow Flaws, as a Function of RT_{NDT} Shift for the C50P Cooldown and for 42 Other PWR Cooldown Transients Simulated for a Shallow Flaw at RT_{NDT} Shift of 100°F

Figure 4-4 shows the calculated CPI and CPF for a PWR subjected to the C50P cooldown described in 2.1.2.4. It should be noted that all CPF values calculated were zero for this transient and thus are not shown on this figure. The frequency of occurrence of the C50P cooldown can be assumed to be 1.0 event per year since this is a 'realistic' PWR cooldown, based on BTP 5-3 [7]. As a result, the CPI and CPF are equal to the annual frequency of crack initiation and TWCF, respectively. This figure shows that no matter how high the RT_{NDT} shift applied within the range studied, the CPI are below 1E-07, and the CPF is zero, thus implying TWCF=0 events per year for this transient. Also shown on Figure 4-4 are the CPI And CPF values calculated for 42 actual PWR cooldown transients at a RT_{NDT} shift value of 100°F. The CPI values for these 42 actual cooldowns range from ~$5x10^{-12}$ to ~$2x10^{-5}$ and most CPF values calculated were zero, with a maximum of ~$1x10^{-10}$, indicating a TWCF of ~$1x10^{-10}$ for the worst case actual cooldown modeled in this study.

The cooldown transient having a frequency of occurrence equal to 1.0 for BWRs is the saturation cooldown, and in that sense, the S50 cooldown for a BWR is analog to the C50P cooldown for a PWR. All simulations performed in this study with the S50 cooldown for a BWR resulted in CPI and CPF of zero, implying a TWCF of zero per year for a saturation cooldown in a BWR.

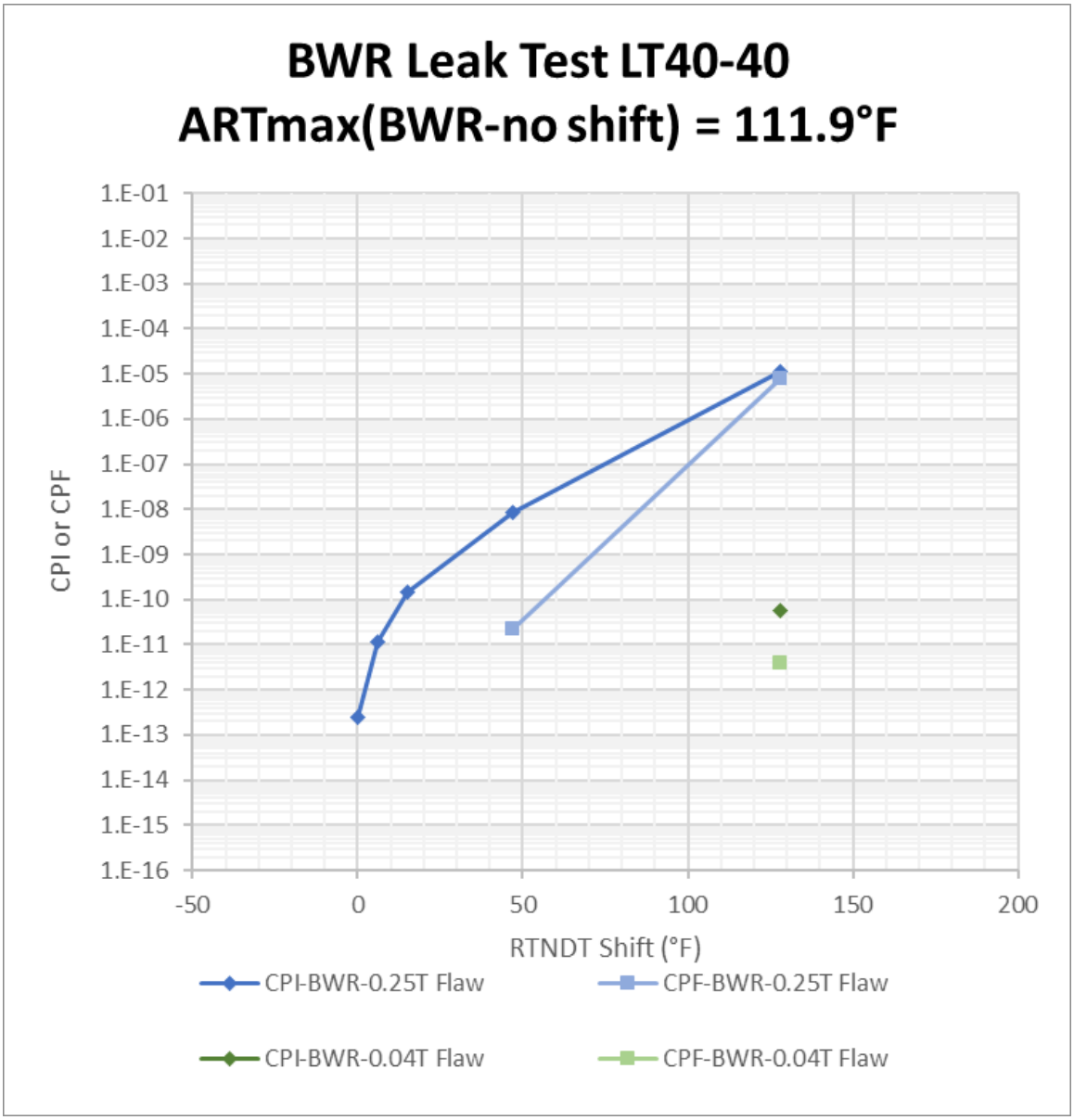

Figure 4-5: CPI and CPF for BWR, ¼ T and Shallow Flaws, as a Function of RT_{NDT} Shift for the LT40-40 Leak Test

Figure 4-5 shows the CPI and CPF for a BWR subjected to the LT40-40 leak test transient described in 3.1.2.5. For this transient, the ¼ T flaw CPI and CPF are orders of magnitude larger than the shallow flaw CPI and CPF, and both the CPI and CPF can reach values around $1x10^{-5}$ for high values of RT_{NDT} shift. However, since the frequency of occurrence of the LT40-40 leak test is estimated to be $1x10^{-3}$ event per

year per BTP 5-3 [7], the overall TWCF (though-Wall Crack Frequency) remains well below the $1x10^{-6}$ per year limit despite the high CPI and CPF calculated in some cases.

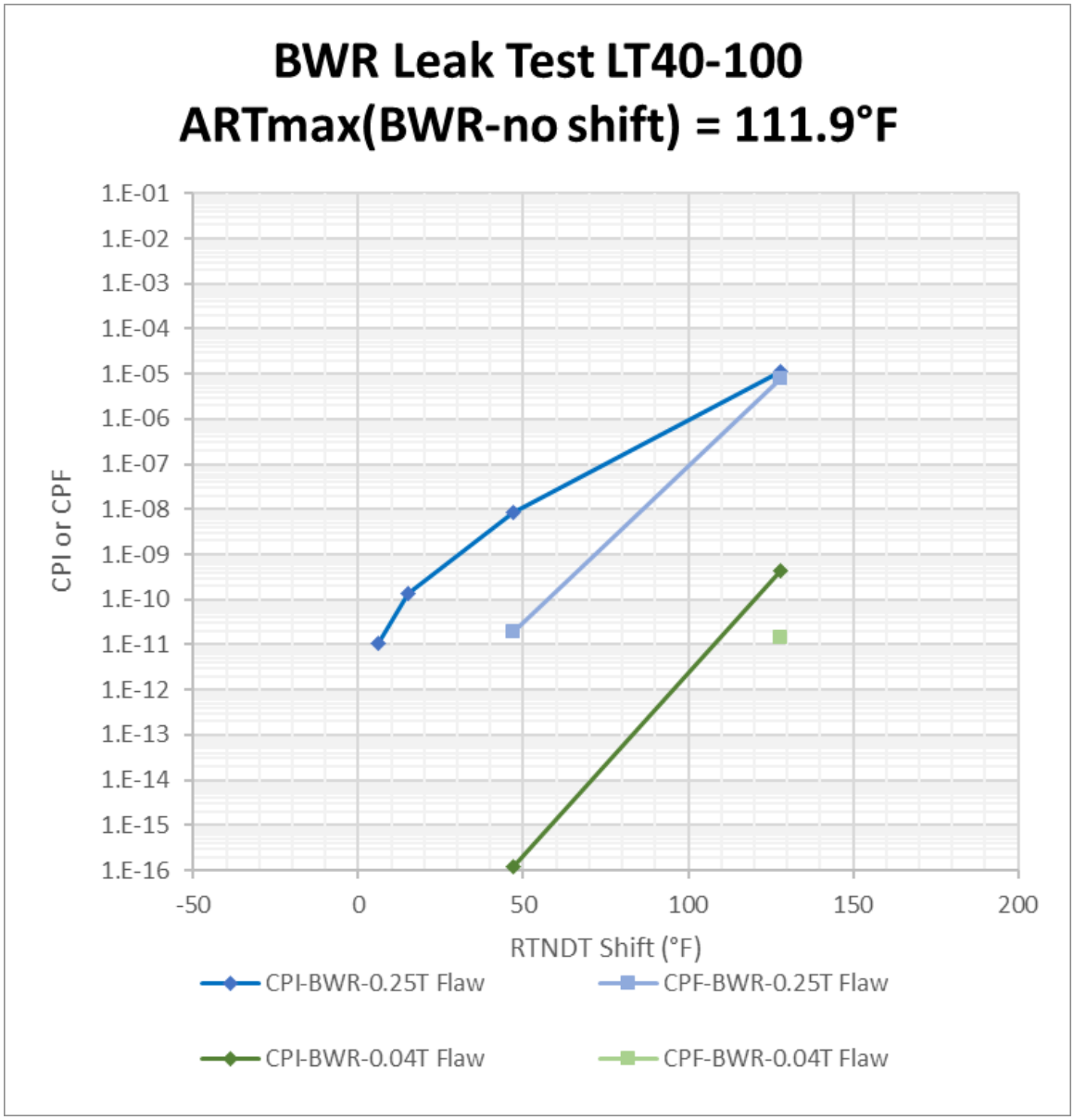

Figure 4-6: CPI and CPF for BWR, ¼ T and Shallow Flaws, as a Function of RT_{NDT} Shift for the LT40-100 Leak Test

Figure 4-6 shows the CPI and CPF for a BWR subjected to the LT40-100 leak test transient described in 3.1.2.6. The results are very similar to those for the LT40-40 leak test. For this transient, the ¼ T flaw CPI and CPF are orders of magnitude larger than the shallow flaw CPI and CPF, and both the CPI and CPF can reach values around $1x10^{-5}$ for high values of RT_{NDT} shift. However, since the frequency of occurrence of the LT40-40 leak test is estimated to be $1x10^{-3}$ event per year per BTP 5-3 [7], the overall TWCF (though-Wall Crack Frequency) remains well below the $1x10^{-6}$ per year limit despite the high CPI and CPF calculated in some cases.

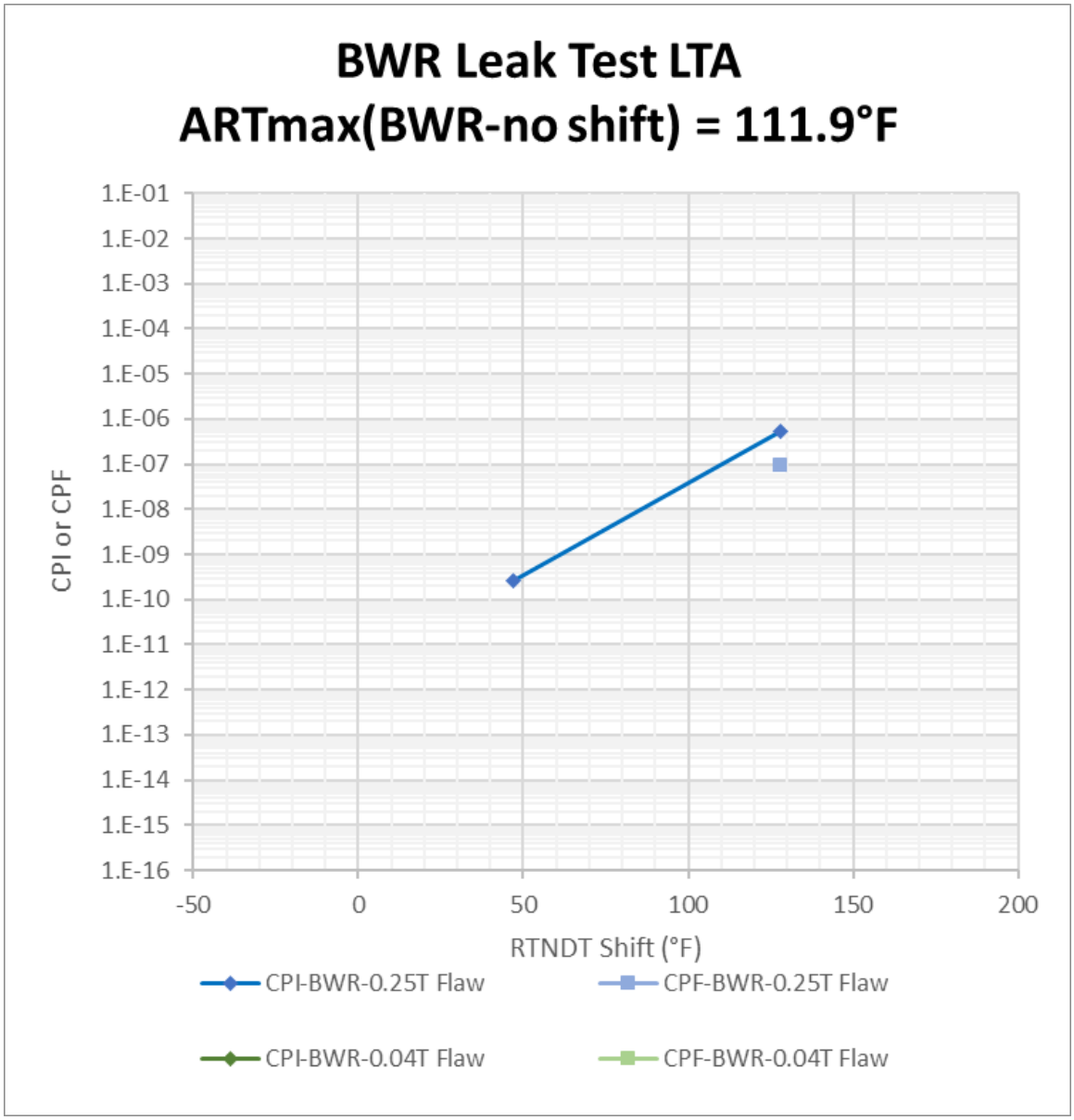

Figure 4-7: CPI and CPF for BWR, ¼ T and Shallow Flaws, as a Function of RT_{NDT} Shift for the LTA Leak Test

Figure 4-7 shows the CPI and CPF for a BWR subjected to the LTA leak test transient described in 3.1.2.7. The frequency of occurrence of the leak test can be assumed to be 1 event per year since this is an actual test that was performed at a plant and because leak testing must be performed as part of return to power operations in BWRs. As a result, the CPI and CPF are equal to the annual frequency of crack initiation and TWCF, respectively. This figure shows that for ¼ T flaws, a high value of RT_{NDT} shift of about 128°F, corresponding to the 99th percentile of RT_{NDT} shift values (see 3.2), can result in a TWCF of $1x10^{-7}$ events per year, which is still below the $1x10^{-6}$ limit on highest allowable TWCF per the regulations. Interestingly, shallow flaws resulted in all values of CPI and CPF being zero, which indicates that shallow flaws are not a complicating factor for BWR leak tests. In fact, ¼ T flaws result in much higher CPI and CPF than shallow flaws do for BWR leak tests, indicating that the BWR leak test issue is not related to the presence of shallow flaws. This is an important point because the BWR leak test issue and the shallow flaw issue have often been incorrectly linked.

In summary, with the modeling assumptions used in this study, the transients resulting in the highest TWCF values are PWR cooldowns along the P-T limit for ¼ T flaws at high values of RT_{NDT} shift. However, the highest calculated TWCF still remained below $1x10^{-6}$ per year.

For BWRs, the transients resulting in the highest TWCF are leak tests, with TWCF reaching close to $1x10^{-7}$ for an actual BWR leak test and TWCF reaching close to $1x10^{-8}$ for leak tests at the P-T limit. However, once again, even the highest calculated TWCF still remained below $1x10^{-6}$ per year.

Realistic cooldown transients resulted in the lowest TWCF values, with most being zero, and the highest reaching around $1x10^{-10}$ per year for one of the actual PWR cooldowns modeled.

5 References

[1] U.S. Nuclear Regulatory Commission, *Regulatory Guide 1.99, Revision 2: Radiation Embrittlement of Reactor Vessel Materials (ML003740284),* Washington, DC: U.S. NRC, May 1988.

[2] ASTM International, *ASTM E900-15: Standard Guide for Predicting Radiation-Induced Transition Temperature Shift in Reactor Vessel Materials,* West Conshohocken, PA: ASTM International, 2015.

[3] B. R. Bass, T. L. Dickson, P. T. Williams, H. B. Klasky and R. H. Dodds, "ORNL/TM-2015/59531/REV-01: The Effect of Shallow Inside-Surface-Breaking Flaws on the Probability of Brittle Fracture of Reactors Subjected to Postulated and Actual Operational Cool-Down Transients: A Status Report," Oak Ridge National Laboratory, Oak Ridge, TN, 2015.

[4] P. T. Williams, T. L. Dickson, B. R. Bass and H. B. Klasky, "ORNL/LTR-2016/309: Fracture Analysis of Vessels – Oak Ridge FAVOR, v16.1, Computer Code: Theory and Implementation of Algorithms, Methods, and Correlations," Oak Ridge National Laboratory, Oak Ridge, TN, 2016.

[5] T. L. Dickson, P. T. Williams, B. R. Bass and H. B. Klasky, "ORNL/LTR-2016/310: Fracture Analysis of Vessels – Oak Ridge - FAVOR, v16.1, Computer Code:User's Guide," Oak Ridge National Laboratory, 2016.

[6] The American Society of Mechanical Engineers, *ASME BPVC.XI-2019, Nonmandatory Appendix G: Fracture Toughness Criteria for Protection Against Failure,* New York, NY: ASME, 2019.

[7] U.S. Nuclear Regulatory Commission, *Closure Memorandum Supporting the Limited Revision of NUREG-0800 Branch Technical Position 5-3 "Fracture Toughness Requirements" (ML16364A285),* Washington, DC: U.S NRC, April 11, 2017.

6 Appendix A: List of FAVOR Analyses

6.1 PWR Analyses

Reactor Type	Flaw	RTNDT Shift	Transient	Run Type	Folder	Case Name
PWR	025T	0F	**P0_PT100**	**Deterministic**	**PWR 025T 0F**	**PWR_025T_0F_P0_PT100**
PWR	025T	-40F	**PT100-100**	**Deterministic**	**PWR 025T -40F**	**PWR_025T_-40F_PT100-100**
PWR	025T	-40F	**PT100-100**	**Probabilistic**	**PWR 025T -40F**	**PWR_025T_-40F_PT100-100**
PWR	003T	-40F	**PT100-100**	**Deterministic**	**PWR 003T -40F**	**PWR_003T_-40F_PT100-100**
PWR	003T	-40F	**PT100-100**	**Probabilistic**	**PWR 003T -40F**	**PWR_003T_-40F_PT100-100**
PWR	025T	0F	**PT100-100**	**Deterministic**	**PWR 025T 0F**	**PWR_025T_0F_PT100-100**
PWR	025T	0F	**PT100-100**	**Probabilistic**	**PWR 025T 0F**	**PWR_025T_0F_PT100-100**
PWR	003T	0F	**PT100-100**	**Deterministic**	**PWR 003T 0F**	**PWR_003T_0F_PT100-100**
PWR	003T	0F	**PT100-100**	**Probabilistic**	**PWR 003T 0F**	**PWR_003T_0F_PT100-100**
PWR	025T	+40F	**PT100-100**	**Deterministic**	**PWR 025T +40F**	**PWR_025T_+40F_PT100-100**
PWR	025T	+40F	**PT100-100**	**Probabilistic**	**PWR 025T +40F**	**PWR_025T_+40F_PT100-100**
PWR	003T	+40F	**PT100-100**	**Deterministic**	**PWR 003T +40F**	**PWR_003T_+40F_PT100-100**
PWR	003T	+40F	**PT100-100**	**Probabilistic**	**PWR 003T +40F**	**PWR_003T_+40F_PT100-100**
PWR	025T	+78F	**PT100-100**	**Deterministic**	**PWR 025T +78F**	**PWR_025T_+78F_PT100-100**
PWR	025T	+78F	**PT100-100**	**Probabilistic**	**PWR 025T +78F**	**PWR_025T_+78F_PT100-100**
PWR	003T	+78F	**PT100-100**	**Deterministic**	**PWR 003T +78F**	**PWR_003T_+78F_PT100-100**
PWR	003T	+78F	**PT100-100**	**Probabilistic**	**PWR 003T +78F**	**PWR_003T_+78F_PT100-100**
PWR	025T	+131F	**PT100-100**	**Deterministic**	**PWR 025T +131F**	**PWR_025T_+131F_PT100-100**
PWR	025T	+131F	**PT100-100**	**Probabilistic**	**PWR 025T +131F**	**PWR_025T_+131F_PT100-100**
PWR	003T	+131F	**PT100-100**	**Deterministic**	**PWR 003T +131F**	**PWR_003T_+131F_PT100-100**
PWR	003T	+131F	**PT100-100**	**Probabilistic**	**PWR 003T +131F**	**PWR_003T_+131F_PT100-100**
PWR	025T	+193F	**PT100-100**	**Deterministic**	**PWR 025T +193F**	**PWR_025T_+193F_PT100-100**
PWR	025T	+193F	**PT100-100**	**Probabilistic**	**PWR 025T +193F**	**PWR_025T_+193F_PT100-100**
PWR	003T	+193F	**PT100-100**	**Deterministic**	**PWR 003T +193F**	**PWR_003T_+193F_PT100-100**

Reactor Type	Flaw	RTNDT Shift	Transient	Run Type	Folder	Case Name
PWR	003T	+193F	**PT100-100**	**Probabilistic**	**PWR 003T +193F**	**PWR_003T_+193F_PT100-100**
PWR	025T	0F	**P0_PT50**	**Deterministic**	**PWR 025T 0F**	**PWR_025T_0F_P0_PT50**
PWR	025T	-40F	**PT100-50**	**Deterministic**	**PWR 025T -40F**	**PWR_025T_-40F_PT100-50**
PWR	025T	-40F	**PT100-50**	**Probabilistic**	**PWR 025T -40F**	**PWR_025T_-40F_PT100-50**
PWR	003T	-40F	**PT100-50**	**Deterministic**	**PWR 003T -40F**	**PWR_003T_-40F_PT100-50**
PWR	003T	-40F	**PT100-50**	**Probabilistic**	**PWR 003T -40F**	**PWR_003T_-40F_PT100-50**
PWR	025T	0F	**PT100-50**	**Deterministic**	**PWR 025T 0F**	**PWR_025T_0F_PT100-50**
PWR	025T	0F	**PT100-50**	**Probabilistic**	**PWR 025T 0F**	**PWR_025T_0F_PT100-50**
PWR	003T	0F	**PT100-50**	**Deterministic**	**PWR 003T 0F**	**PWR_003T_0F_PT100-50**
PWR	003T	0F	**PT100-50**	**Probabilistic**	**PWR 003T 0F**	**PWR_003T_0F_PT100-50**
PWR	025T	+40F	**PT100-50**	**Deterministic**	**PWR 025T +40F**	**PWR_025T_+40F_PT100-50**
PWR	025T	+40F	**PT100-50**	**Probabilistic**	**PWR 025T +40F**	**PWR_025T_+40F_PT100-50**
PWR	003T	+40F	**PT100-50**	**Deterministic**	**PWR 003T +40F**	**PWR_003T_+40F_PT100-50**
PWR	003T	+40F	**PT100-50**	**Probabilistic**	**PWR 003T +40F**	**PWR_003T_+40F_PT100-50**
PWR	025T	+78F	**PT100-50**	**Deterministic**	**PWR 025T +78F**	**PWR_025T_+78F_PT100-50**
PWR	025T	+78F	**PT100-50**	**Probabilistic**	**PWR 025T +78F**	**PWR_025T_+78F_PT100-50**
PWR	003T	+78F	**PT100-50**	**Deterministic**	**PWR 003T +78F**	**PWR_003T_+78F_PT100-50**
PWR	003T	+78F	**PT100-50**	**Probabilistic**	**PWR 003T +78F**	**PWR_003T_+78F_PT100-50**
PWR	025T	+131F	**PT100-50**	**Deterministic**	**PWR 025T +131F**	**PWR_025T_+131F_PT100-50**
PWR	025T	+131F	**PT100-50**	**Probabilistic**	**PWR 025T +131F**	**PWR_025T_+131F_PT100-50**
PWR	003T	+131F	**PT100-50**	**Deterministic**	**PWR 003T +131F**	**PWR_003T_+131F_PT100-50**
PWR	003T	+131F	**PT100-50**	**Probabilistic**	**PWR 003T +131F**	**PWR_003T_+131F_PT100-50**
PWR	025T	+193F	**PT100-50**	**Deterministic**	**PWR 025T +193F**	**PWR_025T_+193F_PT100-50**
PWR	025T	+193F	**PT100-50**	**Probabilistic**	**PWR 025T +193F**	**PWR_025T_+193F_PT100-50**
PWR	003T	+193F	**PT100-50**	**Deterministic**	**PWR 003T +193F**	**PWR_003T_+193F_PT100-50**
PWR	003T	+193F	**PT100-50**	**Probabilistic**	**PWR 003T +193F**	**PWR_003T_+193F_PT100-50**
PWR	025T	-40F	**PT50-50**	**Deterministic**	**PWR 025T -40F**	**PWR_025T_-40F_PT50-50**
PWR	025T	-40F	**PT50-50**	**Probabilistic**	**PWR 025T -40F**	**PWR_025T_-40F_PT50-50**
PWR	003T	-40F	**PT50-50**	**Deterministic**	**PWR 003T -40F**	**PWR_003T_-40F_PT50-50**
PWR	003T	-40F	**PT50-50**	**Probabilistic**	**PWR 003T -40F**	**PWR_003T_-40F_PT50-50**

Reactor Type	Flaw	RTNDT Shift	Transient	Run Type	Folder	Case Name
PWR	025T	0F	**PT50-50**	**Deterministic**	**PWR 025T 0F**	**PWR_025T_0F_PT50-50**
PWR	025T	0F	**PT50-50**	**Probabilistic**	**PWR 025T 0F**	**PWR_025T_0F_PT50-50**
PWR	003T	0F	**PT50-50**	**Deterministic**	**PWR 003T 0F**	**PWR_003T_0F_PT50-50**
PWR	003T	0F	**PT50-50**	**Probabilistic**	**PWR 003T 0F**	**PWR_003T_0F_PT50-50**
PWR	025T	+40F	**PT50-50**	**Deterministic**	**PWR 025T +40F**	**PWR_025T_+40F_PT50-50**
PWR	025T	+40F	**PT50-50**	**Probabilistic**	**PWR 025T +40F**	**PWR_025T_+40F_PT50-50**
PWR	003T	+40F	**PT50-50**	**Deterministic**	**PWR 003T +40F**	**PWR_003T_+40F_PT50-50**
PWR	003T	+40F	**PT50-50**	**Probabilistic**	**PWR 003T +40F**	**PWR_003T_+40F_PT50-50**
PWR	025T	+78F	**PT50-50**	**Deterministic**	**PWR 025T +78F**	**PWR_025T_+78F_PT50-50**
PWR	025T	+78F	**PT50-50**	**Probabilistic**	**PWR 025T +78F**	**PWR_025T_+78F_PT50-50**
PWR	003T	+78F	**PT50-50**	**Deterministic**	**PWR 003T +78F**	**PWR_003T_+78F_PT50-50**
PWR	003T	+78F	**PT50-50**	**Probabilistic**	**PWR 003T +78F**	**PWR_003T_+78F_PT50-50**
PWR	025T	+131F	**PT50-50**	**Deterministic**	**PWR 025T +131F**	**PWR_025T_+131F_PT50-50**
PWR	025T	+131F	**PT50-50**	**Probabilistic**	**PWR 025T +131F**	**PWR_025T_+131F_PT50-50**
PWR	003T	+131F	**PT50-50**	**Deterministic**	**PWR 003T +131F**	**PWR_003T_+131F_PT50-50**
PWR	003T	+131F	**PT50-50**	**Probabilistic**	**PWR 003T +131F**	**PWR_003T_+131F_PT50-50**
PWR	025T	+193F	**PT50-50**	**Deterministic**	**PWR 025T +193F**	**PWR_025T_+193F_PT50-50**
PWR	025T	+193F	**PT50-50**	**Probabilistic**	**PWR 025T +193F**	**PWR_025T_+193F_PT50-50**
PWR	003T	+193F	**PT50-50**	**Deterministic**	**PWR 003T +193F**	**PWR_003T_+193F_PT50-50**
PWR	003T	+193F	**PT50-50**	**Probabilistic**	**PWR 003T +193F**	**PWR_003T_+193F_PT50-50**
PWR	025T	-40F	**C50P**	**Deterministic**	**PWR 025T -40F**	**PWR_025T_-40F_C50P**
PWR	025T	-40F	**C50P**	**Probabilistic**	**PWR 025T -40F**	**PWR_025T_-40F_C50P**
PWR	003T	-40F	**C50P**	**Deterministic**	**PWR 003T -40F**	**PWR_003T_-40F_C50P**
PWR	003T	-40F	**C50P**	**Probabilistic**	**PWR 003T -40F**	**PWR_003T_-40F_C50P**
PWR	025T	0F	**C50P**	**Deterministic**	**PWR 025T 0F**	**PWR_025T_0F_C50P**
PWR	025T	0F	**C50P**	**Probabilistic**	**PWR 025T 0F**	**PWR_025T_0F_C50P**
PWR	003T	0F	**C50P**	**Deterministic**	**PWR 003T 0F**	**PWR_003T_0F_C50P**
PWR	003T	0F	**C50P**	**Probabilistic**	**PWR 003T 0F**	**PWR_003T_0F_C50P**
PWR	025T	+40F	**C50P**	**Deterministic**	**PWR 025T +40F**	**PWR_025T_+40F_C50P**
PWR	025T	+40F	**C50P**	**Probabilistic**	**PWR 025T +40F**	**PWR_025T_+40F_C50P**

Reactor Type	Flaw	RTNDT Shift	Transient	Run Type	Folder	Case Name
PWR	003T	+40F	**C50P**	**Deterministic**	**PWR 003T +40F**	**PWR_003T_+40F_C50P**
PWR	003T	+40F	**C50P**	**Probabilistic**	**PWR 003T +40F**	**PWR_003T_+40F_C50P**
PWR	025T	+78F	**C50P**	**Deterministic**	**PWR 025T +78F**	**PWR_025T_+78F_C50P**
PWR	025T	+78F	**C50P**	**Probabilistic**	**PWR 025T +78F**	**PWR_025T_+78F_C50P**
PWR	003T	+78F	**C50P**	**Deterministic**	**PWR 003T +78F**	**PWR_003T_+78F_C50P**
PWR	003T	+78F	**C50P**	**Probabilistic**	**PWR 003T +78F**	**PWR_003T_+78F_C50P**
PWR	025T	+131F	**C50P**	**Deterministic**	**PWR 025T +131F**	**PWR_025T_+131F_C50P**
PWR	025T	+131F	**C50P**	**Probabilistic**	**PWR 025T +131F**	**PWR_025T_+131F_C50P**
PWR	003T	+131F	**C50P**	**Deterministic**	**PWR 003T +131F**	**PWR_003T_+131F_C50P**
PWR	003T	+131F	**C50P**	**Probabilistic**	**PWR 003T +131F**	**PWR_003T_+131F_C50P**
PWR	025T	+193F	**C50P**	**Deterministic**	**PWR 025T +193F**	**PWR_025T_+193F_C50P**
PWR	025T	+193F	**C50P**	**Probabilistic**	**PWR 025T +193F**	**PWR_025T_+193F_C50P**
PWR	003T	+193F	**C50P**	**Deterministic**	**PWR 003T +193F**	**PWR_003T_+193F_C50P**
PWR	003T	+193F	**C50P**	**Probabilistic**	**PWR 003T +193F**	**PWR_003T_+193F_C50P**
PWR	003T	+100F	**P1C1**	**Deterministic**	**PWR 003T +100F**	**PWR_003T_+100F_P1C1**
PWR	003T	+100F	**P1C1**	**Probabilistic**	**PWR 003T +100F**	**PWR_003T_+100F_P1C1**
PWR	003T	+100F	**P1C2**	**Deterministic**	**PWR 003T +100F**	**PWR_003T_+100F_P1C2**
PWR	003T	+100F	**P1C2**	**Probabilistic**	**PWR 003T +100F**	**PWR_003T_+100F_P1C2**
PWR	003T	+100F	**P1C3**	**Deterministic**	**PWR 003T +100F**	**PWR_003T_+100F_P1C3**
PWR	003T	+100F	**P1C3**	**Probabilistic**	**PWR 003T +100F**	**PWR_003T_+100F_P1C3**
PWR	003T	+100F	**P1C4**	**Deterministic**	**PWR 003T +100F**	**PWR_003T_+100F_P1C4**
PWR	003T	+100F	**P1C4**	**Probabilistic**	**PWR 003T +100F**	**PWR_003T_+100F_P1C4**
PWR	003T	+100F	**P2C1**	**Deterministic**	**PWR 003T +100F**	**PWR_003T_+100F_P2C1**
PWR	003T	+100F	**P2C1**	**Probabilistic**	**PWR 003T +100F**	**PWR_003T_+100F_P2C1**
PWR	003T	+100F	**P2C2**	**Deterministic**	**PWR 003T +100F**	**PWR_003T_+100F_P2C2**
PWR	003T	+100F	**P2C2**	**Probabilistic**	**PWR 003T +100F**	**PWR_003T_+100F_P2C2**
PWR	003T	+100F	**P3C1**	**Deterministic**	**PWR 003T +100F**	**PWR_003T_+100F_P3C1**
PWR	003T	+100F	**P3C1**	**Probabilistic**	**PWR 003T +100F**	**PWR_003T_+100F_P3C1**
PWR	003T	+100F	**P3C2**	**Deterministic**	**PWR 003T +100F**	**PWR_003T_+100F_P3C2**
PWR	003T	+100F	**P3C2**	**Probabilistic**	**PWR 003T +100F**	**PWR_003T_+100F_P3C2**

Reactor Type	Flaw	RTNDT Shift	Transient	Run Type	Folder	Case Name
PWR	003T	+100F	**P4C1**	**Deterministic**	**PWR 003T +100F**	**PWR_003T_+100F_P4C1**
PWR	003T	+100F	**P4C1**	**Probabilistic**	**PWR 003T +100F**	**PWR_003T_+100F_P4C1**
PWR	003T	+100F	**P4C2**	**Deterministic**	**PWR 003T +100F**	**PWR_003T_+100F_P4C2**
PWR	003T	+100F	**P4C2**	**Probabilistic**	**PWR 003T +100F**	**PWR_003T_+100F_P4C2**
PWR	003T	+100F	**P4C3**	**Deterministic**	**PWR 003T +100F**	**PWR_003T_+100F_P4C3**
PWR	003T	+100F	**P4C3**	**Probabilistic**	**PWR 003T +100F**	**PWR_003T_+100F_P4C3**
PWR	003T	+100F	**P5C1**	**Deterministic**	**PWR 003T +100F**	**PWR_003T_+100F_P5C1**
PWR	003T	+100F	**P5C1**	**Probabilistic**	**PWR 003T +100F**	**PWR_003T_+100F_P5C1**
PWR	003T	+100F	**P5C2**	**Deterministic**	**PWR 003T +100F**	**PWR_003T_+100F_P5C2**
PWR	003T	+100F	**P5C2**	**Probabilistic**	**PWR 003T +100F**	**PWR_003T_+100F_P5C2**
PWR	003T	+100F	**P5C3**	**Deterministic**	**PWR 003T +100F**	**PWR_003T_+100F_P5C3**
PWR	003T	+100F	**P5C3**	**Probabilistic**	**PWR 003T +100F**	**PWR_003T_+100F_P5C3**
PWR	003T	+100F	**P5C4**	**Deterministic**	**PWR 003T +100F**	**PWR_003T_+100F_P5C4**
PWR	003T	+100F	**P5C4**	**Probabilistic**	**PWR 003T +100F**	**PWR_003T_+100F_P5C4**
PWR	003T	+100F	**P5C5**	**Deterministic**	**PWR 003T +100F**	**PWR_003T_+100F_P5C5**
PWR	003T	+100F	**P5C5**	**Probabilistic**	**PWR 003T +100F**	**PWR_003T_+100F_P5C5**
PWR	003T	+100F	**P6C1**	**Deterministic**	**PWR 003T +100F**	**PWR_003T_+100F_P6C1**
PWR	003T	+100F	**P6C1**	**Probabilistic**	**PWR 003T +100F**	**PWR_003T_+100F_P6C1**
PWR	003T	+100F	**P7C1**	**Deterministic**	**PWR 003T +100F**	**PWR_003T_+100F_P7C1**
PWR	003T	+100F	**P7C1**	**Probabilistic**	**PWR 003T +100F**	**PWR_003T_+100F_P7C1**
PWR	003T	+100F	**P7C2**	**Deterministic**	**PWR 003T +100F**	**PWR_003T_+100F_P7C2**
PWR	003T	+100F	**P7C2**	**Probabilistic**	**PWR 003T +100F**	**PWR_003T_+100F_P7C2**
PWR	003T	+100F	**P7C3**	**Deterministic**	**PWR 003T +100F**	**PWR_003T_+100F_P7C3**
PWR	003T	+100F	**P7C3**	**Probabilistic**	**PWR 003T +100F**	**PWR_003T_+100F_P7C3**
PWR	003T	+100F	**P7C4**	**Deterministic**	**PWR 003T +100F**	**PWR_003T_+100F_P7C4**
PWR	003T	+100F	**P7C4**	**Probabilistic**	**PWR 003T +100F**	**PWR_003T_+100F_P7C4**
PWR	003T	+100F	**P7C5**	**Deterministic**	**PWR 003T +100F**	**PWR_003T_+100F_P7C5**
PWR	003T	+100F	**P7C5**	**Probabilistic**	**PWR 003T +100F**	**PWR_003T_+100F_P7C5**
PWR	003T	+100F	**P7C6**	**Deterministic**	**PWR 003T +100F**	**PWR_003T_+100F_P7C6**
PWR	003T	+100F	**P7C6**	**Probabilistic**	**PWR 003T +100F**	**PWR_003T_+100F_P7C6**

Reactor Type	Flaw	RTNDT Shift	Transient	Run Type	Folder	Case Name
PWR	003T	+100F	**P7C7**	**Deterministic**	**PWR 003T +100F**	**PWR_003T_+100F_P7C7**
PWR	003T	+100F	**P7C7**	**Probabilistic**	**PWR 003T +100F**	**PWR_003T_+100F_P7C7**
PWR	003T	+100F	**P7C8**	**Deterministic**	**PWR 003T +100F**	**PWR_003T_+100F_P7C8**
PWR	003T	+100F	**P7C8**	**Probabilistic**	**PWR 003T +100F**	**PWR_003T_+100F_P7C8**
PWR	003T	+100F	**P8C1**	**Deterministic**	**PWR 003T +100F**	**PWR_003T_+100F_P8C1**
PWR	003T	+100F	**P8C1**	**Probabilistic**	**PWR 003T +100F**	**PWR_003T_+100F_P8C1**
PWR	003T	+100F	**P8C2**	**Deterministic**	**PWR 003T +100F**	**PWR_003T_+100F_P8C2**
PWR	003T	+100F	**P8C2**	**Probabilistic**	**PWR 003T +100F**	**PWR_003T_+100F_P8C2**
PWR	003T	+100F	**P8C3**	**Deterministic**	**PWR 003T +100F**	**PWR_003T_+100F_P8C3**
PWR	003T	+100F	**P8C3**	**Probabilistic**	**PWR 003T +100F**	**PWR_003T_+100F_P8C3**
PWR	003T	+100F	**P8C4**	**Deterministic**	**PWR 003T +100F**	**PWR_003T_+100F_P8C4**
PWR	003T	+100F	**P8C4**	**Probabilistic**	**PWR 003T +100F**	**PWR_003T_+100F_P8C4**
PWR	003T	+100F	**P8C5**	**Deterministic**	**PWR 003T +100F**	**PWR_003T_+100F_P8C5**
PWR	003T	+100F	**P8C5**	**Probabilistic**	**PWR 003T +100F**	**PWR_003T_+100F_P8C5**
PWR	003T	+100F	**P8C6**	**Deterministic**	**PWR 003T +100F**	**PWR_003T_+100F_P8C6**
PWR	003T	+100F	**P8C6**	**Probabilistic**	**PWR 003T +100F**	**PWR_003T_+100F_P8C6**
PWR	003T	+100F	**P8C7**	**Deterministic**	**PWR 003T +100F**	**PWR_003T_+100F_P8C7**
PWR	003T	+100F	**P8C7**	**Probabilistic**	**PWR 003T +100F**	**PWR_003T_+100F_P8C7**
PWR	003T	+100F	**P9C1**	**Deterministic**	**PWR 003T +100F**	**PWR_003T_+100F_P9C1**
PWR	003T	+100F	**P9C1**	**Probabilistic**	**PWR 003T +100F**	**PWR_003T_+100F_P9C1**
PWR	003T	+100F	**P9C2**	**Deterministic**	**PWR 003T +100F**	**PWR_003T_+100F_P9C2**
PWR	003T	+100F	**P9C2**	**Probabilistic**	**PWR 003T +100F**	**PWR_003T_+100F_P9C2**
PWR	003T	+100F	**P10C1**	**Deterministic**	**PWR 003T +100F**	**PWR_003T_+100F_P10C1**
PWR	003T	+100F	**P10C1**	**Probabilistic**	**PWR 003T +100F**	**PWR_003T_+100F_P10C1**
PWR	003T	+100F	**P11C1**	**Deterministic**	**PWR 003T +100F**	**PWR_003T_+100F_P11C1**
PWR	003T	+100F	**P11C1**	**Probabilistic**	**PWR 003T +100F**	**PWR_003T_+100F_P11C1**
PWR	003T	+100F	**PAC1**	**Deterministic**	**PWR 003T +100F**	**PWR_003T_+100F_PAC1**
PWR	003T	+100F	**PAC1**	**Probabilistic**	**PWR 003T +100F**	**PWR_003T_+100F_PAC1**
PWR	003T	+100F	**PAC2**	**Deterministic**	**PWR 003T +100F**	**PWR_003T_+100F_PAC2**
PWR	003T	+100F	**PAC2**	**Probabilistic**	**PWR 003T +100F**	**PWR_003T_+100F_PAC2**

Reactor Type	Flaw	RTNDT Shift	Transient	Run Type	Folder	Case Name
PWR	003T	+100F	**PBC1**	**Deterministic**	**PWR 003T +100F**	**PWR_003T_+100F_PBC1**
PWR	003T	+100F	**PBC1**	**Probabilistic**	**PWR 003T +100F**	**PWR_003T_+100F_PBC1**
PWR	003T	+100F	**PBC2**	**Deterministic**	**PWR 003T +100F**	**PWR_003T_+100F_PBC2**
PWR	003T	+100F	**PBC2**	**Probabilistic**	**PWR 003T +100F**	**PWR_003T_+100F_PBC2**
PWR	003T	+100F	**PCC1**	**Deterministic**	**PWR 003T +100F**	**PWR_003T_+100F_PCC1**
PWR	003T	+100F	**PCC1**	**Probabilistic**	**PWR 003T +100F**	**PWR_003T_+100F_PCC1**
PWR	003T	+100F	**PCC2**	**Deterministic**	**PWR 003T +100F**	**PWR_003T_+100F_PCC2**
PWR	003T	+100F	**PCC2**	**Probabilistic**	**PWR 003T +100F**	**PWR_003T_+100F_PCC2**
PWR	003T	+100F	**PDC1**	**Deterministic**	**PWR 003T +100F**	**PWR_003T_+100F_PDC1**
PWR	003T	+100F	**PDC1**	**Probabilistic**	**PWR 003T +100F**	**PWR_003T_+100F_PDC1**
PWR	003T	+100F	**PDC2**	**Deterministic**	**PWR 003T +100F**	**PWR_003T_+100F_PDC2**
PWR	003T	+100F	**PDC2**	**Probabilistic**	**PWR 003T +100F**	**PWR_003T_+100F_PDC2**
PWR	003T	+100F	**PEC1**	**Deterministic**	**PWR 003T +100F**	**PWR_003T_+100F_PEC1**
PWR	003T	+100F	**PEC1**	**Probabilistic**	**PWR 003T +100F**	**PWR_003T_+100F_PEC1**
PWR	003T	+100F	**PEC2**	**Deterministic**	**PWR 003T +100F**	**PWR_003T_+100F_PEC2**
PWR	003T	+100F	**PEC2**	**Probabilistic**	**PWR 003T +100F**	**PWR_003T_+100F_PEC2**
PWR	003T	+100F	**PFC1**	**Deterministic**	**PWR 003T +100F**	**PWR_003T_+100F_PFC1**
PWR	003T	+100F	**PFC1**	**Probabilistic**	**PWR 003T +100F**	**PWR_003T_+100F_PFC1**
PWR	003T	+100F	**PFC2**	**Deterministic**	**PWR 003T +100F**	**PWR_003T_+100F_PFC2**
PWR	003T	+100F	**PFC2**	**Probabilistic**	**PWR 003T +100F**	**PWR_003T_+100F_PFC2**

6.2 BWR Analyses

Reactor Type	Flaw	RTNDT Shift	Transient	Run Type	Folder	Case Name
BWR	025T	0F	**P0_PT100**	**Deterministic**	**BWR 025T 0F**	**BWR_025T_0F_P0_PT100**
BWR	025T	-40F	**PT100-100**	**Deterministic**	**BWR 025T -40F**	**BWR_025T_-40F_PT100-100**
BWR	025T	-40F	**PT100-100**	**Probabilistic**	**BWR 025T -40F**	**BWR_025T_-40F_PT100-100**
BWR	004T	-40F	**PT100-100**	**Deterministic**	**BWR 004T -40F**	**BWR_004T_-40F_PT100-100**
BWR	004T	-40F	**PT100-100**	**Probabilistic**	**BWR 004T -40F**	**BWR_004T_-40F_PT100-100**
BWR	025T	0F	**PT100-100**	**Deterministic**	**BWR 025T 0F**	**BWR_025T_0F_PT100-100**
BWR	025T	0F	**PT100-100**	**Probabilistic**	**BWR 025T 0F**	**BWR_025T_0F_PT100-100**
BWR	004T	0F	**PT100-100**	**Deterministic**	**BWR 004T 0F**	**BWR_004T_0F_PT100-100**
BWR	004T	0F	**PT100-100**	**Probabilistic**	**BWR 004T 0F**	**BWR_004T_0F_PT100-100**
BWR	025T	+6F	**PT100-100**	**Deterministic**	**BWR 025T +6F**	**BWR_025T_+6F_PT100-100**
BWR	025T	+6F	**PT100-100**	**Probabilistic**	**BWR 025T +6F**	**BWR_025T_+6F_PT100-100**
BWR	004T	+6F	**PT100-100**	**Deterministic**	**BWR 004T +6F**	**BWR_004T_+6F_PT100-100**
BWR	004T	+6F	**PT100-100**	**Probabilistic**	**BWR 004T +6F**	**BWR_004T_+6F_PT100-100**
BWR	025T	+15F	**PT100-100**	**Deterministic**	**BWR 025T +15F**	**BWR_025T_+15F_PT100-100**
BWR	025T	+15F	**PT100-100**	**Probabilistic**	**BWR 025T +15F**	**BWR_025T_+15F_PT100-100**
BWR	004T	+15F	**PT100-100**	**Deterministic**	**BWR 004T +15F**	**BWR_004T_+15F_PT100-100**
BWR	004T	+15F	**PT100-100**	**Probabilistic**	**BWR 004T +15F**	**BWR_004T_+15F_PT100-100**
BWR	025T	+47F	**PT100-100**	**Deterministic**	**BWR 025T +47F**	**BWR_025T_+47F_PT100-100**
BWR	025T	+47F	**PT100-100**	**Probabilistic**	**BWR 025T +47F**	**BWR_025T_+47F_PT100-100**
BWR	004T	+47F	**PT100-100**	**Deterministic**	**BWR 004T +47F**	**BWR_004T_+47F_PT100-100**
BWR	004T	+47F	**PT100-100**	**Probabilistic**	**BWR 004T +47F**	**BWR_004T_+47F_PT100-100**
BWR	025T	+128F	**PT100-100**	**Deterministic**	**BWR 025T +128F**	**BWR_025T_+128F_PT100-100**
BWR	025T	+128F	**PT100-100**	**Probabilistic**	**BWR 025T +128F**	**BWR_025T_+128F_PT100-100**
BWR	004T	+128F	**PT100-100**	**Deterministic**	**BWR 004T +128F**	**BWR_004T_+128F_PT100-100**
BWR	004T	+128F	**PT100-100**	**Probabilistic**	**BWR 004T +128F**	**BWR_004T_+128F_PT100-100**
BWR	025T	0F	**P0_PT50**	**Deterministic**	**BWR 025T 0F**	**BWR_025T_0F_P0_PT50**
BWR	025T	-40F	**PT100-50**	**Deterministic**	**BWR 025T -40F**	**BWR_025T_-40F_PT100-50**

Reactor Type	Flaw	RTNDT Shift	Transient	Run Type	Folder	Case Name
BWR	025T	-40F	**PT100-50**	**Probabilistic**	**BWR 025T -40F**	**BWR_025T_-40F_PT100-50**
BWR	004T	-40F	**PT100-50**	**Deterministic**	**BWR 004T -40F**	**BWR_004T_-40F_PT100-50**
BWR	004T	-40F	**PT100-50**	**Probabilistic**	**BWR 004T -40F**	**BWR_004T_-40F_PT100-50**
BWR	025T	0F	**PT100-50**	**Deterministic**	**BWR 025T 0F**	**BWR_025T_0F_PT100-50**
BWR	025T	0F	**PT100-50**	**Probabilistic**	**BWR 025T 0F**	**BWR_025T_0F_PT100-50**
BWR	004T	0F	**PT100-50**	**Deterministic**	**BWR 004T 0F**	**BWR_004T_0F_PT100-50**
BWR	004T	0F	**PT100-50**	**Probabilistic**	**BWR 004T 0F**	**BWR_004T_0F_PT100-50**
BWR	025T	+6F	**PT100-50**	**Deterministic**	**BWR 025T +6F**	**BWR_025T_+6F_PT100-50**
BWR	025T	+6F	**PT100-50**	**Probabilistic**	**BWR 025T +6F**	**BWR_025T_+6F_PT100-50**
BWR	004T	+6F	**PT100-50**	**Deterministic**	**BWR 004T +6F**	**BWR_004T_+6F_PT100-50**
BWR	004T	+6F	**PT100-50**	**Probabilistic**	**BWR 004T +6F**	**BWR_004T_+6F_PT100-50**
BWR	025T	+15F	**PT100-50**	**Deterministic**	**BWR 025T +15F**	**BWR_025T_+15F_PT100-50**
BWR	025T	+15F	**PT100-50**	**Probabilistic**	**BWR 025T +15F**	**BWR_025T_+15F_PT100-50**
BWR	004T	+15F	**PT100-50**	**Deterministic**	**BWR 004T +15F**	**BWR_004T_+15F_PT100-50**
BWR	004T	+15F	**PT100-50**	**Probabilistic**	**BWR 004T +15F**	**BWR_004T_+15F_PT100-50**
BWR	025T	+47F	**PT100-50**	**Deterministic**	**BWR 025T +47F**	**BWR_025T_+47F_PT100-50**
BWR	025T	+47F	**PT100-50**	**Probabilistic**	**BWR 025T +47F**	**BWR_025T_+47F_PT100-50**
BWR	004T	+47F	**PT100-50**	**Deterministic**	**BWR 004T +47F**	**BWR_004T_+47F_PT100-50**
BWR	004T	+47F	**PT100-50**	**Probabilistic**	**BWR 004T +47F**	**BWR_004T_+47F_PT100-50**
BWR	025T	+128F	**PT100-50**	**Deterministic**	**BWR 025T +128F**	**BWR_025T_+128F_PT100-50**
BWR	025T	+128F	**PT100-50**	**Probabilistic**	**BWR 025T +128F**	**BWR_025T_+128F_PT100-50**
BWR	004T	+128F	**PT100-50**	**Deterministic**	**BWR 004T +128F**	**BWR_004T_+128F_PT100-50**
BWR	004T	+128F	**PT100-50**	**Probabilistic**	**BWR 004T +128F**	**BWR_004T_+128F_PT100-50**
BWR	025T	-40F	**PT50-50**	**Deterministic**	**BWR 025T -40F**	**BWR_025T_-40F_PT50-50**
BWR	025T	-40F	**PT50-50**	**Probabilistic**	**BWR 025T -40F**	**BWR_025T_-40F_PT50-50**
BWR	004T	-40F	**PT50-50**	**Deterministic**	**BWR 004T -40F**	**BWR_004T_-40F_PT50-50**
BWR	004T	-40F	**PT50-50**	**Probabilistic**	**BWR 004T -40F**	**BWR_004T_-40F_PT50-50**
BWR	025T	0F	**PT50-50**	**Deterministic**	**BWR 025T 0F**	**BWR_025T_0F_PT50-50**
BWR	025T	0F	**PT50-50**	**Probabilistic**	**BWR 025T 0F**	**BWR_025T_0F_PT50-50**
BWR	004T	0F	**PT50-50**	**Deterministic**	**BWR 004T 0F**	**BWR_004T_0F_PT50-50**

Reactor Type	Flaw	RTNDT Shift	Transient	Run Type	Folder	Case Name
BWR	004T	0F	**PT50-50**	**Probabilistic**	**BWR 004T 0F**	**BWR_004T_0F_PT50-50**
BWR	025T	+6F	**PT50-50**	**Deterministic**	**BWR 025T +6F**	**BWR_025T_+6F_PT50-50**
BWR	025T	+6F	**PT50-50**	**Probabilistic**	**BWR 025T +6F**	**BWR_025T_+6F_PT50-50**
BWR	004T	+6F	**PT50-50**	**Deterministic**	**BWR 004T +6F**	**BWR_004T_+6F_PT50-50**
BWR	004T	+6F	**PT50-50**	**Probabilistic**	**BWR 004T +6F**	**BWR_004T_+6F_PT50-50**
BWR	025T	+15F	**PT50-50**	**Deterministic**	**BWR 025T +15F**	**BWR_025T_+15F_PT50-50**
BWR	025T	+15F	**PT50-50**	**Probabilistic**	**BWR 025T +15F**	**BWR_025T_+15F_PT50-50**
BWR	004T	+15F	**PT50-50**	**Deterministic**	**BWR 004T +15F**	**BWR_004T_+15F_PT50-50**
BWR	004T	+15F	**PT50-50**	**Probabilistic**	**BWR 004T +15F**	**BWR_004T_+15F_PT50-50**
BWR	025T	+47F	**PT50-50**	**Deterministic**	**BWR 025T +47F**	**BWR_025T_+47F_PT50-50**
BWR	025T	+47F	**PT50-50**	**Probabilistic**	**BWR 025T +47F**	**BWR_025T_+47F_PT50-50**
BWR	004T	+47F	**PT50-50**	**Deterministic**	**BWR 004T +47F**	**BWR_004T_+47F_PT50-50**
BWR	004T	+47F	**PT50-50**	**Probabilistic**	**BWR 004T +47F**	**BWR_004T_+47F_PT50-50**
BWR	025T	+128F	**PT50-50**	**Deterministic**	**BWR 025T +128F**	**BWR_025T_+128F_PT50-50**
BWR	025T	+128F	**PT50-50**	**Probabilistic**	**BWR 025T +128F**	**BWR_025T_+128F_PT50-50**
BWR	004T	+128F	**PT50-50**	**Deterministic**	**BWR 004T +128F**	**BWR_004T_+128F_PT50-50**
BWR	004T	+128F	**PT50-50**	**Probabilistic**	**BWR 004T +128F**	**BWR_004T_+128F_PT50-50**
BWR	025T	-40F	**S50**	**Deterministic**	**BWR 025T -40F**	**BWR_025T_-40F_S50**
BWR	025T	-40F	**S50**	**Probabilistic**	**BWR 025T -40F**	**BWR_025T_-40F_S50**
BWR	004T	-40F	**S50**	**Deterministic**	**BWR 004T -40F**	**BWR_004T_-40F_S50**
BWR	004T	-40F	**S50**	**Probabilistic**	**BWR 004T -40F**	**BWR_004T_-40F_S50**
BWR	025T	0F	**S50**	**Deterministic**	**BWR 025T 0F**	**BWR_025T_0F_S50**
BWR	025T	0F	**S50**	**Probabilistic**	**BWR 025T 0F**	**BWR_025T_0F_S50**
BWR	004T	0F	**S50**	**Deterministic**	**BWR 004T 0F**	**BWR_004T_0F_S50**
BWR	004T	0F	**S50**	**Probabilistic**	**BWR 004T 0F**	**BWR_004T_0F_S50**
BWR	025T	+6F	**S50**	**Deterministic**	**BWR 025T +6F**	**BWR_025T_+6F_S50**
BWR	025T	+6F	**S50**	**Probabilistic**	**BWR 025T +6F**	**BWR_025T_+6F_S50**
BWR	004T	+6F	**S50**	**Deterministic**	**BWR 004T +6F**	**BWR_004T_+6F_S50**
BWR	004T	+6F	**S50**	**Probabilistic**	**BWR 004T +6F**	**BWR_004T_+6F_S50**
BWR	025T	+15F	**S50**	**Deterministic**	**BWR 025T +15F**	**BWR_025T_+15F_S50**

Reactor Type	Flaw	RTNDT Shift	Transient	Run Type	Folder	Case Name
BWR	025T	+15F	**S50**	**Probabilistic**	**BWR 025T +15F**	**BWR_025T_+15F_S50**
BWR	004T	+15F	**S50**	**Deterministic**	**BWR 004T +15F**	**BWR_004T_+15F_S50**
BWR	004T	+15F	**S50**	**Probabilistic**	**BWR 004T +15F**	**BWR_004T_+15F_S50**
BWR	025T	+47F	**S50**	**Deterministic**	**BWR 025T +47F**	**BWR_025T_+47F_S50**
BWR	025T	+47F	**S50**	**Probabilistic**	**BWR 025T +47F**	**BWR_025T_+47F_S50**
BWR	004T	+47F	**S50**	**Deterministic**	**BWR 004T +47F**	**BWR_004T_+47F_S50**
BWR	004T	+47F	**S50**	**Probabilistic**	**BWR 004T +47F**	**BWR_004T_+47F_S50**
BWR	025T	+128F	**S50**	**Deterministic**	**BWR 025T +128F**	**BWR_025T_+128F_S50**
BWR	025T	+128F	**S50**	**Probabilistic**	**BWR 025T +128F**	**BWR_025T_+128F_S50**
BWR	004T	+128F	**S50**	**Deterministic**	**BWR 004T +128F**	**BWR_004T_+128F_S50**
BWR	004T	+128F	**S50**	**Probabilistic**	**BWR 004T +128F**	**BWR_004T_+128F_S50**
BWR	025T	0F	**P0_LT40-40**	**Deterministic**	**BWR 025T 0F**	**BWR_025T_0F_P0_LT40-40**
BWR	025T	-40F	**LT40-40**	**Deterministic**	**BWR 025T -40F**	**BWR_025T_-40F_LT40-40**
BWR	025T	-40F	**LT40-40**	**Probabilistic**	**BWR 025T -40F**	**BWR_025T_-40F_LT40-40**
BWR	004T	-40F	**LT40-40**	**Deterministic**	**BWR 004T -40F**	**BWR_004T_-40F_LT40-40**
BWR	004T	-40F	**LT40-40**	**Probabilistic**	**BWR 004T -40F**	**BWR_004T_-40F_LT40-40**
BWR	025T	0F	**LT40-40**	**Deterministic**	**BWR 025T 0F**	**BWR_025T_0F_LT40-40**
BWR	025T	0F	**LT40-40**	**Probabilistic**	**BWR 025T 0F**	**BWR_025T_0F_LT40-40**
BWR	004T	0F	**LT40-40**	**Deterministic**	**BWR 004T 0F**	**BWR_004T_0F_LT40-40**
BWR	004T	0F	**LT40-40**	**Probabilistic**	**BWR 004T 0F**	**BWR_004T_0F_LT40-40**
BWR	025T	+6F	**LT40-40**	**Deterministic**	**BWR 025T +6F**	**BWR_025T_+6F_LT40-40**
BWR	025T	+6F	**LT40-40**	**Probabilistic**	**BWR 025T +6F**	**BWR_025T_+6F_LT40-40**
BWR	004T	+6F	**LT40-40**	**Deterministic**	**BWR 004T +6F**	**BWR_004T_+6F_LT40-40**
BWR	004T	+6F	**LT40-40**	**Probabilistic**	**BWR 004T +6F**	**BWR_004T_+6F_LT40-40**
BWR	025T	+15F	**LT40-40**	**Deterministic**	**BWR 025T +15F**	**BWR_025T_+15F_LT40-40**
BWR	025T	+15F	**LT40-40**	**Probabilistic**	**BWR 025T +15F**	**BWR_025T_+15F_LT40-40**
BWR	004T	+15F	**LT40-40**	**Deterministic**	**BWR 004T +15F**	**BWR_004T_+15F_LT40-40**
BWR	004T	+15F	**LT40-40**	**Probabilistic**	**BWR 004T +15F**	**BWR_004T_+15F_LT40-40**
BWR	025T	+47F	**LT40-40**	**Deterministic**	**BWR 025T +47F**	**BWR_025T_+47F_LT40-40**
BWR	025T	+47F	**LT40-40**	**Probabilistic**	**BWR 025T +47F**	**BWR_025T_+47F_LT40-40**

Reactor Type	Flaw	RTNDT Shift	Transient	Run Type	Folder	Case Name
BWR	004T	+47F	LT40-40	Deterministic	BWR 004T +47F	BWR_004T_+47F_LT40-40
BWR	004T	+47F	LT40-40	Probabilistic	BWR 004T +47F	BWR_004T_+47F_LT40-40
BWR	025T	+128F	LT40-40	Deterministic	BWR 025T +128F	BWR_025T_+128F_LT40-40
BWR	025T	+128F	LT40-40	Probabilistic	BWR 025T +128F	BWR_025T_+128F_LT40-40
BWR	004T	+128F	LT40-40	Deterministic	BWR 004T +128F	BWR_004T_+128F_LT40-40
BWR	004T	+128F	LT40-40	Probabilistic	BWR 004T +128F	BWR_004T_+128F_LT40-40
BWR	025T	0F	P0_LT40-100	Deterministic	BWR 025T 0F	BWR_025T_0F_P0_LT40-100
BWR	025T	-40F	LT40-100	Deterministic	BWR 025T -40F	BWR_025T_-40F_LT40-100
BWR	025T	-40F	LT40-100	Probabilistic	BWR 025T -40F	BWR_025T_-40F_LT40-100
BWR	004T	-40F	LT40-100	Deterministic	BWR 004T -40F	BWR_004T_-40F_LT40-100
BWR	004T	-40F	LT40-100	Probabilistic	BWR 004T -40F	BWR_004T_-40F_LT40-100
BWR	025T	0F	LT40-100	Deterministic	BWR 025T 0F	BWR_025T_0F_LT40-100
BWR	025T	0F	LT40-100	Probabilistic	BWR 025T 0F	BWR_025T_0F_LT40-100
BWR	004T	0F	LT40-100	Deterministic	BWR 004T 0F	BWR_004T_0F_LT40-100
BWR	004T	0F	LT40-100	Probabilistic	BWR 004T 0F	BWR_004T_0F_LT40-100
BWR	025T	+6F	LT40-100	Deterministic	BWR 025T +6F	BWR_025T_+6F_LT40-100
BWR	025T	+6F	LT40-100	Probabilistic	BWR 025T +6F	BWR_025T_+6F_LT40-100
BWR	004T	+6F	LT40-100	Deterministic	BWR 004T +6F	BWR_004T_+6F_LT40-100
BWR	004T	+6F	LT40-100	Probabilistic	BWR 004T +6F	BWR_004T_+6F_LT40-100
BWR	025T	+15F	LT40-100	Deterministic	BWR 025T +15F	BWR_025T_+15F_LT40-100
BWR	025T	+15F	LT40-100	Probabilistic	BWR 025T +15F	BWR_025T_+15F_LT40-100
BWR	004T	+15F	LT40-100	Deterministic	BWR 004T +15F	BWR_004T_+15F_LT40-100
BWR	004T	+15F	LT40-100	Probabilistic	BWR 004T +15F	BWR_004T_+15F_LT40-100
BWR	025T	+47F	LT40-100	Deterministic	BWR 025T +47F	BWR_025T_+47F_LT40-100
BWR	025T	+47F	LT40-100	Probabilistic	BWR 025T +47F	BWR_025T_+47F_LT40-100
BWR	004T	+47F	LT40-100	Deterministic	BWR 004T +47F	BWR_004T_+47F_LT40-100
BWR	004T	+47F	LT40-100	Probabilistic	BWR 004T +47F	BWR_004T_+47F_LT40-100
BWR	025T	+128F	LT40-100	Deterministic	BWR 025T +128F	BWR_025T_+128F_LT40-100
BWR	025T	+128F	LT40-100	Probabilistic	BWR 025T +128F	BWR_025T_+128F_LT40-100
BWR	004T	+128F	LT40-100	Deterministic	BWR 004T +128F	BWR_004T_+128F_LT40-100

Reactor Type	Flaw	RTNDT Shift	Transient	Run Type	Folder	Case Name
BWR	004T	+128F	**LT40-100**	**Probabilistic**	**BWR 004T +128F**	**BWR_004T_+128F_LT40-100**
BWR	025T	0F	**P0_LTA**	**Deterministic**	**BWR 025T 0F**	**BWR_025T_0F_P0_LTA**
BWR	025T	-40F	**LTA**	**Deterministic**	**BWR 025T -40F**	**BWR_025T_-40F_LTA**
BWR	025T	-40F	**LTA**	**Probabilistic**	**BWR 025T -40F**	**BWR_025T_-40F_LTA**
BWR	004T	-40F	**LTA**	**Deterministic**	**BWR 004T -40F**	**BWR_004T_-40F_LTA**
BWR	004T	-40F	**LTA**	**Probabilistic**	**BWR 004T -40F**	**BWR_004T_-40F_LTA**
BWR	025T	0F	**LTA**	**Deterministic**	**BWR 025T 0F**	**BWR_025T_0F_LTA**
BWR	025T	0F	**LTA**	**Probabilistic**	**BWR 025T 0F**	**BWR_025T_0F_LTA**
BWR	004T	0F	**LTA**	**Deterministic**	**BWR 004T 0F**	**BWR_004T_0F_LTA**
BWR	004T	0F	**LTA**	**Probabilistic**	**BWR 004T 0F**	**BWR_004T_0F_LTA**
BWR	025T	+6F	**LTA**	**Deterministic**	**BWR 025T +6F**	**BWR_025T_+6F_LTA**
BWR	025T	+6F	**LTA**	**Probabilistic**	**BWR 025T +6F**	**BWR_025T_+6F_LTA**
BWR	004T	+6F	**LTA**	**Deterministic**	**BWR 004T +6F**	**BWR_004T_+6F_LTA**
BWR	004T	+6F	**LTA**	**Probabilistic**	**BWR 004T +6F**	**BWR_004T_+6F_LTA**
BWR	025T	+15F	**LTA**	**Deterministic**	**BWR 025T +15F**	**BWR_025T_+15F_LTA**
BWR	025T	+15F	**LTA**	**Probabilistic**	**BWR 025T +15F**	**BWR_025T_+15F_LTA**
BWR	004T	+15F	**LTA**	**Deterministic**	**BWR 004T +15F**	**BWR_004T_+15F_LTA**
BWR	004T	+15F	**LTA**	**Probabilistic**	**BWR 004T +15F**	**BWR_004T_+15F_LTA**
BWR	025T	+47F	**LTA**	**Deterministic**	**BWR 025T +47F**	**BWR_025T_+47F_LTA**
BWR	025T	+47F	**LTA**	**Probabilistic**	**BWR 025T +47F**	**BWR_025T_+47F_LTA**
BWR	004T	+47F	**LTA**	**Deterministic**	**BWR 004T +47F**	**BWR_004T_+47F_LTA**
BWR	004T	+47F	**LTA**	**Probabilistic**	**BWR 004T +47F**	**BWR_004T_+47F_LTA**
BWR	025T	+128F	**LTA**	**Deterministic**	**BWR 025T +128F**	**BWR_025T_+128F_LTA**
BWR	025T	+128F	**LTA**	**Probabilistic**	**BWR 025T +128F**	**BWR_025T_+128F_LTA**
BWR	004T	+128F	**LTA**	**Deterministic**	**BWR 004T +128F**	**BWR_004T_+128F_LTA**
BWR	004T	+128F	**LTA**	**Probabilistic**	**BWR 004T +128F**	**BWR_004T_+128F_LTA**

7 Appendix B: Analysis of Other PWR Transients

This Appendix describes the characteristics and analysis results for 6 PWR transients that were not deemed to be 'normal' PWR cooldowns, as opposed to the transients presented in Section 2.1.2.4. It is important to note that no information was available regarding how representative these transients are of actual PWR fleet operations. These transients were simply some of those that were made available to NRC by Westinghouse in 2013 through an informal exchange of data.

7.1 Transient P7C1: Partial Cooldown

Figure 7-1 shows the pressure and temperature time history for the P7C1 transient. This transient appears to be a partial cooldown from operating pressure and temperature. It is possible that this partial cooldown and hold at lower pressure and temperature was performed for some online maintenance activities, but this is not known with certainty.

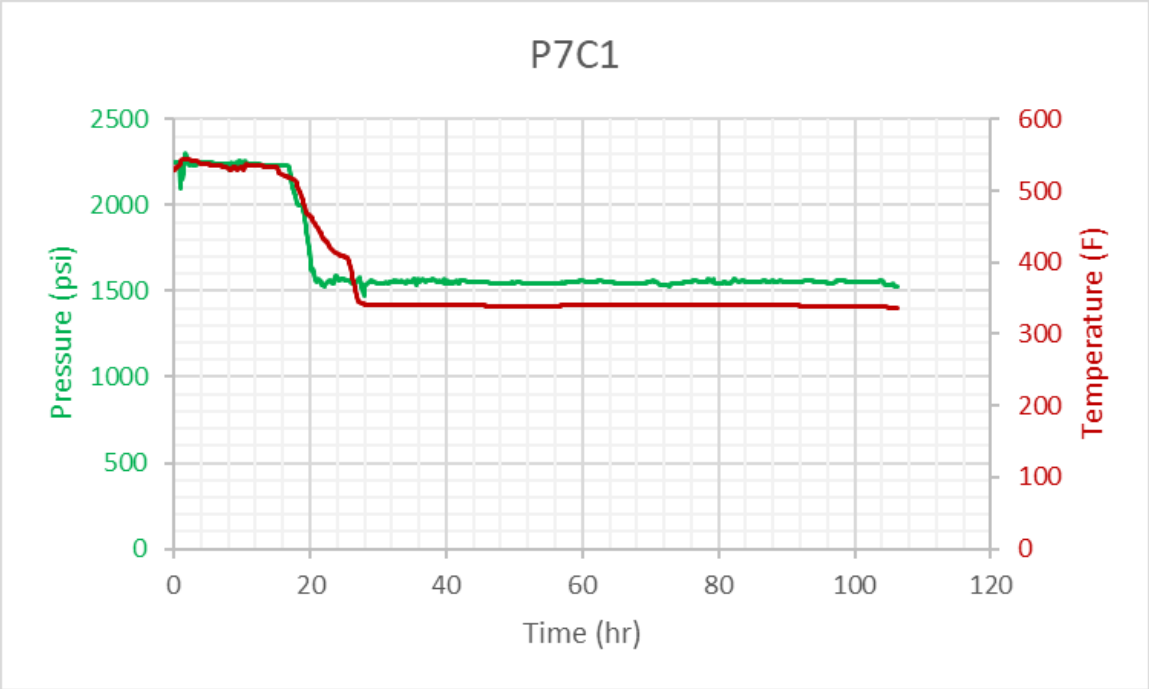

Figure 7-1: PWR P7C1 Transient Characteristics

Figure 7-2 shows the P7C1 transient on a P-T diagram, along with the percentiles of actual cooldowns as described in Section 2.1.2.4, the PT50-50 transient described in Section 2.1.2.2, and the saturation line. Although the transient initially followed the path of a 'normal' PWR cooldown, the pressure was then held constant a little above 1500 psi while the temperature was dropped from about 470°F to 330°F.

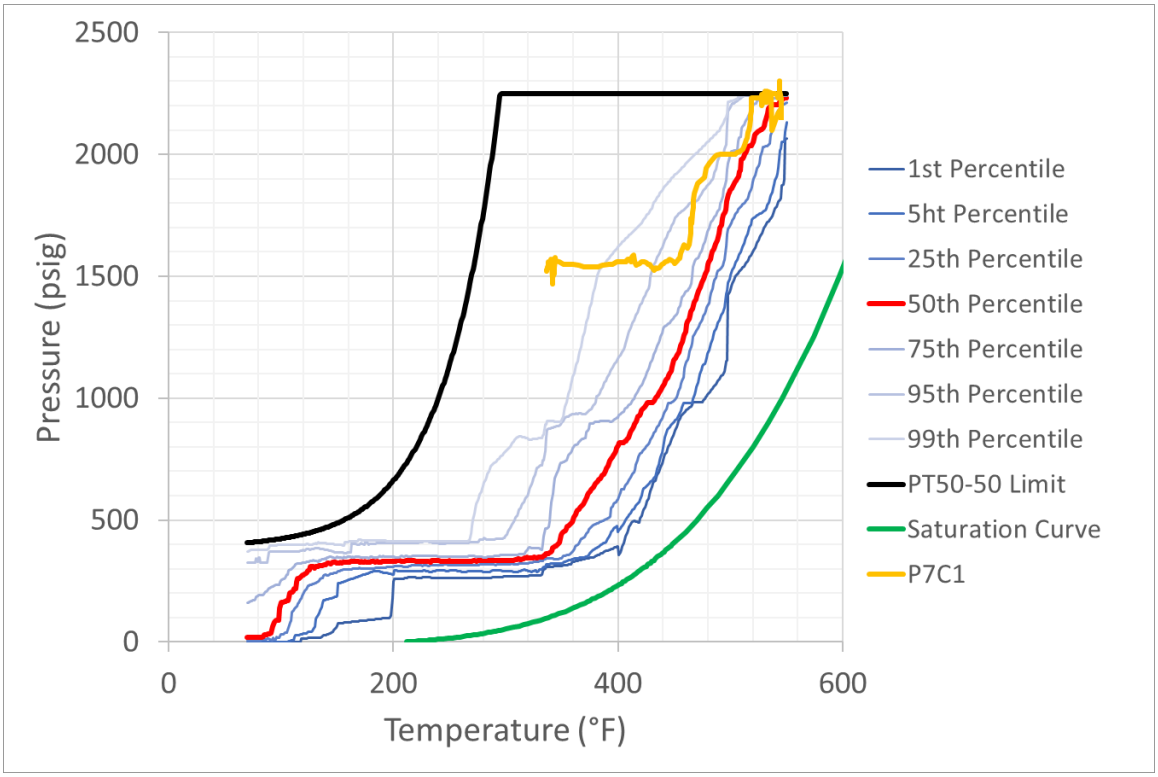

Figure 7-2: P-T Curve for Transient P7C1 Overlaid on P-T Histories Corresponding to Various Percentiles of the Population of PWR Cooldowns Considered (Along with the PT50-50 Limit and the Saturation Curve)

Figure 7-3 shows the K histories versus time for a 0.03 T shallow flaw of aspect ratios of 2, 6, 10, and infinity, along with the K_{Ia} arrest toughness and the 50th percentile of the K_{Ic} fracture toughness distribution. Overall, the K values remain very low and mostly below the arrest toughness. A FAVOR calculation performed for this transient for a small internal surface breaking flaw of depth 0.03 T and aspect ratio of 6 resulted in a CPI of 6.1E-14 and a CPF of 4.5E-16, both extremely low. Such a result is consistent with the very low K values and their position relative to the K_{Ia} curve.

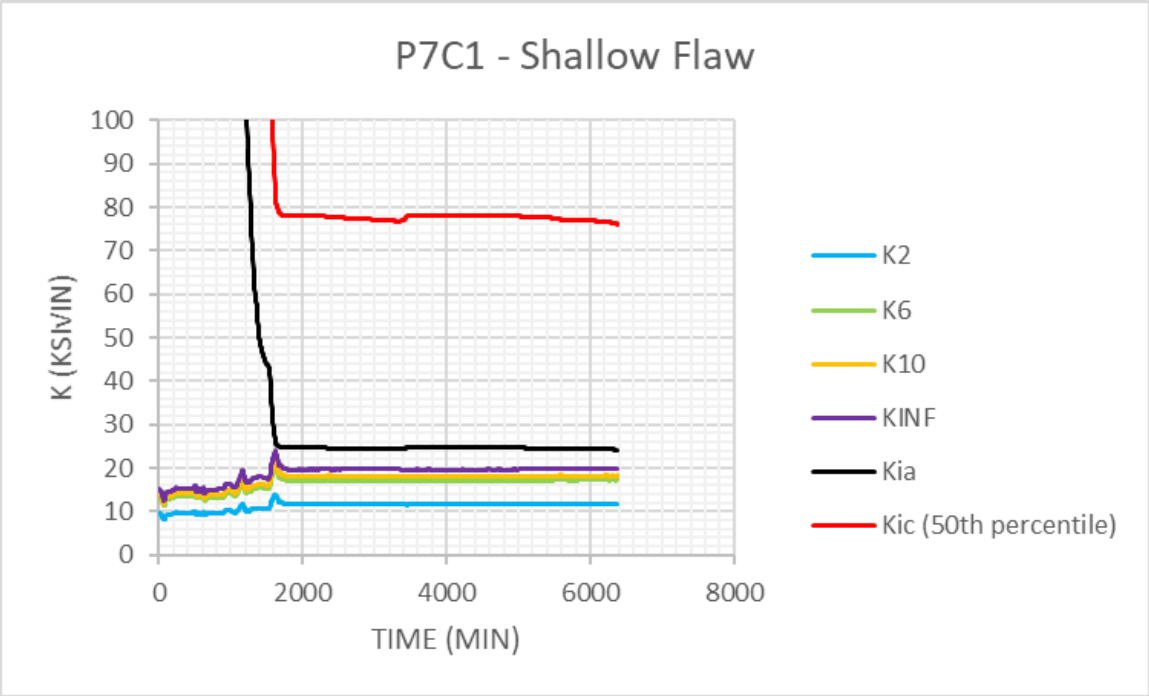

Figure 7-3: Stress Intensity Factor for the PWR P7C1 Transient for a 0.03 T Flaw for Flaw Aspect Ratios of 2, 6, 10 and Infinity

7.2 Transient P7C5: High-Pressure Cooldown

Figure 7-4 shows the pressure and temperature time history for the P7C5 transient. This transient appears to be cooldown from operating pressure and temperature down to about 200°F and 400 psi. This cooldown distinguishes itself from the cooldowns discussed in Section 2.1.2.4 because the high pressure is maintained while the temperature is reduced all the way down to about 360°F.

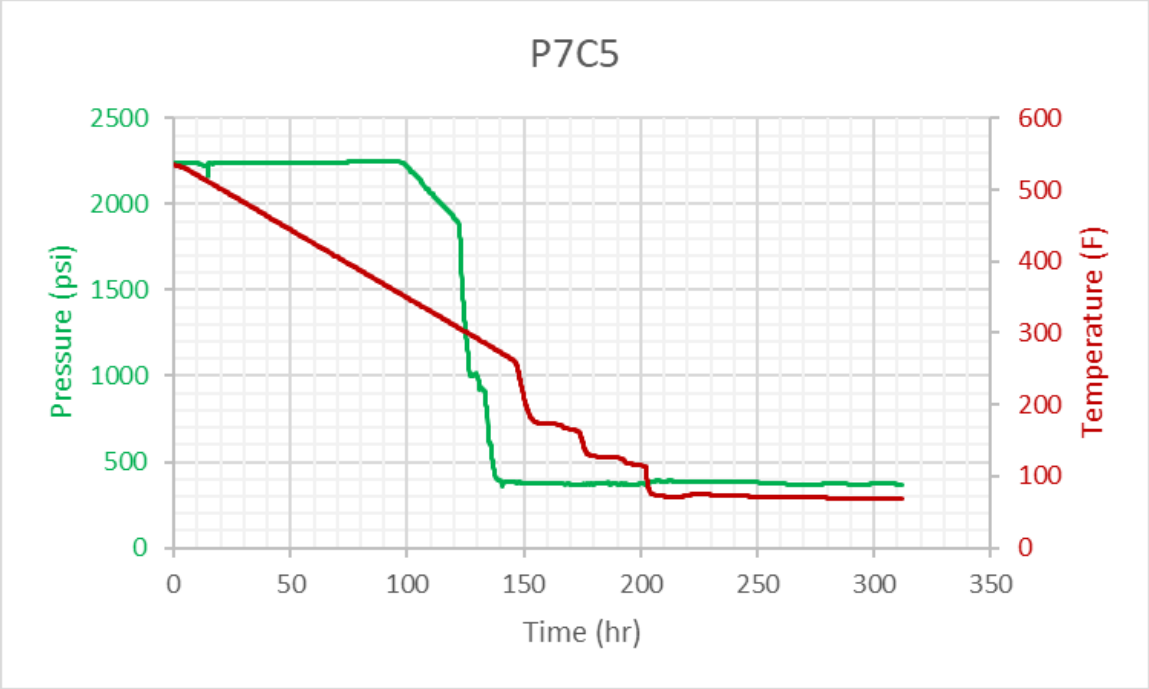

Figure 7-4: PWR P7C5 Transient Characteristics

Figure 7-5 shows the P7C5 transient on a P-T diagram, along with the percentiles of actual cooldowns as described in Section 2.1.2.4, the PT50-50 transient described in Section 2.1.2.2, and the saturation line. This cooldown is different from other cooldowns studied here because it is at or close to the P-T limit until the temperature reaches about 300°F, which appears to be unusual, and may not be allowed in many plants due to various limitations on pumps and other parts of the primary that may be more limiting than the vessel beltline from a P-T limit perspective.

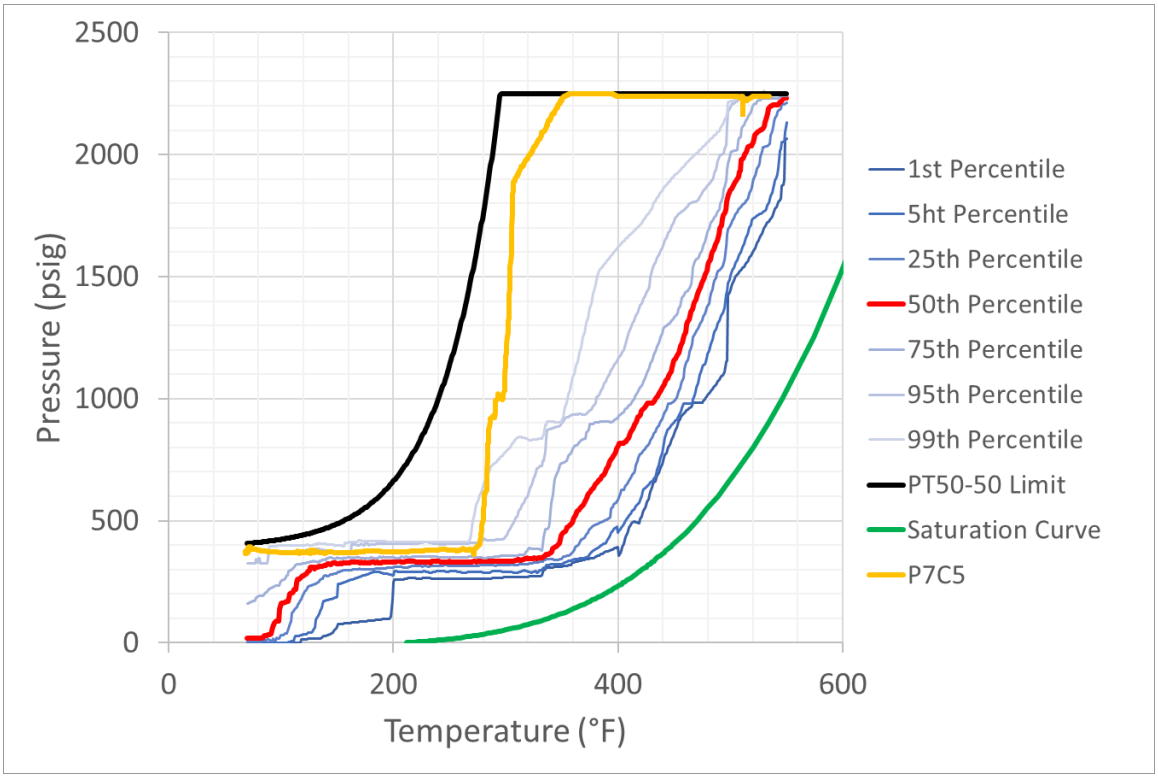

Figure 7-5: P-T Curve for Transient P7C5 Overlaid on P-T Histories Corresponding to Various Percentiles of the Population of PWR Cooldowns Considered (Along with the PT50-50 Limit and the Saturation Curve)

Figure 7-6 shows the K histories versus time for a 0.03 T shallow flaw of aspect ratios of 2, 6, 10, and infinity, along with the K_{Ia} arrest toughness and the 50th percentile of the K_{Ic} fracture toughness distribution. Overall, the K values are low early in the transient despite the high pressure. This is expected for shallow flaws because the K values are more driven by thermal stresses than pressure for such flaws. The K values exceed K_{Ia} later in the transient as the thermal stresses build up from the temperature reduction, and this occurs despite the pressure being low after about 8000 minutes. A FAVOR calculation performed for this transient for a small internal surface breaking flaw of depth 0.03 T and aspect ratio of 6 resulted in a relatively high CPI of 6.7E-6 but a CPF of only 4.8E-14, posing no real failure risk for the vessel.

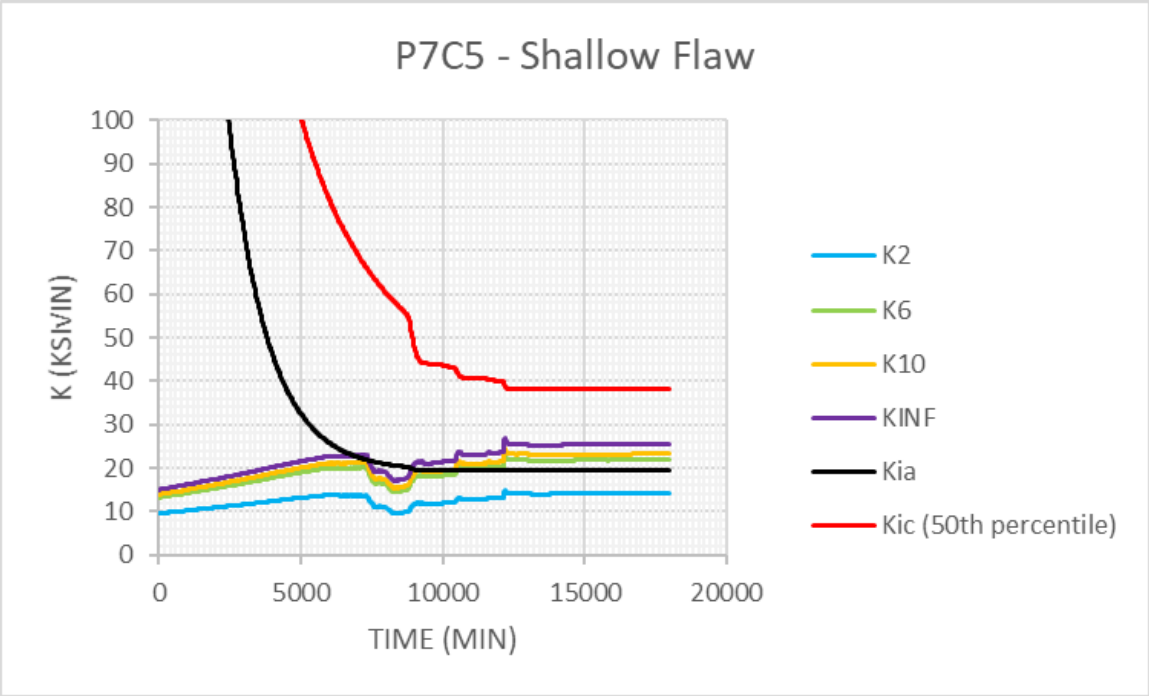

Figure 7-6: Stress Intensity Factor for the PWR P7C5 Transient for a 0.03 T Flaw for Flaw Aspect Ratios of 2, 6, 10 and Infinity

7.3 Transient P7C6: Unusual Cooldown

Figure 7-7 shows the pressure and temperature time history for the P7C6 transient. This transient does represent a cooldown from operating pressure and temperature down to about 85°F and 400 psi, but it is unusual in the sense that there was a repressurization between 110 hours and 160 hours. This could have been a failed attempt to return to operation after a period of lower pressure and temperature for online maintenance, but this cannot be confirmed.

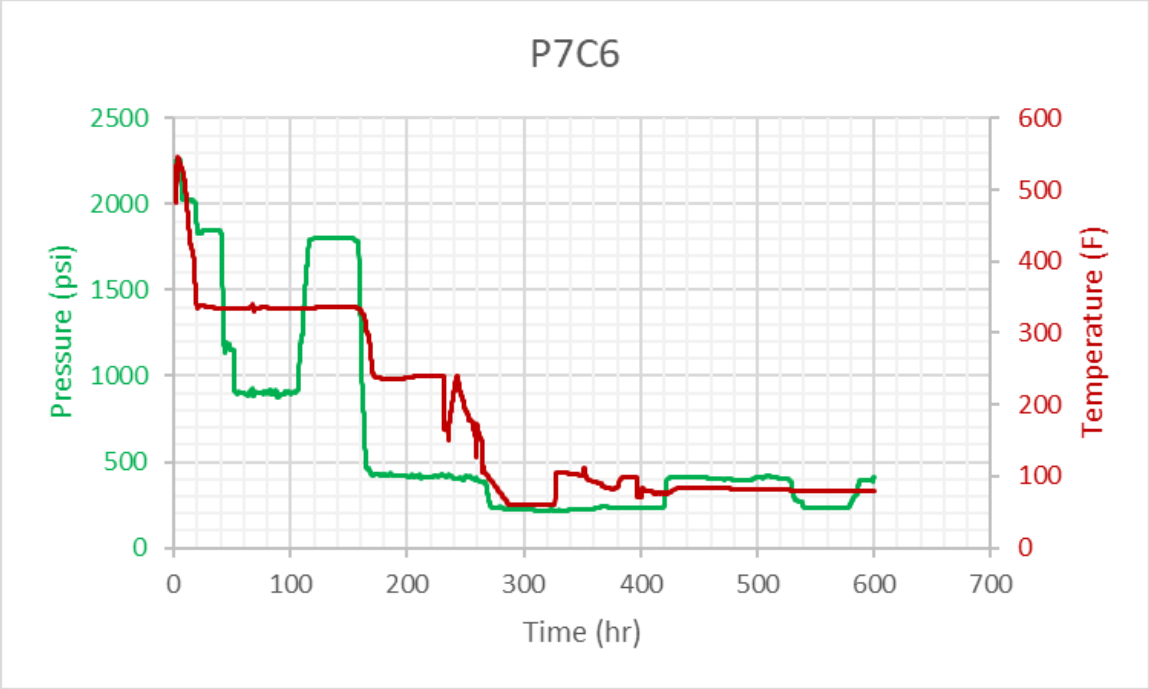

Figure 7-7: PWR P7C6 Transient Characteristics

Figure 7-8 shows the P7C6 transient on a P-T diagram, along with the percentiles of actual cooldowns as described in Section 2.1.2.4, the PT50-50 transient described in Section 2.1.2.2, and the saturation line. This cooldown is different from other cooldowns studied here because of the sustained pressure between 500°F and about 330°F. In addition, the pressure fluctuations around 330°F and later around 80°F, as well as the temperature fluctuation around 400 psi appear to be atypical. Nonetheless, the transient falls overall well below the P-T limit, although it exceed the 99th percentile of 'normal' cooldowns from Section 2.1.2.4 for temperature above ~330°F.

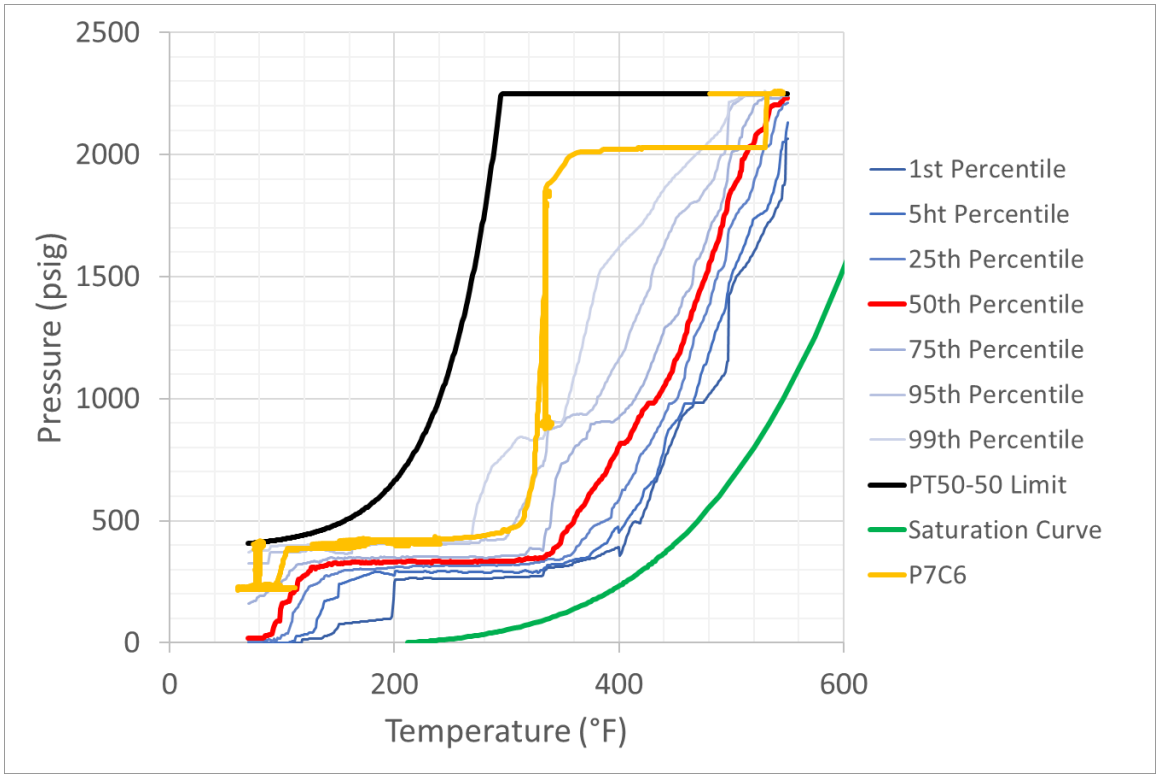

Figure 7-8: P-T Curve for Transient P7C6 Overlaid on P-T Histories Corresponding to Various Percentiles of the Population of PWR Cooldowns Considered (Along with the PT50-50 Limit and the Saturation Curve)

Figure 7-9 shows the K histories versus time for a 0.03 T shallow flaw of aspect ratios of 2, 6, 10, and infinity, along with the K_{Ia} arrest toughness and the 50th percentile of the K_{Ic} fracture toughness distribution. Overall, the K values are low early in the transient despite the high pressure and repressurization. This is expected for shallow flaws because the K values are more driven by thermal stresses than pressure for such flaws. The K values exceed K_{Ia} later in the transient as the thermal stresses build up from the temperature reduction, and this occurs despite the pressure being low after about 16000 minutes. A FAVOR calculation performed for this transient for a small internal surface breaking flaw of depth 0.03 T and aspect ratio of 6 resulted in a relatively high CPI of 1.4E-5 but a CPF of only 3.9E-10, posing no real failure risk for the vessel.

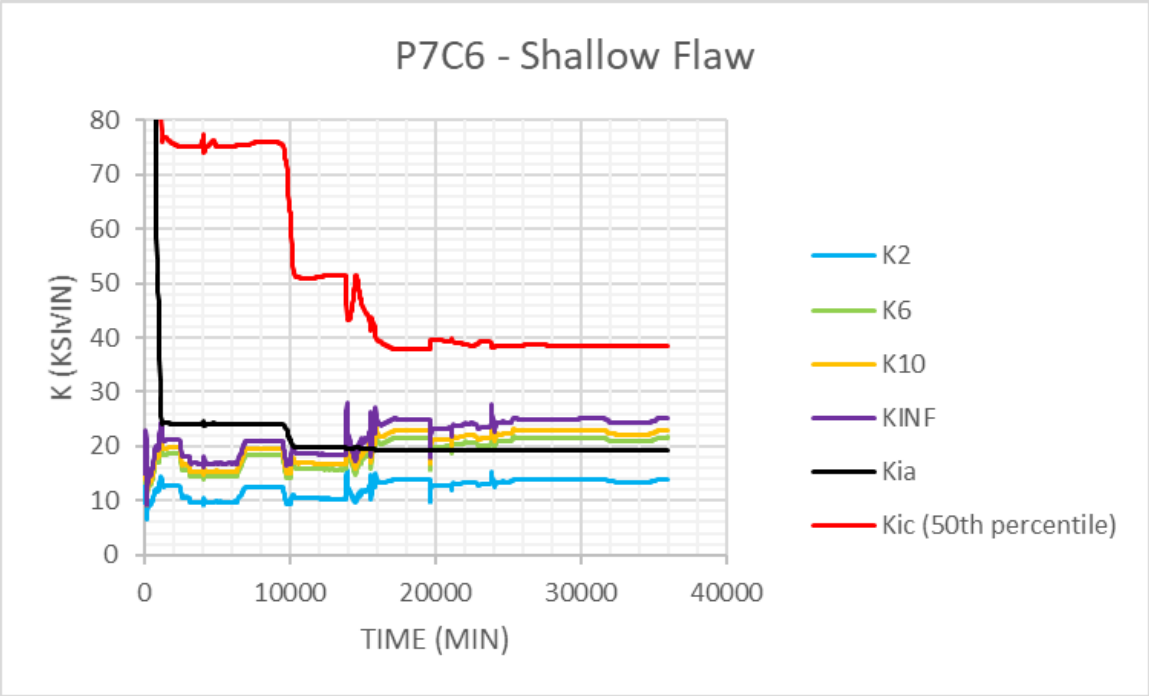

Figure 7-9: Stress Intensity Factor for the PWR P7C6 Transient for a 0.03 T Flaw for Flaw Aspect Ratios of 2, 6, 10 and Infinity

7.4 Transient P7C8: Partial Cooldown Followed by Heatup

Figure 7-10 shows the pressure and temperature time history for the P7C8 transient. This transient appears to be a partial cooldown from operating pressure and temperature, followed by the beginning of a return to operating conditions. It is possible that this partial cooldown and hold at lower pressure and temperature was performed for some online maintenance activities, but this is not known with certainty. In many ways, this transient is similar to the P7C1 transient described in 7.1.

Figure 7-10: PWR P7C8 Transient Characteristics

Figure 7-11 shows the P7C8 transient on a P-T diagram, along with the percentiles of actual cooldowns as described in Section 2.1.2.4, the PT50-50 transient described in Section 2.1.2.2, and the saturation line. Although the transient initially followed the path of a 'normal' PWR cooldown, the pressure was then held constant a little above 1500 psi while the temperature was dropped from about 450°F to 325°F, and then pressure and temperature were both increased in the direction of a return to operating conditions. The first part of this transient is very similar to the P7C1 transient (see Figure 7-2)

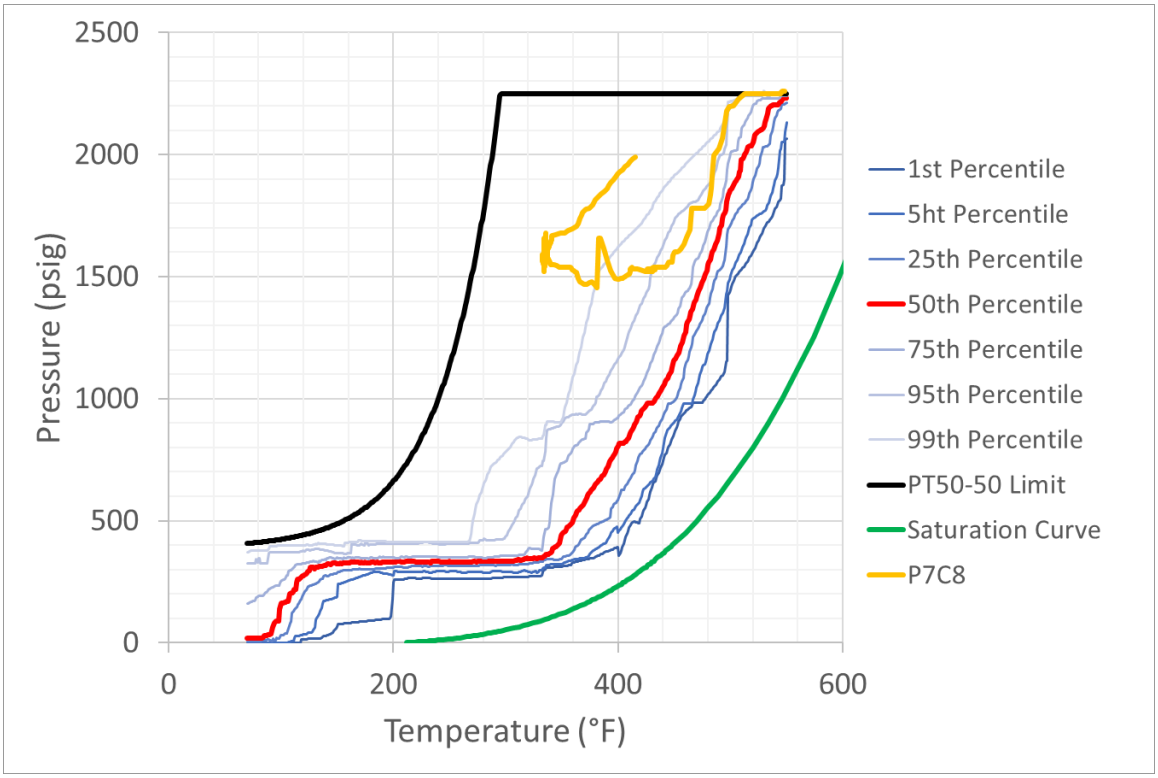

Figure 7-11: P-T Curve for Transient P7C8 Overlaid on P-T Histories Corresponding to Various Percentiles of the Population of PWR Cooldowns Considered (Along with the PT50-50 Limit and the Saturation Curve)

Figure 7-12 shows the K histories versus time for a 0.03 T shallow flaw of aspect ratios of 2, 6, 10, and infinity, along with the K_{Ia} arrest toughness and the 50th percentile of the K_{Ic} fracture toughness distribution. Overall, the K values remain very low and entirely below the arrest toughness. A FAVOR calculation performed for this transient for a small internal surface breaking flaw of depth 0.03 T and aspect ratio of 6 resulted in a CPI and a CPF of zero. Such a result is consistent with the very low K values and their position relative to the K_{Ia} curve. The reason why the CPI and CPF are lower for this transient than for transient P7C1 is that P7C1 experienced a more rapid drop in temperature around 1750 minutes, resulting in a brief and small spike in K values that does not occur for transient P7C8 (see Figure 7-3).

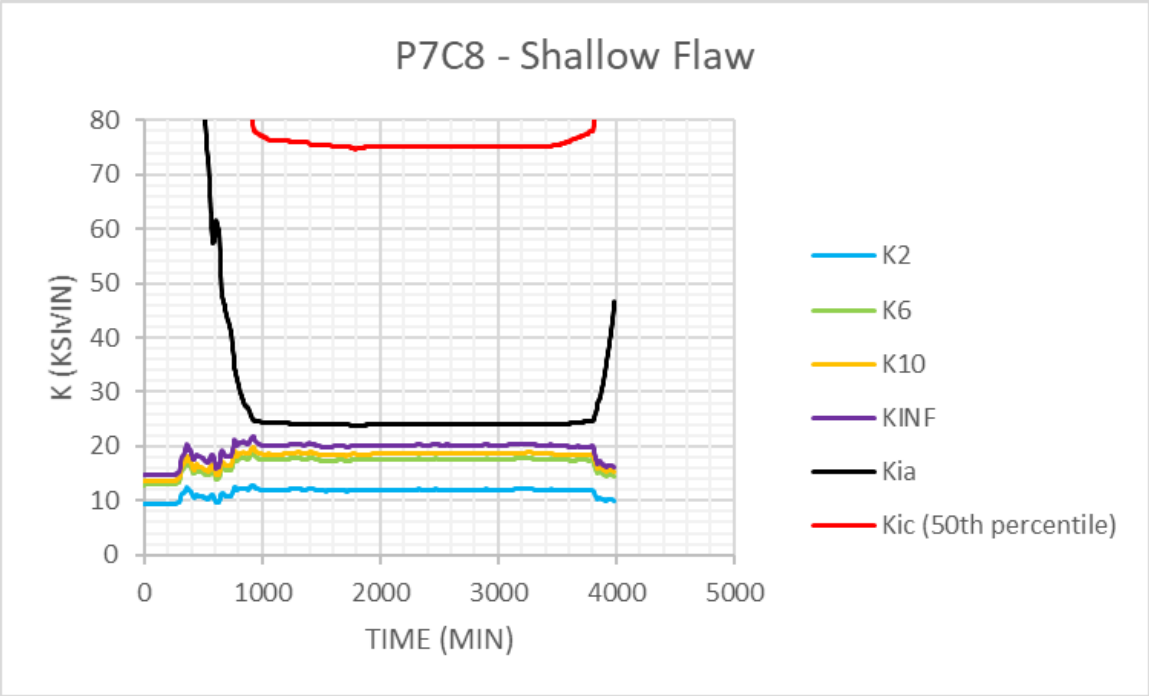

Figure 7-12: Stress Intensity Factor for the PWR P7C8 Transient for a 0.03 T Flaw for Flaw Aspect Ratios of 2, 6, 10 and Infinity

7.5 Transient P8C3: Cooldown Followed by Partial Heatup

Figure 7-13 shows the pressure and temperature time history for the P8C3 transient. This transient appears to be a complete cooldown from operating pressure and temperature, followed by the beginning of a return to operating conditions. It is possible that this complete cooldown and hold at zero pressure and ambient temperature was performed for some short duration maintenance activities, or as a result of a reactor trip and subsequent return to power, but this is not known with certainty. In many ways, this transient is similar to the many of the normal cooldowns described in Section 2.1.2.4, except that it is followed by the beginning of a return to operating conditions.

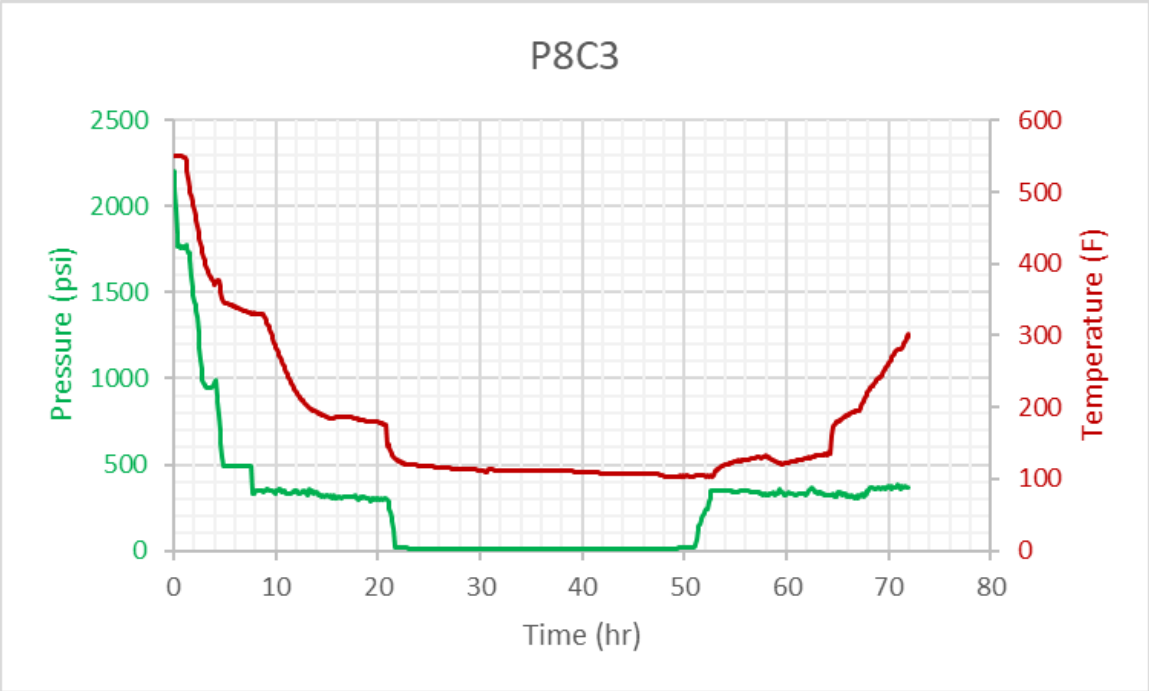

Figure 7-13: PWR P8C3 Transient Characteristics

Figure 7-14 shows the P8C3 transient on a P-T diagram, along with the percentiles of actual cooldowns as described in Section 2.1.2.4, the PT50-50 transient described in Section 2.1.2.2, and the saturation line. This cooldown very similar to many of the normal cooldowns studied in Section 2.1.2.4, and lies between the 25th and 75th percentiles of the Section 2.1.2.4 cooldowns for most of the transient. Even the return to power seems to be following roughly the same path.

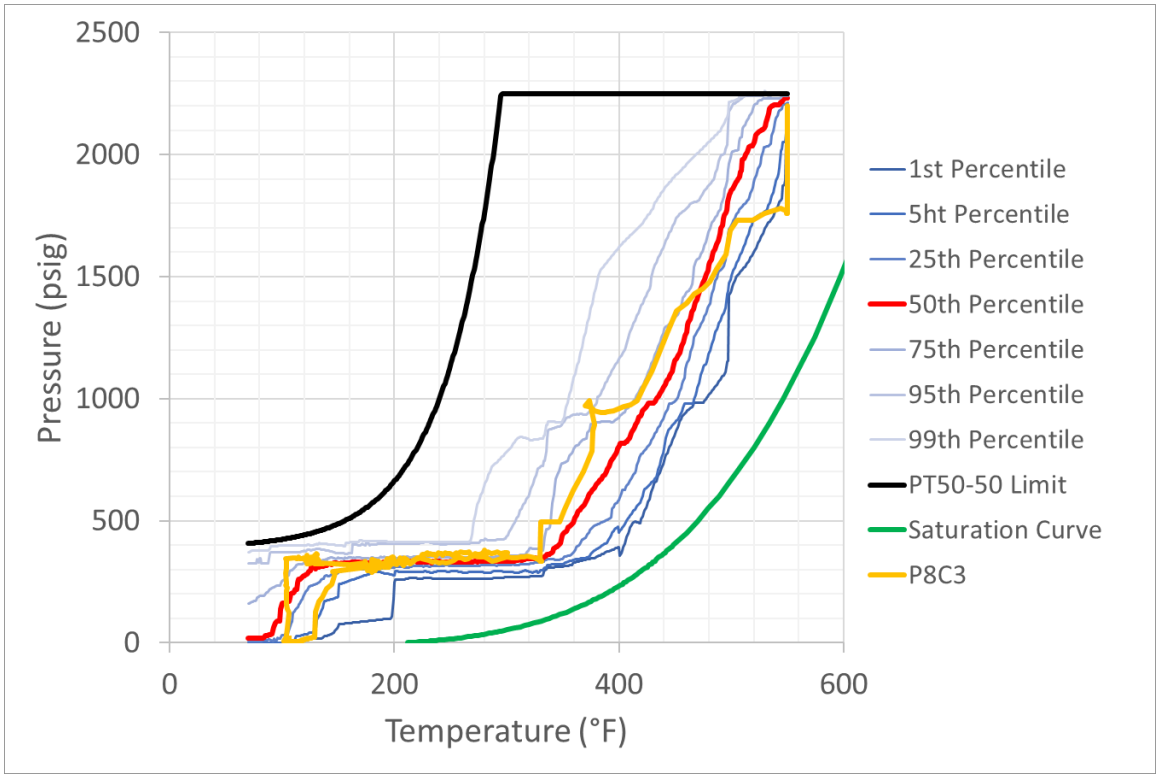

Figure 7-14: P-T Curve for Transient P8C3 Overlaid on P-T Histories Corresponding to Various Percentiles of the Population of PWR Cooldowns Considered (Along with the PT50-50 Limit and the Saturation Curve)

Figure 7-15 shows the K histories versus time for a 0.03 T shallow flaw of aspect ratios of 2, 6, 10, and infinity, along with the K_{Ia} arrest toughness and the 50th percentile of the K_{Ic} fracture toughness distribution. Overall, the K values remain low with a small spike around 1250 minutes, which relates to a relatively rapid drop in temperature, which drives the thermal K up for the shallow flaw. The K values do exceed the K_{Ia} line for most of the low temperature portion of the transient, despite there being no pressure applied, but this is expected as it is driven by the thermal stresses for the shallow flaw. It is interesting to note the expected decrease in K as the temperature is increased during the return to operating conditions at the end of the transient. A FAVOR calculation performed for this transient for a small internal surface breaking flaw of depth 0.03 T and aspect ratio of 6 resulted in a relatively high CPI of 1.9E-6 but a CPF of zero, posing zero failure risk for the vessel, as would be hoped for in normal operations as seem to be the case for this transient.

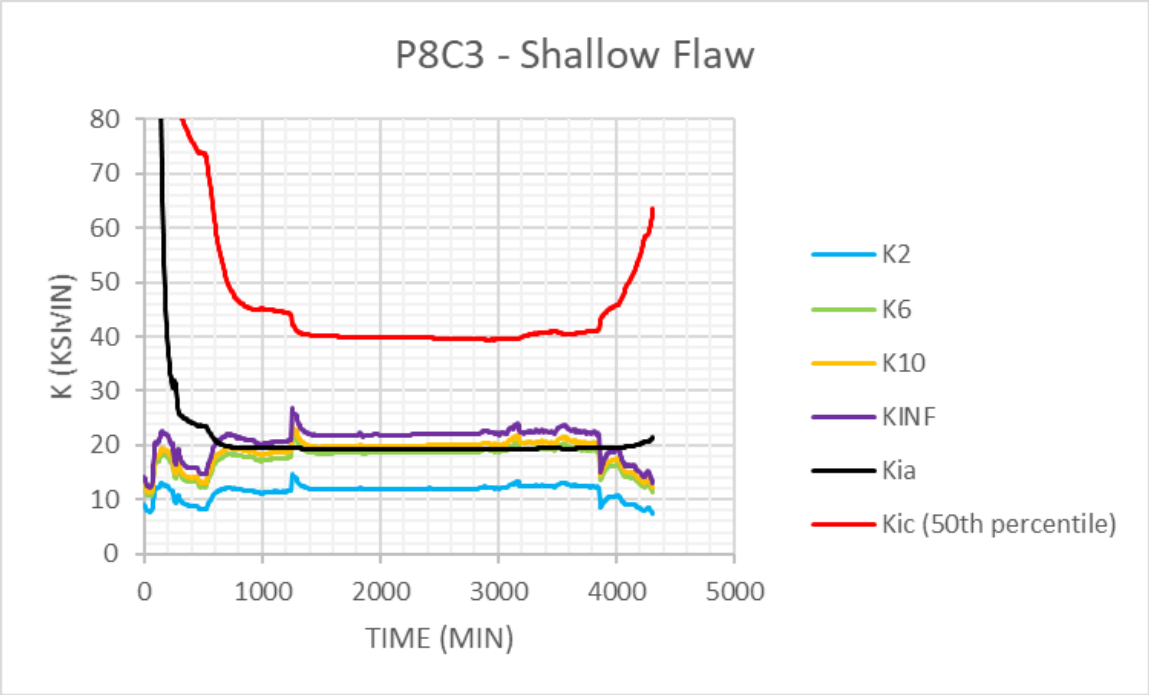

Figure 7-15: Stress Intensity Factor for the PWR P8C3 Transient for a 0.03 T Flaw for Flaw Aspect Ratios of 2, 6, 10 and Infinity

7.6 Transient PBC1: Cooldown with Pressure Hold and Low Temperature Pressure Spike

Figure 7-16 shows the pressure and temperature time history for the PBC1 transient. This transient does represent a cooldown from operating pressure and temperature, but it is unusual in the sense that there was a repressurization exceeding the RCS operating pressure at 58 hours. This repressurization exceed all RCS pressure limits as it reaches about 3000 psi and occurs over a period of roughly 1 hour. Since NRC would have notified of such an even of it had occurred in the vessel or other portion of the RCS, one possibility is that the pressure sensor that recorded this data was isolated from the main RCS when this occurred and that the pressure spike was localized in a system that is open to the RCS during normal operation but was isolated at the time of the pressure spike. Of course, this scenario cannot be confirmed, so for the purpose of the analysis, it was assumed that this data truly represented vessel conditions, which is almost certainly not the case here.

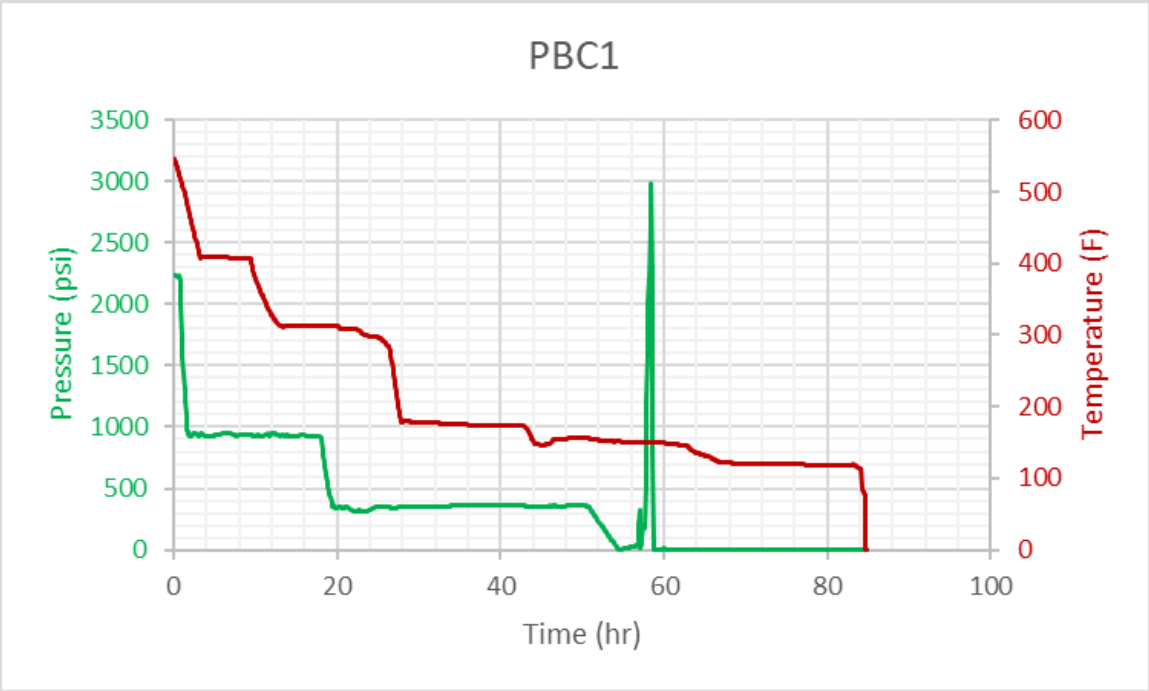

Figure 7-16: PWR PBC1 Transient Characteristics

Figure 7-17 shows the PBC1 transient on a P-T diagram, along with the percentiles of actual cooldowns as described in Section 2.1.2.4, the PT50-50 transient described in Section 2.1.2.2, and the saturation line. This spears to be a stepwise cooldown where the pressure was reduced in large increments at almost constant temperature, followed by reductions in temperature at almost constant pressure, rather than a cooldown where pressure and temperature were reduced simultaneously. There were several other such stepwise cooldowns among the cooldowns studied in Section 2.1.2.4, and this transient would have likely been grouped with the 'normal' cooldowns if it were not for the late pressure spike. As described above, this pressure spike is not believed to have been experienced by the vessel itself, but rather by an isolated portion of the primary. Nonetheless, the transient was analyzed as if this was the pressure in the vessel.

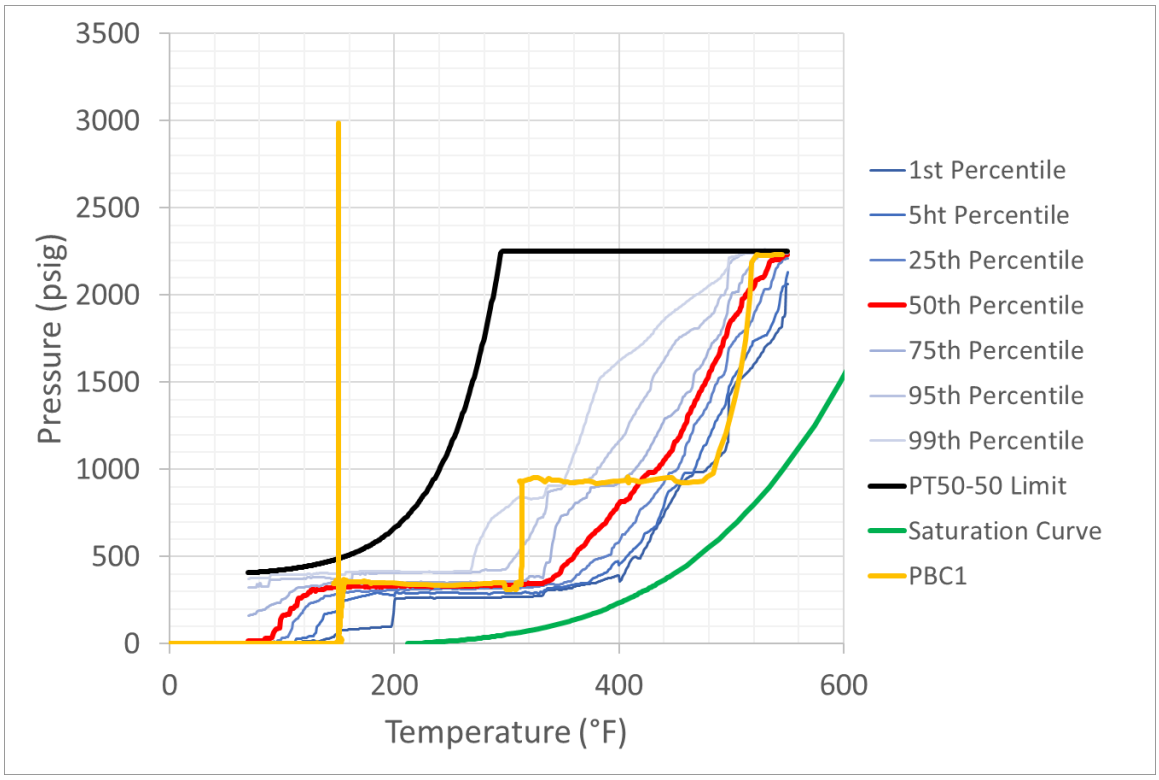

Figure 7-17: P-T Curve for Transient PBC1 Overlaid on P-T Histories Corresponding to Various Percentiles of the Population of PWR Cooldowns Considered (Along with the PT50-50 Limit and the Saturation Curve)

Figure 7-18 shows the K histories versus time for a 0.03 T shallow flaw of aspect ratios of 2, 6, 10, and infinity, along with the K_{Ia} arrest toughness and the 50th percentile of the K_{Ic} fracture toughness distribution. As is the case for all the transients presented in 2.1.2.4 and in this Appendix, the K values remain below K_{Ia} initially. There is a pike in K values around 1600 minutes associated with a rapid drop in temperature, and again at the very end of the transient also associated with a temperature drop. These K increases are related to tensile thermal stresses experienced by the shallow flaw upon cooling down events. The biggest spike in K, however, is experienced at about 3500 minutes, and drives the CPI and CPF values calculate with FAVOR. In fact, a FAVOR calculation performed for this transient for a small internal surface breaking flaw of depth 0.03 T and aspect ratio of 6 resulted in a very high CPI of 1.40E-3 and a CPF of 1.38E-3 (almost equal to CPI), which is 3 orders of magnitude higher than normally acceptable. It is important to underline that this transient is not believed to have been experienced by the vessel, and could be related to a sensor malfunction or a primary system piping configuration.

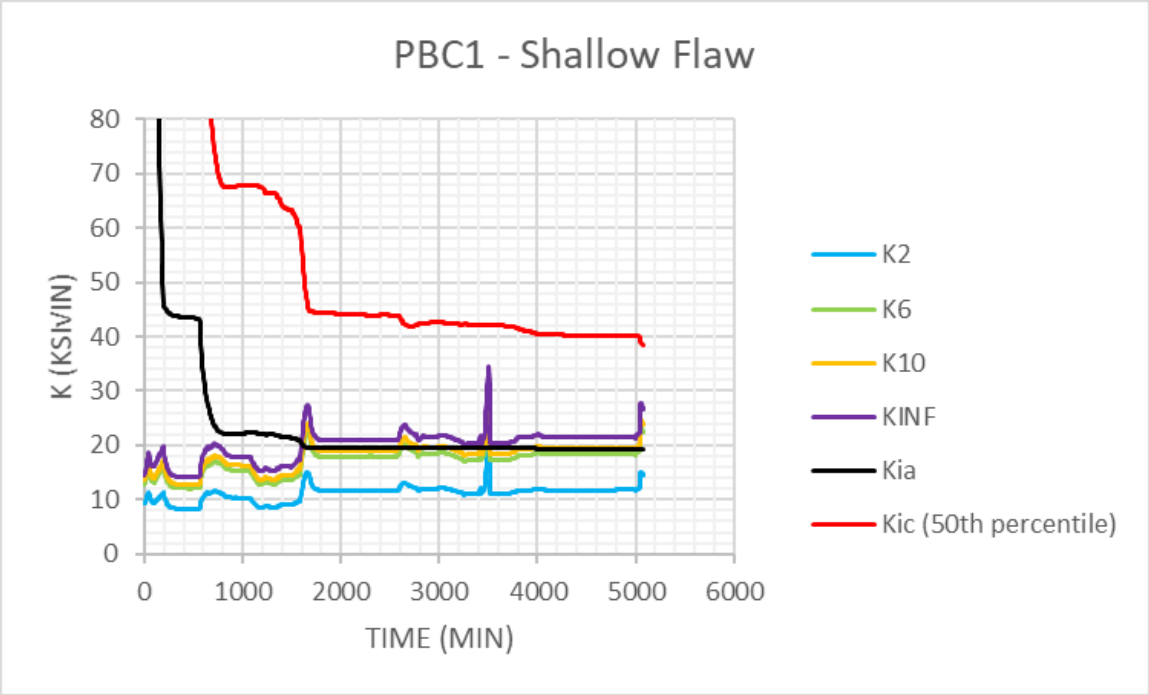

Figure 7-18: Stress Intensity Factor for the PWR PBC1 Transient for a 0.03 T Flaw for Flaw Aspect Ratios of 2, 6, 10 and Infinity